Thiophene - based DNA binders for sensing, nano-bioelectronics, and therapeutic purposes

IRINA MIHAELA DORIN

A thesis submitted for Degree of Doctor of Philosophy

School of Chemistry

Cardiff University

December 2010

ProQuest LLC
789 East Eisenhower Parkway
P.O. Box 1346
Ann Arbor, MI 48106-1346

DECLARATION

This work has not previously been accepted in substance for any degree and is not concurrently submitted in candidature for any degree.

Signed ..... (candidate) Date 23.12.2010

STATEMENT 1

This thesis is being submitted in partial fulfillment of the requirements for the degree of PhD

Signed ..... (candidate) Date 23.12.2010

STATEMENT 2

This thesis is the result of my own independent work/investigation, except where otherwise stated.
Other sources are acknowledged by explicit references.

Signed ..... (candidate) Date 23.12.2010

STATEMENT 3

I hereby give consent for my thesis, if accepted, to be available for photocopying and for inter-library loan, and for the title and summary to be made available to outside organisations.

Signed ..... (candidate) Date 23.12.2010

Summary

The development of cationic conjugated oligohetero-aromatics as building blocks for conjugated polymeric DNA binders with exciting spectroscopic and electronic properties is a prerequisite for genosensors and programmable self assembly of nanobioelectronic systems.

As an example of such systems, we have synthesised a series of cationic conjugated oligoheteroaromatics using Pd cross-coupling reactions such as the Suzuki-Mirayaura and Stille cross-coupling in combination with microwave-assisted Pd catalysis to synthesise the conjugated oligoheteroaromatic frameworks. The interactions of these oligoheteroaromatics with duplex DNA were studied and all the compounds showed interesting optoelectronic properties which change markedly upon binding to duplex DNA. As a result, these cationic conjugated oligoheteroaromatics are able to detect double-stranded DNA. The affinities of the studied oligoheteroaromatics are typically in the order of 10^4 M^{-1} and binding modes vary between groove binding and intercalation.

Additionally, we have demonstrated that cationic conjugated oligoheteroaromatics self assemble in aqueous solutions, forming various aggregate structures such as micelles via π-π stacking interactions. Self aggregation of cationic oligoheteroaromatics in aqueous solution needs to be taken in account when quantifying the binding of cationic oligoheteroaromatics with duplex DNA, but the resulting quantitative information on the self assembly of cationic oligoheteroaromatics can also open new interesting prospects for material science.

...to my parents...

For the love and care

For the value you have taugh

For the support you always given

I am truly holy and grateful to have parents like you....

ACKNOWLEDGEMENTS

First of all I would like to thank my supervisor Dr. Niek Buurma for giving me the opportunity to work on this research. You have made me to see the nice part of doing chemistry in a moment when I was struggling.

Thank you Niek! Thank you for your extraordinary support, encouragements and assistant, for every undertaking during my PhD in Cardiff University.

I am also very thankful for Professor Barry Carpenter and Dr. James Redman for serving as my examiners for the six monthly examinations. An extra thanks to Rob Richardson for many chemistry discussions we had and for proof reading of my thesis. I also acknowledge to Dr. Jim Thomas and Dr. Peter Griffiths for accepting to be my examiners and to read my thesis.

I enjoyed working in the POC, in the nice atmosphere, with a lot of people from around the world, Spain, Italy, Kurdistan, USA, South Arabia, India, UK. I am very pleased to the members of Buurma's group in particular to Mazin, Ismail and Andy. During these years you guys been as brothers for me. I really appreciate that! I also wish thank the members of Barry's group and Eric's group. My regards go to Larry, for the funny times spent in the Lab together, especially at the very beginning when we were the first people here in POC. It has been a great pleasure to meet people from other research groups, especially from Peter's group and to socialise with them. Thank you all of you guys for having a good time.

I also thank those who worked with me to create the work described in this thesis, to M.Sc and B.Sc students and Erasmus students.

I thank to Romanian community in Cardiff. It was great to join you for orthox church services, every Sunday morning.

I also thank to my "Bulinuta", for his efforts to travel frequently from Iasi to Cardiff to support me and to make our love to resist over these three years.

Finally I would like to give a big thank to my parents, for their love and support throughout my life. An especial place in my heart is offer to my mother, for her continue encouragements and help to get where I am now. Thank you Mom and Dad!

TABLE OF CONTENTS

Chapter 1

INTRODUCTION

Abstract:

To exploit the possibilities of targeting DNA for various medical purposes to the fullest, there is a strong need for new drugs, biosensors, etc. interacting sequence-selectively with DNA. The preferred target for synthetic sequence-selective duplex DNA binders is the minor groove. Chapter 1 describes both the advantages and the challenges accompanying targeting this binding mode. Of particular interest to us are chemical systems displaying variable optoelectronic properties that are able to recognise nucleic acids and as a result can be used for sensing and bio-nanoelectronic applications. In this context, the chapter offers examples of cationic polythiophenes that possess favourable electronic and spectroscopic properties and that bind to DNA in aqueous solution. Additionally, the chapter describes general methods for synthesis of conjugated polymers and oligomers.

1 General introduction of thesis

All biological processes are fundamentally chemical reactions and depend in general on the properties and interactions between molecules. This means that biology is strongly entwined with chemistry. Of particular interest at the interface between the two domains are non-covalent self-assembling systems consisting of bio(macro)molecules and chemical systems displaying variable optoelectronic properties. Combining the versatility of the molecules of life with technology-defining molecular electronics in particular opens up a wealth of applications, including the ultimate miniaturisation of biosensors and the programmable self-assembly of nanobioelectronic systems. In biosensor design, to selectively target DNA offers not only new prospects for gene discovery and disease diagnosis, but could provide an enormous contribution to drug discovery. Having said that, we focus in this thesis on DNA as the biomacromolecule of choice, but approaches involving other biomacromolecules are being developed by others.[1-7] In order to detect DNA, an optoelectronic element called a transducer needs to be attached to the recognition element. The transducer will be able to convert the signal resulting from the hybridisation with DNA into a read-out signal. From this point of view, electrically conducting polymers are known to posses several features that enable them to act as exceptional materials for the attachment of biomolecules and rapid electron transfer for the development of efficient biosensors.

1.1 Biological processes involving DNA

It is a generally accepted reality of life that all (known) living organisms depend upon deoxyribonucleic acid (DNA) and ribonucleic acid (RNA) for their continued existence. Additionally, enzymes and proteins are needed to drive cellular processes. Knowing that all of these entities are present in a living organism, then the main question which appears in one's mind is: "how are DNA, RNA and proteins connected"? The answer comes from the fact that different DNA sequences form codons, or triplets of nucleotides which correspond to particular amino acids. Also, a series of codons in a specific region represent the complete code for a specific protein.

According to the "central dogma of molecular biology", the information encoded in DNA is transferred through RNA to proteins in the cell (Figure 1.1). This involves several important cellular processes surrounding the DNA such as replication, transcription and translation.

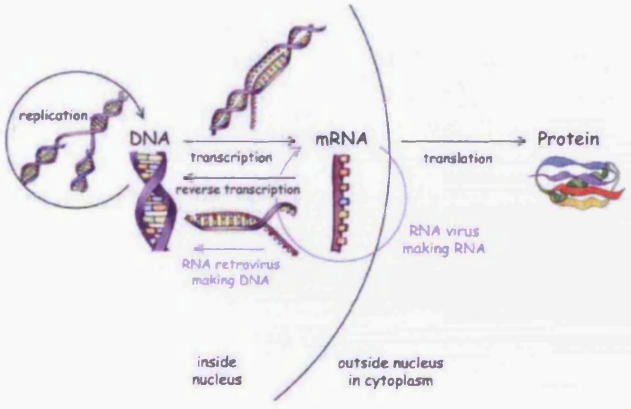

Figure 1.1 Cartoon representation of the "central dogma of molecular biology".[8]

When the cell divides, DNA duplicates by a process known as replication. The information is transferred to messenger RNA (mRNA) using the DNA as a template during the transcription process. Finally, it can be transferred to the ribosome in the cytoplasm where the proteins are produced through translation. Each of these processes involves the contribution of various types of proteins called enzymes.

1.2 DNA structure

It has been 66 years since Oswald Avery, Colin MacLeod, and MacLyn McCarty demonstrated DNA to be the carrier of genetic information.[9] Later it was found that the molecule itself was the genetic code material, so a race in the scientific world was begun in order to find the structure of this polynucleotide. Investigations on the structure of nucleic acids continued and in 1962 Watson, Crick and Wilkins were awarded the Nobel Prize in Medicine for their elucidation on the structure of nucleic acids. According to Watson and Crick's model[10] DNA is a double helix, composed of two antiparallel, complementary strands which are held together by hydrogen bonding between the purine and pyrimidine bases (Figure 1.2). Nucleobases in each strand are attached via the glycosidic bonds to the C_1 of the deoxyribose sugar backbone. The sugar units in the backbones are joined together through the 3'-hydroxyl and 5'-hydroxyl groups by phosphodiester groups. These linker groups are orientated outside of the double helix in order to minimize repulsion betweens the strands, while the nucleotides are inside of the helix, stacking along the direction of the helix axis.

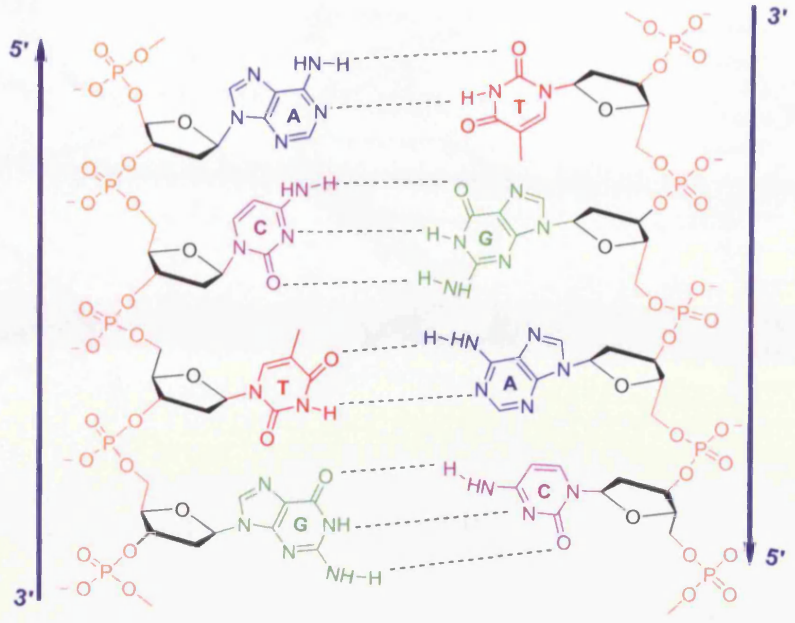

Figure 1.2 The chemical structure of DNA (B-DNA)

The four types of nucleobases in the structure of DNA are: adenine (A), thymine (T), guanidine (G) and cytosine (C). The combination of these bases leads to only two types of base pairs. Adenine on one DNA strand is always paired with thymine on the complementary strand, while guanine is always paired with cytosine. The G•C base pairs contain three H-bonds whereas A•T base pairs contain two H-bonds, making G•C base pairs more stable than A•T base pairs. The A•T and G•C base pairings are energetically favored in B-DNA. Additionally, the sugar and phosphate groups can exhibit various torsional effects on the secondary structure of the nucleic acids,[11] allowing double stranded DNA to adopt several conformations depending on base-pairs sequences and conditions, *viz.* A-, B- and Z-DNA (Figure 1.3).

Figure 1.3 Nucleic acid duplex conformations: a) A-DNA (NDB ID: AD0003), b) B-DNA (NDB ID: BDJ019) and Z-DNA (NDB ID: ZD0016)

Although, A-and B-DNA posses right-handed helical structure, they differ in geometry and dimensions. A-DNA contains 11 base pairs per helix, with C3'-endo conformation for the sugar unit, while the B-DNA enclosed 10.4 base pair per helix turn with 3.45 Å distance between the stacked bases and C2'-endo conformation for the sugar unit. Z-DNA shows a left-handed conformation, with 12 base pairs per helix. In addition, diverse structural DNA conformations such as G-quadruplex, *i*-motif and triplex DNA are well known (Figure 1.4).

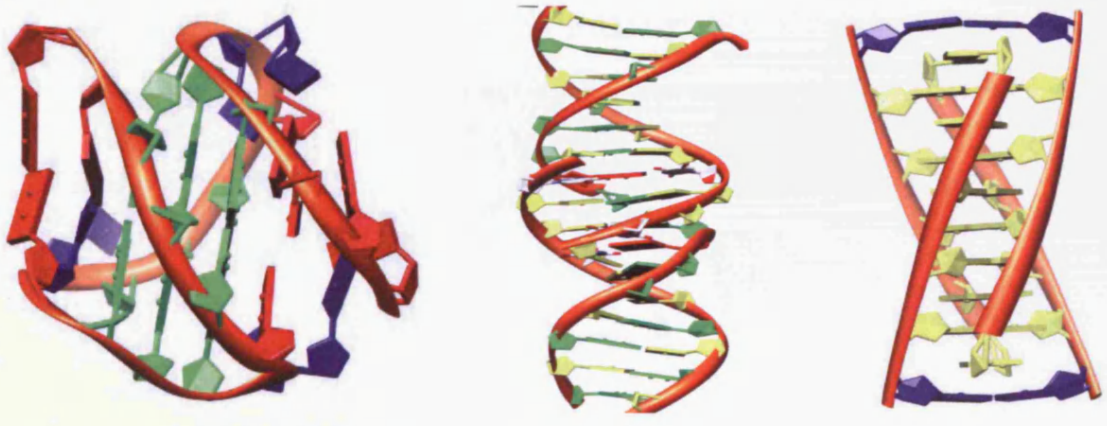

Figure 1.4 Other DNA conformations: a) G-quadruplex DNA (PDB: ID 2HY9); b) triplex DNA (NDB ID: BD0017) and c) *i*-motif (NDB ID: BD0017).

G-quadruplexe nucleic acid structures are formed by certain sequences which are predominant in G•C base pairs. The four-stranded quadruplex structures are stabilised by hydrogen bonding and further by metal ions in the center of the helix.[12] In another example of the wealth of nucleic acid structures, oligonucleotides bind in the major groove of B-DNA forming triplex DNA structures.[13] The *i*-DNA motif is also a four stranded arrangement formed as a result of intercalation of two parallel duplexes with opposite polarities by CC^+ base pairs.[14]

There are various physical forces that stabilise the formation of the DNA double helix, *viz.* hydrogen bonding between the bases on both DNA strands; hydrophobic interactions between the aromatic rings in adjacent stacked base pairs; metal cations surrounding the negatively charged phosphates shielding electrostatic repulsions; and hydration along the minor and major grooves of DNA *(vide infra)*.

1.3 B-DNA grooves

As a consequence of the geometry of the base pairs and the double-helical structure of the two strands, DNA has two grooves that are not equal in size (Figure 1.5).

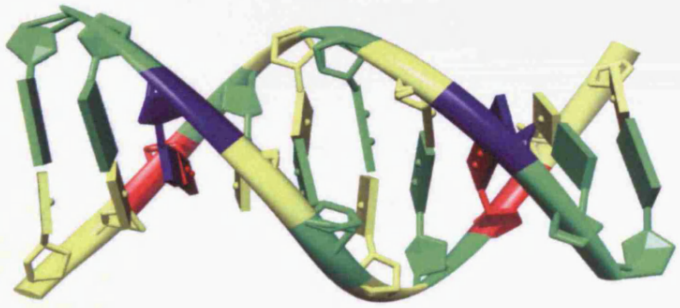

Figure 1.5 Major and minor grooves of DNA (NBD ID: BD0036)

The narrow groove with an average width of 11 Å is known as the minor groove. The second groove is 22 Å in average width and is known as the major groove.[15] The grooves are defined by upper and lower edges of each base pair which form the "floors" of the grooves and by the sugar-phosphate backbone of the DNA which form the "walls". As a consequence, the grooves have clearly different stereochemical environments (Figure 1.6).

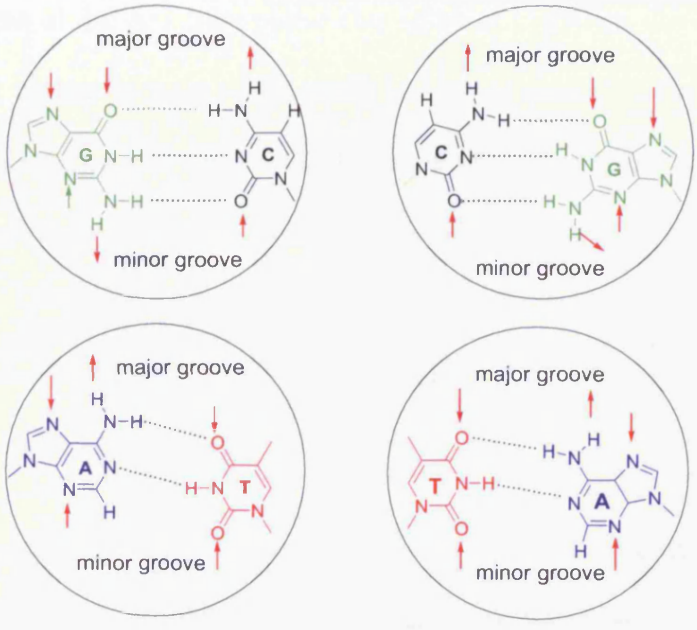

Figure 1.6 H-bond donor and acceptor characteristic for all base pairs in the minor and major groove of DNA

In the major groove of DNA, there is a pattern of H-bond donors and acceptors along with groups that can partake in steric interactions that is unique for different base pairs. For example, the edge of the A•T base pair at the floor of the major groove presents two hydrogen bond acceptors (H_A), one donor (H_D) and a methyl group on the thymine base which permits discrimination between the bases. C•G base pairs also show two hydrogen bond acceptors and one hydrogen bond donor but in a different pattern to the A•T base pair.

In the minor groove, however, each base pair shows symmetric hydrogen bond patterns. Apart from differences in hydrogen bonding and steric factors, several studies indicate different characteristics of water molecules in both grooves. For example, in the minor groove of stretches of A•T base pairs, water molecules in crystal structures suggest an ordered structure forming a zig-zag "spine of hydration".[16] In this fashion, water molecules H-bond to the N3 and O2 atoms of the A•T base pairs. This spine of hydration does not appear to exist for G•C base pairs, maybe because of the steric hindrance caused of the N2 hydrogen-bond donors in the G•C sequence and intermolecular packing constraint. In contrast, in the major groove, most of the water molecules are disordered and there is no recognisable hydration pattern.

1.4 Small molecules DNA interactions

DNA possesses a rich structure and small organic molecules can bind covalently or non-covalently to DNA in many different ways. The formation of covalent DNA-ligand complexes is an irreversible process whereas the non-covalent binding to ds-DNA is typically a reversible process.

One of the most studied covalent complexes is that formed with cisplatin that is known to lead to cell death when it binds to DNA.[17-19] Cisplatin covalently attaches to the nitrogen on the DNA bases, bending or kinking the DNA structure. It was found that chromosomal proteins recognise the bent cisplatin-DNA complex compromising the DNA repairing process, as well as replication and transcription.[20-22] In some cases, the cytotoxity of cisplatin decreases when repair DNA mechanism is active.[23]

DNA also provides various modes for ligands to bind reversibly to DNA. The modes include electrostatic interactions, groove binding or intercalation between the base pairs. It is very important to determine the type of binding mode because small molecules influence DNA repair, transfection or transcription mechanisms and its resulting efficiency. Which binding mode is preferable depends on the DNA sequence and the structural features (e.g. shape, size and polarity) of the bound ligand. Usually, small molecules bind to DNA by either of two main binding modes: intercalation and minor groove-binding. Representative groove-binders and intercalators are shown in Figure 1.7.

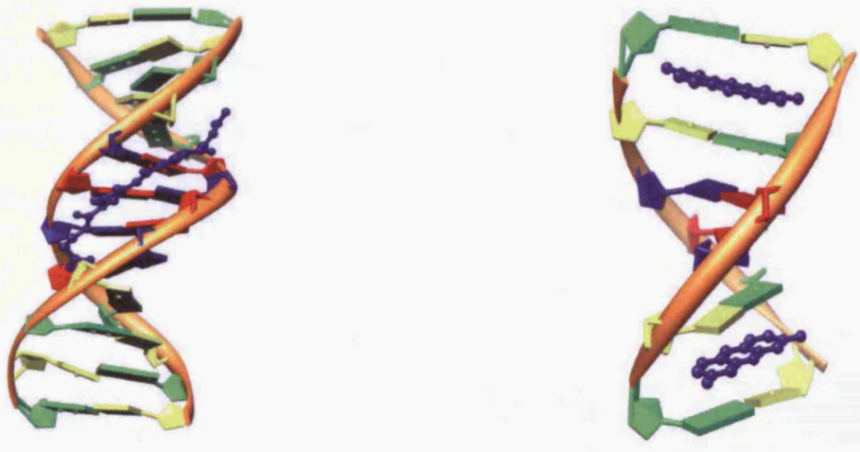

Figure 1.7 The minor groove and intercalation binding modes. Netropsin binding to DNA (NDB ID: GDLB05) (left). Proflavine binding to DNA (NDB ID: DD0103) (right).

1.4.1. Electrostatic interactions

DNA is a polyelectrolyte with high charge density due to phosphate groups which are negatively charged. As a consequence, cationic organic molecules bind to the phosphate backbone by electrostatic interactions. Electrostatic interactions are influenced by charge,

hydrophobicity and size of the ligand. Simple cations such as Na^+ or Ca^{2+} neutralise negative charges on the DNA,[24, 25] therefore, the binding of small molecules to DNA is affected by the ionic strength of the medium. High ionic strength destroys the balance between counter-ions and negatively charged phosphate groups, decreasing the binding affinity of organic molecules to DNA. However, contributions from cationic charges play an important role in solubilisation in aqueous solution. Hence, the electrostatic component is also used to design DNA grooves binders and intercalators *(vide infra)*.

1.4.2. Intercalators

The intercalation concept was introduced by Lerman in 1961 in his studies on the interaction of acridines with DNA.[26, 27] Classic examples of intercalators include proflavine, ethidium bromide, acridine orange, phenanthridinium, actinomycin, daunomycin (Scheme 1.1).

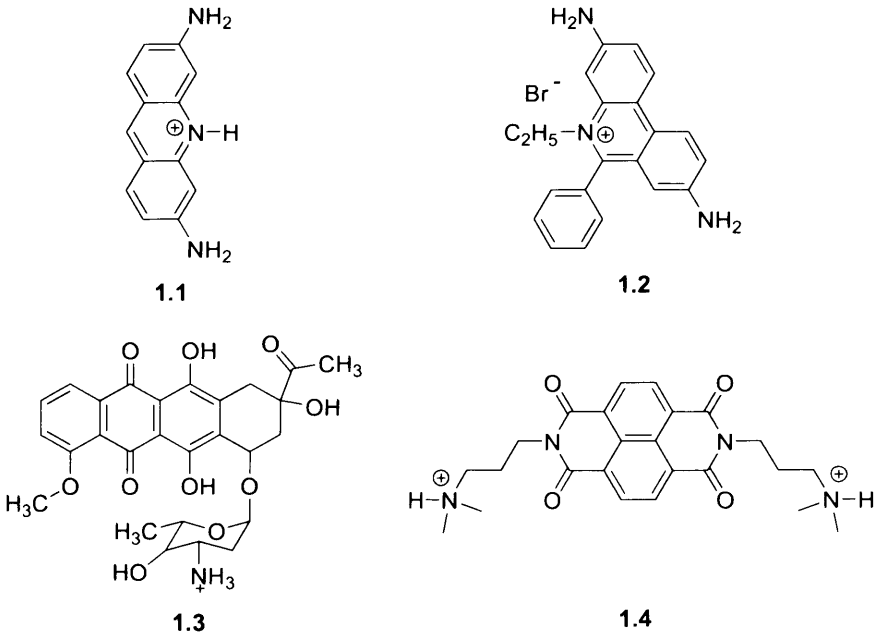

Scheme 1.1

Intercalators are usually planar, aromatic systems that bind to DNA by insertion between base pairs. Intercalation, which is typically enthalpically driven, causes significant changes of the nucleic acid structure – lengthening and geometrically distorting the DNA helix.[28]

The conformation of neighboring binding sites also changes during the intercalation process. As a result intercalation blocks the accommodation of a second intercalator between base pairs adjacent to a bound intercalator.[29] This is called the "neighbor exclusion principle".[30]

The main driving forces behind intercalation are π-π stacking interactions and Van der Waals dispersion interactions between the planar aromatic molecule and the base pairs of DNA.[31, 32]

Intercalators are often characterised by low affinity for DNA, but an increase is observed if the intercalators bear a positive charge *(vide infra)*. Many organic intercalators have been used in antitumor chemotherapy,[33] DNA cleavage,[34, 35] fluorescent DNA intercalators[36, 37] and various other purposes.[38] Daunomycin is the most studied intercalator due to its use as an anticancer drug. The drug preferentially recognises G•C rich DNA sequences that also contain A•T base pairs.[28, 39, 40] X-ray studies on interactions of daunomycin with d(CGTACG) showed that the fused aromatic ring intercalates between the C and N of the 5'-GCN-3' sequence while the amino sugar group, surprisingly, binds to an A•T base pair outside the intercalation site (Figure 1.8).

Figure 1.8 X - ray structure of daunomycin bound to d(CGTACG). The structure was obtained from the Nucleic Acids Database (NDB DDF018) and rendered using Chimera.

Another interesting example of intercalators is provided by naphthalene diimide **1.4** which binds to DNA by a threading intercalation mode with the aromatic system inserted between the base pairs while one cationic substituent binds in the major groove and the other one in the minor grove.[41] Unfused polyaromatic systems can also stack between the base pairs when they bind to DNA (Scheme 1.2).[42, 43]

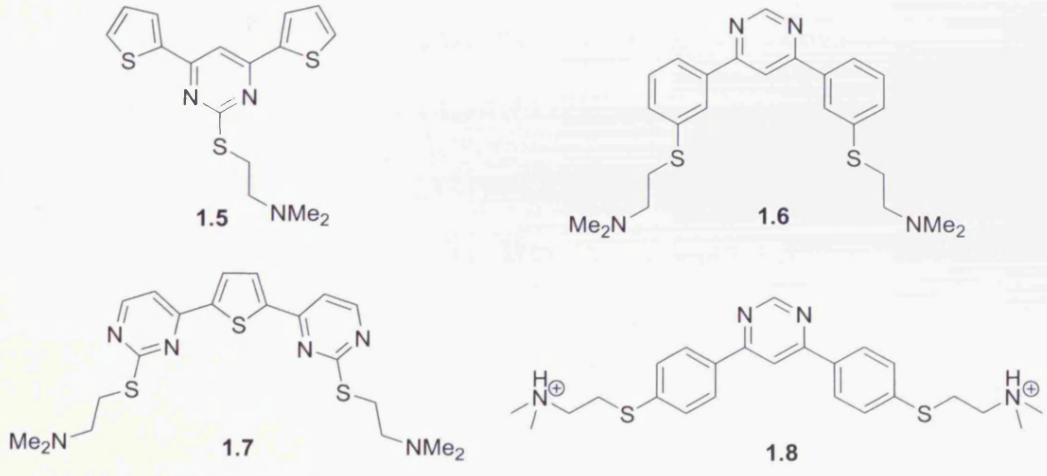

Scheme 1.2

Recent studies by Chaires and coworkers showed that dicationic biarylpyrimidine **1.8** (Scheme 1.2) binds selectively to poly(dA)•poly(rU) through intercalation with a binding stoichiometry of 10 base pairs.[44] The ligand also showed preference for triplex and quadruplex nucleic acids.

Interestingly, chromophore systems consisting one or two phenothiazine rings (Scheme 1.3) have been found to act as DNA photocleaving agents after binding by intercalation.[45]

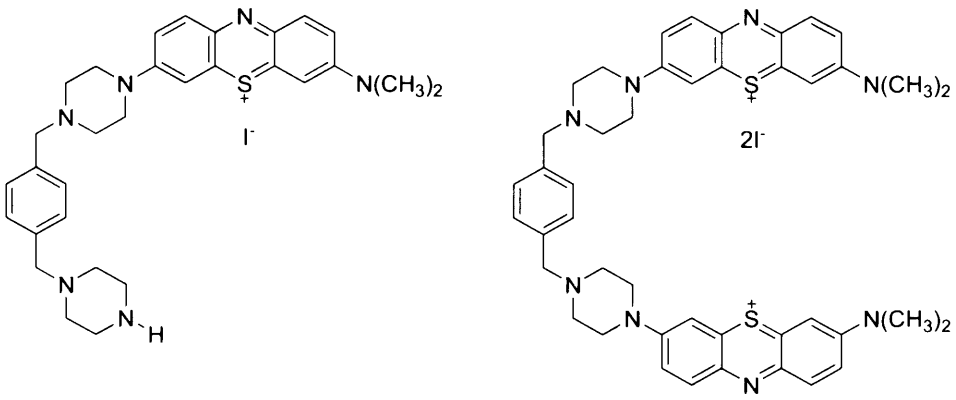

1.9 **1.10**

Scheme 1.3

When bound to calf thymus DNA, phenothiazines stabilise the duplex and monointercalate between the base pairs. Phenothiazines **1.9-1.10** exhibit strong UV-visible absorption between 600-800 nm, and as a consequence can be used for photodynamic cancer therapy.

Only a few examples of neutral polar dyes that interact with duplex DNA through intercalation have been reporteted.[46] In this respect, Dupont and coworkers[30, 47] claimed the first examples of highly polar dyes based on 2,1,3-benzothiadiazoles (Scheme 1.4) which were found to be excellent candidates for optical ds-DNA detection.

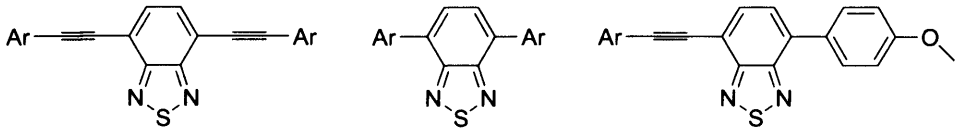

1.11 **1.12** **1.13**

Scheme 1.4

Some of these molecules possess a triple bond C-C spacer between the aromatic rings in order to facilitate the correct geometry and electronic properties required for acting as an intercalating agent for DNA duplex.

1.4.3. Groove binders

Groove binding modes can involve either the minor or major groove. Most of the proteins that interact with DNA bind in the major groove allowing sequence-specific recognition. As a result, binding of other ligands in the major groove can be directly competitive with biologically relevant interactions. Alternatively, smaller molecules can bind in the minor groove which is generally unoccupied and, therefore, more available for co-ordination.[48] Most of the minor groove binders posses several structural features which underlay selectivity in their coordination with ds-DNA. First, small molecules need adequate curvature that matches the curvature of the minor groove of B-DNA. Moreover, the interior walls of the minor groove are hydrophobic and, therefore, the minor groove is preferred by drugs with a hydrophobic framework. Almost all minor groove binders carry positive charges and, as a result, electrostatic interactions with the negative phosphate ions of the DNA backbone are considered to be important driving forces for the interactions. Additionally, typical minor groove binders form hydrogen bonds with the DNA bases. All these forces contribute to the

formation of stable ligand-DNA complexes in the minor groove. Finally, molecular dynamic simulation studies showed that binding by minor groove binders have important consequences for the hydration of the minor groove of DNA. When binding occurs in the minor groove, the water molecules involved in the "spine of hydration" *(vide supra)* are replaced by binders.[49] The minor groove binding mode was first proposed in 1974 for netropsin by Wartell *et al.*[50] The binding selectivity of netropsin for A•T-rich DNA was attributed to "shape selective recognition" and to hydrogen bond formation between the base pairs and the amide NH groups of the N-methylpyrrole-carboxamides.[51, 52] Whereas binding of netropsin to DNA always occurs in 1:1 fashion along four consecutive A•T base pairs, its analogue distamycin can bind in 1:1 as well as in 2:1 fashion in the minor groove along five base pairs (Figure 1.9).[53, 54]

Figure 1.9 The groove binding modes of netropsin and distamycin with DNA duplexes: a): 1:1 binding of netropsin to the 5'-CGCAATTGCG-3' sequence (NDB ID: GDL B05); (b): 1:1 binding of distamycin to the 5'-CGCAAATTTGCG-3' sequence (NDB ID: GDL 003); (c): side-by-side binding of distamycin to the 5'-GTATATAC-3' sequence (NDB ID: GDH060).

The binding of distamycin to DNA depends strongly on the DNA sequence.[55] Distamycin binds most strongly to sequences of A•T base pairs, but on replacing one of the five A•T base pairs with a G•C base pair, the minor groove can accommodate two molecules of distamycin. Although, the A•T sequence specificity found for netropsin and distamycin was maintained for their analogue lexitropsin **1.14**, surprisingly lexitropsin **1.15** shows some ability to recognise G•C base pairs.[56] For example, the X-ray diffraction data showed that lexitropsin **1.15** was capable to bind side-by-side to 5'-CATGGCCATG sequence in the minor groove.[57]

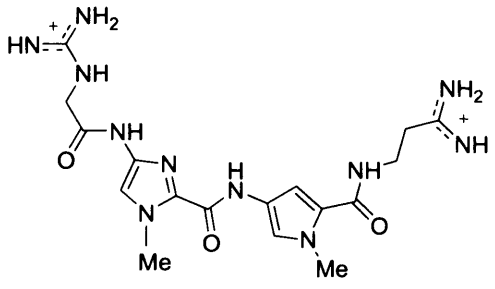

1.14

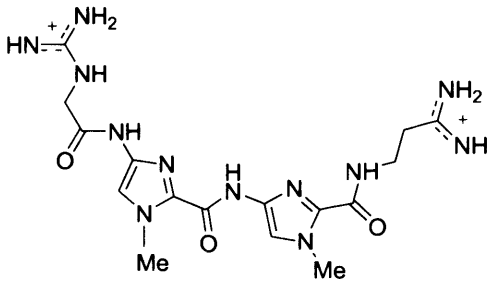

1.15

Scheme 1.5

Recently, Suckling and co-workers developed selective minor groove DNA binders that recognise short DNA sequences and function as selective antibacterial agents.[58] One of the first goals in the work was to modify ligand features by increasing its lipophilicity and maximising hydrophobic interactions within the minor groove of DNA. With this aim, the authors introduced C-alkylthiazole in place of *N*-methylimidazole to provide binding to G•C sites (Scheme 1.6).

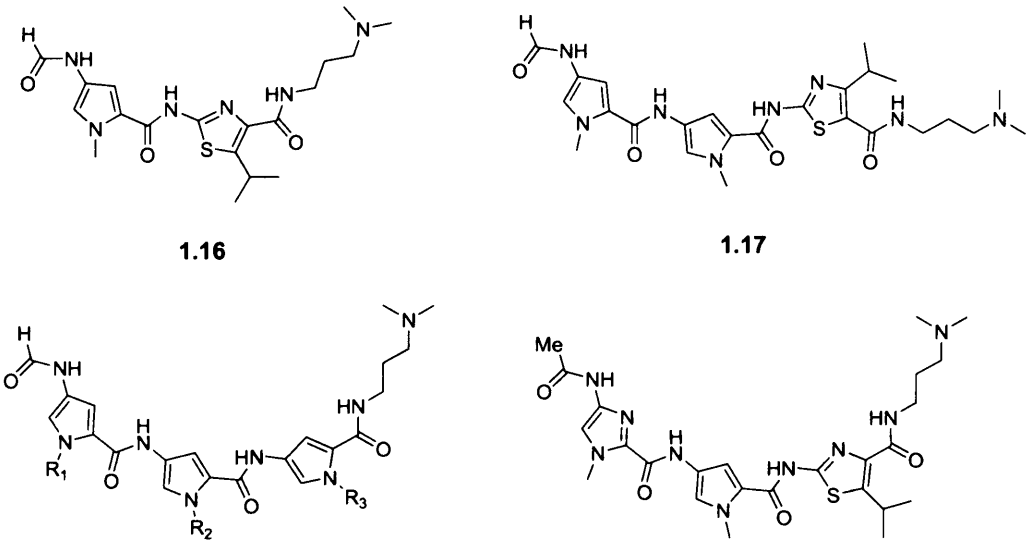

1.16 **1.17**

R_1, R_2, R_3 = Me, *i*-Pr

1.18 **1.19**

Scheme 1.5 Structures of thiazotropsin

Most of the polyamide minor groove binders **1.16-1.19** (Scheme 1.5) contain formyl groups as head group and tertiary aliphatic amines as tail group. As a result, polyamides **1.16-1.19** are protonated under physiological conditions, showing lower antibacterial activity. A first attempt to increase the antibacterial activity of polyamides **1.17-1.19** was to replace the formyl groups with hydrophobic groups containing hydrogen bond atoms or substituents (*e.g.* 3-MeO benzoyl, 3-NO-pyrrolyl, 2,3-di-pyridyl) and to introduce in their structure protonated tertiary aliphatic amines. Unfortunately, even these compounds did not show sufficient biological activity to warrant investigation *in vitro* and a new strategy of replacing the amide group with an alkene led to an increase of the anti-bacterial activity of **1.20** and **1.21** (Scheme 1.6) by an order of magnitude.

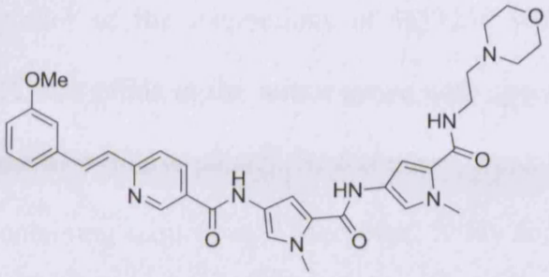

1.20

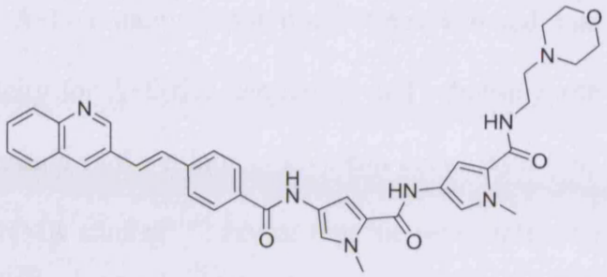

1.21

Scheme 1.6

Another well-known DNA binder, Hoechst 33258 (**1.22**) has shape similarities with netropsin and distamycin, although it contains a π-conjugated oligoheteroaromatic system. H33258 possesses enough rotational flexibility around the bonds connecting the aromatic rings to adopt the optimum shape to fit in the minor groove (Figure 1.10).

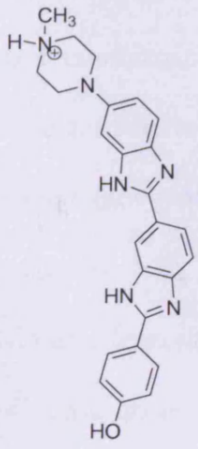

1.22

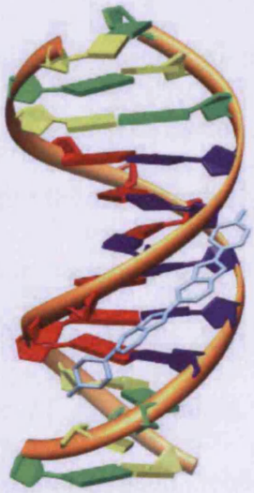

Figure 1.10 Structure of H33258 (left). Complex between H33258 and d(CGCAAATTTGCG)$_2$ (NDB ID: GDL028) (right)

Studies of the interactions of H33258 with A•T-containing polynucleotides showed that H33258 binds in the minor grove with specificity for A•T-rich sequences and a binding site size of 4-5 base pairs.[59] Nevertheless, weak binding in the minor groove can occur with G•C containing sequences.[60] Moreover, X-ray and NMR studies[61-65] reveal that the imidazole ring is orientated towards the floor of the minor groove and each nitrogen atom is capable of forming a bifurcated hydrogen bond with adjacent adenine-N3 or thymine-O2 atoms on the edge of the A•T base pairs. On the basis of these findings, H33258 has emerged as a model for the synthesis of new π-conjugated minor groove binders. For example, minor groove DNA binders containing symmetric bisbenzimidazoles were developed by Neidle and coworkers and these molecules were found to bind in the minor groove of A•T-rich regions of DNA dodecanucleotides.[66, 67] In other examples, *o*-, *m*- and *p*- isomers of bis-2-(pyridyl)-1*H*-benzimidazoles showed different binding affinity to A•T specific DNA which could be attributed to the ligand conformation.[68] The majority of current synthetic minor groove binders bind sequence-selectively to A•T base pairs. The selectivity for A•T is probably due to hydration effects in the minor groove making binding there particularly thermodynamically favourable, while the guanine NH_2 protruding into the minor groove hinders the binding at G•C-rich sequence. Nevertheless, some efforts have been made to develop structures which selectively target G•C base pairs. Prime examples of such binders with selectivity for sequences other than A•T were pioneered by Boykin and Wilson, who designed diamidine structures (Scheme 1.7) selective for ATGA and GCTCG sequences.[69-73]

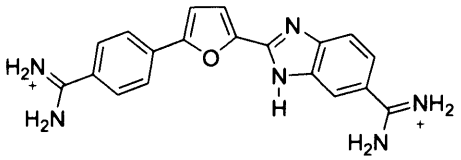

1.23

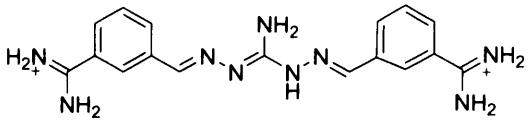

1.24

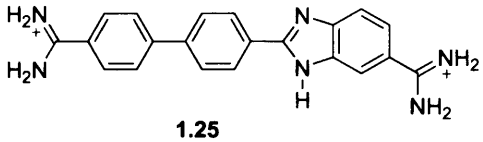

1.25

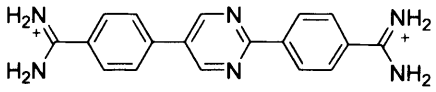

1.26

Scheme 1.7

Furamidine **1.23** in Scheme 1.7 is one of the most discussed minor groove binders since it forms dimers which stack in an antiparallel arrangement in the minor groove and it is capable of recognising G•C-containing sites more strongly than A•T sequences.[72-76] In contrast, when replacing the furan ring by thiophene the resulting compound binds weakly to G•C base pairs, but 30 times more strongly to A•T base pairs.[77, 78]

Inspired by sequence-selective natural compounds netropsin and distamycin, Dervan's hairpin polyamides (DHP) are a class of molecules that provide modular and programmable sequence recognition of double-stranded DNA.[79, 80] DHPs consist of amide-coupled heterocycles based on *N*-methylimidazole (Im), *N*-methylpyrrole (Py) and *N*-methyl-3-hydroxypyrrole (Hp) that bind in a side-by-side manner in the minor groove in addition to forming 1:1 complexes with A•T base pairs. The 2:1 binding mode for this class of molecules was initially demonstrated for 1-methylimidazole-2-carboxamide netropsin (2-Im-N) which specifically bind to 5'-TGAT (Figure 1.11).[81]

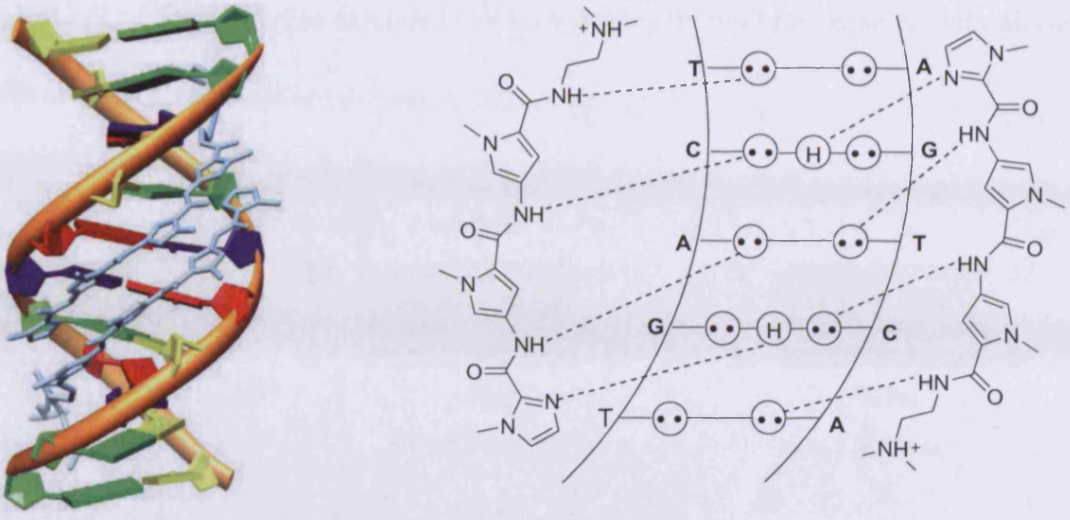

Figure 1.11 X-Ray structure (left) and hydrogen bonds view of side-by-side dimer of 2-Im-N bound to d(TGACT) (NDB ID: BDD003).

The effect of the inclusion of a pyridine ring on the recognition of base pairs in the minor groove was demonstrated by analogues of (2-Im-N) with pyridine replacing the 1-methylimidazole. These compounds were found to have affinity for both A•T- and G•C-containing sequences.[82] Also, *N*-methylimidazole paired opposite *N*-methylpyrrole recognises the G•C sequences, while the reverse pair targets C•G sequences.[82] Surprisingly, the pyrrole/pyrrole pairing shows similar strength binding for both A•T and T•A base pairs in the minor groove. However, if one of the pyrrole rings is replaced by *N*-methyl-3-hydroxypyrrole, then this new pair and its reverse will target T•A or A•T sequences selectively.[83] Attempts to get DHPs to recognise sequences longer than five base pairs fail. The reason for this is that the polyamide curvature no longer matches the curvature of the minor groove of DNA.[84] To avoid this problem, Dervan and coworkers developed polyamides linked head-to-

head or turn-to-tail which recognise extended DNA sequences without losing selectivity along 10 base pairs (Figure 1.12).[85, 86]

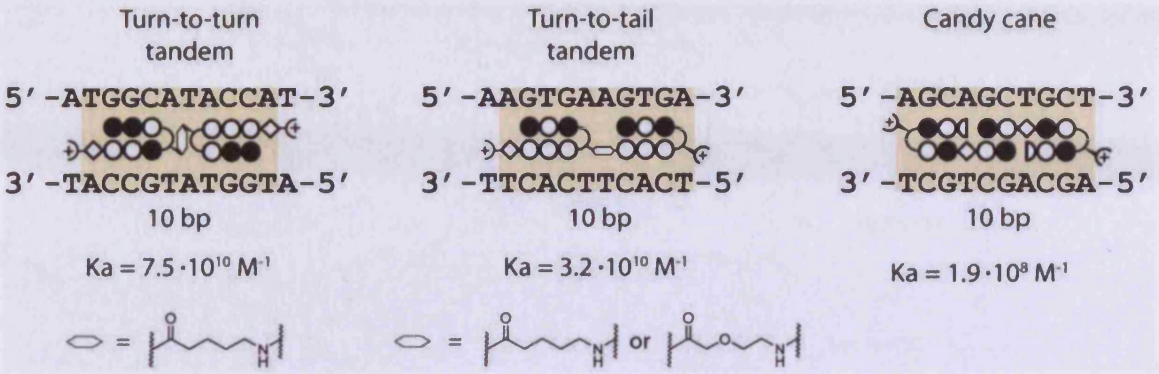

Figure 1.12 Cartoon representations of polyamide models for binding to extended DNA sequences. Picture taken from reference 79.

Dervan's group also developed an eight ring hairpin polyamide[87] by covalently connecting two antiparallel polyamide strands using a γ-aminobutyric acid linker. The hairpin possesses a crescent-shape comparable to the curvature of the minor groove. The steric hindrance in the minor groove induced by the presence of $-NH_2$ group is tolerated by the imidazole ring because it can hydrogen bond with it, offering specificity for G•C base pairs (Figure 1.13). Additionally, the linker has been found to target A·T sequence instead of G•C, possible for steric reasons.

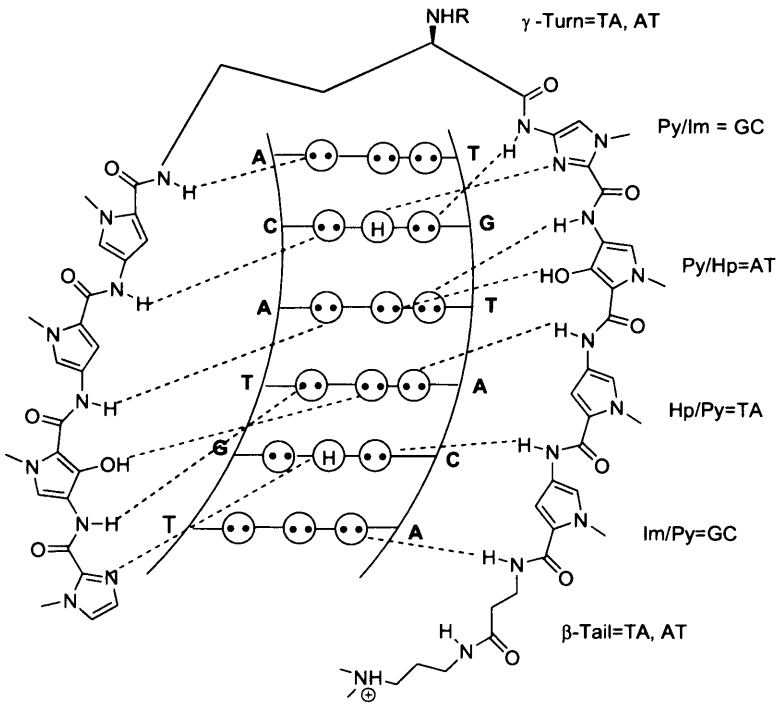

Figure 1.13 Hydrogen bonding model for hairpin polyamide interacting with $d(TGTACA)_2$.

1.5 Conjugated polymers for biosensing

Conducting polymers have received much attention since Alan Heeger, Alan G. MacDiarmid and Hideki Shirakawa were awarded the Nobel Prize in Chemistry in 2000 for their discovery of conducting polyacetylene.[88] Conducting polymers feature π–delocalisation along the main chain, a low band gap and interesting electrical and optical properties.[89] A combination of all these properties leads them to be used as organic semiconductors for electronic devices such as field-effect transistors (FET),[90, 91] organic light-emitting diodes (OLEDs),[92, 93] flexible displays and organic photovoltaics.[94] Due to their rigid structure and interchain forces, conducting polymers are insoluble in many organic solvents, infusible and very difficult to

process. Different long side chains are introduced onto the polymer backbone to avoid these difficulties. For example, cationic or anionic charged side chains present on the conjugated framework make the polymer soluble in aqueous solution. As a result, cationic polythiophenes[4, 95-98] and polypyrroles[99] are known to interact with bio(macro)molecules. The electronic structure of conducting polymers is sensitive to changes in the polymeric chain environment and other perturbations in the chain conformation caused by DNA hybridisation. Additionally, optical and electrical properties of the conducting polymers can be modified on its interaction with a target bio(macro)molecule *(vide infra)*. These favourable electronic and spectroscopic properties render conjugated polymers promising components for biosensors applications.[4, 98, 100] Unfortunately, in the literature there are no studies which identify the binding location and the nature of the interaction of the polythiophenes with nucleobases. The binding to both single stranded DNA and duplex DNA are sufficiently strong that they are difficult to quantify. Even the stoichiometry of interaction has yet to be defined. Moreover, the interaction of short oligomeric materials, like cationic terthiophenes, with DNA has received very little attention to date. A variety of experimental approaches have been used to probe DNA hybridization. We focus in this section on optical and electrochemical detection but other approaches are available. All these methods have in common that sequence selectivity is the result of the selectivity of ssDNA for its complementary sequence and not of selectivity of the conjugated polymer for particular sequences.

1.5.1. Optical detection

The use of oligo- and polythiophenes as fluorescent probes for studies of biological events was reviewed recently by Åslund *et al.*[3] Some of these structures are shown in Scheme 1.8.

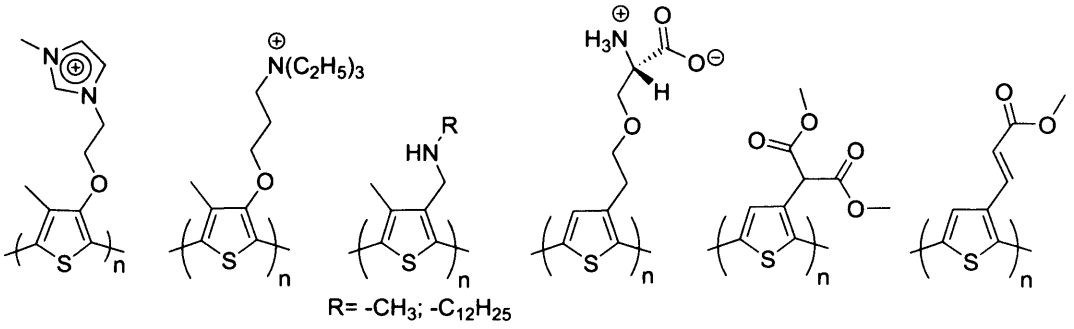

1.27 **1.28** **1.29** **1.30** **1.31** **1.32**

Scheme 1.8

The concept of using a cationic polythiophene for the optical detection of the hybridisation of DNA was first introduced by Leclerc and coworkers (Figure 1.14).[97, 98] As a result of the free rotation of the thiophene rings, these polythiophenes adopt a random coil conformation when they are free in aqueous solution. Addition of single-stranded DNA produces a significant red-shift of the polythiophenes in the UV-visible spectrum, which is attributed to "planarising" of the cationic polythiophene and π-stacking between the ssDNA-cationic polythiophene complexes.[4,101] Addition of the complementary single-stranded target sequence results in the formation of the complex of duplex DNA with the cationic polythiophene and a concomitant blue-shift in the UV-visible absorption spectrum, though the resulting spectrum is still red-shifted compared to the free cationic polythiophene. Because of the region in which the spectroscopic changes take place in combination with the extent of the shift in λ_{max}, the

optical changes can be observed as colour changes by the naked eye. In practice, an aqueous solution of cationic polythiophene changes colour from yellow to red upon addition of the single-stranded probe sequences and back to yellow when the complementary single stranded target DNA was added. Additionally, an induced CD signal characteristic of a right-handed twisted helical polythiophene-structure appears upon interaction with duplex DNA[1] suggesting that the polythiophene binds in either the major or minor groove.

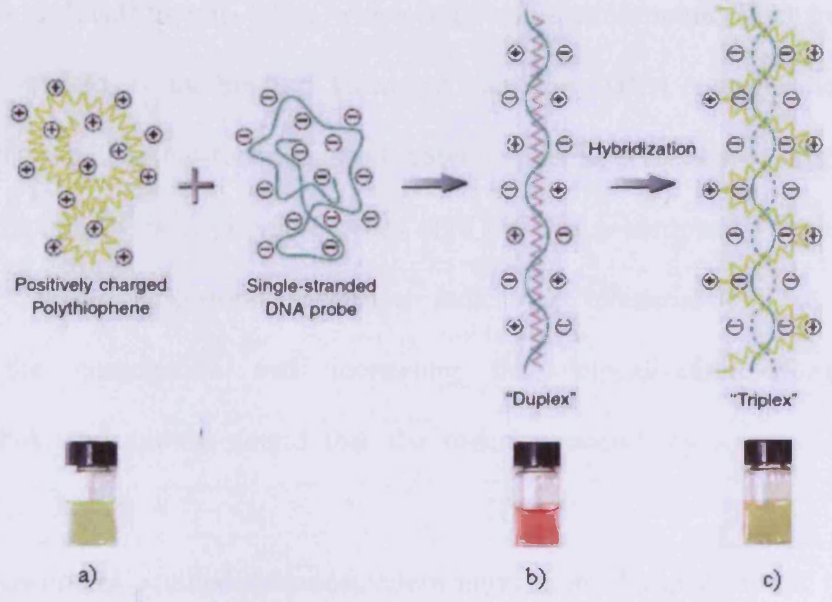

Figure 1.14 Optical detection of dsDNA. Reproduced from reference 98.

Fluorometric detection of oligonucleotide hybridisation can also be achieved since poly(3-alkoxy-4-methylthiophene) **1.27** (Scheme 1.8) shows florescence quenching in its aggregated form.[97, 102] Upon heating an aqueous solution of poly(3-alkoxy-4-methylthiophene)s to 55 °C, the polymer showed fluorescence corresponding to its uncomplexed form, while a decrease of the fluorescence intensity and a blue shift of the maximum emission could be observed when

1 equivalent of the ss-oligonucleotide probe was added. A dramatic increase in the fluorescence intensity was observed upon addition of the complementary ssDNA.

Related systems for the detection of dsDNA were reported by Ewbank *et al.* [96] The authors designed amine-functionalised polythiophenes **1.29** (Scheme 1.8) in order to non-specifically interact with ds-DNA and to detect conformational changes in the DNA structure upon interaction. No circular dichroism signal was observed for the interaction of polythiophenes with calf thymus DNA, which suggests no conformational changes occur with the polythiophenes due to the binding. However, increasing DNA concentration led to a CD signal indicating that amine-functionalised polythiophenes get chirally ordered by DNA. Also, the interaction of these polythiophenes with DNA is accompanied by a bathochromic shift in the UV-Vis absorption spectrum, indicating "planarisation" of the polymer, maximising the conjugation and increasing the delocalisation along the chain. Using AT DNA, the authors found that the ordering occurs by a right handed helical conformation.

Inganas and coworkers[4] studied the noncovalent interaction of a zwitterionic polythiophene-derivative, poly(3-[(S)-5-amino-5-carboxyl-3-oxapentyl]-2,5-thiophenylene hydrochloride (POWT) **1.30** (Scheme 1.8) with DNA. The interaction of single-stranded DNA with POWT again induces a planar conformation of the polymer chains and aggregation (Figure 1.15). The authors explained this phenomenon by electrostatic interactions between negatively charged phosphate groups of ssDNA with the positive amino groups on the polymer chain. On the other hand, the interactions with complementary oligonucleotides added to the complex lead to separation of the polymer chains and a less planar backbone.

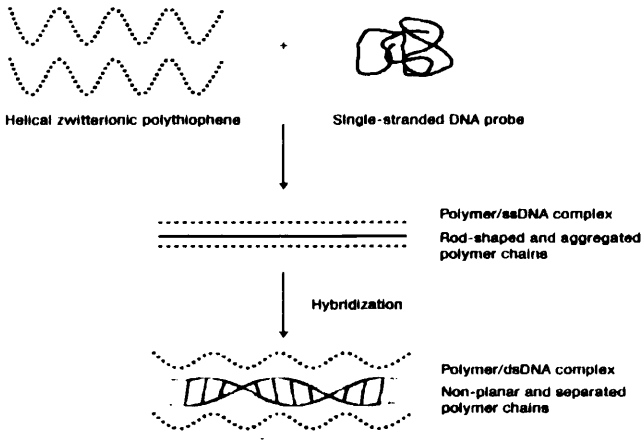

Figure 1.15 Formation of polythiophene/DNA complexes. Geometrical changes of the polythiophene on addition of ssDNA and dsDNA. Picture taken from reference 4.

More recently, Alemán and coworkers[103] reported the interaction of poly(3-thiophene-3-yl-acrylic acid methyl ester) **1.31** and poly(2-thiophene-3-yl-malonic acid dimethyl ester) **1.32** (Scheme 1.8) with plasmid DNA. Two restriction enzymes (*e.g.* EcoRI and BamHI) were added to the polymer-DNA mixture in order to cut the DNA at specific nucleotide sequences 5'-G/AATTC-3' (EcoRI) respective 5'-G/GATCC-3'(BamHI). As a result, the interaction between the polymer and DNA occur specifically at the restriction sites. The authors showed using UV-visible spectroscopy there were differences in the interaction patterns of polymers with plasmid DNA. These differences are caused by different features of various polymers (*i.e.* one polar side group compared to two polar side groups in the structure of **1.32**) and by the different abilities of the polymers to act as hydrogen bonding acceptors. In addition, circular dichroism studies showed that the interaction of the polythiophenes **1.31** and **1.32** (Scheme 1.8) with plasmid produces ellipticity changes and alteration of the secondary structure of the DNA. Finally, these results enhanced that an unfolding of the

double helix is produced during the interaction between the conducting polymers and DNA and this promotes the intercalation of the conducting polymer between the DNA strands (Figure 1.16).

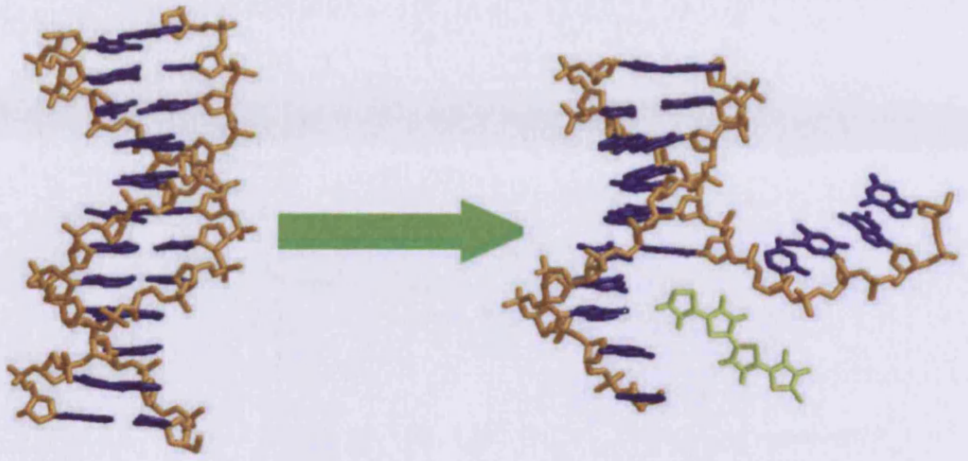

Figure 1.16 Mechanism of interactions of polythiophenes bearing polar groups with double stranded DNA. Picture taken from reference 103.

Most of the biosystems described above suffer from non-specific polymer-biomolecule interactions and this may diminish their sensitivity or selectivity. For this reason, an oligothiophene moiety can be linked covalently to a specific single-stranded oligonucleotide that is complementary to the target sequence. Barbarella *et al.* reported oligothiophene isocyanates that are capable covalently binding to bovine serum albumin and DNA and subsequently showed that binding of these isocyanates to biomolecules does not lead to fluorescence quenching.[2]

In another example, a fluorescent oligothiophene *N*-succinimidyl ester was covalently linked to proteins and to 3'-amino-modified oligonucleotides. These constructs were used as markers for detection and quantification of biopolymers in clinical diagnosis.[104] These biosystems

have higher fluorescence intensities compared to their analogues based on fluorescein and did not show photobleaching after continuous irradiation. Additionally, deoxyuridines labeled with oligothiophenes at the 5-position (Figure 1.17) showed changes in the emission intensity upon hybridization.[105]

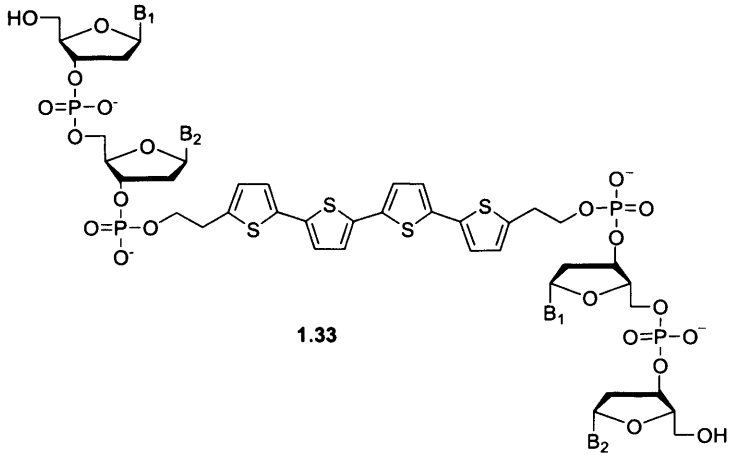

B_1B_2 =TT, AA, TA

Figure 1.17 Molecular structure of oligothiophene-labeled oligonucleotides

Bäuerle *et al.*[106] described the synthesis of thymine-2'-desoxyadenosine functionalised oligothiophenes via a "click reaction" using the Cu(I)-catalysed Huisgen 1,3-dipolar cycloaddition (Figure 1.18). These structures allow selective detection of the hybridisation with complementary nucleosides via intermolecular forces leading to self aggregated superstructures in both solution and in the solid state.

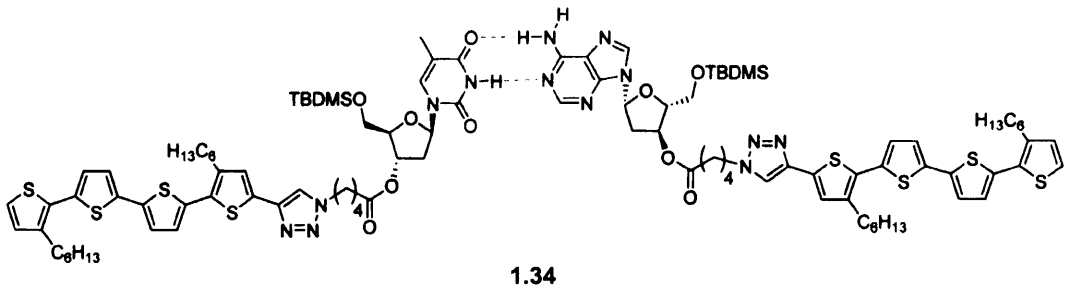

1.34

Figure 1.18 Oligothiophene-nucleoside conjugates for recognition of A-T base pairs

1.5.2. Electrochemical detection

Beside fluorescence detection, electrochemical detection is another popular method used to study DNA sequences. Apart from its simplicity, low instrumentation costs and high sensitivity, the method offers the best potential for miniaturization.[107, 108]

Promising recent advances in electrochemical detection of DNA include hybridisation detection of single-stranded DNA on surfaces using cyclic voltammetry or electrochemical impedance spectroscopy.[109-112]

The first attempts to electrochemically detect the DNA hybridisation were reported by Garnier and co-workers,[113] who covalently attached a ssDNA probe to a polypyrrole backbone. A decrease in current and a shift to more positive oxidation potential could be observed in the cyclic voltammogram for the polypyrrole-oligonucleotide construct upon hybridisation. Such modifications in electronic properties of polypyrrole were attributed to the changes in the polymer conformation that occur upon duplex formation resulting from binding of the target strand to the polymer-oligonucleotide conjugate. Following this method a variety of functionalised polythiophenes have been synthesised and used to

electrochemically detect DNA hybridisation.[114] For example, Lee *et al.* reported terthiophene **1.35** carrying a carboxyl group which can be easily electropolymerised on a glass carbon electrode (Scheme 1.9).[115]

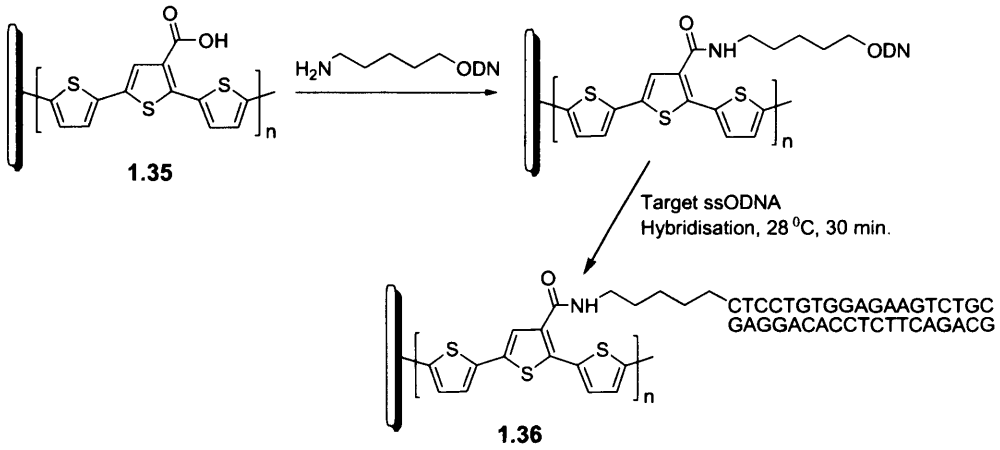

Scheme 1.9

Oligonucleotide-functionalised polythiophene **1.36** showed good specificity to complementary ds-DNA and is able to transduce this recognition into molecular signal that is sent to the supporting electrode through the conducting polythiophene chain. Surprisingly, the biosensor in Scheme 1.9 functions without using active labels such as ferrocene. Using impedance spectroscopy the authors observed a decrease of the impedance after hybridisation with the complementary DNA sequence, suggesting that double stranded DNA is more conductive than single stranded DNA. No differences in the impedance were observed for non-complementary target DNA.

Other examples use peptide nucleic acids instead of DNA for immobilisation on the electrode surface.[116-118] This is considered to be an advantage because PNA show higher thermal

stability than DNA. The thermal stability of nucleic acids is usually affected by the presence of imperfect matches.[119] Leclerc and coworkers[120] designed a ferrocene-functionalised cationic polythiophene **1.37** which was applied as the sensing element for label-free detection of DNA. The scheme for electrochemical detection of target DNA is present in Figure 1.19.

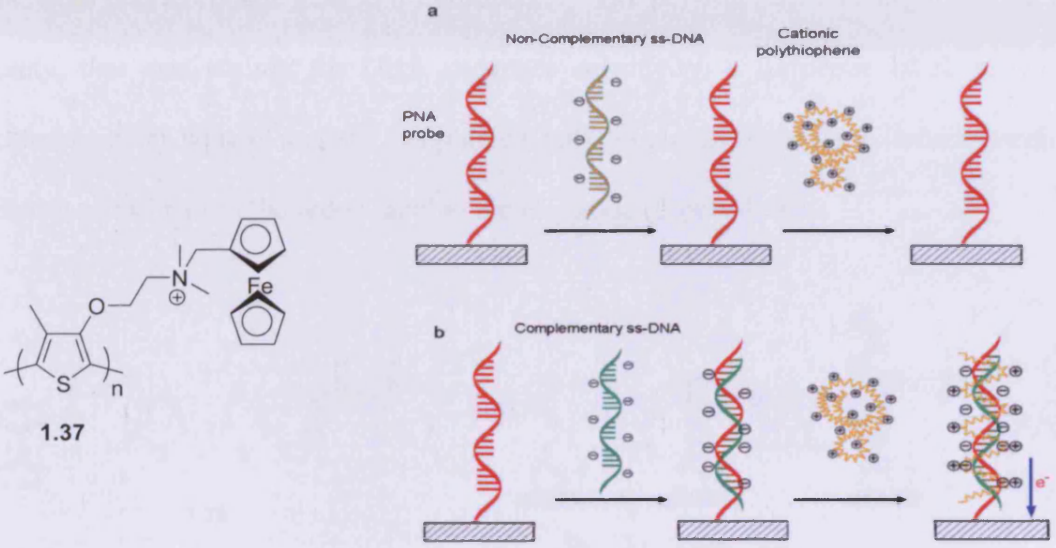

Figure 1.19 Schematic description of non formation of polythiophene/PNA conjugate (a) and formation of polythiophene/hybridised nucleic acid triplex (b).[120]

A cysteine linker was used in order to covalently immobilize a peptide nucleic acid (PNA) sequence (5'-TTGAACCATCCACCA-3') on the gold electrode. The cationic water-soluble polythiophene **1.37** does not bind to neutral PNA (Scheme 1.20a). However, after hybridisation with the complementary negatively charged DNA sequence, the resulting duplex interacted with the cationic polythiophene through electrostatic interactions. This led to electron transfer between the redox-active ferrocene units and the gold electrode that could be measured using square wave voltammetry.

A well-defined peak characteristic for oxidation of the ferrocenyl group was observed at 585 mV upon hybridisation. This method showed a limit of detection of 0.5 nM, but this could be improved to 0.01 nM using a nanogold-modified electrode.[121] In another example, Zhang *et al.* developed a sequence-specific electrochemical DNA sensor which uses a cationic multi-functional polythiophene **1.38** as a transducer.[122] The polythiophene incorporates: an acridine moiety, that acts mainly for DNA sequence selectivity; a ferrocene label, providing the electrochemical signal; and the conjugated polythiophene framework, which mediates the electron transfer from the redox label to the electrode (Figure 1.20).

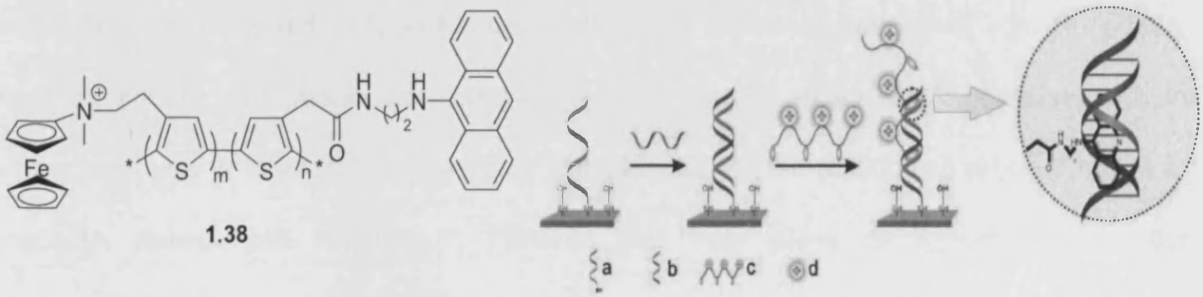

Figure 1.20 The electrochemical detection of dsDNA. The notations are: ssDNA (5'-SH-$(CH_2)_6$-ATGATGTTCGTTGTGTAGGATTTGC-3') immobilised on gold electrode (a); target DNA (5'GCAAATCCTACACA ACGAACATAT-3') (b); cationic polythiophene (c); ferrocene unit attached to the polymer (d).[122]

After hybridisation of PNA with non-complementary single-stranded DNA, the cationic polythiophene interacts with the charged dsDNA backbone, conferring clear hybridisation detection in cyclic and differential pulse voltammetry. The polymer preferable interacts with dsDNA through the acridine intercalator while the contribution of the electrostatic interactions is negligible.

1.5.3 General methods for synthesis of conjugated polymers and oligomers

The development of new applications for (semi)conducting polymers[94] resulted in intensive studies of this class of polymer in the last decade. Advance in the molecular electronic applications of conjugated polymers are closely related to advances in the synthesis of conjugated systems. In general, functional mixed conjugated polymers and oligomers are synthesised using a variety of metal- cross-coupling reactions.[123-125] The Stille cross-coupling reaction involves the coupling of an arylhalide or triflate with an organotin compound. Additionally, the Stille coupling reaction is compatible with a variety of functional groups and is therefore the preferred method for the synthesis of mixed oligomers of, *e.g.,* thiophene, furan and pyrrole. The Suzuki cross-coupling reaction couples an arylhalide or triflate with an arylboronic acid or ester. Basic conditions are required for the reaction to proceed and it is generally, though not exclusively, believed that base plays an import role in the transmetallation step, activating the boron species. Microwave-assisted catalysis offers many advantages over the traditional synthesis by decreasing the undesirable processes that can compete with the cross-coupling reaction giving fewer side-products at the end of the reaction. Moreover, this method reduces the time of the reaction and the products are obtained in a very high yield. Other methods for the synthesis of conjugated polythiophenes employ an oxidative homocoupling reaction in the presence of catalytic amount of $FeCl_3$ in chloroform.[126, 127] This method was preferred for the synthesis of luminescent conjugated polymers used for DNA-hybridisation,[128, 97]or protein folding.[129, 130]

Cross-coupling reactions are usually catalysed by low valent transition metal complexes, mainly of Ni or Pd.[131] For example, Ni(II) is the catalyst for Kumada cross-coupling reactions

while Pd(0) catalyst or its precursors are more efficient in Stille and Suzuki cross-coupling reactions. A variety of Pd catalysts are commercially available, *e.g.* $Pd(PPh_3)_4$, $Pd(OAc)_2$, $PdCl_2(MeCN)_2$, $Pd(dba)_2$ or $Pd(dppf)Cl_2$. The discovery of new Pd catalysts containing N-heterocyclic carbenes (NHC) as ligands has made an enormous impact in the field of Pd mediated cross-coupling reactions.[132, 133] Compared to $Pd(PPh_3)_4$, Pd-NHC precatalysts show enhanced stability and high activity. A particular example that should be mentioned here is the high reactivity and selectivity of the PEPPSI-iPr catalyst due to a bulky ligand (*N*, *N'*-diarylimidazole) present in the catalyst structure. The electronic and steric properties of the ligand are crucial in the formation of the intermediates needed in the catalytic cycle. The general palladium-promoted catalytic cycle proposed for aryl-aryl coupling reactions is presented in Scheme 1.10.

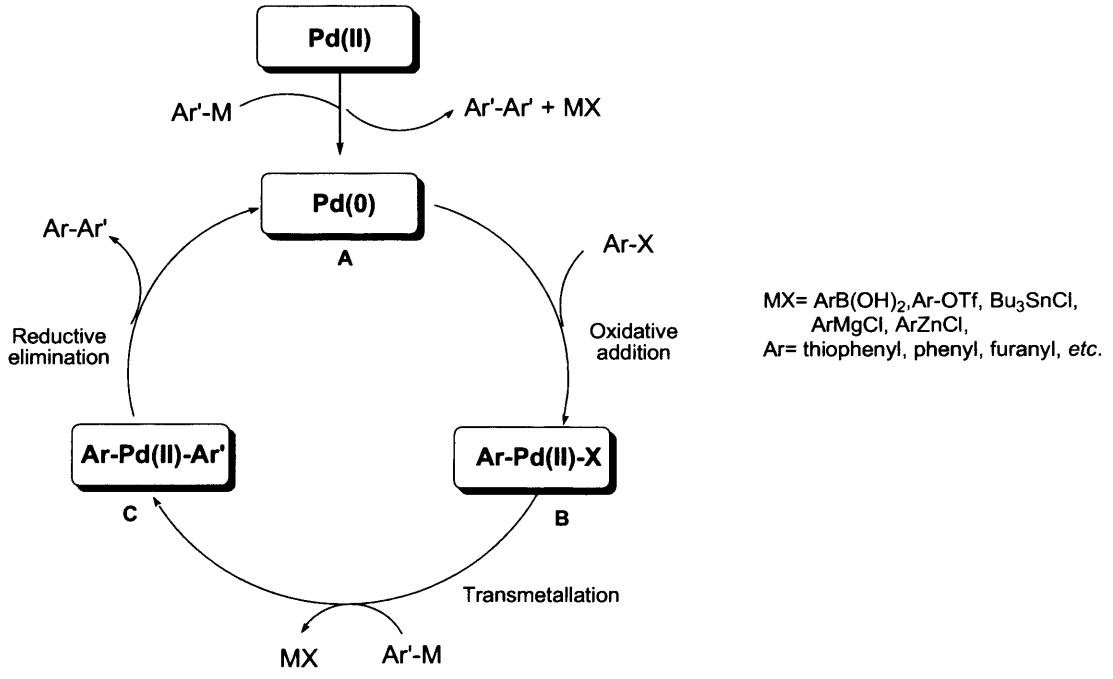

Scheme 1.10 A general catalytic cycle for palladium-cataylsed, cross-coupling reactions

If a pre-catalyst, Pd(II) complex is used, the catalytic cycle includes a supplementary step which involves the reduction of Pd(II) to an active Pd(0) species (A). The first step in the catalytic cycle is the oxidative addition of arylhalide (Ar-X) to the active palladium(0) complex **(A)** to form the *cis* intermediate Ar-Pd(II)-X **(B)** which rapidly isomerises to the *trans* conformation. This step is often the rate-determining step in the catalytic cycle. In the transmetallation step, the organometallic (ArM) attacks the palladium centre forming the Ar-Pd(II)-Ar' intermediate **(C)**. The mechanism for this transmetalation remains unclear. The transmetalation is highly dependent on the reaction conditions and on the organometallic species involved in the reaction and often requires nucleophilic activation of the metal. Finally, reductive elimination produces the desired product Ar-Ar' and regenerates the Pd^0 catalyst, so that the catalytic cycle continues. A main condition for the elimination step to occur is that the intermediate **C** adopts a *cis*-conformation. If the intermediate is in the *trans*-conformation, it must first isomerise to the corresponding *cis*-conformer before reductive elimination can occur. Specific examples of Ar-Ar bond formation will be discussed in Section 4.1.

1.6 Aims of the thesis

The aim of this thesis is to design and develop new cationic conjugated heterocycle-based oligomers which have the potential to be used as building blocks for DNA-binding compounds with exciting spectroscopic and electronic properties. Such compounds could also form the building blocks for genosensors and for self-assembling nanobioelectronics. For genosensors detecting duplex DNA to be selective and for self-assembly of structures

involving DNA to be programmable, we have to address sequence selectivity of these conjugated oligomers for binding DNA. The preferred target for synthetic sequence-selective duplex DNA binders is the minor groove and in this thesis we focused on this binding mode. The overall design is illustrated for oligothiophenes in Scheme 1.11.

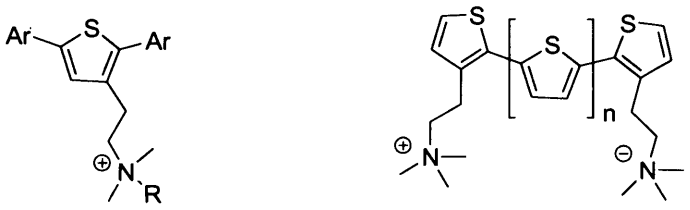

Ar = thiophene, furan, phenyl, pyridine
R= CH_3, CH_2CH_2OH, $CH_2CH_2OCH_2CH_2OH$

Scheme 1.11

Our ligand design involves various coupling heteroaromatics in such a way as to maintain the conjugation along the entire molecule. This will allow significant changes in optical and electronic properties upon interaction with double stranded DNA. We selected oligothiophenes as our first set of DNA binders because the intrinsic curvature of oligothiophenes is similar to the average curvature of the minor groove of DNA, but other cationic oligoheteroaromatics containing mixed heteroaromatics are also of interest. In particular, changing the heteroatoms in the aromatic rings modifies the angle between the rings, changing the curvature of the molecule. As a result, different oligoheteroaromatics should show different binding affinity and different sequence selectivity for the minor groove of DNA. We also introduced a permanent positive charge. The charged is tethered to the "back" of the molecule, directed outward from the minor groove, enabling optimum electrostatic interactions with the negatively-charged backbone of duplex DNA.

Introducing oligoethylene chains on the ammonium group should not only prevent the self-aggregation *(vide infra)* but also the aggregation of ligand-DNA complexes in solution. The reason for using relatively short oligoheteroaromatics is that the effects of the structure variation on binding affinity and selectivity are easily monitored for such systems with intermediate binding affinity, in comparison to the cationic polythiophenes.

This proposed DNA binder design addresses both the optical properties exhibited by cationic polythiophenes and the sequence selectivity introduced by Dervan's polyamides. Additionally, it is noted that this design addresses requirements for genosensors and for conjugated polymers for use in self-assembling bionanoelectronics but not for therapeutic DNA binders. For example, the permanent charge and the presence of thiophenes are likely to lead to poor transmembrane mobility[58] and hepatotoxicity,[134] respectively. Nevertheless, as therapeutic DNA binders and building blocks for genosensors and nanobioelectronic components share a common target, considerable synergy between the fields is anticipated. In order to provide information about these new building blocks to be used as biosensors, it is of vital importance to understand the non-covalent interactions that occur when these molecules bind to dsDNA. A crucial requirement for high performance biosensor device is an efficient control over the aggregation phenomena of the conjugated oligomers in aqueous solution. As a result we have to identify and quantify the aggregation modes that drive the molecules from a disordered state to an aggregation state and to include these studies into DNA binding studies.

References

1. Zambianchi, M.; Barbieri, A.; Ventola, A.; Favaretto, L.; Bettini, C.; Galeotti, M.; Barbarella, G., *Bioconjugate Chem.* **2007,** *18* (3), 1004-1009.
2. Barbarella, G.; Zambianchi, M.; Pudova, O.; Paladini, V.; Ventola, A.; Cipriani, F.; Gigli, G.; Cingolani, R.; Citro, G., *J. Am. Chem. Soc.* **2001,** *123* (47), 11600-11607.
3. Aslund, A.; Nilsson, K. P. R.; Konradsson, P., *J Chem Biol* **2009,** *2* (4), 161-75.
4. Nilsson, K. P. R.; Inganas, O., *Nat. Mater.* **2003,** *2* (6), 419-424.
5. Nilsson, K. P. R.; Hammarstrom, P., *Adv. Mater.* **2008,** *20* (13), 2639-2645.
6. Schillinger, E. K.; Mena-Osteritz, E.; Hentschel, J.; Borner, H. G.; Bauerle, P., *Adv. Mater.* **2009,** *21* (16), 1562-1564.
7. Klok, H. A.; Rosler, A.; Gotz, G.; Mena-Osteritz, E.; Bauerle, P., *Org. Biomol. Chem.* **2004,** *2* (24), 3541-3544.
8. Amsel, S. "Genetics, Cloning, and the Human Genome Project" The Central Dogma of Genetics. Exploring Nature Educational Resource.<http://exploringnature.org/db/detail.php?dbID=106&detID=2454>.
9. Avery, O. T.; MacLeod, C. M.; McCarty, M., *J. Exp. Med.* **1944,** *79* (2), 137-158.
10. Watson, J. D.; Crick, F. H., *Nature* **1974,** *248* (5451), 765.
11. Blackburn, G. M.; Gait, M. J.; Loakes, D.; Williams, D. M., *Nucleic Acids in Chemistry and Biology 3rd Edition Introduction and Overview*. Royal Soc Chemistry: **2006**.
12. Guschlbauer, W.; Chantot, J. F.; Thiele, D., *J. Biomol. Struct. Dyn.* **1990,** *8* (3), 491-511.
13. Gilbert, D. E.; Feigon, J., *Curr. Opin. Struct. Biol.* **1999,** *9* (3), 305-314.
14. Gehring, K.; Leroy, J. L.; Gueron, M., *Nature* **1993,** *363* (6429), 561-565.
15. Wing, R.; Drew, H.; Takano, T.; Broka, C.; Tanaka, S.; Itakura, K.; Dickerson, R. E., *Nature* **1980,** *287* (5784), 755-758.
16. Shui, X. Q.; McFail-Isom, L.; Hu, G. G.; Williams, L. D., *Biochemistry* **1998,** *37* (23), 8341-8355.
17. Johnson, N. P.; Hoeschele, J. D.; Kuemmerle, N. B.; Masker, W. E.; Rahn, R. O., *Chem. Biol. Interact.* **1978,** *23* (2), 267-271.
18. Sorenson, C. M.; Eastman, A., *Cancer Res.* **1988,** *48* (16), 4484-4488.
19. Sorenson, C. M.; Eastman, A., *Cancer Res.* **1988,** *48* (23), 6703-6707.
20. Takahara, P. M.; Rosenzweig, A. C.; Frederick, C. A.; Lippard, S. J., *Nature* **1995,** *377* (6550), 649-652.
21. Chu, G., *J. Biol. Chem.* **1994,** *269* (2), 787-790.
22. Aliosman, F.; Berger, M. S.; Rairkar, A.; Stein, D. E., *J. Cell. Biochem.* **1994,** *54* (1), 11-19.
23. Siddik, Z. H., *Oncogene* **2003,** *22* (47), 7265-7279.
24. Shui, X. Q.; Sines, C. C.; McFail-Isom, L.; Van Derveer, D.; Williams, L. D., *Biochemistry* **1998,** *37* (48), 16877-16887.
25. McFail-Isom, L.; Shui, X. Q.; Williams, L. D., *Biochemistry* **1998,** *37* (49), 17105-17111.

26. Lerman, L. S., *J. Mol. Biol.* **1961,** *3* (1), 18-30.
27. Luzzati, V.; Lerman, L. S.; Masson, F., *J. Mol. Biol.* **1961,** *3* (5), 634-639.
28. Chaires, J. B.; Dattagupta, N.; Crothers, D. M., *Biochemistry* **1982,** *21* (17), 3933-3940.
29. Rao, S. N.; Kollman, P. A., *Proc. Natl. Acad. Sci. U.S.A.* **1987,** *84* (16), 5735-5739.
30. Neto, B. A. D.; Lapis, A. A. M., *Molecules* **2009,** *14* (5), 1725-1746.
31. Boresch, S.; Karplus, M., *J. Mol. Biol.* **1995,** *254* (5), 801-807.
32. Strekowski, L.; Wilson, B., *Mutat. Res. Fundam. Mol. Mech. Mugag.* **2007,** *623*, 3-13.
33. Denny, W. A., *Anti-Cancer Drug Des.* **1989,** *4* (4), 241-263.
34. Viola, G.; Dall'Acqua, F.; Gabellini, N.; Moro, S.; Vedaldi, D.; Ihmels, H., *Chembiochem* **2002,** *3* (6), 550-558.
35. Lee, Y. A.; Lee, S.; Cho, T. S.; Kim, C.; Han, S. W.; Kim, S. K., *J. Phys. Chem. B* **2002,** *106* (43), 11351-11355.
36. Strekowski, L.; Mokrosz, J. L.; Wilson, W. D.; Mokrosz, M. J.; Strekowski, A., *Biochemistry* **1992,** *31* (44), 10802-10808.
37. Armitage, B. A., *DNA Binders and Related Subjects* **2005,** *253*, 55-76.
38. Cholody, W. M.; Kosakowska-Cholody, T.; Hollingshead, M. G.; Hariprakasha, H. K.; Michejda, C. J., *J. Med. Chem.* **2005,** *48* (13), 4474-4481.
39. Moore, M. H.; Hunter, W. N.; Destaintot, B. L.; Kennard, O., *J. Mol. Biol.* **1989,** *206* (4), 693-705.
40. Chaires, J. B., *Biophys. J.* **1983,** *41* (2), 286a-287a.
41. Tanious, F. A.; Yen, S. F.; Wilson, W. D., *Biochemistry* **1991,** *30* (7), 1813-1819.
42. Strekowski, L.; Wilson, W. D.; Mokrosz, J. L.; Strekowska, A.; Koziol, A. E.; Palenik, G. J., *Anti-Cancer Drug Des.* **1988,** *2* (4), 387-398.
43. Strekowski, L.; Chandrasekaran, S.; Wang, Y. H.; Edwards, W. D.; Wilson, W. D., *J. Med. Chem.* **1986,** *29* (7), 1311-1315.
44. Wheelhouse, R. T.; Garbett, N. C.; Buurma, N. J.; Chaires, J. B., *Angew. Chem. Int. Ed.* **2010,** *49* (18), 3207-3210.
45. Wilson, B.; Fernandez, M. J.; Lorente, A.; Grant, K. B., *Tetrahedron* **2008,** *64* (16), 3429-3436.
46. Valis, L.; Mayer-Enthart, E.; Wagenknecht, H. A., *Bioorg. Med. Chem. Lett.* **2006,** *16* (12), 3184-3187.
47. Neto, B. A. D.; Lapis, A. A. M.; Mancilha, F. S.; Batista, E. L., Jr.; Netz, P. A.; Rominger, F.; Basso, L. A.; Santos, D. S.; Dupont, J., *Mol. Biosyst.* **2010,** *6* (6).
48. Gottesfeld, J. M.; Neely, L.; Trauger, J. W.; Baird, E. E.; Dervan, P. B., *Nature* **1997,** *387* (6629), 202-205.
49. Nguyen, B.; Neidle, S.; Wilson, W. D., *Accounts Chem. Res.* **2009,** *42* (1), 11-21.
50. Wartell, R. M.; Larson, J. E.; Wells, R. D., *J. Biol. Chem.* **1974,** *249* (21), 6719-6731.
51. Zimmer, C.; Wahnert, U., *Prog. Biophys. Mol. Biol.* **1986,** *47* (1), 31-112.
52. Kopka, M. L.; Yoon, C.; Goodsell, D.; Pjura, P.; Dickerson, R. E., *Proc. Natl. Acad. Sci. U.S.A.* **1985,** *82* (5), 1376-1380.
53. Pelton, J. G.; Wemmer, D. E., *Proc. Natl. Acad. Sci. U.S.A.* **1989,** *86* (15), 5723-5727.

54. Lah, J.; Carl, N.; Drobnak, I.; Sumiga, B.; Vesnaver, G., *Acta Chim. Slov.* **2006,** *53*(3), 284-291.
55. Lah, J.; Vesnaver, G., *J. Mol. Biol.* **2004,** *342* (1), 73-89.
56. Neidle, S., *Nat. Prod. Rep.* **2001,** *18* (3), 291-309.
57. Kopka, M. L.; Goodsell, D. S.; Han, G. W.; Chiu, T. K.; Lown, J. W.; Dickerson, R. E., *Structure* **1997,** *5* (8), 1033-1046.
58. Suckling, C. J., *J. Phys. Org. Chem.* **2008,** *21* (7-8), 575-583.
59. Harshman, K. D.; Dervan, P. B., *Nucleic Acids Res.* **1985,** *13* (13), 4825-4835.
60. Moon, J. H.; Kim, S. K.; Sehlstedt, U.; Rodger, A.; Norden, B., *Biopolymers* **1996,** *38* (5), 593-606.
61. Teng, M.; Usman, N.; Frederick, C. A.; Wang, A. H. J., *Nucleic Acids Res.* **1988,** *16* (6), 2671-2690.
62. Carrondo, M.; Coll, M.; Aymami, J.; Wang, A. H. J.; Vandermarel, G. A.; Vanboom, J. H.; Rich, A., *Biochemistry* **1989,** *28* (19), 7849-7859.
63. Quintana, J. R.; Lipanov, A. A.; Dickerson, R. E., *Biochemistry* **1991,** *30* (42), 10294-10306.
64. Spink, N.; Brown, D. G.; Skelly, J. V.; Neidle, S., *Nucleic Acids Res.* **1994,** *22* (9), 1607-1612.
65. Parkinson, J. A.; Barber, J.; Douglas, K. T.; Rosamond, J.; Sharples, D., *Biochemistry* **1990,** *29* (44), 10181-10190.
66. Neidle, S.; Mann, J.; Rayner, E. L.; Baron, A.; Opoku-Boahen, Y.; Simpson, I. J.; Smith, N. J.; Fox, K. R.; Hartley, J. A.; Kelland, L. R., *Chem. Commun.* **1999,** (10), 929-930.
67. Mann, J.; Baron, A.; Opoku-Boahen, Y.; Johansson, E.; Parkinson, G.; Kelland, L. R.; Neidle, S., *J. Med. Chem.* **2001,** *44* (2), 138-144.
68. Chaudhuri, P.; Ganguly, B.; Bhattacharya, S., *J. Org. Chem.* **2007,** *72* (6), 1912-1923.
69. Munde, M.; Ismail, M. A.; Arafa, R.; Peixoto, P.; Collar, C. J.; Liu, Y.; Hu, L. X.; David-Cordonnier, M. H.; Lansiaux, A.; Bailly, C.; Boykin, D. W.; Wilson, W. D., *J. Am. Chem. Soc.* **2007,** *129*, 13732-13743.
70. Wang, L.; Bailly, C.; Kumar, A.; Ding, D.; Bajic, M.; Boykin, D. W.; Wilson, W. D., *Proc. Natl. Acad. Sci. U.S.A.* **2000,** *97* (1), 12-16.
71. Wang, L.; Kumar, A.; Boykin, D. W.; Bailly, C.; Wilson, W. D., *J. Mol. Biol.* **2002,** *317* (3), 361-374.
72. Bailly, C.; Tardy, C.; Wang, L.; Armitage, B.; Hopkins, K.; Kumar, A.; Schuster, G. B.; Boykin, D. W.; Wilson, W. D., *Biochemistry* **2001,** *40* (33), 9770-9779.
73. Nguyen, B.; Hamelberg, D.; Bailly, C.; Colson, P.; Stanek, J.; Brun, R.; Neidle, S.; Wilson, W. D., *Biophys. J.* **2004,** *86* (2), 1028-1041.
74. Tanious, F.; Wilson, W. D.; Wang, L.; Kumar, A.; Boykin, D. W.; Marty, C.; Baldeyrou, B.; Bailly, C., *Biochemistry* **2003,** *42* (46), 13576-13586.
75. Nguyen, B.; Tardy, C.; Bailly, C.; Colson, P.; Houssier, C.; Kumar, A.; Boykin, D. W.; Wilson, W. D., *Biopolymers* **2002,** *63* (5), 281-297.

76. Lansiaux, A.; Tanious, F.; Mishal, Z.; Dassonneville, L.; Kumar, A.; Stephens, C. E.; Hu, Q. Y.; Wilson, W. D.; Boykin, D. W.; Bailly, C., *Cancer Res.* **2002,** *62* (24), 7219-7229.
77. Mallena, S.; Lee, M. P. H.; Bailly, C.; Neidle, S.; Kumar, A.; Boykin, D. W.; Wilson, W. D., *J. Am. Chem. Soc.* **2004,** *126* (42), 13659-13669.
78. Nguyen, B.; Tanious, F. A.; Mallena, S.; Kumar, A.; Boykin, D. W.; Wilson, W. D., *Abstr. Pap. Am. Chem. Soc.* **2006,** *231*, 23-MEDI.
79. Dervan, P. B.; Edelson, B. S., *Curr. Opin. Struct. Biol.* **2003,** *13* (3), 284-299.
80. Dervan, P. B., *Bioorg. Med. Chem.* **2001,** *9* (9), 2215-2235.
81. Mrksich, M.; Wade, W. S.; Dwyer, T. J.; Geierstanger, B. H.; Wemmer, D. E.; Dervan, P. B., *Proc. Natl. Acad. Sci. U.S.A.* **1992,** *89* (16), 7586-7590.
82. Wade, W. S.; Mrksich, M.; Dervan, P. B., *J. Am. Chem. Soc.* **1992,** *114* (23), 8783-8794.
83. Kielkopf, C. L.; Bremer, R. E.; White, S.; Szewczyk, J. W.; Turner, J. M.; Baird, E. E.; Dervan, P. B.; Rees, D. C., *J. Mol. Biol.* **2000,** *295* (3), 557-567.
84. Kelly, J. J.; Baird, E. E.; Dervan, P. B., *Proc. Natl. Acad. Sci. U.S.A.* **1996,** *93* (14), 6981-6985.
85. Herman, D. M.; Baird, E. E.; Dervan, P. B., *Chem.-Eur. J.* **1999,** *5* (3), 975-983.
86. Weyermann, P.; Dervan, P. B., *J. Am. Chem. Soc.* **2002,** *124* (24), 6872-6878.
87. Hsu, C. F.; Phillips, J. W.; Trauger, J. W.; Farkas, M. E.; Belitsky, J. M.; Heckel, A.; Olenyuk, B. Z.; Puckett, J. W.; Wang, C. C. C.; Dervan, P. B., *Tetrahedron* **2007,** *63* (27), 6146-6151.
88. Shirakawa, H., *Angew. Chem. Int. Ed.* **2001,** *40* (14), 2575-2580.
89. Jaiswal, M.; Menon, R., *Polym. Int.* **2006,** *55*, 1371-1384.
90. Murphy, A. R.; Frechet, J. M. J., *Chem. Rev.* **2007,** *107*, 1066-1096.
91. Melucci, M.; Barbarella, G.; Zambianchi, M.; Benzi, M.; Biscarini, F.; Cavallini, M.; Bongini, A.; Fabbroni, S.; Mazzeo, M.; Anni, M.; Gigli, G., *Macromolecules* **2004,** *37* (15), 5692-5702.
92. Walzer, K.; Maennig, B.; Pfeiffer, M.; Leo, K., *Chem. Rev.* **2007,** *107* (4), 1233-1271.
93. Huang, Q.; Meerheim, R.; Fehse, K.; Schwartz, G.; Reineke, S.; Walzer, K.; Leo, K., *Sid International Symposium, Digest of Technical Papers, Vol XXXVIII, Books I and II* **2007,** *38*, 1282-1285.
94. Kirchmeyer, S.; Reuter, K., *J. Mater. Chem.* **2005,** *15* (21), 2077-2088.
95. Dore, K.; Dubus, S.; Ho, H. A.; Levesque, I.; Brunette, M.; Corbeil, G.; Boissinot, M.; Boivin, G.; Bergeron, M. G.; Boudreau, D.; Leclerc, M., *J. Am. Chem. Soc.* **2004,** *126* (13), 4240-4244.
96. Ewbank, P. C.; Nuding, G.; Suenaga, H.; McCullough, R. D.; Shinkai, S., *Tetrahedron Lett.* **2001,** *42* (2), 155-157.
97. Ho, H. A.; Boissinot, M.; Bergeron, M. G.; Corbeil, G.; Dore, K.; Boudreau, D.; Leclerc, M., *Angew. Chem. Int. Ed.* **2002,** *41* (9), 1548-1551.
98. Ho, H. A.; Najari, A.; Leclerc, M., *Accounts Chem. Res.* **2008,** *41* (2), 168-178.
99. KorriYoussoufi, H.; Garnier, F.; Srivastava, P.; Godillot, P.; Yassar, A., *J. Am. Chem. Soc.* **1997,** *119* (31), 7388-7389.

100. Najari, A.; Ho, H. A.; Gravel, J. F.; Nobert, P.; Boudreau, D.; Leclerc, M., *Anal. Chem.* **2006,** *78* (22), 7896-7899.
101. Bjork, P.; Thomsson, D.; Mirzov, O.; Wigenius, J.; Inganas, O.; Scheblykin, I. G., *Small* **2009,** *5* (1), 96-103.
102. Ho, H. A.; Leclerc, M., *J. Am. Chem. Soc.* **2003,** *125* (15), 4412-4413.
103. Teixeira-Dias, B.; del Valle, L. J.; Estrany, F.; Armelin, E.; Oliver, R.; Aleman, C., *Eur. Polym. J.* **2008,** *44* (11), 3700-3707.
104. Barbarella, G.; Zambianchi, M.; Ventola, A.; Fabiano, E.; Della Sala, F.; Gigli, G.; Anni, M.; Bolognesi, A.; Polito, L.; Naldi, M.; Capobianco, M., *Bioconjugate Chem.* **2006,** *17* (1), 58-67.
105. Alesi, S.; Brancolini, G.; Melucci, M.; Capobianco, M. L.; Venturini, A.; Camaioni, N.; Barbarellala, G., *Chem.-Eur. J.* **2008,** *14* (2), 513-521.
106. Jatsch, A.; Kopyshev, A.; Mena-Osteritz, E.; Bauerle, P., *Org. Lett.* **2008,** *10* (5), 961-964.
107. Gooding, J. J., *Electroanalysis* **2002,** *14* (17), 1149-1156.
108. Bakker, E.; Telting-Diaz, M., *Anal. Chem.* **2002,** *74* (12), 2781-2800.
109. Ronkainen, N. J.; Halsall, H. B.; Heineman, W. R., *Chem. Soc. Rev.* **2010,** *39* (5), 1747-1763.
110. Peng, H.; Zhang, L. J.; Soeller, C.; Travas-Sejdic, J., *Biomaterials* **2009,** *30* (11), 2132-2148.
111. Keighley, S. D.; Estrela, P.; Li, P.; Mighorato, P., *Biosens. Bioelectron.* **2008,** *24* (4), 906-911.
112. Keighley, S. D.; Li, P.; Estrela, P.; Mighorato, P., *Biosens. Bioelectron.* **2008,** *23* (8), 1291-1297.
113. Garnier, F.; Korri-Youssoufi, H.; Srivastava, P.; Mandrand, B.; Delair, T., *Synth. Met.* **1999,** *100* (1), 89-94.
114. Li, G. T.; Kossmehl, G.; Welzel, H. P.; Engelmann, G.; Hunnius, W. D.; Plieth, W.; Zhu, H. S., *Macromol. Chem. Phys.* **1998,** *199* (4), 525-533.
115. Lee, T. Y.; Shim, Y. B., *Anal. Chem.* **2001,** *73* (22), 5629-5632.
116. Mateo-Marti, E.; Briones, C.; Pradier, C. M.; Martin-Gago, J. A., *Biosens. Bioelectron.* **2007,** *22* (9-10), 1926-1932.
117. Steichen, M.; Decrem, Y.; Godfroid, E.; Buess-Herman, C., *Biosens. Bioelectron.* **2007,** *22* (9-10), 2237-2243.
118. Nielsen, P. E., *Curr. Opin. Biotechnol.* **2001,** *12* (1), 16-20.
119. Wang, J., *Biosens. Bioelectron.* **1998,** *13* (7-8), 757-762.
120. Le Floch, F.; Ho, H. A.; Harding-Lepage, P.; Bedard, M.; Neagu-Plesu, R.; Leclerc, M., *Adv. Mater.* **2005,** *17* (10), 1251-1254.
121. Hvastkovs, E. G.; Buttry, D. A., *Analyst* **2010,** *135* (8), 1817-29.
122. Zhang, L. Y.; Sun, H.; Li, D.; Song, S.; Fan, C. H.; Wang, S., *Macromol. Rapid Commun.* **2008,** *29* (19), 1626-1626.
123. Babudri, F.; Farinola, G. M.; Naso, F., *J. Mater. Chem.* **2004,** *14* (1), 11-34.
124. Alberico, D.; Scott, M. E.; Lautens, M., *Chem. Rev.* **2007,** *107* (1), 174-238.
125. McGlacken, G. P.; Bateman, L. M., *Chem. Soc. Rev.* **2009,** *38* (8), 2447-2464.

126. Sato, M.; Tanaka, S.; Kaeriyama, K., *Synth. Met.* **1986,** *14* (4), 279-288.
127. Yoshino, K.; Hayashi, S.; Sugimoto, R., *Jpn. J. Appl. Phys., Part 2* **1984,** *23* (12), 899-900.
128. Nilsson, K. P. R.; Inganas, O., *Nat. Mater.* **2003,** *2* (6), 419-424.
129. Nilsson, K. P. R.; Olsson, J. D. M.; Konradsson, P.; Inganas, O., *Macromolecules* **2004,** *37* (17), 6316-6321.
130. Nilsson, K. P. R.; Rydberg, J.; Baltzer, L.; Inganas, O., *Proc. Natl. Acad. Sci. U.S.A.* **2003,** *100* (18), 10170-10174.
131. Hassan, J.; Sevignon, M.; Gozzi, C.; Schulz, E.; Lemaire, M., *Chem. Rev.* **2002,** *102* (5), 1359-1469.
132. Marion, N.; Nolan, S. P., *Accounts Chem. Res.* **2008,** *41* (11), 1440-1449.
133. Ye, J. S.; Chen, W.; Wang, D., *Dalton Trans.* **2008,** (30), 4015-4022.
134. Larrey, D., *J. Hepatol.* **2000,** *32*, 77-88.

Chapter 2

MODELS AND PHYSICAL TECHNIQUES

Abstract:

Many ligands of biological interest are planar aromatic molecules that cause a common difficulty when studying their binding properties, viz. their self aggregation in aqueous solution competes with binding. At high ligand concentration, the ligand exists as aggregated species which, upon addition of (or to) DNA, will (at least formally) dissociate into monomeric ligand prior to DNA binding. A solution to this hurdle in the analysis of DNA-binding DNA is to determine and thermodynamically quantify ligand self aggregation and then to take ligand aggregation into account during analysis of data for DNA-binding studies. Different mathematical models that describe aggregation equilibria of organic molecules in solution are discussed at the beginning of this chapter. These models can be used to analyse self aggregation data obtained using a variety of physical techniques such as ^{1}H-NMR, PGSE-NMR, surface tension, small angle neutron scattering (SANS) and isothermal titration calorimetry (ITC). In addition to these techniques for studying self aggregation, the chapter briefly describes the biophysical techniques (e.g. UV-Vis and CD spectroscopy, Job plot, viscosity and isothermal titration calorimetry) which can be used to quantify the interaction of small organic molecules with duplex DNA.

2.1 Aggregation and DNA binding

Although there are a multitude of small molecules that sequence-selectively recognise duplex DNA (Chapter 1), there is a continuous interest in designing and synthesising additional DNA-targeting small organic molecules, especially for drug discovery. Most of the small molecules designed to target DNA possess particular molecular features, *e.g.* planar aromatic structure, which make them good intercalators or minor groove binders, but which also facilitate self aggregation in aqueous solution.

Some of the key interactions that stabilise drug-DNA complexes and drive ligand self aggregation are hydrophobic and Van der Waals interactions. One explanation of the hydrophobic effect states that water molecules undertake a structural rearrangement in a so-called "hydrophobic hydration shell" of hydrophobic solutes allowing the formation of stronger hydrogen bonds.[1] This rearrangement leads to a loss of entropy because water molecules are more restricted in the hydration shell than in bulk water. The release of water molecules from the hydrophobic hydration shell then provides the entropic driving force for hydrophobic interactions.

Both intercalators and groove binders exhibit DNA binding as well as self-aggregation. For example, intercalators such as ethidium bromide[2, 3] or acridine orange[3] as well as end-stacking camptothecins[4] self aggregate in aqueous solution. Some minor groove binders such as Hoechst 33258 (H33258),[5] daunomycin[6] and its analogue doxorubicin[7] and methylene blue[8] have also been shown to self aggregate in aqueous solution.

Whether ligand self aggregation is a problem depends on the technique used for the study of DNA interactions. A variety of physical techniques can be used to quantify and determine the modes of binding of small molecules to DNA.[9-14] Some of these techniques use low concentrations of ligand, so the ligand molecules exist as monomers. This is the case for UV-Vis, circular dichroism and fluorescence titrations, when ligand self aggregation is often negligible and, therefore, does not interfere with the interpretation of DNA binding data. Unfortunately, several other techniques require high ligand concentrations (*e.g.* ^{1}H-NMR and isothermal titration calorimetry). In the case of ITC, the presence of high ligand concentration in the injection syringe causes (de)aggregation heat effects due to the self aggregation of the ligand before injection. The (de)aggregation heat effects are typically non-constant because the gradual increase in ligand concentration in the calorimeter cell leads to building up of pre-existing aggregates in the cell. As a result, ligand aggregation interferes with DNA binding and needs to be taken into account during data analysis in order to obtain meaningful DNA binding parameters. In an alternative approach, Chaires and coworkers introduced model-free ITC protocols in order to avoid the problems caused by aggregation when they studied the binding of daunorubicin to DNA.[15] Model-free ITC provides statistically meaningful values for the enthalpy of interactions even though binding constants cannot be determined.

2.2 Modes of self aggregation

Non-covalent self aggregation in solution is a common phenomenon for aromatic molecules and has attracted a wide range of applications in supramolecular chemistry, medicinal chemistry, molecular electronics and dye chemistry.[16-19] There are two main ways in which aromatic molecules can self aggregate in aqueous solution, *viz.* cooperatively or non-cooperatively.

2.2.1 Non-cooperative self aggregation

The term "non-cooperative" self aggregation refers to the formation of aggregates, where cooperativity does not play a role in aggregation.[20] Non-cooperative aggregation can be described as a gradual increase in the aggregation number and consequently the size of the aggregates. In the case of isodesmic self aggregation, the association constants for every growing step are equal and do not depend on the size of the aggregates. There are also situations when molecules do not form aggregated species higher than dimers in aqueous solution.[21-23] In this case, the aggregation could be limited to dimerisation by either the size and geometry of the molecule, the nature of substituents present in the molecule, the solvent or a combination of these factors.[24]

2.2.2 Cooperative self aggregation

Cooperative self aggregation involves preferential formation of aggregates with an aggregation number >2 and includes for example micellisation. Micelle-forming ligands (or surfactants) are characterised by an aggregation number and a critical micelle concentration (cmc).

Below the cmc, surfactant molecules typically form dimers, trimers, tetramers, etc. These aggregates are referred to as premicellar aggregates. Above the cmc, surfactant micelles, surfactant monomers and small surfactant aggregates coexist.

Determination of the thermodynamic parameters which characterise each mode of self aggregation requires analysis of experimental data with appropriate models describing self aggregation.

2.3. Mathematical models

2.3.1 Monomer-dimer formation

The monomer-dimer equilibrium for a ligand L can be defined by equation 2.1 and it is characterised by association constant K_{dim}.

$$L + L \leftrightarrow L_2 \; ; K_{dim} = \frac{[L_2]}{[L]^2} \tag{2.1}$$

where [L] and [L_2] are the concentrations of the monomer and dimer species in solution, respectively.

The total molar concentration of ligand L present in solution (*i.e.*in the monomers and molecules in dimers) is given by equation 2.2.

$$[L]_{tot} = [L] + 2[L_2] \tag{2.2}$$

Combining equations 2.1 and 2.2, the mass balance equation for a dimerising ligand L (Equation 2.3) is expressed as a function of K_{dim} and $[L]_{tot}$.

$$[L]_{tot} = [L](1 + 2K_{dim}[L]) \tag{2.3}$$

Rearranging equation 2.3, quadratic equation 2.4 is obtained:

$$2K_{dim}[L]^2 + [L] - [L]_{tot} = 0 \quad (2.4)$$

The monomer concentration in solution is calculated by solving quadratic equation (2.4), giving equation 2.5.

$$[L] = \frac{-1 + \sqrt{8K_{dim}[L]_{tot} + 1}}{4K_{dim}} \quad (2.5)$$

The mole fraction of monomer species can be defined as: $\alpha_{mon}=[L]/[L]_{tot}$ while the mole fraction of molecules existing in dimers can be written as $\alpha_{dim} = 2[L_2]/[L]_{tot}$. Considering equation 2.5,α_{mon} and α_{dim} can be expressed as a function K_{dim} and $[L]_{tot}$ (Equations 2.6 and 2.7).[24]

$$\alpha_{mon} = \frac{-1 + \sqrt{8K_{dim}[L]_{tot} + 1}}{4K_{dim}[L]_{tot}} \quad (2.6)$$

$$\alpha_{dim} = \frac{4K_{dim}[L]_{tot} + 1 - \sqrt{8K_{dim}[L]_{tot} + 1}}{4K_{dim}[L]_{tot}} \quad (2.7)$$

2.3.2 Isodesmic self aggregation model

The stepwise aggregation process can be defined by equations 2.8-2.11.

$$L + L \leftrightarrow L_2 \qquad K_2 = \frac{[L_2]}{[L]^2} \quad (2.8)$$

$$L_2 + L \leftrightarrow L_3 \qquad K_3 = \frac{[L_3]}{[L_2] \cdot [L]} = \frac{[L_3]}{K_2 \cdot [L]^3} \quad (2.9)$$

$$L_3 + L \leftrightarrow L_4 \qquad K_4 = \frac{[L_4]}{[L_3] \cdot [L]} = \frac{[L_4]}{K_2 \cdot K_3 \cdot [L]^4} \quad (2.10)$$

$$L_{n-1} + L \leftrightarrow L_n \qquad K_n = \frac{[L_n]}{[L_{3n-1}] \cdot [L]} = \frac{[L_n]}{(K_2 \cdots\cdots K_{n-1} \cdot [L]^n)} \tag{2.11}$$

The isodesmic self aggregation model is the simplest model describing the formation of extended aggregates.[18, 25] The model assumes that the association constants characteristic for every growing step are equal and do not depend on the size of the aggregates. For isodesmic aggregation the equilibrium constants in equations 2.8-2.11 are therefore identical (Equation 2.12).

$$K = K_2 = K_3 = \cdots = K_n = K_{agg} \tag{2.12}$$

Accordingly, the concentration of n-mer [L_n] can be deduced from equations 2.8-2.11 and is given by equation 2.13.

$$[L_n] = K_{agg}^{n-1}[L]^n \tag{2.13}$$

The total concentration of molecules is given by equation 2.14:

$$[L]_{tot} = [L] + 2K_{agg}[L]^2 + 3K_{agg}^2[L]^3 + \cdots\cdots + nK_{agg}^n[L]^n \tag{2.14}$$

Considering the series expansion (Equation 2.15) for 0< x <1,

$$(1 + 2x + 3x^2 + 4x^3 + \cdots) = \frac{x}{(1-x)^2} \tag{2.15}$$

Equation 2.14 becomes equation 2.16, which resembles equation 2.4.

$$[L]_{tot} = \frac{[L]}{\left(1 - K_{agg}[L]\right)^2} \tag{2.16}$$

Solving quadratic equation 2.16 leads to the ligand monomer concentration (Equation 2.17).

$$[L] = \frac{\left(2K_{agg}[L]_{tot} + 1 - \sqrt{4K_{agg}[L]_{tot} + 1}\right)}{2K_{agg}^2[L]_{tot}} \tag{2.17}$$

Defining the mole fraction of monomeric L asα_{mon} = $[L]/[L]_{tot}$, where $[L]_{tot}$ is the total ligand concentration, the mole fraction of aggregated L is $\alpha_{agg}=1-\alpha_{mon}$, (Equation 2.18).

$$\alpha_{agg} = 1 - \frac{2K_{agg}[L]_{tot} + 1 - \sqrt{4K_{agg}[L]_{tot} + 1}}{2K_{agg}^2[L]_{tot}^2} \tag{2.18}$$

2.3.3 *n*-merisation model

As one of the possible models describing micellisation, we use the most simplistic *n*-merisation model which assumes that aggregates of one single aggregation number *n* are formed. The model does not take in account any relevant counterions. Moreover, the model includes only one size of micelle. Thus micellisation is considered as a one-step process where *n* ligand molecules L associate forming a single aggregate containing *n* molecule (Equation 2.19).

$$nL \rightleftarrows L_n \qquad K_{n-mer} = \frac{[L_n]}{[L]^n} \tag{2.19}$$

The equilibrium constant $K_{\text{n-mer}}$ can be expressed in terms of a formal equilibrium constant for addition of single monomers to the micelle, $K'_{\text{n-mer}}$ leading to equation 2.20.

$$[L_n] = (K'_{n-mer}[L])^{n-1}[L] \tag{2.20}$$

For $n>>1$, the critical micelle concentration is given by expression 2.21 because $K'_{\text{n-mer}}\cdot[L]$ cannot significantly exceed 1.

$$[L] = \frac{1}{K'_{n-mer}} = cmc \tag{2.21}$$

Hence,

$$\ln cmc = \frac{1}{RT}\Delta G_{mic} \quad (2.22)$$

where ΔG_{mic} is the free energy of micellisation.

2.3.4 Kegeles' model

An alternative model to describe micellisation involves Kegeles' model. Kegeles defined the equilibria involved in micellisation as in equations 2.23–2.27.[26] The key assumption behind Kegeles' model is that the monomers arrange themselves on a shell-like surface with a limited number of n+1 spaces available to the monomers. As a result of its definition, the Kegeles model includes a distribution of micellar sizes.

$$[L_1]/[L_0] = K_{0,1} \cdot [L_0] \quad (2.23)$$

$$[L_2]/[L_1] = K_{1,2} \cdot [L_0] \quad (2.24)$$

$$[L_3]/[L_2] = K_{2,3} \cdot [L_0] \quad (2.25)$$

$$\vdots$$

$$[L_{i+1}]/[L_i] = K_{i,i+1} \cdot [L_0] \quad (2.26)$$

$$\vdots$$

$$[L_{n+1}]/[L_n] = K_{n,n+1} \cdot [L_0] \quad (2.27)$$

The equilibrium constants ($K_{0,1}$ … $K_{n,n+1}$) combine a statistical factor describing the likelihoods of monomer loss and monomer gain for different micelle sizes, as related to the number of monomers present per aggregate, i+1, with an intrinsic equilibrium constant K (Equation 2.28).

$$[L_{i+1}]/[L_i] = \frac{n-(i-1)}{n} \cdot \frac{i}{i+1} \cdot K \cdot [L_f] \quad (2.28)$$

Here, $[L_f]$ is the concentration of monomers, while $[L_{i+1}]$ is the concentration of ligand taken up in (i+1)-mers.

Equation 2.29 gives the total concentration of L taken up in each (i+1)-mer.

$$(i+1)\cdot[L_{i+1}] = \frac{n!}{(n-i)!}\cdot\left(\frac{K\cdot[L_f]}{n}\right)^i\cdot[L_f] \qquad (2.29)$$

Summation over i=1 to n gives the total concentration of L in all "Kegeles aggregates", starting from dimers up to the maximum size aggregates which contain n+1 monomers (Equation 2.30).

$$\sum_{i=1}^{n}\frac{n!}{(n-i)!}\cdot\left(\frac{K\cdot[K]_f}{n}\right)^i\cdot[L]_f = \sum_{i=1}^{n}(i+1)\cdot[L_{i+1}] = 2[L_2]+3[L_3]+\cdots+(n+1)[L_{n+1}] \quad (2.30)$$

The introduction of Kegeles' f-term involves a further multiplication by f. This term is taken as an absolute constant and is called cooperativity factor. According to Kruif *et al.*[27] this factor f should be higher than 10^{-2}. In contrast, Kegeles estimated f to be approximately 10^{-4}.[28] Unfortunately, the precise meaning and the expected values of this factor remain unclear.

2.4 Techniques used for quantification of self aggregation in aqueous solution

Self associated assemblies of small conjugated molecules in aqueous solution can be studied using a multitude of physical techniques such as ^{1}H-NMR, pulsed gradient spin echo NMR (PGSE-NMR), surface tension, small angle neutron scattering (SANS), and isothermal titration calorimetry (ITC). These techniques allow distinction between cooperative and non-cooperative self aggregation. Applications of these techniques include determination of critical

micelle concentrations (cmc) or estimation of size, shape and aggregation number. In addition, ITC permits the determination of thermodynamic parameters of self aggregation, *e.g.* association constant, enthalpy, entropy and Gibbs energy.

2.4.1 ^{1}H- Nuclear magnetic resonance (NMR) spectroscopy

Nuclear magnetic resonance (NMR) spectroscopy probes the structure and properties of organic molecules. In the case of self aggregation, the physical environment around the molecule changes as the solvation shell around the free molecule in aqueous solution is replaced by the hydrophobic environment of the molecule in the aggregate. In a typical experiment, the chemical shifts for selected protons are measured and are plotted against ligand concentration. The two theoretical models that describe non-cooperative self aggregation can be used to analyse experimental data and to calculate the equilibrium constant and thermodynamic parameters of self association (Section 2.2). In case of dimerisation, the dependence of the observed chemical shift as a function of the concentration is given by equation 2.31.[29, 30]

$$\delta = \delta_m + (\delta_{dim} - \delta_m)\left(1 + \frac{1 - \sqrt{4K_{dim}[L]_{tot} + 1}}{2K_{dim}[L]_{tot}}\right) \tag{2.31}$$

where δ_m and δ_{dim} are the monomer and dimer chemical shifts, respectively, in solution and K_{dim} is the dimerisation constant as defined before. For aromatic molecules that show formation of aggregates higher than dimers, the observed chemical shift is given by equation 2.32.

$$\delta = \delta_m + (\delta_{agg} - \delta_m)\left(1 + \frac{1 - \sqrt{8K_{agg}[L]_{tot} + 1}}{4K_{agg}[L]_{tot}}\right) \tag{2.32}$$

where δ is the observed chemical shift, δ_m is the monomer chemical shift and δ_{agg} is the chemical shift of ligand molecules in the aggregates. K_{agg} is the aggregation equilibrium constant. Unfortunately, many association equilibria involve cooperative self association and this makes it hard to determine the parameters of the association process.

2.4.2 Pulsed Gradient Spin Echo NMR (PGSE-NMR)

Pulsed-gradient spin-echo NMR has become an valuable tool for measuring the diffusion coefficient of molecules in solution.[31] The diffusion coefficients used to provide information about the random translational movement of the molecules driven by thermal energy.

Basic principles of PGSE-NMR

In the basic theory of PGSE NMR (or diffusion NMR), magnetic field gradients are applied on the static magnetic field ($\boldsymbol{B}_0$) in order to spatially distinguish NMR-active nuclei through their Larmor frequencies. In the three dimensional coordinate system, the gradient **g** is described by equation 2.33.[32]

$$g = \frac{\partial B_z}{\partial x} i + \frac{\partial B_z}{\partial y} j + \frac{\partial B_z}{\partial z} k \qquad (2.33)$$

where **i**, **j**, **k** are the unit vectors in the x, y and z directions of the main static magnetic field $\boldsymbol{B}_0$. The total magnetic field at position r is then given by equation 2.34.

$$B = B_0 + g \cdot r \qquad (2.34)$$

As a result the nuclear spin will have the Larmor frequency given by the equation 2.35.

$$\omega = \gamma\{B_0 + \Delta B\} \qquad (2.35)$$

with γ the gyromagnetic ratio and $\Delta B = g \cdot r$

By applying a gradient along the z-axis, the Larmor frequency changes with the z position of the spin. These changes in frequency provide the background for a spin echo (SE) experiment. Two equal rectangular gradient pulses are inserted, one into each τ period of the spin echo sequence as illustrated in Figure 2.1.

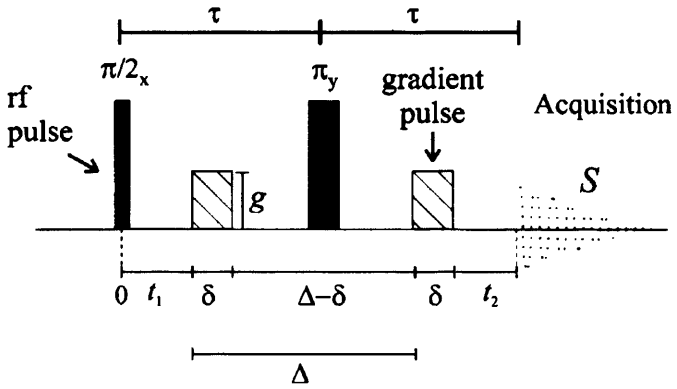

Figure 2.1 The basic pulse sequence for a spin-echo experiment. Picture taken from reference 32.

When a π/2 radiofrequency (RF) pulse is applied, the magnetisation changes orientation from the z-axis into the x-y plane perpendicular to the static field. If one applies a pulse gradient of duration δ and magnitude G during the first τ period at time t_1, then the dephasing of the spins varies along the z-axis due to the applied inhomogeneity of the magnetic field. Applying a π RF pulse at the end of time t_1 in combination with a second gradient pulse will repeal the dephasing effect leading to a spin echo. Two situations should be taken into consideration when the second gradient pulse (equal in magnitude and duration to the first one) is applied at time $t_1+\Delta$. In the first (extreme) case, the spins do not undertake any translational motion with reference to the z-axis and the two applied gradient pulses cancel out and the phases refocus leading (in theory) to a full spin echo signal. In the second case, if the spin shows translational

movement, the phase shift of the spin after the second period will be different in magnitude to the one at the end of the first period. In this case, the second gradient pulse does not completely refocus the magnetisation and an attenuated spin echo signal is observed.

Analysing PGSE-NMR data

A number of ^{1}H-NMR spectra are recorded while increasing the gradient pulses. The diffusion coefficient is calculated by measuring the integral of a chosen proton and fitting the exponential attenuation of the signal to equation 2.36.[33]

$$A(\delta, G, \Delta) = A_0 exp[(-kD_s)] \tag{2.36}$$

with

$$k = -\gamma^2 G^2 \left(\frac{30\Delta(\sigma + \delta)^2 - (10\delta^3 + 30\sigma\delta^2 + 35\sigma^2\delta + 14\sigma^3)}{30} \right) \tag{2.37}$$

Where $A(\delta,G,\Delta)$ is the observed amplitude of the signal, A_0 the signal in the absence of the field gradient pulses and γ is the gyromagnetic ratio, Δ is the diffusion time, σ is the gradient ramp time, δ is the gradient pulse length, and G is the gradient field strength.

Considering that free monomers and micelles are present in solution at equilibrium, the calculated diffusion coefficient is an average of the diffusion coefficients of the monomers and the micelles. A two state mobility model (Equation 2.38) can therefore be used to determine the diffusion coefficient of the micelle.

$$D_s = p_{mon} D_{mon} + (1 - p_{mon}) D_{micelle} \tag{2.38}$$

where p_{mon} is the mole fraction of the monomers in solution and is expressed by equation 2.39.

$$p_{mon} = \frac{cmc}{c_{tot}} \tag{2.39}$$

with D_{mon} and $D_{micelle}$ the monomer and micellar diffusion coefficients, respectively.

Above the cmc, the monomer concentration is constant and equal to the cmc. Below the cmc, all the surfactant is present as monomers – the diffusion coefficient does not vary with the concentration and is equal to the diffusion coefficient of monomers. There is a correlation between the diffusion coefficient and the size of the micellar aggregates, and this is given by the Stokes-Einstein equation 2.40, assuming spherical aggregates.

$$D_n = \frac{K \cdot T}{6 \cdot \pi \cdot \alpha \cdot \eta \cdot r_n} \tag{2.40}$$

where r_n is the hydrodynamic radius of the n-mer, η is the viscosity, k is the Boltzmann constant and T is the temperature. Assuming that the micelles are spherical, the volume of the n-mer micelle can be calculated using equation 2.41.

$$V_{micelle} = \frac{4\pi r_n^3}{3} \tag{2.41}$$

with r_n as defined before.

The aggregation number (N) is approximated as the ratio of the volume of the micelles ($V_{micelle}$) and the volume of a single surfactant molecule (V_{mon}). The volume of one monomer can be determined based on, *e.g.*, its crystal structure and takes in account both the volume of the hydrophobic conjugated chain and the volume of hydrophilic part of the monomer.

Distinguishing between stepwise self aggregation and dimerisation

The two main processes involving non-cooperative self aggregation are stepwise self aggregation and dimerisation. PSGE-NMR can be used to distinguish between these two processes.[34] The diffusion coefficient of a molecule in solution, D_{obs}, is plotted as a function of its concentration and the data is analysed in terms of either a dimerisation or a stepwise aggregation model. Such models are based on the observation that the measured diffusion coefficient is expressed by equation 2.42, representing the mass-weighted average of diffusion constants characteristic for different aggregates in solution.

$$D_{obs} = \sum_{n=1}^{n=\infty} x_n \cdot D_n \tag{2.42}$$

Here, x_n is the fraction of compound present in the form of n-mers and D_n is the diffusion coefficients for these n-mers. Assuming that the aggregates are spherical, relative diffusion coefficients can be calculated using the Stokes-Einstein equation (Equation 2.40). For the case of isodesmic self aggregation, the molar fraction of n-mers ϕ_n can be calculated from equation 2.43.[34]

$$\emptyset_n = \frac{n \cdot K_{agg}^{n-1} \cdot \left[\left\{\frac{2 \cdot K_{agg} \cdot [comp]_{tot} + 1 - \sqrt{4 \cdot K_{agg} \cdot [comp]_{tot} + 1}}{2 \cdot K_{agg}^2 \cdot [c]_{tot}}\right\}^n\right]}{[comp]_{tot}} \tag{2.43}$$

Equation 2.43can be reduced to the dimerisation process and the molar fraction of the dimers is given by equation (2.44) where n is summation counter.

$$\emptyset_n = n \cdot \left(\frac{K_{dim}^{n-1} \cdot \left(\frac{-1 + \sqrt{1 + 8 \cdot K_{dim} \cdot [comp]_{tot}}}{4 \cdot K_{dim}} \right)^n}{[comp]_{tot}} \right) \tag{2.44}$$

For stepwise self aggregation, combining equations 2.40, 2.42 and 2.43, gives equation 2.45, allowing calculation of D_{obs} as a function of concentration.

$$D_{obs} = \sum_{n=1}^{n=\infty} \{x_n \cdot D_i\} \approx \sum_{n=1}^{n=max\ terms} \left\{ \frac{n \cdot K^{n-1} \cdot \left[\left\{ \frac{\left(2 \cdot K \cdot [comp]_{tot} + 1 - \sqrt{(4 \cdot K \cdot [comp]_{tot} + 1)}\right)}{(2 \cdot K^2 \cdot [comp]_{tot})} \right\}^n \right]}{[comp]_{tot}} \cdot \frac{k \cdot T}{6 \cdot \pi^{0.666} \cdot \eta \cdot \{\frac{3}{4} \cdot n \cdot V_i\}^{0.333}} \right\} \tag{2.45}$$

In case of dimerisation, D_{obs} is given by equation 2.46.

$$D_{obs} = \sum_{n=1}^{n=2} \{x_n \cdot D_i\} = \frac{k \cdot T}{6 \cdot \pi^{0.666} \cdot \eta \cdot \{\frac{3}{4} \cdot 1 \cdot V_i\}^{0.333}} \cdot \left(\frac{\left(\frac{\left(-1 + \sqrt{(1 + 8 \cdot K \cdot [comp]_{tot})}\right)}{(4 \cdot K)} \right)}{[comp]_{tot}} \right) + \frac{k \cdot T}{6 \cdot \pi^{0.666} \cdot \eta \cdot \{\frac{3}{4} \cdot 2 \cdot V_i\}^{0.333}} \cdot 2 \cdot \left(\frac{\left\{ K \cdot \left(\frac{\left(-1 + \sqrt{(1 + 8 \cdot K \cdot [comp]_{tot})}\right)}{(4 \cdot K)} \right)^2 \right\}}{[comp]_{tot}} \right) \tag{2.46}$$

The concentration dependence predicted by equation 2.45 is significantly different from that predicted by equation 2.46, allowing distinction between isodesmic self aggregation and dimerisation.

2.4.3 Surface tension

The surface tension is a physical property of a liquid observed at the liquid-gas interface due to the intermolecular forces acting between the molecules. The surface tension phenomenon is due to packing of molecules and the interactions between those molecules at the interface. Usually, these interactions are based on London dispersion forces, dipole-dipole attractions, and hydrogen bonding. In bulk solution, a molecule is involved equally in interactions with all other neighboring molecules and as a result all the forces are cancelled. In contrast, at the interface due to the attraction forces being greater towards the bulk liquid, molecules are pulled

inward and are counter-balanced only by the liquid's resistance to compression.[35] As a result, the interface possesses a higher free energy than the inner bulk liquid. A cartoon representation of the unbalanced forces in solution and at the interface is given in Figure 2.2.

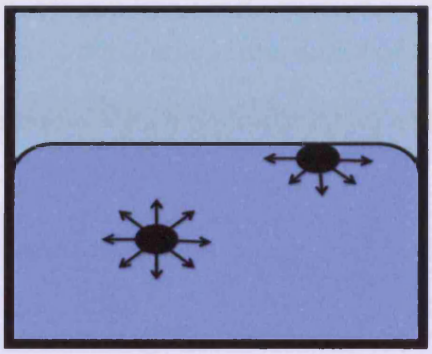

Figure 2.2 The diagram of the forces on the molecule in liquid state and at the interface

Different hydrophobic and hydrophilic groups have different minimum surface tensions depending on the packing of the molecule and on the interactions between the molecules at the interface. Moreover, reducing the interactions by applying a physical factor (*e.g.* temperature) will lower the surface tension. Plotting the surface tension of a solute (surfactant) against its concentration, the amount of surfactant adsorbed at the interface can be calculated using the Gibbs adsorption equation 2.47.

$$\Gamma_i = -\frac{1}{RT} \cdot \frac{\partial \gamma_i}{\partial \ln a_i} \qquad (2.47)$$

where γ_i is the surface tension of any component, a_i is the activity of any component in bulk solution, R is the gas constant and T is the temperature, Γ_i represents the excess of the i component per unit area of the surface. The concentration of surfactant in bulk solution is very

low below the cmc. In this case the solute activity can be replaced by solute concentration the solute concentration, c (Equation 2.48).

$$\Gamma_i = -\frac{1}{RT} \cdot \frac{\partial \gamma_i}{\partial \ln c} \tag{2.48}$$

The critical micelle concentration is determined from a plot of the surface tension as a function of the natural log of the concentration, which typically shows a break at the cmc.

2.4.4 Small angle neutron scattering (SANS)

In general, small angle neutron scattering (SANS) is used to characterise colloidal systems. SANS data is used to estimate the size and shape of aggregates, from which the aggregation numbers can be deduced. Aggregation numbers can be compared with those determined using other techniques (*e.g.* diffusion NMR and ITC). SANS experiments require a neutron beam produced either by nuclear fission in a reactor-based neutron source or by spallation in an accelerator-based neutron source. Several neutron facilities are available worldwide (*e.g.* France, USA, Japan, *etc.*), including the pulsed neutron source at ISIS, near Oxford, in the UK (Figure 2.3).[36]

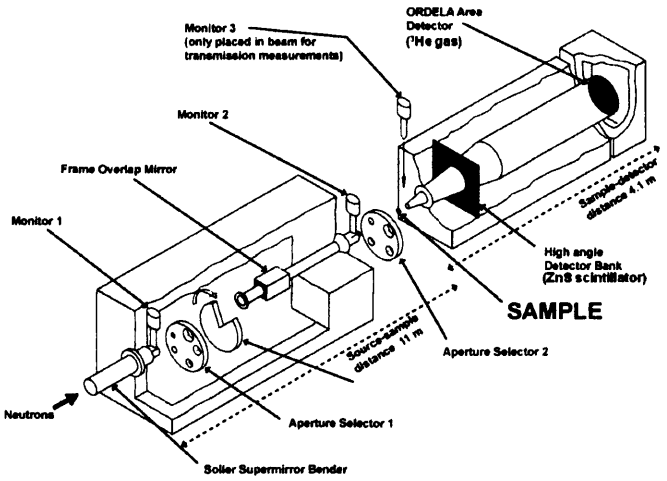

Figure 2.3 Schematic representation of the spallation neutron source at ISIS facility, Oxford, UK. Picture taken from the ISIS website.[36]

At ISIS, the neutrons are produced by bombarding a heavy tantalum (Ta) metal target with high energy particles (*e.g.* protons) from an accelerator in a process known as spallation.[37] The resulting neutrons possess high kinetic energy and are slowed down by passing through liquid nitrogen. Before passing through the sample, the neutron beam passes through a collimator in order for the beam to become the appropriate size and it is then further shaped by a series of apertures. A monitor is used to measure the speed at which the neutrons travel through the sample. This monitor produces an output proportional to the incident beam flux. The neutrons are scattered by the sample and produce a diffraction pattern that is recorded on large two dimensional detectors in an evacuated tank. The nuclei of any atoms in the path of the neutron beam scatter the neutrons. As a result the location of the nuclei determines the scattering properties. Figure 2.4 shows a schematic representation of a SANS experiment.

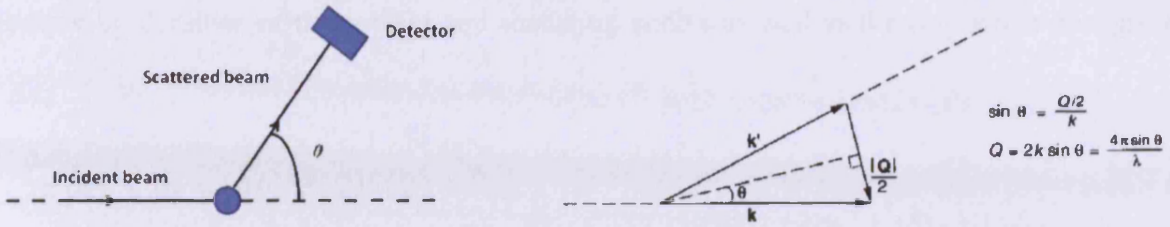

Figure 2.4 Representation of the neutron reflection and direction of the scattering vector Q

The SANS experiment measures the intensity of the scattered neutrons which is expressed in terms of scattering (wave) vector (Q). This scattering vector is equal to the modulus of the resultant between incident wave (K_0) and scattered vectors (K_s) and its value is given by equation 2.49.[38]

$$Q = |Q| = \left|K' - K\right| = \frac{4\pi n}{\lambda} sin\,\theta/2 \tag{2.49}$$

where K' and K_s are the incident and the scattered wave vectors respectively, θ is the scattering angle and η is the refractive index of the medium. Additionally, the flux of the neutrons $I(\lambda,\theta)$ incident on the area of the detector is described by equation 2.50.[38]

$$I(\lambda,\theta) = I_0(\lambda,\theta)\,\Delta\Omega\,\eta(\lambda)TV\frac{d\sigma}{d\Omega}(Q) \tag{2.50}$$

where $I_0(\lambda,\theta)$ is the incident neutron flux, $\Delta\Omega$ is the scattering angle, η the detector efficiency, T sample transmission and V is the volume. The differential cross-section $\frac{\partial\sigma}{\partial\Omega}(Q)$ (Equation 2.51) is dependent on the concentration of the scattering body (N_p), the volume of the scattering body (V_p), the form factor $P(Q)$ and structure factors $S(Q)$, the difference of the neutron

scattering densities of the solvent and scattering bodies as well as the incoherent background B_{inc}.

$$\frac{\partial\sigma}{\partial\Omega}(Q) = N_p V_p^2 (\Delta\rho)^2 P(Q) S(Q) + B_{inc} \quad (2.51)$$

Information about the size and shape of the particles can be obtained by analysing the form factor $P(Q)$. Different mathematical expressions are available for $P(Q)$ depending on the shape of the particles (*e.g.* sphere, spherical shells, cylinders, disc). Spherical micelles can be modeled using a solid sphere model (Equation 2.52) in order to calculate the hydrodynamic radius.[38]

$$P(Q) = \left[\frac{3(sinQR - QRcosQR)}{(QR)^3}\right]^2 \quad (2.52)$$

2.5. Techniques used for quantifying the binding to DNA

DNA-binding properties can be studied using a variety of biophysical techniques including UV-visible and circular dichroism (CD) spectroscopy, Job plots, viscometry and isothermal titration calorimetry (ITC). These methods will be briefly described below.

2.5.1. UV-visible spectroscopy

When a ligand chromophore interacts with DNA, its spectroscopic properties often change. This change is typically the result of the change in environment of the chromophore from solvation in aqueous solution to the more hydrophobic environment offered by DNA or a change in effective conjugation length as the result of conformational requirements of DNA

binding. Changes in absorption can involve a decrease or increase in extinction coefficient (hypochromicity and hyperchromicity, respectively) and shifts to a lower or a higher wavelength (blue and red shifts). If an isosbestic point is found when plotting these changes in absorption, this suggests that one single distinct binding process takes place between the ligand and DNA and only two species are involved in the process, *viz.* free and bound ligand. The changes in the ligand absorption properties can be used to quantify the interaction of ligands with ds-DNA. If full spectra have been recorded, titration curves can be extracted from the UV-visible data. A binding model can then be fitted to the data in order to determine the binding constants (K) and binding site sizes (n). A first model was proposed by Scatchardin 1949.[39] Unfortunately this linear model is inadequate for complicated systems with more than a single 1:1 binding stoichiometry. A neighbor exclusion model known as the McGhee-von Hippel model was developed to analyse the non-specific binding of ligands to homogeneous DNA lattices containing a multitude of free binding sites.[40] An alternative to the McGhee-von Hippel model is the multiple independent binding sites (MIS) model. Contrary to the McGhee-von Hippel model, the MIS model considers that binding sites do not "communicate" with each other, and are therefore independent. As a consequence there is no cooperativity or anticooperativity in this model. Our version of the MIS model takes ligand dilution into account through explicit incorporation of both the DNA concentration and the ligand concentration for every titration data point.

The model is derived starting from the complexation equilibrium (Equation 2.53).

$$L_f + bs_f \leftrightarrow L_b \qquad (2.53)$$

The terms L_f and bs_f are the free ligand and the free binding sites in solution, respectively, and L_b is the ligand bound in the complex. The equilibrium is characterised by the association constant as defined by equation 2.54.

$$K = \frac{[L]_b}{[L]_f[bs]_f} \tag{2.54}$$

In equation 2.54, $[L]_b$ is the concentration of bound ligand, $[L]_f$ is the concentration of free ligand in solution and $[bs]_f$ is the concentration of free binding sites in solution. The total concentration of ligand and the total concentration of binding sites are expressed by equations 2.55 and 2.56. Additionally, in the complex, the concentration of bound ligand is equal to the concentration of bound (*i.e.* occupied) binding sites (Equation 2.57).

$$[L]_{tot} = [L]_f + [L]_b \tag{2.55}$$

$$[bs]_{tot} = [bs]_f + [bs]_b \tag{2.56}$$

$$[L]_b = [bs]_b \tag{2.57}$$

Based on equations 2.55 and 2.56, the concentrations of free ligand and free binding sites can be expressed in terms of the total ligand concentration $[L]_{tot}$, the total binding sites concentration $[bs]_{tot}$ and the concentration of bound ligand $[L]_b$. As a consequence the association constant can be rewritten in terms of equation 2.58.

$$K = \frac{[L]_b}{([L]_{tot} - [L]_b)([bs]_{tot} - [L]_b)} \tag{2.58}$$

Rearrangement of equation 2.58 leads to a quadratic equation 2.59.

$$K[L]_b{}^2 - (1 + K[bs]_{tot} + K[L]_{tot})[L]_b + K[bs]_{tot}[L]_{tot} = 0 \tag{2.59}$$

Solving for $[L]_b$, the two roots for quadratic equation 2.59 are given by equation 2.60.

$$[L]_b = \frac{1 + K[bs]_{tot} + K[L]_{tot} \pm \sqrt{(1 + K[bs]_{tot} + K[L]_{tot})^2 - 4K^2[bs]_{tot}[L]_{tot}}}{2K} \quad (2.60)$$

For titrations involving DNA, the concentration expressed in terms of base pairs is turned into the concentration of binding sites by dividing by the binding site size N (in base pairs). Also adding terms representing signal strength and base lines, equation 2.60 turns into equation 2.61.

$$\text{signal}_{obsd} = \text{background} + \text{signal}_{free,m} \cdot [L]_{tot} + \Delta_{binding}\text{signal}_m \cdot \left\{ \frac{1 + K \cdot \frac{x}{N} + K \cdot [L]_{tot} - \sqrt{\left(1 + K \cdot \frac{x}{N} + K \cdot [L]_{tot}\right)^2 - 4 \cdot K^2 \cdot \frac{x}{N} \cdot [L]_{tot}}}{2 \cdot K} \right\} \quad (2.61)$$

For the case of UV-visible titrations, $signal_{obs}$ is the observed absorbance at a given wavelength λ, *background* is the background absorbance at λ, $signal_{free,m}$ is the product of the cuvette pathlength and the molar extinction coefficient at λ, $\Delta_{binding}signal_m$ is the product of the cuvette pathlength and the change in molar extinction coefficient upon binding at λ, K is the equilibrium constant for the binding process, x is the DNA concentration in base pairs for a given data point, N is the binding site size in base pairs, and $[L]_{tot}$ is the total ligand concentration for a given data point.

2.5.2 Circular dichroism (CD) spectroscopy

Circular dichroism spectroscopy is a method to determine the difference in the absorption of left-and right-handed circularly-polarised light which arises as a result of the structural asymmetry in enantiomers. Circular dichroism spectroscopy is related to optical activity and optical rotation dispersion.[41] When used to probe the interactions between a biomolecule and a small molecule, the chiral environment of a biomolecule, *e.g.* DNA, induces chirality in achiral

molecule when they interact with each other resulting in an induced circular dichroism signal for the achiral molecule. For molecules interacting with DNA, the transition moments of the ligand and polynucleotide bases greatly affect the induced CD signal of the binder.[41, 42] For example, the induced CD signal is typically strongly positive if the ligand binds in the minor groove with a transition moment oriented along the groove (Figure 2.5).

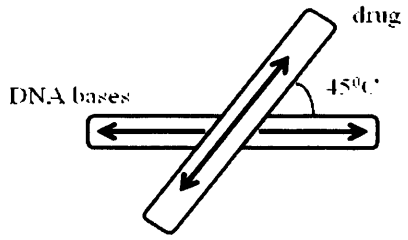

Figure 2.5 Cartoon representation of a minor groove binder with a transition moment oriented along the groove of B-DNA.

The sign of the induced circular dichroism signal varies for a major groove binder due to the multitude of ligand orientations that are accessible in this groove. Additionally, the induced CD signal is also sensitive to ligand organisation, such as the formation of monomers, dimers or n-mers. In the case of the formation of dimers and higher aggregates, an exciton coupled circular dichroism signal (EC-CD) can be observed as a result of the electronic interaction of the nearest neighbours possessing identical transition moments. This signal is indicative for a groove binder, with positive and negative bands to the sides of the absorption maximum of the ligand.

In contrast, an intercalator does not show an exciton CD signal. The ICD signal for an intercalator is dramatically dependent on its displacement relative to the double helix and the nature of the base pairs on either side of the intercalation site. For example, an intercalator

possessing transition moments oriented along its main axis induces a weak and negative CD signal. On the other hand, for an intercalator located in the centre of the DNA helix, the induced circular dichroism signal is positive if the transition moments are perpendicular to the intercalator long axis.

2.5.3 Method of continuous variation (Job plot)

The method of continuous variation applied to various analytical techniques (UV-visible, fluorescence, CD or ^{1}H-NMRspectroscopy) is especially useful for the determination of the stoichiometry of a DNA-ligand complex. In this method, different volumes of biomolecule and ligand solutions, each at a fixed concentration, are mixed in such way that the molar fraction of the ligand is varied while the total summed concentration of DNA and DNA binder is held constant. The spectrophotometric signal of each solution is measured and the changes are plotted against the mole fraction of one of the components. The observed inflection point leads to the stoichiometry of the interaction, in our case the binding site size. First, Job[43] applied the continuous variation method to simple enzymatic systems with one binding process. Later, the method was extended to more complicated systems, including biomolecules with n equivalent and non-interacting sites.

If we consider a biomacromolecule M interacting with n moles of ligand L we define the equilibrium binding process as in equation 2.62.

$$M + nL \leftrightarrow ML + (n-1)L \leftrightarrow ML_2 + (n-2)L \leftrightarrow \cdots \leftrightarrow ML_n \qquad (2.62)$$

Thus, the dissociation constant is expressed by equation 2.63 where $[M]_0$ and $[L]_0$ are the total concentrations of the biomacromolecule and the ligand, respectively.

$$K_d = \frac{[bs]_f \cdot [L]_f}{[L]_b} = \frac{(n[M]_0 - \sum_{i=0}^{n} i[ML_i]) \cdot ([L]_0 - \sum_{i=0}^{n} i\,[ML_i])}{\sum_{i=0}^{n} i[ML_i]} \quad (2.63)$$

The summation over all the forms of DNA-ligand complex is equal to the concentration of bound ligand (Equation 2.64).

$$\sum_{i=0}^{n} i[ML_i] = [ML] + 2[ML_2] + \cdots + n[ML_n] \quad (2.64)$$

If the summed concentration of DNA and ligand is kept constant and equal to C_0, then we have

$$[M]_0 + [L]_0 = C_0 \quad (2.65)$$

Rearranging equation 2.65, gives equation 2.66.

$$\frac{[M]_0}{C_0} + \frac{[L]_0}{C_0} = 1 \quad (2.66)$$

The molar fraction of DNA (χ) and ligand (γ) are defined as in equation 2.67.

$$\chi = \frac{[M]_0}{C_0}; \quad \gamma = \frac{[L]_0}{C_0} \quad (2.67)$$

Equation 2.67 is rewritten as equation 2.68.

$$\gamma + \chi = 1 \quad (2.68)$$

$[M]_0$ and $[L]_0$ can be calculated using equations 2.69 and 2.70.

$$[M]_0 = C_0 \cdot \chi \quad (2.69)$$

$$[L]_0 = C_0 \cdot \gamma = C_0(1 - \chi) \quad (2.70)$$

We introduce S as representing all the forms of DNA-ligand complex (Equation 2.71)

$$S = \sum_{i=0}^{n} i[ML_i] \quad (2.71)$$

We substitute equations 2.69-2.71 into equation 2.63, and rearrange, giving equation 2.72.

$$K_d \cdot S = (n \cdot C_0 \cdot \chi - S) \cdot [C_0 \cdot (1 - \chi) - S] \tag{2.72}$$

The derivative of equation 2.72with respect to χ leads to equation 2.73.

$$K_d \cdot \left(\frac{dS}{d\chi}\right) = (n \cdot C_0 \cdot \chi - S) \cdot \left(-C_0 - \frac{dS}{d\chi}\right) + [C_0 \cdot (1 - \chi) - S] \cdot \left(n \cdot C_0 - \frac{dS}{d\chi}\right) \tag{2.73}$$

If the molar fraction of DNA tends to zero ($\chi \rightarrow 0$), the summed concentration of ligand-DNA complexes also tends to zero and equation 2.73 assumes the form of equation 2.74.

$$K_d \cdot \left(\frac{dS}{d\chi}\right)_{\chi \rightarrow 0} = C_0 \left[n \cdot C_0 - \left(\frac{dS}{d\chi}\right)_{\chi \rightarrow 0}\right] \tag{2.74}$$

The tangent or limiting slope of the Job plot obtained for ($\chi \rightarrow 0$) is given by equation 2.75.

$$\left(\frac{dS}{d\chi}\right)_{\chi \rightarrow 0} = \frac{n \cdot {C_0}^2}{K_d + C_0} \tag{2.75}$$

Similarly, when the mole fraction of the ligand goes to zero ($\gamma \rightarrow 0$ or $\chi \rightarrow 1$), S goes to zero and equation 2.73becomes equation 2.76.

$$K_d \cdot \left(\frac{dS}{d\chi}\right) = nC_0 \cdot \left[-C_0 - \left(\frac{dS}{d\chi}\right)_{\chi \rightarrow 1}\right] \tag{2.76}$$

Rearranging equation 2.76 gives equation 2.77 for the tangent (limiting slope) of S as a function χ.

$$\left(\frac{dS}{d\chi}\right)_{\chi \rightarrow 1} = -\frac{n \cdot {C_0}^2}{K_d + C_0} \tag{2.77}$$

At the intersection point of the two tangents described by equations 2.75 and 2.77, we have

$$\frac{\chi_i \cdot n \cdot {C_0}^2}{K_d + C_0} = \frac{\gamma_i \cdot n \cdot {C_0}^2}{K_d + n \cdot C_0} \tag{2.78}$$

Rearranging the terms in equation 2.78 leads to equation 2.79.

$$\frac{\gamma_i}{\chi_i} = \frac{K_d + n \cdot C_0}{K_d + C_0} \tag{2.79}$$

Therefore, if the total sum of concentrations C_0 is high relative to K_d (*i.e.*$C_0 >> K_d$), then the binding stoichiometry n can be determined based on the molar ratio of ligand and biomolecule at the inflection point (Equation 2.80).

$$\frac{\gamma_i}{\chi_i} = \frac{n \cdot C_0}{C_0} = n \tag{2.80}$$

2.5.4 Viscosity

Measuring the viscosity is effective in probing the modes of interaction of DNA with a binder in aqueous solution.[44-46] Intercalation of a ligand between the DNA base pairs causes the separation of the bases at the binding site, hence, the DNA length will increase. This causes an increase in the viscosity of the DNA solution. In contrast, a minor groove binder does not modify the length of the DNA it binds to, causing either a very small change (positive or negative) or no change in the viscosity of the DNA solution. The relative viscosity of the DNA solution (η) in the presence and absence of the ligand is calculated using equation 2.81.

$$\eta = \frac{t - t_0}{t_0} \tag{2.81}$$

where t is the observed flow time of the DNA solution in viscometer and t_0 is the flow time of the buffer.

According to Cohen and Eisenberg,[47] the change in the viscosity of the free and bound DNA (L / L_0) is given by solving equation 2.82.

$$\frac{L}{L_0} = \left[\frac{\eta}{\eta_0} \cdot \frac{f(p)_0}{f(p)}\right]^{1/3} \approx 1 + r \tag{2.82}$$

where L is the contour length of rod-like macromolecules, p is the axial ratio of the rods, r is ratio of bound complex to DNA,and η is the intrinsic viscosity of DNA solution at different binding ratios r. The subscripts zero in equation 2.82 indicate the absence of the binder. The viscosity data is plotted as relative viscosity $(\eta/\eta_0)^{1/3}$ versus the binding ratio r. An increase or no increase in the viscosity of the DNA solution is observed depending on the type of DNA binders.

2.6 Isothermal titration calorimetry - common technique for both ligand self aggregation and DNA binding

Isothermal titration calorimetry (ITC) provides a powerful tool to study ligand-biomolecule interactions in (aqueous) solution. ITC measures the heat taken up or released during a binding event and allows determination of the binding affinity, binding site size and the enthalpy (ΔH), and, therefore, also the free energy (ΔG) and entropy (ΔS) changes for the binding event(s). Because ITC experiments typically require relatively high concentrations of ligand and biomolecules (here DNA), self aggregation needs to be taken in account (See section 2.1). This can be done and ITC is in fact a helpful source of information on both DNA binding and self aggregation.

2.6.1 Detailed ITC instrumentation

A schematic representation of an isothermal titration calorimeter is shown in Figure 2.5. The isothermal titration calorimeter consists of two identical cells; *viz.* a reference cell, that typically contains water, and a sample cell containing a solution of a host molecule. The syringe containing a concentrated solution of the guest (ligand) injects programmed volumes into the calorimeter sample cell at programmed time intervals. If interactions are broken or formed, the making or breaking of interactions is often accompanied by the uptake or release of heat which leads to a difference in temperature ΔT between the sample and reference cells. The cells are in an isothermal jacket and both are allowed to equilibrate to constant temperature by addition or removal of heat. The relative energy flow required to keep both cells at constant temperature is measured and integrated with respect to time. This process provides the total uptake or release of heat accompanying the making or breaking of interactions in the calorimeter sample cell. The process is repeated until a full titration profile has been obtained.

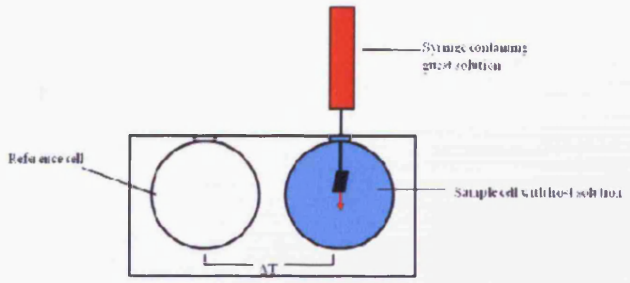

Figure 2.6 Schematic diagram of an ITC instrument

2.6.2 ITC data analysis (IC-ITC)

As mentioned before, ITC experiments require high concentrations of ligand in the syringe and, as a consequence, self aggregation needs to be factored into data analysis. Unfortunately, when considering ligand self aggregation in combination with binding processes, the mass balance equations describing the equilibrium systems involved in DNA-binding are complex and frequently these equations cannot be solved analytically. As an alternative, we use custom written data analysis software called IC-ITC[34, 48] that allows numerical analysis of calorimetric data for combined self aggregation and DNA binding in order to find the thermodynamic parameters for the various equilibria involved (Scheme 2.1). Briefly, this numerical analysis involves equilibrium concentrations determined numerically using the Newton-Raphson algorithm[49] and simulated annealing[50] to optimise thermodynamic parameters, so that they best reproduce the experimental calorimetric data.

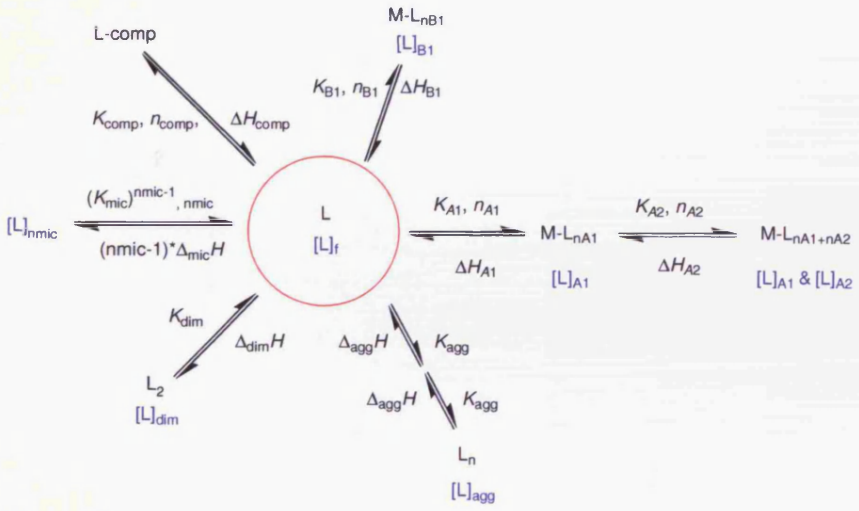

Scheme 2.1 Possible equilibria involved in both ITC self aggregation and DNA binding data analysis

The analysis of binding isotherms using IC-ITC[34] requires in the first instance calculating all relevant total concentrations (*e.g.* biomolecule, ligand, competing ligand) in the cell after every injection and solving the mass balance equation (Equation 2.83).

$$-[\mathrm{L}]_{\mathrm{tot}} + \sum_{X}[\mathrm{L}]_{X} = 0 \qquad (2.83)$$

Equation 2.83 represents the sum of concentrations of ligand taken up in the different complexes X. The expression for the concentration of ligand taken up in complexes $[L]_x$ (Equation 2.84) includes the free ligand concentration, total macromolecule concentrations $[M]_{tot}$ and interaction parameters $\mathbf{a}_X$ for the individual complexation events, *i.e.* equilibrium constants and stoichiometries.

$$[L]_X = f([L]_f, [M]_{tot}, a_X) \qquad (2.84)$$

IC-ITC requires expressions of the type of equation 2.84 for the concentrations of the ligand L taken up in all types of aggregates. Additionally, IC-ITC calculates the error margins and covariances for different variables during the optimisation.

2.6.3 Isosdesmic self aggregation and ITC

For the case of aggregates formed through step-wise self aggregation, the contribution of the ligand taken up in aggregates to the overall mass balance equation is given by equation 2.85.

$$[L]_{aggregates} = \frac{[L]_f}{\{1 - K_{agg} \cdot [L]_f\}^2} \qquad (2.85)$$

where $[L]_{aggregates}$ is the concentration of the ligand taken up in the aggregates, $[L]_f$ is the free ligand concentration and K_{agg} is association constant.

The heat effects are calculated using the "concentration of interactions". For stepwise self aggregation, the concentration of interactions $[int]_{aggregates}$ is calculated using equation (2.86).

$$[int]_{aggregates} = \frac{K_{agg} \cdot \{[L]_f\}^2}{\{1 - K_{agg} \cdot [L]_f\}^2} \quad (2.86)$$

2.6.4 Dimerisation model and ITC

The concentration of ligand taken up in the dimers $[L]_{dim}$ is given by equation 2.87.

$$[L]_{dim} = 2 \cdot K_{dim} \cdot \{[L]_f\}^2 \quad (2.87)$$

where K_{dim} is dimerisation equilibrium constant and $[L]_f$ is free ligand concentration.

The concentration of the interactions taken up in the dimers $[int]_{dim}$ is expressed by equation 2.88.

$$[int]_{dim} = K_{dim} \cdot \{[L]_f\}^2 \quad (2.88)$$

2.6.5 n-merisation model in ITC

For the case of n-merisation, the contribution of n-mers to the overall mass balance equation is given by equation 2.89.

$$[L]_{n-mer} = n \cdot K^{n-1} \cdot [L]_f{}^n \quad (2.89)$$

with n the number of monomers in the aggregates and K^{n-1} the n-merisation equilibrium constant. The concentration of the interactions in n-mers, $[int]_{n\text{-}mer}$, is given by equation 2.90.

$$[int]_{n-mer} = (n-1) \cdot K^{n-1} \cdot [L]_f{}^n \quad (2.90)$$

2.6.6 Kegeles shell model in ITC

The total concentration of ligand taken up in each (i+1)-mer is giving by equation 2.91.

$$f \cdot \frac{n!}{(n-i)!} \cdot \left(\frac{K \cdot [L]_f}{n}\right)^i \cdot [L]_f = (i+1) \cdot [L_{i+1}] \tag{2.91}$$

with n themaximum number of monomers which can be added to one pre-existing monomer on Kegeles' shell and i-number of monomers per aggregate, f a cooperativity multiplication factor, and K the micellisation equilibrium constant.

The concentration of interaction is expressed by equation 2.92.

$$f \cdot \frac{n!}{(n-i)!} \cdot \left(\frac{K \cdot [L]_f}{n}\right)^i \cdot [L]_f = (i+1) \cdot [int_{i+1}] \tag{2.92}$$

2.6.7 Two consecutive DNA binding events

The DNA binding model assumes two consecutive binding modes A1 and A2. During the first binding event A1, n_{A1} ligand molecules occupy the A1 binding sites on the macromolecule creating n_{A2} binding sites which are involved in a second binding event A2. The concentrations of ligand bound in sites A1 and A2 can be calculated using equations 2.93 and 2.94, for $n_{A1} \neq 0$ (for $n_{A1}=0$, $[L]_{A2}=0$).

$$[L]_{A1} = \frac{K_{A1} \cdot [M]_{tot} \cdot n_{A1} \cdot [L]_f + \frac{n_{A1}}{n_{A2}} \cdot K_{A1} \cdot K_{A2} \cdot [M]_{tot} \cdot n_{A2} \cdot ([L]_f)^2}{\left\{1 + K_{A1} \cdot [L]_f + K_{A1} \cdot K_{A2} \cdot ([L]_f)^2\right\}} \tag{2.93}$$

$$[L]_{A2} = \frac{K_{A1} \cdot K_{A2} \cdot [M]_{tot} \cdot n_{A2} \cdot ([L]_f)^2}{\left\{1 + K_{A1} \cdot [L]_f + K_{A1} \cdot K_{A2} \cdot ([L]_f)^2\right\}} \tag{2.94}$$

Similarly, the concentration of the ligand taken up in the complex for a parallel binding event B1 can be calculated using equation 2.95.

$$[L]_{B1} = \frac{K_{B1} \cdot [M]_{tot} \cdot n_{B1} \cdot [L]_f}{\{1 + K_{B1} \cdot [L]_f\}} \tag{2.95}$$

Typically, mass balance equation 2.83 can only be solved numerically, which is done using the Newton-Raphson algorithm.[49] The Newton-Raphson algorithm finds the roots x for which the mass balance equation, here notated f(x) expressed in terms of $[L]_f$, is equal to zero (Equation 2.96).

$$x_{i+1} = x_i - \frac{f(x_i)}{f'(x_i)} \tag{2.96}$$

Equation 2.96 is valid if the physically meaningful roots satisfy equation 2.97.

$$[L]_f \in <0,[L]_{tot}> \tag{2.97}$$

Heat effects for individual types of interactions *i* involved in the formation of complex X are based on interactions broken or formed in the active cell volume (Equation 2.09). This includes heat effects from interactions in the syringe.

$$q_{iX} = \Delta_{int-X}H \cdot V_{cell} \cdot \{[int]_{X,i-1} - [int]_{X,i}\} - \Delta_{int-X}H \cdot \Delta V_i \cdot \{[int]_{X,syringe} - [int]_{X,i-1}\} \tag{2.98}$$

In equation 2.98, q_{iX} is the heat effect for injection *i* accompanying making or breaking of the interactions involved in complex X, $\Delta_{int-X}H$ is the enthalpy change for forming the interactions involved in complex X, and V_{cell} and ΔV_i are the volumes of the cell and of injection *i*, respectively. Heat effects for every injection are the sum of all heat effects resulting from making and breaking all types of interactions (Equation 2.99).

$$q_i = q_b + \sum_X q_{iX} \tag{2.99}$$

where q_{iX} is the heat effects resulting from interactions for all complexes X and q_b is a constant which corrects for the experimental baseline. The contributions of the ligand to the formation of the aggregates were derived from equations presented earlier in the aggregation chapter and these include dimerisation, isosdesmic self aggregation, micellisation. The next step in analysing the ITC data involves the optimisation of variable parameters that best reproduce the experimental data. The goodness of the fit is quantified by $\Sigma dev^2/dof$ as defined in equation 2.100.

$$\sum dev^2/dof = \frac{\sum_{i=1}^{N}[q_i - q(i;a)]^2}{dof} \tag{2.100}$$

where (vector) **a** is a set of thermodynamic parameters describing all interactions *i.e.* it combines all $\mathbf{a}_X$, $q(i;\mathbf{a})$ is the calculated heat effect for injection i for thermodynamic parameters **a**, and *dof* is the number of degrees of freedom, *i.e.* the number of data points minus the number of optimisable parameters. $\Sigma dev^2/dof$ is minimised, using the simulated annealing (SA) algorithm.[51]

During the simulated annealing optimisation, the probability P that a new parameter set is accepted is given by equation (2.101).

$$P = e^{-\left[\frac{\Delta(\Sigma dev^2/dof)}{RT}\right]} \tag{2.101}$$

where T is a virtual temperature, R represents a virtual gas constant and $\Delta\Sigma dev^2/dof$ is the change in $\Sigma dev^2/dof$ for the tested change in the parameter set. As a consequence, increases in $\Sigma dev^2/dof$ will be accepted less and less frequently upon gradually lowering the virtual

temperature *T*. Post fitting, error margins are visualised through the SA "trajectories" which are saved during the optimisation. Reducing the D+1 dimensional trajectory (with D the number of variables that are optimised and the extra variable being $\Sigma dev^2/dof$) to a three dimensional surface, the error margins can be visualised. In practice, dividing the range of values for two particular variables into X and Y consecutive ranges of values (bins) will result in a combination of X by Y bins of ranges of the values for two of the optimisable parameters. For each combination (bin), the lowest $\Sigma dev^2/dof$ is indentified and this value is plotted against the optimisable parameters.

2.6.8 Calorimetry and Van't Hoff plot

ITC is another technique that is able to distinguish between dimerisation and stepwise self aggregation. The equations describing the heat effects of dimerisation and stepwise self aggregation are identical, apart from a factor of 2, such that if K_{dim}=A then K_{agg}=A/2 and if ΔH_{dim}=B then ΔH_{agg}=B/2. The factor of 2 differences, however, allows the use of Van't Hoff[52] and Clark Glew[53] equations to distinguish between the two processes. The Van't Hoff and Clark Glew equations describe the temperature dependence of equilibrium constant and are derived starting from equation 2.102.

$$\Delta G = \Delta H - T\Delta S = -RTlnK \qquad (2.102)$$

According to the Gibbs - Helmholtz equation, at fixed pressure equation 2.55 holds.

$$\frac{d[\Delta G]/T}{dT} = -\frac{\Delta H}{T^2} \qquad (2.103)$$

Hence,

$$\frac{d\,lnK}{dT} = -\frac{\Delta H}{RT^2} \tag{2.104}$$

Using the integrated form of equation 2.104, we express the dependence of the equilibrium constant K as a function of temperature T (Equation 2.105).

$$ln[K(T)] = ln[K(\theta)] + \int_{\theta}^{T} \left[\frac{\Delta H}{RT^2}\right] \cdot dT \tag{2.105}$$

The heat capacity (ΔC_p) is given by equation 2.106.

$$\Delta C_p = \left(\frac{d\Delta H}{dp}\right)_T \tag{2.106}$$

If we assume that ΔC_p is independent of temperature, ΔH is a linear function of temperature and is given by equation 2.107.

$$\Delta H(T) = \Delta H(\theta) + \Delta C_p(T - \theta) \tag{2.107}$$

Following substitution of equations (2.106) and (2.107) into (2.105), some rearrangements yield the Clark Glew equation (Equation 2.108).

$$[K(T)] = ln[K(\theta)] + \frac{\Delta H(\theta)}{R} \cdot \left[\frac{1}{\theta} - T^{-1}\right] + \left[\frac{\Delta C_p}{R}\right] \cdot [T^{-1} \cdot \theta - 1 - ln(T^{-1} \cdot \theta)] \tag{2.107}$$

Equation 2.108 shows that plotting ln(K) against 1/T allows the determination of the enthalpy and heat capacity of the interaction. Alternatively, we can predict the values for ln(K) at different temperatures, based on the equilibrium constant at 25 °C, together with the enthalpies and heat capacities of self aggregation as determined calorimetrically.

References

1. Frank, H. S., *J. Chem. Phys.* **1945,** *13* (11), 478-492.
2. Davies, D. B.; Djimant, L. N.; Veselkov, A. N., *J. Chem. Soc., Faraday Trans.* **1996,** *92* (3), 383-390.
3. Veselkov, A. N.; Djimant, L. N.; Karawajew, L. S.; Kulikov, E. L., *Stud. Biophys.* **1985,** *106* (3), 171-180.
4. Mazzini, S.; Bellucci, M. C.; Dallavalle, S.; Fraternali, F.; Mondelli, R., *Org. Biomol. Chem.* **2004,** *2* (4), 505-513.
5. Loontiens, F. G.; Regenfuss, P.; Zechel, A.; Dumortier, L.; Clegg, R. M., *Biochemistry* **1990,** *29* (38), 9029-9039.
6. Chaires, J. B.; Dattagupta, N.; Crothers, D. M., *Biochemistry* **1982,** *21* (17), 3927-3932.
7. Hayakawa, E.; Furuya, K.; Ueno, H.; Kuroda, T.; Moriyama, M.; Kondo, A., *Chem. Pharm. Bull.* **1991,** *39* (4), 1009-1012.
8. Braswell, E. H., *J. Phys. Chem.* **1984,** *88* (16), 3653-3658.
9. Chen, Z. J.; Stepanenko, V.; Dehm, V.; Prins, P.; Siebbeles, L. D. A.; Seibt, J.; Marquetand, P.; Engel, V.; Wurthner, F., *Chem.-Eur. J.* **2007,** *13* (2), 436-449.
10. Stoncius, S.; Orentas, E.; Butkus, E.; Ohrstrom, L.; Wendt, O. F.; Warnmark, K., *J. Am. Chem. Soc.* **2006,** *128* (25), 8272-8285.
11. Giuseppone, N.; Schmitt, J. L.; Allouche, L.; Lehn, J. M., *Angew. Chem. Int. Ed.* **2008,** *47* (12), 2235-2239.
12. Arnaud, A.; Bouteiller, L., *Langmuir* **2004,** *20* (16), 6858-6863.
13. Obert, E.; Bellot, M.; Bouteiller, L.; Andrioletti, F.; Lehen-Ferrenbach, C.; Boue, F., *J. Am. Chem. Soc.* **2007,** *129* (50), 15601-15605.
14. Seki, T.; Yagai, S.; Karatsu, T.; Kitamura, A., *J. Org. Chem.* **2008,** *73* (9), 3328-3335.
15. Haq, I.; Jenkins, T. C.; Chowdhry, B. Z.; Ren, J. S.; Chaires, J. B., *Energetics of Biological Macromolecules, Part C* **2000,** *323*, 373-405.
16. Davis, J. T., *Angew. Chem. Int. Ed.* **2004,** *43* (6), 668-698.
17. Murakami, K., *Dyes Pigm.* **2002,** *53* (1), 31-43.
18. Zhao, D. H.; Moore, J. S., *Org. Biomol. Chem.* **2003,** *1* (20), 3471-3491.
19. Muller-Dethlefs, K.; Hobza, P., *Chem. Rev.* **2000,** *100* (1), 143-167.
20. Martin, R. B., *Chem. Rev.* **1996,** *96* (8), 3043-3064.
21. West, W.; Pearce, S., *J. Phys. Chem.* **1965,** *69* (6), 1894-&.
22. Yang, Y. C.; Ward, J. R.; Seiders, R. P., *Inorg. Chem.* **1985,** *24* (12), 1765-1769.
23. Wurthner, F.; Yao, S.; Debaerdemaeker, T.; Wortmann, R., *J. Am. Chem. Soc.* **2002,** *124* (32), 9431-9447.
24. Chen, Z. J.; Lohr, A.; Saha-Moller, C. R.; Wurthner, F., *Chem. Soc. Rev.* **2009,** *38* (2), 564-584.
25. van der Schoot, P.; Michels, M. A. J.; Brunsveld, L.; Sijbesma, R. P.; Ramzi, A., *Langmuir* **2000,** *16* (26), 10076-10083.
26. Kegeles, G., *J. Phys. Chem.* **1979,** *83* (13), 1728-1732.
27. Mikheeva, L. M.; Grinberg, N. V.; Grinberg, V. Y.; Khokhlov, A. R.; de Kruif, C. G., *Langmuir* **2003,** *19* (7), 2913-2921.

28. Tai, M. S.; Kegeles, G., *Biophys. Chem.* **1984,** *20* (1-2), 81-87.

29. Evstigneev, M. P.; Mykhina, Y. V.; Davies, D. B., *Biophys. Chem.* **2005,** *118* (2-3), 118-127.
30. Davies, D. B.; Veselkov, D. A.; Kodintsev, V. V.; Evstigneev, M. P.; Veselkov, A. N., *Mol. Phys.* **2000,** *98* (23), 1961-1971.
31. Cohen, Y.; Avram, L.; Frish, L., *Angew. Chem. Int. Ed.* **2005,** *44* (4), 520-554.
32. Price, W. S., *Concepts Magn. Reson.* **1997,** *9* (5), 299-336.
33. Paul, A.; Griffiths, P. C.; Pettersson, E.; Stilbs, P.; Bales, B. L.; Zana, R.; Heenan, R. K., *J. Phys. Chem. B* **2005,** *109* (33), 15775-15779.
34. Buurma, N. J.; Haq, I., *J. Mol. Biol.* **2008,** *381* (3), 607-621.
35. Evans, D. F.; Wennerstrom, H., *The Colloidal Domain: Where Physics, Chemistry, Biology and Technology Meet, 2nd Ed.* **1999**, 539-597.
36. ISIS www.ISIS.rl.uk
37. King, S. M., *Small Angle Neutron Scattering; ISIS Facility; Oxford:* **2003**.
38. Eastoe, J., *Scattering Techniques* **2003**.
39. Scatchard, G., *Ann. N.Y. Acad. Sci.* **1949,** *51* (4), 660-672.
40. McGhee, J. D.; Hippel, P. H. V., *J. Mol. Biol.* **1974,** *86* (2), 469-489.
41. Eriksson, M.; Norden, B., *Drug-Nucleic Acid Interactions* **2001,** *340*, 68-98.
42. Garbett, N. C.; Ragazzon, P. A.; Chaires, J. B., *Nat. Protoc.* **2007,** *2* (12), 3166-3172.
43. Job, P., *Ann Chim.* **1928,** *9*, 113-203.
44. Suh, D.; Chaires, J. B., *Bioorg. Med. Chem.* **1995,** *3* (6), 723-728.
45. Lerman, L. S., *J. Mol. Biol.* **1961,** *3* (1), 18-30.
46. Satyanarayana, S.; Dabrowiak, J. C.; Chaires, J. B., *Biochemistry* **1993,** *32* (10), 2573-2584.
47. Cohen, G.; Eisenber.H, *Biopolymers* **1969,** *8* (1), 45-55.
48. Buurma, N. J.; Haq, I., *Methods* **2007,** *42* (2), 162-172.
49. Press, W. H.; Flannery, B. P.; Teukolsky, S. A.; Vetterling, W. T., *Numerical Recipes in Pascal* **2004**, 270.
50. Kirkpatrick, S.; Gelatt, C. D.; Vecchi, M. P., *Science* **1983,** *220* (4598), 671-680.
51. Metropolis, N.; Rosenbluth, A. W.; Rosenbluth, M. N.; Teller, A. H.; Teller, E., *J. Chem. Phys.* **1953,** *21* (6), 1087-1092.
52. Van't-Hoff, J. H., *Etudes de Dynamique Chimique* **1884**.
53. Clarke, E. C. W.; Glew, D. N., *Trans. Faraday Soc.* **1966,** *62*, 539-547.

Chapter 3

SYNTHESIS OF CONJUGATED OLIGOHETEROAROMATICS

Abstract:

Literature examples of oligo- and polythiophene synthesis are presented in this chapter, with an emphasis on those using Stille and Suzuki cross-coupling reactions. The synthesis and characterisation of short cationic conjugated oligoheteroaromatics that are building blocks for conjugated polymeric DNA binders is described. The preparation of extended substituted oligothiophenes via microwave Pd assisted catalysis is similarly reported.

3.1 Introduction

Generally, oligo- and polythiophenes are the most important classes of π-conjugated materials owing to their frequent use as active components in organic electronic devices and molecular electronics. Due to their stability in various oxidation states; their optical and redox properties; and their self-assembling properties in solid state or in bulk solution (Section 4.1), a multitude of various functionalised oligo- and polythiophenes have been established and characterised.[1] Thiophene chemistry is already well-known, but it is remarkable that thiophenes are building blocks for transition metal-catalysed cross-coupling reactions.[2] Additionally, the high polarisability of sulfur atoms in thiophene rings stabilises the conjugated chain and leads to excellent charge transport properties – one of the most important requirements for applications in organic and molecular electronics.[3] This section briefly introduces examples of oligo- and polythiophenes synthesised by different methods, *e.g.*, Pd mediated cross-coupling reaction and oxidative coupling reactions.

3.1.1 Literature examples of oligo- and polythiophene synthesis by Pd cross-coupling reactions

In 1994, the first functionalised bithiophene **3.1** obtained *via* Stille cross-coupling was reported. Only a few years later this substituted bithiophene was employed in the regioselective synthesis of head-to-head and tail-to-tail substituted quarter- and sexi-oligothiophenes **3.2** and **3.3** (Scheme 3.1).[4]

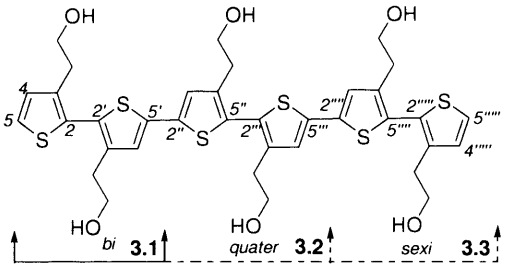

Scheme 3.1

The same group further reported the synthesis and application of oligothiophene isothiocyanates as luminescent markers for biomolecules.[5] Conjugated framework **3.4** was again synthesised by a Stille cross-coupling reaction (Scheme 3.2). The synthetic sequence for the transformation of the alcohol into corresponding isothiocyanate **3.5** involved four steps: synthesis of mesylate, followed by the formation of the azide, then the azide was reduced to an amine and subsequently transformed into the isothiocyanate.

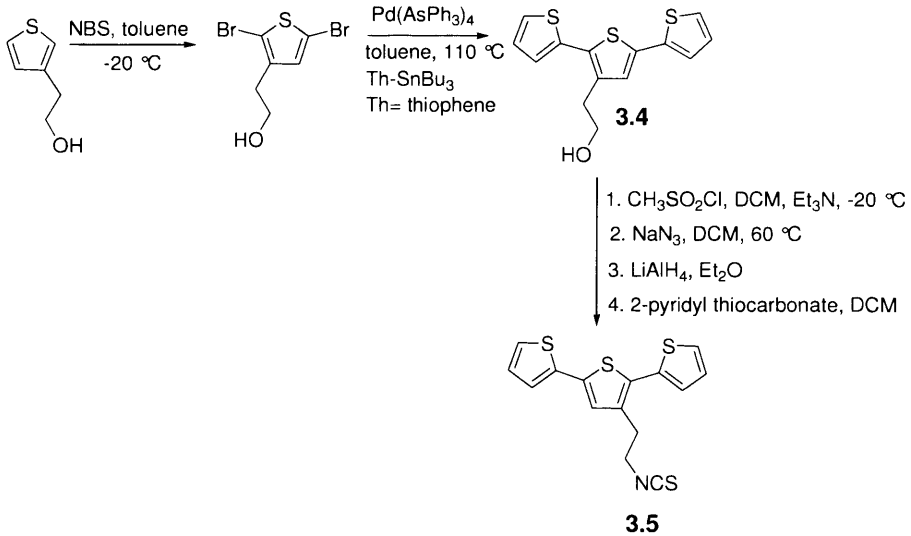

Scheme 3.2

In the same year, Ewbank *et al.* reported regioregular polythiophenes carrying an alkylamine as a side chain using a CuO-modified Stille coupling reaction (Scheme 3.3).[6] Polymer **3.6** was soluble in water, but not highly conjugated, adopting a twisted conformation.

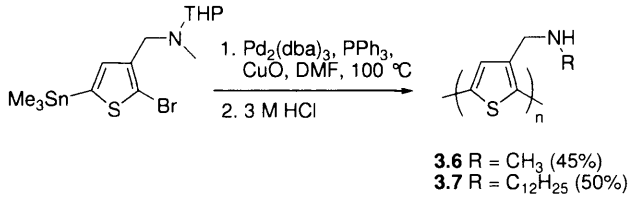

3.6 R = CH_3 (45%)
3.7 R = $C_{12}H_{25}$ (50%)

Scheme 3.3

The disadvantage of the Stille cross-coupling reaction is the use of an organotin reagent which is very toxic. From this point of view, Suzuki reactions are preferable because they are more environmentally friendly. In 1998, Bidan *et al.*[7] proposed the synthesis of oligo(3-octylthiophenes) **3.9** by repetitive use of Suzuki cross-coupling reactions (Scheme 3.4). One of the two α–reactive positions on the thiophene ring was blocked throughout the entire synthesis by a non-reactive chloride group in order to control the chain growth. To obtain unprotected oligo(3-octylthiophenes) **3.9**, protected **3.8** was subject of the reductive dehalogenation with H_2 over Pd/C or by using tributyl tinhydride in the presence of AIBN.

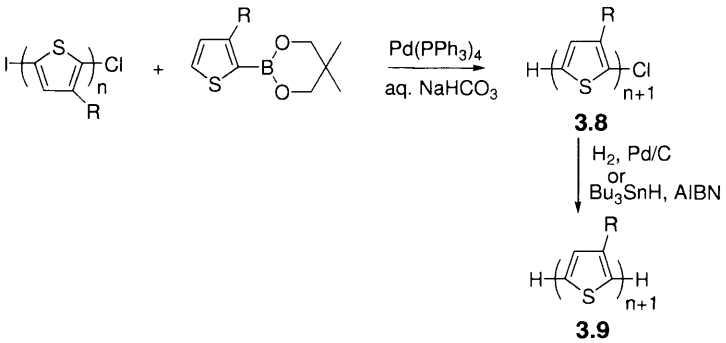

Scheme 3.4

One year later, Bäurle *et al.*[8] developed a selective method for the synthesis a head-to-tail (HT) coupled oligo(3-dodecylthiophenes) (Scheme 3.5). First, one reactive position on the oligothiophene was blocked using a benzyl ester allowing selective iodination on the other end. Secondly, boronated bithiophene **3.10** was coupled with iodinated species **3.11** by a Suzuki cross-coupling reaction to build up the benzyl ester-substituted oligothiophenes **3.12.**

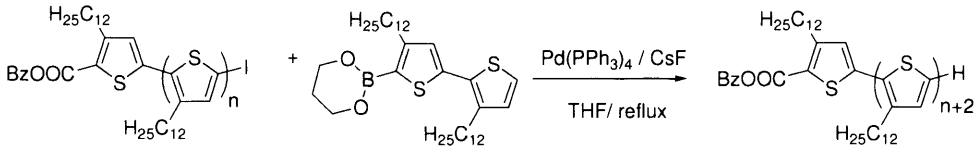

Scheme 3.5

The same idea was used later, when substituted thiophene **3.13** was coupled by Suzuki reaction with boronic ester **3.12** to obtain the head to tail dihexyl bithiophene **3.14** (Scheme 3.6).[9]

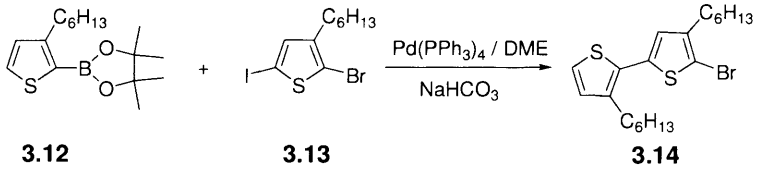

Scheme 3.6

Due to the reactivity difference between aryl bromines and iodides in Suzuki reactions, the bromide functionality of **3.14** was left unreacted during the reaction and was later involved in another cross-coupling type reaction, *viz.* a Negishi reaction (Scheme 3.7).

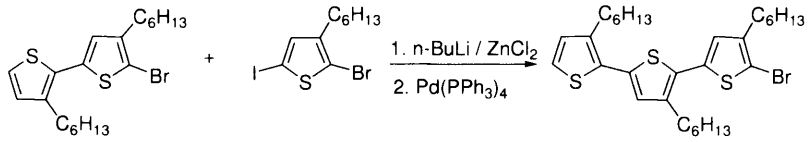

3.15

Scheme 3.7

Recently, bromo-substituted thiophene **3.16** was coupled with bisborylated thiophene to give the terthiophene **3.17.**[10] Oxidative polymerisation of terthiophene **3.17** led to the zwitterionic polythiophenes **3.18** with 3-5 repetitive units (Scheme 3.8).

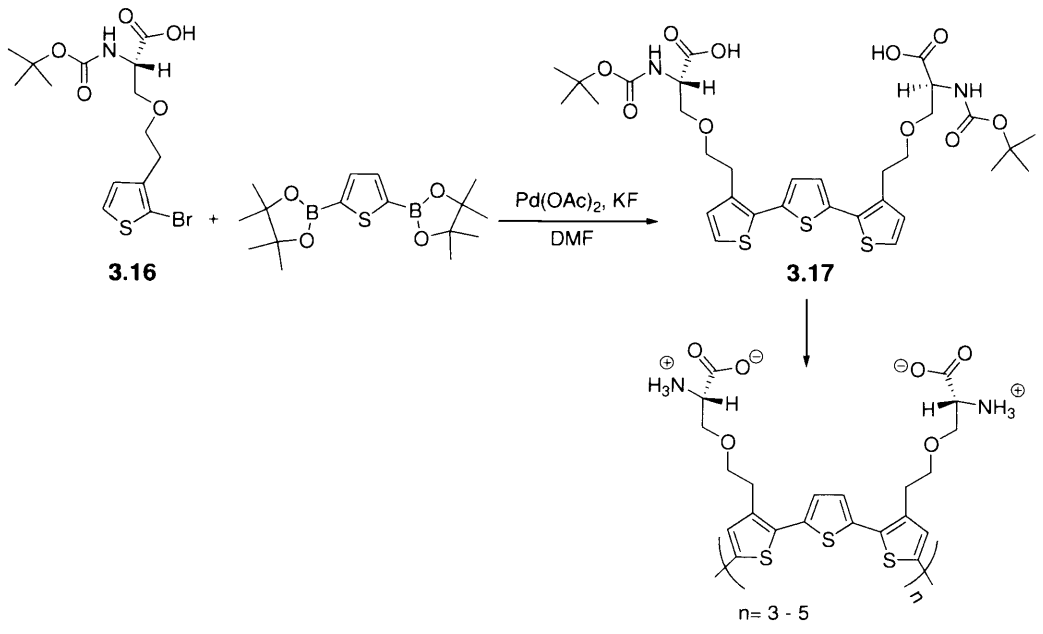

3.16 **3.17** **3.18**

Scheme 3.8

In some of these examples, the Suzuki cross-coupling reaction shows formation of by-products resulting from demetallation or dehalogenation of the starting materials or from homo-coupling of boronic acids or esters in the presence of oxygen.[11, 12] Moreover, catalyst

traces could be present at the end of any cross-coupling reaction and these could alter the electronic properties of the conjugated materials. To overcome all these obstacles, variations of cross-coupling reactions are available. These methods include either microwave irradiation,[13, 14] solid-phase strategies[15] and the development of MIDA esters as protective groups for boronic acids.[16, 17] An example of solid phase strategies is the synthesis of head-to-tail oligo(3-hexylthiophene) **3.20** on a chloromethylated polystyrene resin support (Scheme 3.9).[18] Bithiophene carboxylic acid **3.19** was immobilized on the resin support using an ester linker and the oligothiophene was built-up by repetitive iodination and Suzuki cross-coupling reactions. To release the oligomer from the support, a transesterification reaction was applied followed by a treatment with iodomethane.

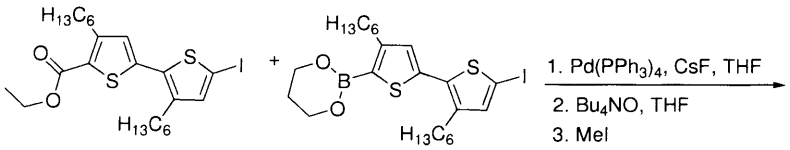

3.19

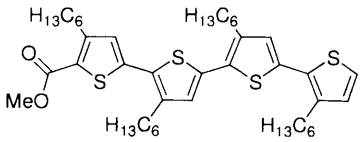

3.20

Scheme 3.9

3.1.2 Literature examples of oligo- and polythiophenes by Pd-microwave assisted catalysis

In 2002, Barbarella and coworkers[19] showed the efficient use of microwave-assisted catalysis in the synthesis of soluble oligothiophenes **3.21** and **3.22** *via* Suzuki cross coupling reactions

(Scheme 3.10). The reaction time did not exceed 5 min and no side-products could be observed at the end of the reaction. When the reaction was performed under standard conditions, *i.e.* without microwave irradiation, the oligothiophenes were obtained in very poor yield.

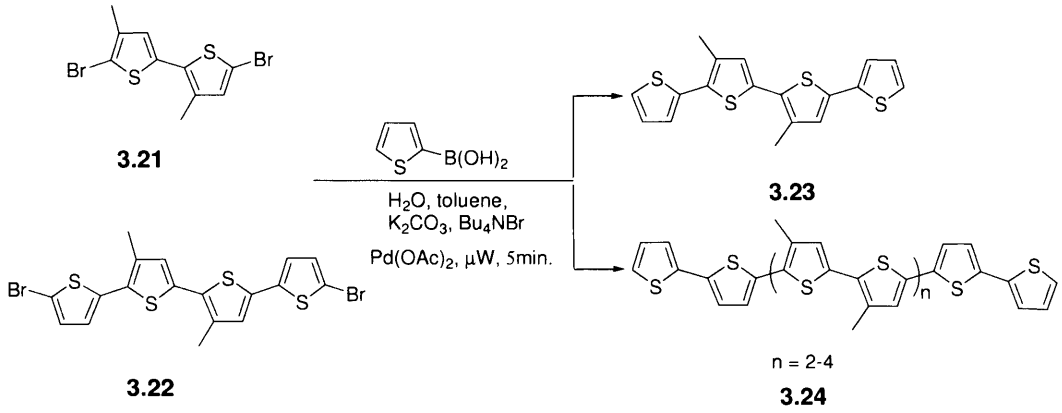

Scheme 3.10

Several attemps to use the microwave irradiation in the synthesis oligothiophenes **3.23** and **3.24** by a Stille coupling of dibromo substituted bithiophene **3.21** or dibromo substituted quaterthiophene **3.22** with 2-tributylstannyl thiophene were unsuccessful.[19] Barbarella's hypothesis is that both halogen exchange reaction and subsequent coupling of metallated-halogenated intermediates compete against the desired Stille cross coupling reaction. Two years later, McCulloch and colaborators[20] published interesting results on the synthesis of polythiophenes by a microwave-assisted Stille coupling reaction (Scheme 3.11). The solvent effect in this reaction seems to be very important in order for efficient microwave heating. The solvent needs to solubilise the polymer product and have a high boiling point. By using chlorobenzene as a solvent for this coupling reaction, the authors synthesised

poly(3,3''-dioctyl-2,2':5'2''-terthiophene) **3.25** which could be successfully used as a semiconducting layer in the fabrication of organic field-effect transistor devices (OFET).

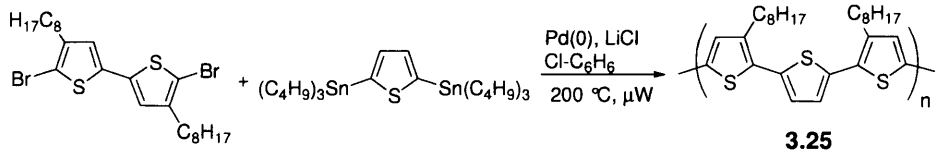

3.25

Scheme 3.11

The success of the PEPPSI-iPr catalyst in basic cross-coupling reactions has led to extensive application of this catalyst.[21] An example is the use of PEPPSI-iPr catalyst in combination with microwave-assisted catalysis to obtain terthiophene **3.26.**[22] This building block was subsequently polymerised by an oxidative homocoupling reaction in the presence of $FeCl_3$ and TBA-triflate as an oxidant (Scheme 3.12).

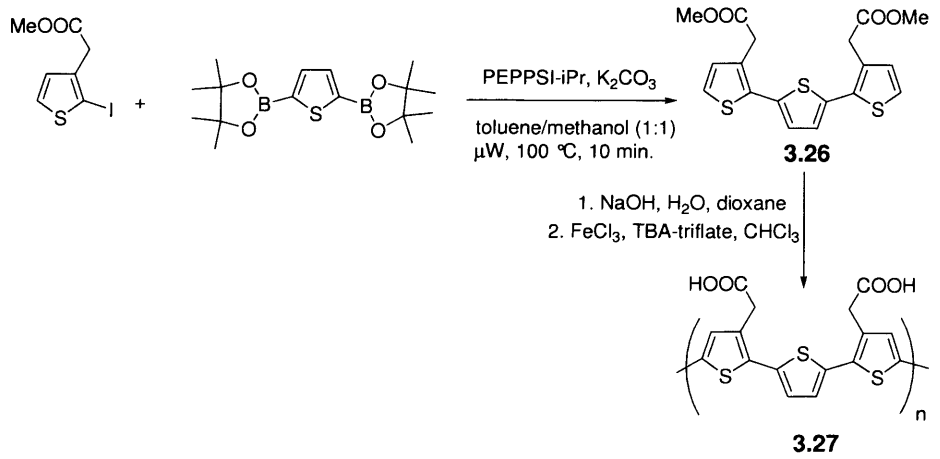

3.26

3.27

Scheme 3.12

As an alternative, the solvent-free microwave-assisted catalysis using Al_2O_3 as a solid support allows the synthesis of extended oligothiophenes in high yield (Scheme 3.13).[23] While the coupling of dibromo bithiophene **3.28** with thiophene boronic acid afforded the quaterthiophene **3.29** in 81% yield (path A), the coupling of monobromo thiophene **3.30** with

diborolane bithiophene **3.31** reduced the yield to 40% (path B). The isolated yield could be controlled by choosing the appropriate bromide and borolane derivatives. Furthermore, the same quaterthiophene was obtained by coupling 2-bromobithiophene **3.32** with bis(pinacolato)-diboron **3.33** through the *in situ* generation of thiophene boronic ester (path C).

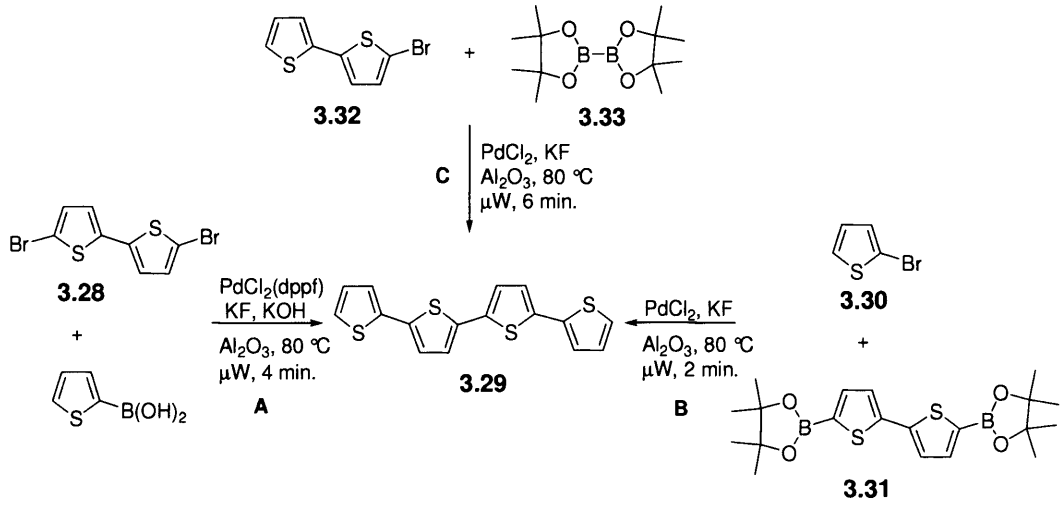

Scheme 3.13

Other synthetic routes used chitosan or silica supported Pd-catalysts for the synthesis of quaterthiophene **3.29.**[24] Although the reaction needs a longer time to reach completition, *e.g.* 100 min, the Pd catalyst was reusable up to 10 times. Compared to the solvent-free microwave-assisted reaction this method provides greater yields and uses thienyl diiodides instead of thienyl dibromides. Moreover, this approach is "greener" than the existing homogeneous Pd catalysis.

3.1.2 Literature examples of oligo- and polythiophenes by oxidative coupling reactions

Oxidative polymerisation of thiophene with $FeCl_3$ in chloroform is currently the most commonly exploited oxidative method to synthesise 3- and 3,4-substituted polythiophenes (Scheme 3.14).

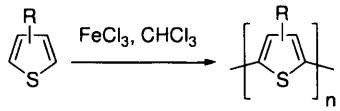

Scheme 3.14

Choosing suitable substituents at the 3-position in polythiophenes offers the possibility to improve the solubility and processability of poly(alkylthiophene)s. However, polymerisation of unsymmetrical thiophenes will result in regio-irregular coupling of thiophene rings along the polymer chain.[25, 26] As a result a mixture of head-to-tail (HT), head-to-head (HH) and tail-to-tail (TT) coupled monomers can be obtained (Scheme 3.15).

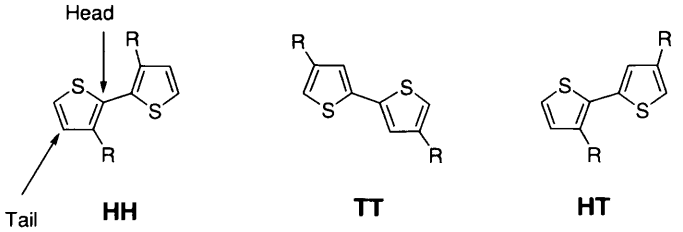

Scheme 3.15

Moreover, the polymer will show different chain lengths as a consequence of the side-chain reactions which can take place on the α–position of the polythiophene.[10, 27] Leclerc and coworkers showed that head-to-tail coupling is preferred for the synthesis of 3-alkoxy-4-

methyl polythiophene as a consequence of the presence of the alkoxy group which possesses more flexibility compared than the methyl group.[28]

Synthesis of oligothiophenes can be also carried out by oxidative homocoupling reactions of lithiothiophenes in the presence of $CuCl_2$. Following this method, oligothiophenes containing a dodecyl chain as a solubiliser group was first reported in 1996 by Bäuerle *et al.* (Scheme 3.16).[29]

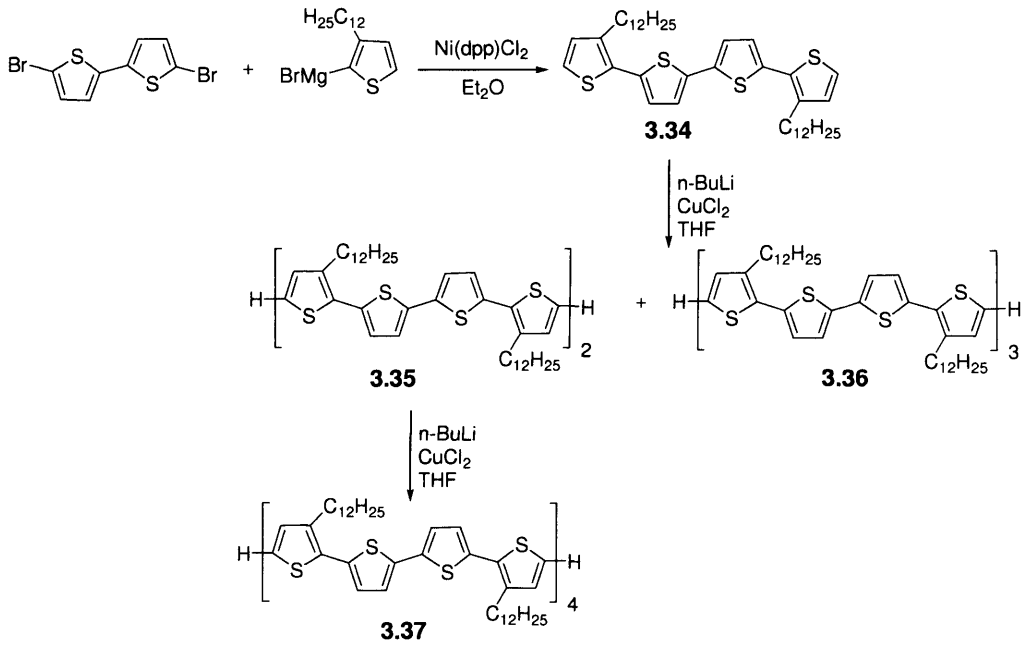

Scheme 3.16

The lithiation of quaterthiophene **3.34** with 1 eq. of n-BuLi in THF led, after oxidation, to the formation of a mixture of oligothiophenes **3.35** and **3.36**. The two oligomers could be isolated in 30% and 8% yield respectively, after purification several times. Using the same steps, octomer **3.35** was coupled to obtain oligothiophene **3.37** in 19% yield after purification. Usually the α-protons in longer thiophenes are more acidic than the shorter ones.

As a consequence the lithiation by deprotonation always includes the dilithiaton and formation of the dimer as a byproduct. Additionally, the reaction is less selective with increasing chain length of the oligothiophene. Preliminary investigations of oxidative homocoupling of 3-substituted thiophene have been also done in Buurma's group.[30] Two substituted thiophene **3.38** were coupled by direct lithiation reaction followed by transmetallation with copper salts. The resulted organocuprate intermediate was then oxidised to **3.39** (Scheme 3.17).

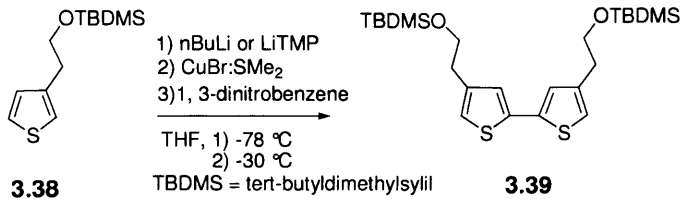

3.38 **3.39**

Scheme 3.17

3.1.3 Regioselectivity of lithiation reactions of thiophenes

A series of investigations have been done in order to find a highly selective method to synthesise 3,5-and 2,3-disubstituted thiophenes. The treatment of THP protected 3-ethanolthiophene with alkyllithium base like ^{n}BuLi in hexane led to a very selective formation of 2,3-disubstituted thiophene **3.40** in 98% yield. In contrast, when TBDMS protected thiophene was treated with 1.0 equivalents of LiTMP (a hindered amide base) in THF, the major product was 3,5-disubstituted thiophenes **3.41.**

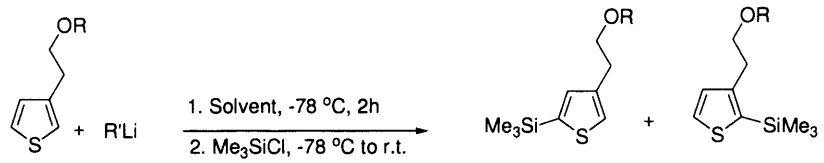

Scheme 3.18

These results can be explained by both steric hinderence of the bulky protecting group and the solvent which act against the chelating effect of the side chain (Figure 3.1).

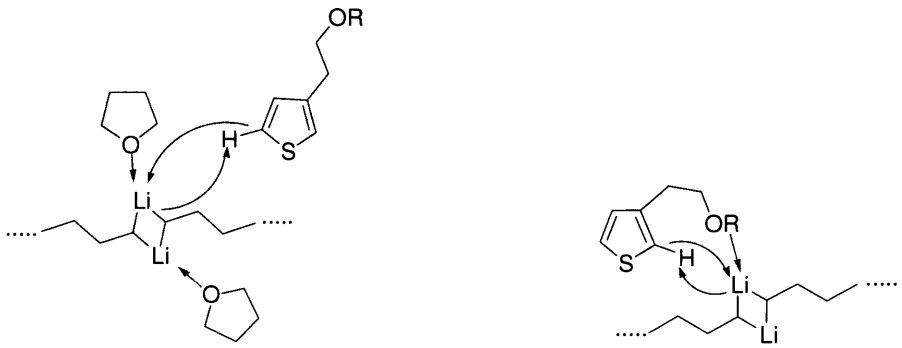

a) b)

Figure 3.1 Influence of the solvent in the lithiation reaction: a) Lithium coordinated by THF; b) Lithium coordinated by oxygen atom in hexane.

It is known that hexane is not an electron donor solvent and as a consequence the only electron donor present in solution is the oxygen atom on the thiophene side chain. This oxygen directs the lithiation to the nearest favourable position, leading to formation of **3.40** as a major product (Figure 3.1b). In contrast, THF is a better electron donor than hexane and is able to form aggregates with lithium atoms. In this case, the THP protecting group does no longer acts against the chelating effect of the side chain, directing the deprotonation to the

other side (Figure 3.1a). These studies helped us to find a selective lithiation method to functionalise 3-ethanolthiophene needed for the synthesis of dicationic terthiophenes *(vide infra).*

3.2 Results and discussions

3.2.1 Synthesis of mono-cationically substituted oligoheteroamatics

A series of conjugated monocationic oligoheteroaromatics were designed and synthesised starting from commercially available 3-(2-hydroxyethyl)thiophene (Scheme 3.19).

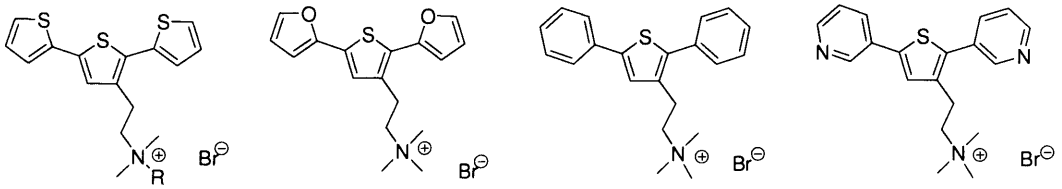

3.41 R=CH_3
3.42 R= CH_2CH_2OH
3.43 R=$CH_2CH_2OCH_2CH_2OH$

3.44 **3.45** **3.46**

Scheme 3.19

The bromination of 3-(2-hydroxyethyl)thiophene **3.47** with two equivalents of *N*-bromo-succinimide at room temperature in DMF led to 2,5-dibromo-3-(2-hydroxyethyl)thiophene **3.48** in 85% yield (Scheme 3.20).

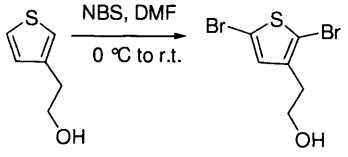

3.47 **3.48**

Scheme 3.20

The dibromide **3.48** was further used as building block in the construction of cationic oligothiophenes **3.41-3.46** (Scheme 3.21).

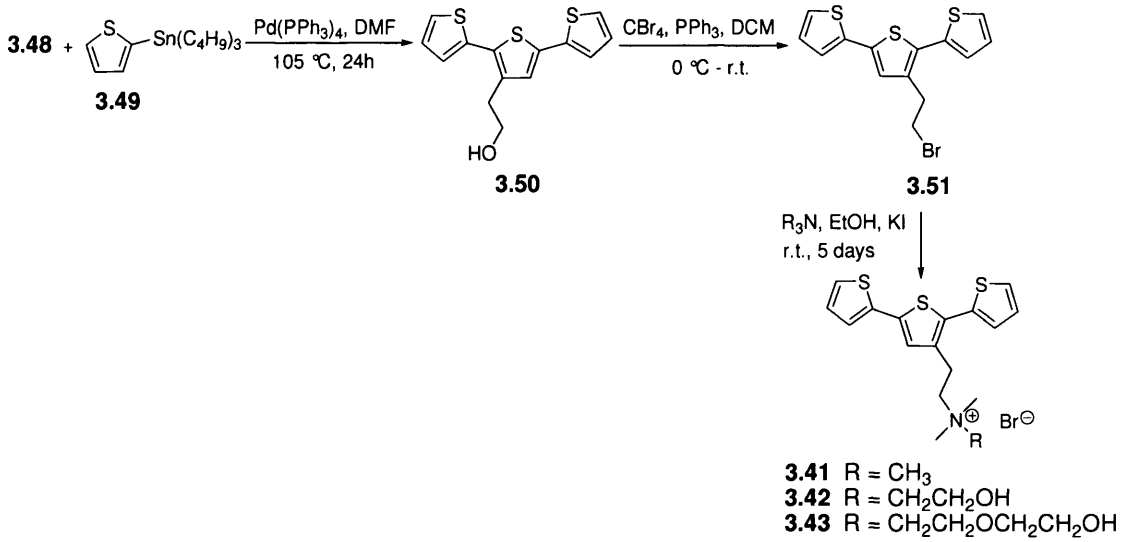

Scheme 3.21

The key synthetic step was the synthesis of the conjugated oligoheteroaromatic framework using Stille cross-coupling reactions. We modified the Stille procedure previously reported by Barbarella and coworkers, replacing the $Pd(AsPh_3)_4$ catalyst and the solvent. 2,5-dibromo-3-(2-hydroxyethyl)thiophene **3.48** was coupled with 2-(tributylstannyl)thiophene **3.49**, in the presence of $Pd(PPh_3)_4$ as a catalyst in DMF at 105 °C, and 3'-(2-hydroxyethyl)-2, 2':5', 2''-terthiophene **3.50** was obtained in 78% yield. Following the coupling reaction to give conjugated oligothiophene **3.51**, an Appel reaction[31] was used for converting the hydroxyl group into the bromide. A side chain alcohol was treated with a mixture of CBr_4 and PPh_3, both in excess. Initially, this step was a problematic step in our synthesis and different conditions were tested in order to optimise the reaction. If the water is present in the reaction,

this has a very unfavorable effect on the yield. Additionally, it has been found that the reaction depends on the nature of CBr_4. If the reaction is performed with 1.5 equivalents of new CBr_4, only traces of product could be observed. Adding additional new CBr_4 and PPh_3 (5 equivalents in excess) does not drive the reaction to completion and we do not obtain the desired product. When 1.5 equivalents of a mixture of old CBr_4 and PPh_3 were added to a solution of terthiophene **3.50** in extra dry DCM, at 0 °C under a nitrogen atmosphere, bromide **3.51** was obtained as a solid in 82% yield. Remarkably, restarting a sealed bromination reaction involving new CBr_4 through the addition of old CBr_4 does not work. The final step for the synthesis of cationic terthiophenes **3.41–3.43** involved the conversion of the terminal bromide **3.51** into the corresponding quaternary ammonium salt by a substitution reaction. The step consists of adding the required amines *viz.* trimethylamine, *N*,*N*-dimethylethanolamine or 2-(2-dimethylaminoethoxy)ethanol in ethanolic solution in the presence of catalytic amount of KI. This gave ammonium salts **3.41–3.43** in moderate yield. Based on the success of the synthetic schemes used for **3.41–3.43**, we decided to apply the same strategies for the synthesis of cationic oligoheteroaromatic **3.44** (Scheme 3.22).

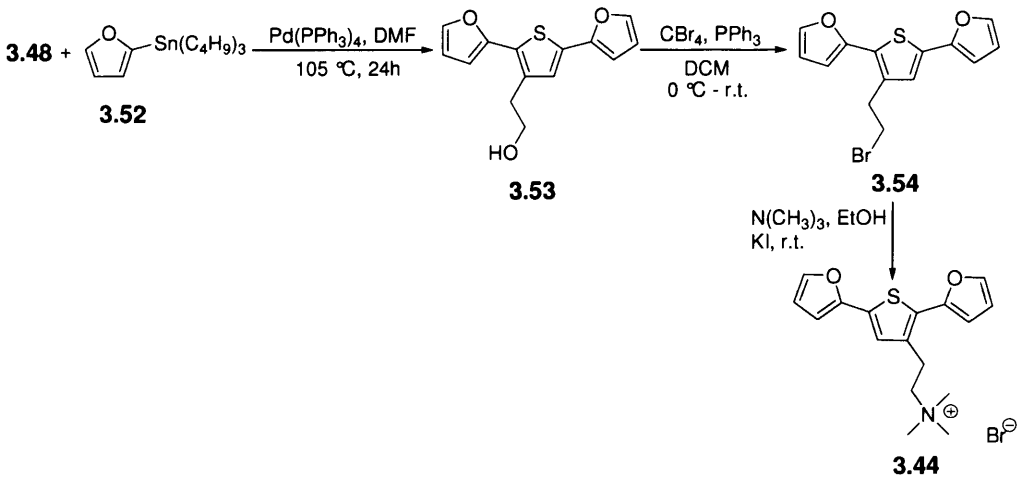

Scheme 3.22

Again, we chose to perform a Stille cross-coupling reaction for the synthesis of conjugated 2-(2,5-di(furan-2-yl)thiophene-3-yl)ethanol **3.53.** 2,5-dibromo-3-(2-hydroxyethyl)thiophene **3.48** was reacted with 2-(tributylstannyl)furan **3.52,** in the presence of $Pd(PPh_3)_4$ as catalyst, in DMF at 105 °C, affording **3.53** in 90% yield. The optimised conditions mentioned for the Appel reaction (*vide supra*) were replicated during the synthesis of bromide **3.54**. The desired bromide **3.54** was obtained in 73 % yield. In the last step, bromide **3.54** was treated with a large excess of trimethylamine solution in ethanol producing ammonium salt **3.44** in 41% yield.

The use of a Suzuki cross-coupling reaction was investigated in the synthesis of cationic **3.45** (Scheme 3.23).

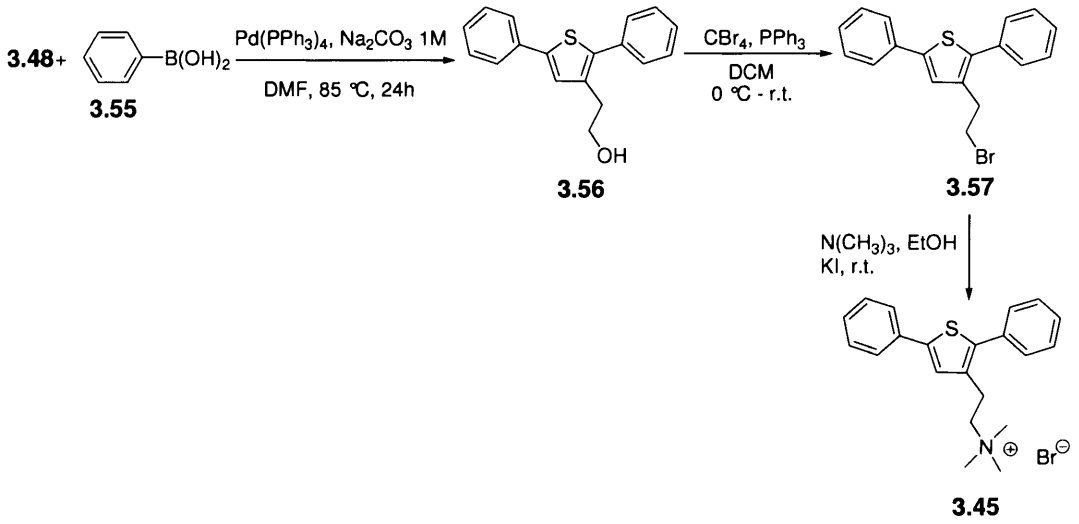

Scheme 3.23

The Suzuki coupling reaction is a challenging step in this synthesis of **3.43** with regard to reaction conditions, yield and purification of the desired product. A first attempt at the Suzuki coupling reaction was carried out in THF for 4 days, in the presence of $Pd(PPh_3)_4$ catalyst and aq. 1M $NaHCO_3$ solution as a base. This reaction was found not to have worked well as we as expected, achieving the desired product in a mediocre yield of 39%. Furthermore, purification of the crude product presented problems due to both mono- and di-substituted products eluting with a very similar retention factor. In a second attempt, the solvent was changed from THF to DMF, reducing the reaction time dramatically and leading to di-substituted product formation in 67% yield. The further steps in the synthesis of **3.45** were exactly the same as those carried out for cationic terthiophene **3.41–3.43** after the coupling reaction. The crude quaternary ammonium salt **3.45** was obtained as colourless needle-like crystals with a yield of 62 %.

Analogously, a ligand containing thiophene and pyridine moieties was synthesised starting from the same building block **3.48** (Scheme 3.24).

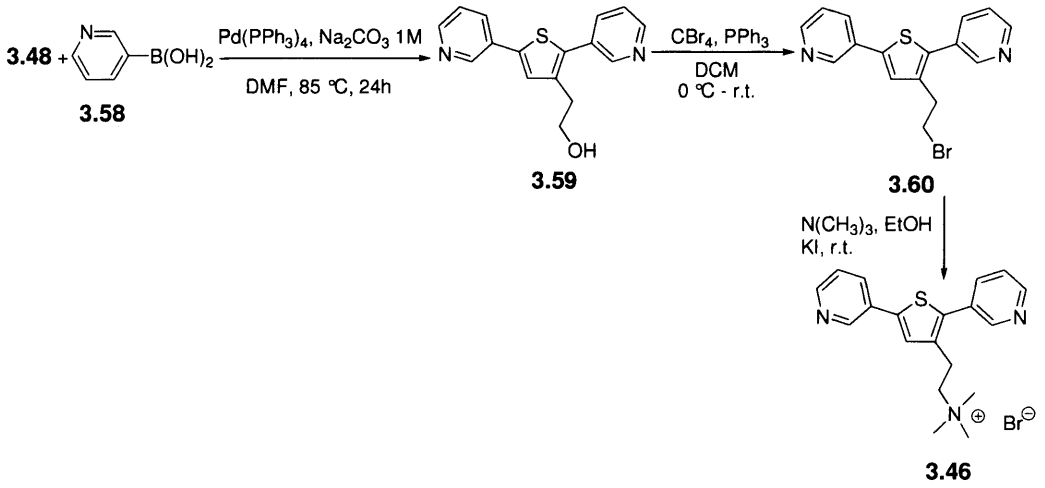

Scheme 3.24

The bromination reaction was the most unpredictable step in the synthetic route towards pyridine containing cationic oligomer. Bromide **3.60** is very unstable and it decomposes in the neat state. The decomposition of **3.60** is likely the result of intermolecular nucleophilic attack of the pyridine ring on the primary bromide. Immediate addition of trimethylamine solution in ethanol gave **3.46** in 53% yield.

3.2.2 Synthesis of dicationic oligothiophenes

Both dicationic oligothiophenes **3.61** and **3.62** (Scheme 3.25) were synthesised starting from the same commercially available 2-(3-thienyl)ethanol **3.47**.

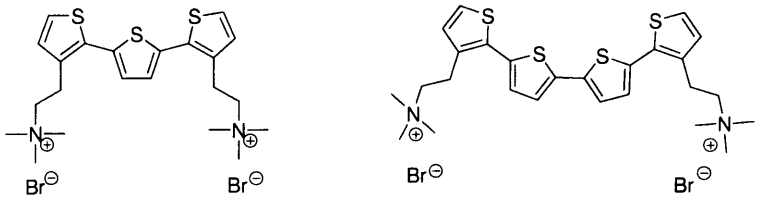

3.61 **3.62**

Scheme 3.25

Two routes were investigated for the synthesis of dicationic terthiophene **3.61** and these use different palladium-catalysed coupling reactions for the construction of the conjugated framework. The first route involved used a Stille cross-coupling reaction. To perform this route, the synthesis of tin intermediate **3.64** was required (Scheme 3.26).

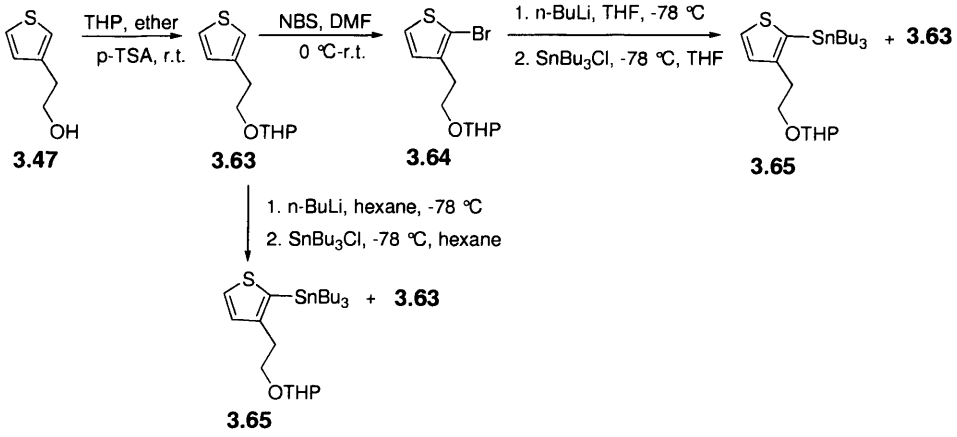

3.47 **3.63** **3.64** **3.65**

3.65

Scheme 3.26

First 3'-(2-hydroxyethyl)thiophene was protected with 3,4-dihydro-2H-pyran to give the 3-[2-(tetrahydroxypyranyloxy)ethyl]thiophene **3.63** in 80% yield. Based on earlier studies in Buurma's group on the selectivity of lithiation (*vide supra*), we lithiated **3.63** with n-BuLi in hexane. Unfortunately, the subsequent quenching of the lithiated species with tributyltin chloride provided the desired product **3.64** in only 10% yield. Because of disappointing yield

of the stannylation, we tested another route for the synthesis of **3.61**. The protected thiophene **3.63** was selectively brominated to give the monobrominated **3.64** in 70% yield. Li-Hal exchange and treatment of the subsequent thienyl lithium gave stannane **3.65** in 35% yield. Some debrominated 3-ethanolthiophene **3.63** was observed along with **3.65**. Moreover, other tin species were formed during the reaction (Bu_3Sn-$SnBu_3$, Bu_3Sn-O-$SnBu_3$). It was very difficult to purify **3.65** because it destanyllated when we carried out a purification by flash chromatography. This made impossible to use the intermediate **3.65** in a further Stille cross coupling reaction.

The second potential route for the synthesis of the conjugated framework of the dicationic terthiophene **3.62** involved a Suzuki cross-coupling reaction and uses commercially available 2,5-thiophenediboronic acid. 3-(2-hydroxyethyl)thiophene **3.48** was reacted with 1 equivalent of *N*-bromosuccinimide in DMF to obtain **3.66** in 77% yield (Scheme 3.27). Monobrominated thiophene **3.66** is a highly versatile building block in the construction of several oligothiophenes including dicationic oligothiophenes **3.61** and **3.62**.

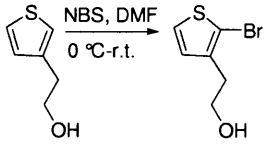

3.47 **3.66**

Scheme 3.27

Based on the literature reports,[22] we decided to apply a microwave-assisted Suzuki coupling in combination with PEPPSI-iPr as a catalyst for the synthesis of terthiophene **3.68** (Scheme 3.28).

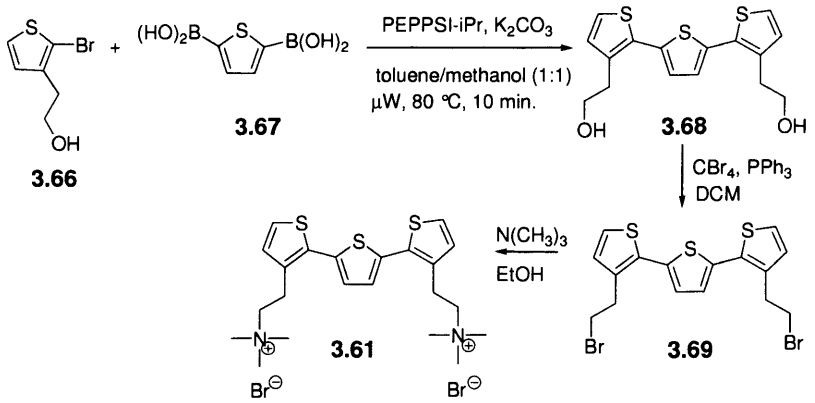

Scheme 3.28

3,3''-Di(2-hydroxyethyl)-2,2':5',2''-terthiophene **3.68** was obtained in 91% yield from previously synthesised **3.66** and commercially available 2,5-thiophenediboronic acid **3.67**. In the next step, the conversion of the side chain hydroxyl in bromide **3.69** was accomplished in 81% yield. Finally, **3.69** was treated with excess trimethylamine to give **3.61** in 68% yield. The same strategy was applied to the synthesis of dicationic quaterthiophene **3.62** (Scheme 3.29).

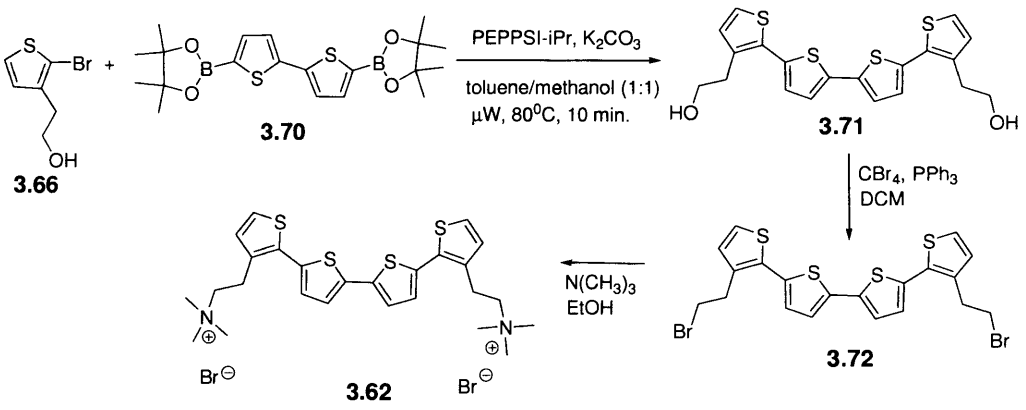

Scheme 3.29

The previously synthesised monobrominated thiophene **3.66,** was used in the microwave assisted Suzuki cross-coupling reaction with commercially available 2,2'-bithiophene-5,5'-diboronic acid bis(pinacol) ester **3.70** and the quaterthiophene **3.71** was obtained in 87% yield. In order to convert the hydroxyl functionality of **3.71** into the corresponding bromide **3.72,** the conjugated quaterthiophene **3.71** was treated with CBr_4 and PPh_3 in dry DCM. This gave **3.72** in 80% yield. The final step of the synthesis involved converting the terminal bromides into the corresponding quaternary ammonium salts **3.62** (72% yield).

3.3 Conclusions

Building on our proposed design for conjugated oligoheteroaromatics as building blocks for sequence selective conjugated polymers, we have synthesised a series of cationic oligoheteroaromatics. The key synthetic step is the synthesis of the conjugated oligoheteroaro-matic framework using Stille or Suzuki cross-coupling reactions. For synthesis of monocationic oligothiophenes we used classical Suzuki reaction, while the microwave-assisted catalysis was efficiently applied for synthesis of extended dicationic thiophenes. The Appel reaction was used for converting the hydroxyl group into the bromide. The final step of the synthesis involved conversion of the terminal bromide into a quaternary ammonium salt.

Acknowledgements

Dr. Rob Richardson is most gratefully acknowledged for stimulating discussions on many aspects of this chapter. I thank Simon Pascal, an Erasmus student in Burrma's group for

studies on regioselectivity of lithiation reactions of thiophenes. I also thank Josh Taylor for his help on the synthesis of intermediate **3.45**. I also thank Dr. Mark C. Bagley and Vincenzo Fusillo for their help with microwave-assisted reactions. Robert Jenkins is thanked for NMR technical support and Dave Walker for obtaining high resolution mass spectra.

3.5 Materials and methods

All starting materials were procured from known commercial sources and used without further purification. Solvents such as DCM, THF, Ether were dried using an MBraun solvent purification system. The Stille cross-coupling reaction was carried out under an N_2 atmosphere and the solvent was previously degassed. Suzuki cross-coupling reactions were carried out under an N_2 atmosphere under microwave heating. Solvents used in the Suzuki reactions were degassed using the freeze-pump-thaw method. The Pd catalyst was transferred to the reaction mixture under N_2 atmosphere using a glove bag. A computer controlled CEM-DISCOVER microwave reactor was used for irradiation. Microwave-assisted syntheses were conducted in 10 ml closed reactor tubes (maximum 5 ml working volume) under continuous stirring. The samples were irradiated for 10 minutes at 80 °C, applying 100 W power. Flash column chromatography was carried out using 60 Å silica. All oligothiophenes show strong fluorescence and were readily visualised on TLC plates using UV light. ^{1}H-NMR, ^{13}CNMR and 2D-NMR spectra were recorded at 400 MHz on a Bruker B-ACS-6 or at 500 MHz on a Bruker Avance 500 instrument. High resolution mass spectra were recorded using a Water Micromass LCT Premier.

3.5 Experimental procedures

Synthesis of 2,5-dibromo-3-(2-hydroxyethyl)thiophene **3.48**

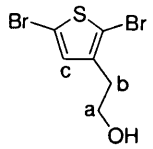

To a solution of 2.5 g (19.5 mmol) 2-(3-thienyl)ethanol in 25 cm^3 DMF at 0 °C, was slowly added dropwise a solution of 10.4 g (58.5 mmol) NBS in 100 cm^3 DMF over 20 min. The reaction mixture was stirred at 0 °C for a further 30 min. The ice bath was removed and the reaction was carried out over 2 days, keeping in the dark. The mixture was then poured into a saturated Na_2CO_3 solution and extracted with ethyl acetate. The ethyl acetate fractions were washed several times with water and the solvent was removed under reduced pressure. The crude product was purified using silica gel chromatography with hexane / ethylacetate (2:1) as eluent. The product was obtained as yellow oil in 85% yield.

^{1}H-NMR (500 MHz, $CDCl_3$): δ(ppm): 6.74 (s, 1H, c), 3.68 (t, J = 6.5 Hz, 2H, a), 2.67 (t, J = 6.4 Hz, 2H, b), 1.60 (s, H, -OH). **^{13}C-NMR (126 MHz, $CDCl_3$): δ(ppm):** 139.13, 131.28, 110.85 (thiophene *C*), 61.81 (-CH_2OH), 32.77 (-CH_2Th). EI-HRMS calculated for [$C_6H_6O_2Br_2S_3$] 285.8486; found 285.8487

Synthesis of 3'-(2-hydroxyethyl)-2, 2':5', 2''-5 terthiophene **3.50**

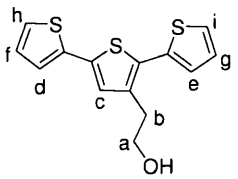

A 25 cm^3 single-necked Schlenk tube equipped with a condenser, nitrogen inlet and a magnetic stirrer was charged with 1.0 g (3.49 mmol) 2,5-dibromo-3-(2-hydroxy-

ethyl)thiophene dissolved in 7 cm^3 DMF and 3.12 g (8.74 mmol) of 2-(tributylstannyl)-thiophene. The mixture was degassed several times during 15 min and brought under N_2 atmosphere. Finally, 1 mol % $Pd(PPh_3)_4$ was added. The mixture was heated to 100 °C for one day, maintaining vigorous stirring and with exclusion of oxygen and light. The reaction was quenched with water to remove inorganic salts and extracted several times with DCM. The product was purified by gradient column chromatography over silica gel, starting with petroleum ether as eluent and continuing with a mixture of petroleum ether / ethylacetate (3:7). The compound was obtained as a white-yellow solid in 78 % yield.

^{1}H-NMR (500 MHz, $CDCl_3$): δ(ppm): 7.34 (dd, *J* = 1.2, 6.4 Hz, 1H, h/i), 7.23 (dd, *J* = 1.2, 6.4 Hz, 1H, h/i), 7.18-7.22 (m, 2H, d & e), 7.08-7.12 (m, 2H, c & f/g), 7.04 (dd, *J* = 3.6 , 8.4 Hz, 1H, f/g), 3.94 (t, 2H, *J* = 6.8 Hz, a), 3.05 (t, 2H, *J* =25 6.8 Hz, b), 1.55 (s, 1H, -OH). **^{13}C-NMR (126 MHz, $CDCl_3$): δ(ppm):** 136.89, 135.79, 135.28, 130.92, 127.89, 127.60, 126.53, 125.75, 124.59, 123.81 (thiophene *C*), 62.69 (-CH_2OH), 32.43(-CH_2Th). EI-HRMS calculated for [$C_{14}H_{12}OS_3$] 292.0050, found 292.0050.

Synthesis of 3-(2-bromoethyl)-2,5-di(thiophen-2-yl)thiophene **3.51**

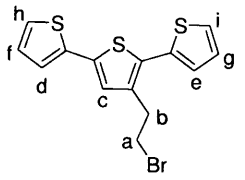

0.58 g (2.2 mmol) of PPh_3 was added portion-wise over a period of 10 min. to a cooled (0 °C) solution of 0.73g (2.2 mmol) old CBr_4 and 0.43 g (1.47 mmol) of **3.50** in anhydrous DCM (25 cm^3). The mixture was stirred, under N_2 atmosphere and in the dark, at 0 °C for 30 min. and subsequently at room temperature for 24 h. The reaction was monitored by ^{1}H-NMR. The crude was purified by flash column chromatography over silica gel, using hexane / ethylacetate (9:1) as eluent, yielding the title compound as a solid in 82% yield.

^{1}H-NMR (500 MHz, $CDCl_3$): δ(ppm): 7.20 (dd, *J* = 1.5, 6.5 Hz, 1H, h/i), 7.09 (dd, *J* = 1.0, 6.0 Hz, 1H, h/i), 7.00-7.04 (m, 2H, d & e), 6.95 (dd, *J* = 3.5, 8.5 Hz, 1H, f/g), 6.91 (s, 1H, c), 6.90 (dd, *J* = 3.5 , 8.4 Hz, 1H, f/g), 3.88 (t, 2H, *J* = 8.0 Hz, 45 b), 3.02 (t, 2H, *J* = 8.0 Hz, c). **^{13}C-NMR (126 MHz, $CDCl_3$): δ(ppm):** 136.70, 136.00, 135.93, 134.83, 131.40, 126.89, 127.63, 126.44, 125.96, 125.89, 124.71, 123.91, (thiophene *C*), 32.71 (CH_2Br), 31.05 (CH_2Th). **ES-HRMS** calcd for [$C_{14}H_{11}BrS_3$] 353.9206, found 353.9206.

Synthesis of 3'-(2-[*N*,*N*,*N*-trimethylammonium]ethyl)-2,2':5',2''-terthiophene bromide **3.41**

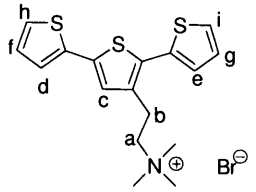

A 25 cm^3 capped round bottom flask was charged with 0.2 g (0.204 mmol) 3'-(2-bromoethyl)-2,2':5',2''-terthiophene **3.51**. A 20% solution of trimethylamine in ethanol was added in excess (20 cm^3), leaving limited head space to limit trimethylamine evaporation. A catalytic amount of KI was added to the mixture. The flask was capped tightly, shielded from light, and left to stir for four days at room temperature. The solvent was removed to yield the crude product as a brown liquid. The crude product was dissolved in water and washed with DCM. Water was removed by freeze drying. The solid was redissolved in a small amount of ethanol and precipitated in ether at 0 °C. The suspension was transferred to an eppendorf and centrifuged for 10 minutes, resulting in a white-yellow solid pellet. The supernatant was removed, and the pellet was dried using high vacuum to afford **3.41** in 59 % yield. As a result of self-aggregation, the ^{1}H-NMR spectrum is concentration dependent and several peaks are broad.

^{1}H- NMR (500 MHz, D_2O): δ(ppm): 7.28 (d, *J* = 4.5 Hz, 1H, h/i), 7.08 (d, *J* = 3.5 Hz, 1H, h/i), 6.97 (s, 1H, c), 6.72- 6.93 (m, 4H, d, e, f & g), 3.08 (t, 2H, *J* = 9.0 Hz, a), 2.92 (s, 9H, -

NCH_3), 2.84 (t, 2H, J = 9.0 Hz, b). **^{13}C-NMR (126 MHz, D_2O): δ(ppm):** 136.17, 135.75, 133.79, 131.77, 131.59, 128.40, 75 128.30, 126.77, 126.27, 125.34, 124.16 (thiophene *C*), 65.36 (-CH_2Th), 63.78 (-CH_2N), 52.98 (-NCH_3). **ES-HRMS** calculated for $[C_{17}H_{20}NS_3]^+$ 334.0758, found 334.0746.

Synthesis of 3'-(2-[*N*,*N*-dimethyl-*N*-(2-hydroxyethyl)ammonium]ethyl)-2,2':5',2''-terthiophene bromide **3.42**

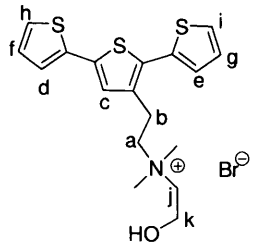

In a 25 cm^3 capped round bottom flask, 0.2 g (0.204 mmol) of 3'-(2-bromoethyl)-2,2':5',2''-terthiophene **3.51** was dissolved in 20 cm^3 ethanol. An excess of ethanolamine (5 cm^3) was added. A catalytic amount of KI was added to the mixture. The flask was capped tightly, shielded from light, and left to stir for four days at room temperature. The solvent was partially removed under reduced pressure and the product was precipitated in ether at 0 °C. The suspension was transferred to an eppendorf and centrifuged for 10 minutes resulting in a white-yellow solid pellet. The supernatant was removed, and the pellet was dried using high vacuum to afford the pure compound in 40 % yield.

^{1}H-NMR (400 MHz, D_2O): δ(ppm): 7.26 (dd, 1H, h/i), 7.07 (d, J = 4.5 Hz, 1H, h/i), 6.80-8.99 (s &m, 4H, c, d, e & f/g), 6.75 (dd, 1H, f/g), 3.79 (2H, k), 3.26 (2H, j), 3.16 (t, 2H, a), 2.91 (s & t, 8H). Low solubility precluded recording a **^{13}C-NMR** spectrum for this compound. **ES-HRMS** calculated for $[C_{18}H_{22}NOS_3]^+$ 364.0864, found 364.0870.

Synthesis of 3'-(2-[*N*,*N*-dimethyl-*N*-(2-(2-hydroxyethoxy)ethyl)ammonium]ethyl)-,2':5',2''-terthiophene bromide **3.43**

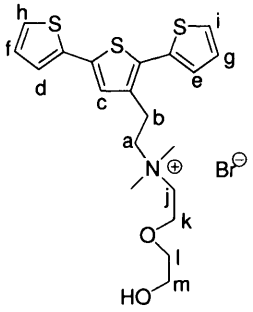

In a 25 cm^3 capped round bottom flask, 0.2 g (0.204mmol) of 3'-(2-bromoethyl)-2,2':5',2''-terthiophene **3.51** was dissolved in 20 cm^3 ethanol. An excess of 2-(2-aminoethoxy)ethanol (5 cm^3) was added. A catalytic amount of KI was added to the mixture. The flask was capped tightly, shielded from light and left to stir for four days at room temperature. The solvent was partially removed under reduced pressure and the product was precipitated in ether at 0 °C. The suspension was transferred to an eppendorf and centrifuged for 10 minutes resulting in a white-yellow solid pellet. The supernatant was removed, and the pellet was dried using high vacuum to afford the title compound in 48 % yield.

^{1}H-NMR (500 MHz, D_2O): δ(ppm): 7.30 (d, J = 4.5 Hz, 1H, h/i), 7.10 (d, J = 4.5 Hz, 1H, h/i), 6.99 (s, 1H, c), 6.91- 6.95 (m, 1H, f/g), 6.86-6.90 (m, 2H,d and e), 6.75-6.80 (m, 1H, f/g), 3.66-3.72 (m, 2H, m), 3.51 (t, J = 4.0 Hz, 2H, k/l), 3.34-3.44 (m, 4H, j & k/l), 3.16 (t, J = 9.0 Hz, 2H, a), 2.95 (s, 6H, -NCH_3), 2.89 (t, J = 9.0 Hz, 2H, b). **^{13}C-NMR (126 MHz, $CHCl_3$): δ(ppm):** 136.14, 135.94, 133.73, 132.00, 131.57, 128.45, 128.36, 126.92, 126.87, 126.23, 125.43, 124.16 (thiophene *C*), 71.98, 64.02, 63.69, 63.14, 60.29, 51.63. **EI-HRMS** calc for $[C_{20}H_{26}N\ O_2S_3]^+$ 408.1115, found 408.1126.

Synthesis of 2,5-di(furan-2-yl)-3-(2-hydroxyethyl)thiophene **3.53**

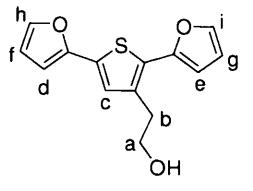

A 25 cm^3 single-necked Schlenk tube equipped with a condenser, nitrogen inlet and a magnetic stirrer was charged with 0.5 g (1.75 mmol) 2,5-dibromo-3-(2-hydroxyethyl)thiophene dissolved in 5 cm^3 DMF and 1.4 ml (4.38 mmol) of 2-(tributylstannyl)furan. The mixture was degassed several times during 15 min and brought under N_2 atmosphere. Finally, 1 mol % $Pd(PPh_3)_4$ was added. The mixture was heated to 100 °C for one day, maintaining vigorous stirring and with exclusion of oxygen and light. The reaction was quenched with water to remove inorganic salts and extracted several times with DCM. The product was purified by gradient column chromatography over silica gel, starting with petroleum ether as eluent and continuing with a mixture of petroleum ether / ethylacetate (3:7). The compound was obtained as a white-yellow solid in 90 % yield.

^{1}H-NMR (500 MHz, $CHCl_3$): δ(ppm): 7.38 (dd, *J* = 1.26 Hz, *J* = 8.6 Hz, 2H, i&h), 7.04 (s, 1H, c), 6.35-6.44 (m, 5H, d,f,e,g), 3.86 (t, *J* = *6.6* Hz 2H, b), 2.99 (t, *J* = 6.6 Hz, 2H, a). **^{13}C-NMR (126 MHz,$CHCl_3$): δ(ppm):** 148.22, 147.59, 140.85, 134.11, 130.72, 130.89, 126.77, 124.32, 110.78, 110.68, 106.92, 104.40 (furan & thiophene *C*), 61.58 (CH_2OH), 31.98 (CH_2Th). **ES-HRMS** calculated for [$C_{14}H_{12}O_2S$] 260.0507, found 260.0503.

Synthesis of 2,5-di(furan-2-yl)-3-(2-bromoethyl)--thiophene **3.54**

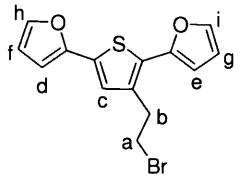

0.76 g (2.3 mmol) of PPh_3 was added portion-wise over a period of 10 min. to a cooled (0 °C) solution of 0.6 g (2.3 mmol) old CBr_4 and 0.4 g (1.5 mmol) of **3.53** in anhydrous DCM (25 cm^3). The mixture was stirred, under N_2 atmosphere and in the dark, at 0 °C for 30 min. and subsequently at room temperature for 24 h. The reaction was monitored by ^{1}H-NMR.

The crude product was purified by flash column chromatography over silica gel, using hexane / ethyl-acetate (9:1) as eluent, yielding the title compound as a solid in 73% yield.

^{1}H-NMR (500 MHz, $CDCl_3$): δ(ppm): 7.38 (dd, *J* = 1.26 Hz, *J* = 8.6 Hz, 2H, i&h), 7.01 (s, 1H, c), 6.39 (m, 4H, d,f,e & g), 3.51 (t, *J* = *6.6* Hz, 2H, b), 3.28 (t, *J* = *6.6* Hz, 2H, a). **^{13}C-NMR (126 MHz, $CDCl_3$): δ(ppm):** 148.52, 147.89, 140.87, 134.21, 130.74, 130.93, 126.79, 124.41, 110.87, 110.78, 106.02, 104.44 (furan & thiophene *C*), 32.73 (CH_2Br), 31.59 (CH_2Th). **ES-HRMS** calculated for $[C_{14}H_{12}O_2S]$ 321.9663, found 321.9663

Synthesis of 3-(2-[*N,N,N*-trimethylammonium]ethyl)-2,5-di(furan-2-yl)thiophene bromide **3.44**

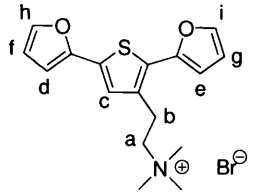

A 10 cm^3 capped round bottom flask was charged with 0.3 g (0.92 mmol) 3-(2-bromoethyl)-2,5-di(furan-2-yl)thiophene **3.54**. A 20% solution of trimethylamine in ethanol was added in excess (8 cm^3), leaving limited head space to limit trimethylamine evaporation. A catalytic amount of KI was added to the mixture. The flask was capped tightly, shielded from light, and left to stir for four days at room temperature. The solvent was removed to yield the crude product as a brown liquid. The solid was redissolved in a small amount of ethanol and precipitated in ether at 0 °C. The suspension was transferred to an eppendorf and centrifuged for 10 minutes, resulting in a brown solid pellet. The supernatant was removed, and the pellet was dried using high vacuum to afford **3.44** in 41% yield.

^{1}H-NMR (500 MHz, D_2O): δ(ppm): 7.49 (dd, *J* = 1.26 Hz, *J* = 8.6 Hz, 2H, i&h), 7.40 (s, 1H, c), 6.47 (m, 4H, d,f,e & g), 3.40 (t, *J* = *6.6* Hz, 2H, b), 3.18 (t, *J* = *6.6* Hz, 2H, a), 3.07 (s, 9H, $-CH_3$). **^{13}C-NMR (126 MHz, D_2O): δ(ppm):** 159.12, 158.81, 151.87, 145.21, 140.75, 140.92, 137.97, 135.51, 121.87, 121.32, 116.02, 114.34 (furan & thiophene *C*), 32.73 (CH_2Br), 31.59 (CH_2Th). **EI-HRMS** calculated for $[C_{17}H_{20}NO_2S]^+$ 302.1215, found 302.1218

Synthesis of 2,5-diphenyl-3-(2-hydroxyethyl)thiophene **3.56**

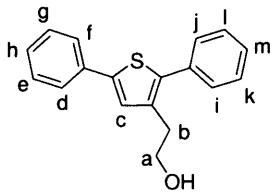

A 25 cm^3 single-necked Schlenk tube equipped with a condenser, nitrogen inlet and a magnetic stirrer was charged with 0.7 g (2.45 mmol) 2,5-dibromo-3-(2-hydroxy-ethyl)thiophene dissolved in 7 cm^3 DMF, 0.9g (7.65 mmol) phenyl boronic acid and 0.5 ml Na_2CO_3 1M. The mixture was degassed several times during 15 min and brought under N_2 atmosphere. Finally, 1 mol % $Pd(PPh_3)_4$ was added. The mixture was heated to 85 °C for one day, maintaining vigorous stirring and with exclusion of oxygen and light. The reaction was quenched with water to remove inorganic salts and extracted several times with DCM. The product was purified by gradient column chromatography over silica gel, starting with petroleum ether as eluent and continuing with a mixture of petroleum ether / ethylacetate (3:7). The compound was obtained as a white-yellow solid in 67 % yield.

^{1}H-NMR (500 MHz, $CDCl_3$): δ(ppm): 7.53 (dd, *J*= 7.20, 2H, *o*-C_6H_5), 7.44 (dd, *J*= 7.16 Hz, 2H, *o*-C_6H_5) 7.39-7.24 (m, 6H, *m*-, *p*-C_6H_5), 7.16 (s, 1H, Th), 3.82 (t, *J*= 5.2 Hz, 1H, b), 2.90 (t, *J*= 7.0 Hz, 2H, a), **^{13}C-NMR (126 MHz, $CDCl_3$): δ(ppm):** 138.47, 134.45, 133.02, 132.84, 128.18, 127.98, 127.87, 126.87, 126.72, 124.85, 123.90 (-C_6H_5), 62.11 (CH_2OH), 32.98 (CH_2Th). **ES-HRMS** calculated for [$C_{18}H_{16}OS$] 280.0922, found 280.0925

Synthesis of 2,5-diphenyl-3-(2-bromoethyl)thiophene **3.57**

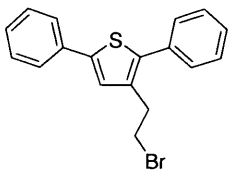

0.13 g (0.39 mmol) of PPh_3 was added portion-wise over a period of 10 min. to a cooled (0 °C) solution of 0.15 g (0.45 mmol) old CBr_4 and 0.11 g (0.39 mmol) of **3.56** in anhydrous DCM (25 cm^3). The mixture was stirred, under N_2 atmosphere and in the dark, at 0 °C for 30 min. and subsequently at room temperature for 24 h. The reaction was monitored by ^{1}H-NMR. The crude was purified by flash column chromatography over silica gel, using hexane / ethyl-acetate (9:1) as eluent, yielding the title compound as a solid in 73% yield.

^{1}H-NMR (500 MHz, $CDCl_3$): δ(ppm): 7.53 (dd, *J*= 7.19 Hz, 2H, o-C_6H_5), 7.43-7.28 (m, 7H, *o*-,*m*-,*p*-C_6H_5), 7.2 (m, 1H, *p*-C_6H_5), 7.15 (s, 1H, Th) 3.47 (t, *J*= 5.2 Hz, 2H, b), 3.17 (t, *J*= 5.2, 2H, a) **^{13}C-NMR (126 MHz, $CDCl_3$): δ(ppm):**138.40, 134.43, 132.98, 132.84, 128.18, 127.91, 127.74, 126.87, 126.62, 124.58, 123.84, 31.40, 30.73. **ES-HRMS** calculated for [$C_{18}H_{15}BrS$] 342.0078, found 342.0078.

Synthesis of 3-(2-[*N*,*N*,*N*-trimethylammonium]ethyl)-2,5-diphenyl-thiophene bromide **3.45**

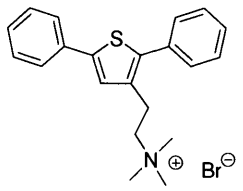

A 10 cm^3 capped round bottom flask was charged with 0.14 g (0.40 mmol) of 2,5-diphenyl-3-(2-bromoethyl)thiophene **3.57**. A 20% solution of trimethylamine in ethanol was added in excess (8 cm^3), leaving limited head space to limit trimethylamine evaporation. A catalytic amount of KI was added to the mixture. The flask was capped tightly, shielded from light, and left to stir for four days at room temperature. The solvent was removed to yield the crude product as a brown liquid. The solid was redissolved in a small amount of ethanol and precipitated in ether at 0 °C. The suspension was transferred to an eppendorf and centrifuged

for 10 minutes, resulting in a brown solid pellet. The supernatant was removed, and the pellet was dried using high vacuum to afford **3.45** in 62% yield.

^{1}H-NMR (500 MHz, D_2O): δ(ppm): 7.70-6.95 (m, 10H, -C_6H_5 & Th), 3.34 (m, 2H, b) 3.06 2.94 (m, 2H, a), 2.94 (s, 9H, -CH_3). Low solubility precluded recording a **^{13}C-NMR** spectrum for this compound. **ES-HRMS** calculated for $[C_{21}H_{24}NS]^+$ 322.1619, found 322.1621.

Synthesis of 2,5-(dipyridyl-3yl)-3-(2-hydroxyethyl)thiophene **3.59**

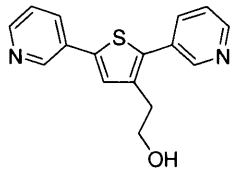

A 25 cm^3 single-necked Schlenk tube equipped with a condenser, nitrogen inlet and a magnetic stirrer was charged with 0.2 g (0.7 mmol) 2,5-dibromo-3-(2-hydroxy-ethyl) thiophene dissolved in 7 cm^3 DMF and 0.26g (2.1 mmol) pyridineboronic acid, and 0.5 ml solution Na_2CO_3 1M. The mixture was degassed several times during 15 min and brought under N_2 atmosphere. Finally, 1 mol % $Pd(PPh_3)_4$ was added. The mixture was heated to 85 °C for one day, maintaining vigorous stirring and with exclusion of oxygen and light. The reaction was quenched with water to remove inorganic salts and extracted several times with DCM. The product was purified by gradient column chromatography over silica gel, using a mixture of DCM / MeOH / Ether (8:1:1). The compound was obtained as a white-yellow solid in 61 % yield. This compound was prepared and characterised by Enora Bertin-Ecoublet.

^{1}H-NMR (500 MHz, CH_3Cl): δ(ppm): 8.82 (d,1H, d/h), 8.73 (s, 1H, c/g), 8.53 (s, 1H), 8.48(d, 1H, d/h), 7.85 (m, 2H) 7.3(m,4H), 7.2(s, 1H, Th), 3.92 (t, 2H, b), 2.91 (t, 2H, a).

Synthesis of 2,5-(dipyridyl-3yl)-3-(2-bromoethyl)thiophene **3.60**

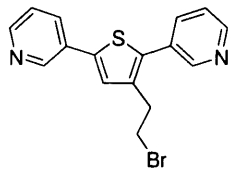

0.14 g (0.53 mmol) of PPh_3 was added portion-wise over a period of 10 min. to a cooled (0 °C) solution of 0.15 g (0.53 mmol) old CBr_4 and 0.1 g (0.35 mmol) of **3.59** in anhydrous DCM (25 cm^3). The mixture was stirred, under N_2 atmosphere and in the dark, at 0 °C for 30 min. and subsequently at room temperature for 24 h. The reaction was monitored by ^{1}H-NMR. The crude was not purified and the solvent was partially removed to avoid decomposition. The compound was not fully characterised.

^{1}H-NMR (500 MHz, CH_3Cl): δ(ppm): 8.82 (s, 1H), 8.69 (s, 1H), 8.58 (d, 1H), 8.48 (d, 1H).It was difficult to identify the protons between 8.0-7.0 ppm because of the side products formed during the Appel reaction.

Synthesis of 3-(2-[*N,N,N*-trimethylammonium]ethyl)-2,5-di(pyridine-3-yl)thiophene **3.46**

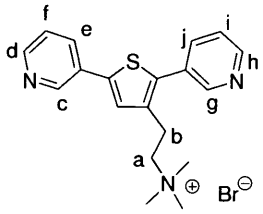

A 10 cm^3 capped round bottom flask was charged with solution of **3.60** in DCM and ethanol from previous reaction. A 20% solution of trimethylamine in ethanol was added in excess (8 cm^3), leaving limited head space to limit trimethylamine evaporation. A catalytic amount of KI was added to the mixture. The flask was capped tightly, shielded from light, and left to stir for four days at room temperature. The solvent was removed to yield the crude product as a

brown liquid. The solid was quenched with ethanol several times in a small amount of ethanol and precipitated in ether at 0 °C. The suspension was transferred to an eppendorf and centrifuged for 10 minutes, resulting in a yellow solid pellet. The supernatant was removed, and the pellet was dried using high vacuum to afford **3.46** in 62% yield.

^{1}H-NMR (400 MHz,D_2O): δ(ppm): 8.51 (s, 1H, c/g), 8.48 (d, 1H, d/h), 8.32 (s, 1H, c/g), 8.25 (d, 1H, d/h), 7.82 (d, 1H, j/e), 7.71 (d, J= , 1H, j/e), 7.4 (m, 1H, f/i), 7.29 (m, 1H, f/i), 7.27 (s, 1H, Th), 3.52 (t, 2H, b), 2.93 (t, 2H, a).

Synthesis of 3-(2-(tetrahydropyranyloxy)ethyl)thiophene **3.63**

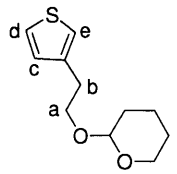

3.00 g (23.4 mmol) of 3-ethanolthiophene were dissolved in 25 ml of dry ether and then 2.17 g (25.8 mmol) of 1,4-dihydro-2Hpyran previously dissolved in 25 ml of ether and 0.25 g (1.45 mmol) of p-TSA were added to the solution. The mixture was stirred at room temperature for about three hours. Afterwards, the solution was washed two times with 15 ml of 10% K_2CO_3 and with 20 ml distilled water. The organic layer was concentrated on a rotavapor to give a colourless liquid. A further purification was operating by passing the compound through a silica gel column using Hexane/Ether (80:20) as eluent. The product was obtained in 85% yield.

^{1}H-NMR ($CDCl_3$; 400 MHz): δ(ppm): 7.23 (dd, *J*= 5.0 Hz, *J*= 1.2 Hz, 1H, d), 7.03 (dd, *J*= 2.9 Hz, *J*=1.1 Hz, 1H, e), 6.99 (dd, *J*=5.0 Hz, *J*= 3.2 Hz, 1H, c), 4.61 (t, *J*= 3.5 Hz, 1H, O-C**H**-O), 3.96 (m, 1H, C-CH_2-CH_a**H_b**), 3.77 (m, 1H, CH-$(CH_2)_3$-CH_a**H_b**), 3.62 (m, 1H, C-CH_2-**CH_a**H_b), 3.48 (m, 1H, CH-$(CH_2)_3$-**CH_a**H_b), 2.94 (t, J=7.02 Hz, 2H, C-CH_2), 1.79 (m, $1H_{THP}$), 1.69 (m, $1H_{THP}$), 1.58 (m, $4H_{THP}$). **^{13}C-NMR ($CDCl_3$; 126 MHz): δ(ppm):** 139.4, 128.6,

125.1, 121.1, 98.8, 67.6, 62.2, 30.8, 30.7, 25.5, 19.5. **ES-HRMS** calculated for [$C_{11}H_{16}O_2S$] 212.0871, found 212.0871

Synthesis of 2-bromo-3-(2-hydroxyethyl)thiophene **3.66**

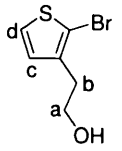

To a solution of 2.61 g (20.36 mmol) 2-(3-thienyl)ethanol in 25 cm^3 DMF at 0 °C, was slowly added dropwise a solution of 3.6 g (20.36 mmol) NBS in 100 cm3 DMF during 15 min. The reaction mixture was stirred at 0 °C for a further 30 min. The ice bath was removed, allowing the reaction mixture to reach room temperature, and the reaction was continued for a further 7 hours, keeping in the dark. The mixture was then poured into a saturated Na_2CO_3 solution and extracted with ethyl acetate. The ethyl acetate fractions were washed several times with water and then the solvent was removed under reduced pressure. The crude product was purified using silica gel chromatography with hexane / ethylacetate (2:1) as eluent. A pale yellow oil was obtained in 77% yield.

^{1}H-NMR (400 MHz, $CDCl_3$): δ(ppm): 7.12 (d, *J* = 5.6 Hz, 1H, e), 6.76 (d, *J* = 5.2 Hz, 1H, c), 3.73 (t, *J* = 6.4 Hz, 2H, a), 2.76 (t, *J* = 6.4 Hz, 2H, b), 1.53 (s, H, -OH). **^{13}C-NMR (126 MHz, $CDCl_3$): δ(ppm):** 138.41, 95 129.00, 126.13, 110.76 (thiophene *C*), 62.95 (-CH_2OH), 33.20 (-CH_2Th). **EI-HRMS** calcd for [C_6H_7BrOS] 205.9401; found 205.9403.

3, 3''-di(2-hydroxyethyl)-2, 2':5', 2''-terthiophene **3.68**

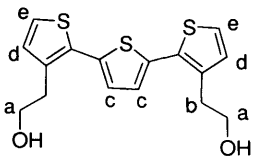

A solution of 0.48 g (2.32 mmol) 2-bromo-3-(2-hydroxyethyl)thiophene in 6 cm^3 of a mixture of toluene and methanol (1: 1) in a microwave reactor tube equipped with a magnetic stirrer bar was degassed using the freeze-pump-thaw method and was flushed with N_2 for 20 minutes. The microwave reactor tube was placed in a glove bag and 0.2 g (1.16 mmol) of 2,5-thiophenediboronic acid and 0.027 g (0.20 mmol) of K_2CO_3 were added. Finally, a catalytic amount of PEPPSI-iPr was added and the solution was irradiated at 80 °C for 10 min, at a fixed power (100 W). The solvent was removed under reduced pressure and the product was purified by column chromatography over silica gel and using dichloromethane/ tetrahydrofuran (8 : 2) as the eluent. The title compound was obtained as a pale yellow solid in 91 % yield.

^{1}H-NMR (400 MHz, CDCl3): δ(ppm): 7.12 (d, *J* = 5.2 Hz, 2H, e), 7.03 (s, 2H, c), 6.90 (d, *J* = 5.2 Hz, 2H, e), 3.80 (t, *J* = 6.4, 25 Hz, 4H, a), 3.01 (t, *J* = 6.4 Hz, 4H, b), 1.47 (s, 2H, -OH). **^{13}C-NMR (126 MHz, CDCl3): δ(ppm):** 135.83, 135.33, 132.02, 130.08, 126.74, 125.52, 124.54 (thiophene *C*), 62.74 (-CH_2OH), 32.63(-CH_2Th). **EI-HRMS** calcd for [$C_{16}H_{16}O_2S_3$] 336.0312; found 336.0302.

Synthesis of 3, 3''-di(2-bromoethyl)-2, 2':5', 2''-terthiophene **3.69**

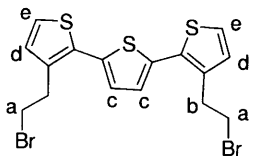

A solution of terthiophene **3.68** (0.21g, 0.63 mmol) in dry DCM (40 cm^3) in a round bottom flask equipped with a magnetic stirrer bar was cooled to 0 °C and CBr_4 (0.53g, 1.59 mmol) was added, followed by 0.83 g of PPh_3 (1.59 mmol) in two portions over a period of 15 min. The reaction was left to stir at 0 °C for a further 30 min. The mixture was allowed to warm up to room temperature and stirred for 24 h. The solvent was removed under reduced pressure

and the crude product was purified by column chromatography using hexane / ethylacetate (9:1) as eluent. The desired product was obtained in 81 % yield.

^{1}H-NMR (400 MHz, $CDCl_3$): δ(ppm): 7.12 (d, *J* = 5.2 Hz, 1H, e), 6.99 (s, 2H, c), 6.95 (d, *J* = 5.2 Hz, 2H, e), 3.51 (t, *J* = 8.0 Hz, 4H, a), 3.01 (t, *J* = 8.0 Hz, 4H, b). **^{13}C-NMR (126 MHz, $CDCl_3$): δ(ppm):** 135.55, 135.52, 132.10, 129.54, 126.57, 124.54 (thiophene *C*), 32.53 (-CH_2Br), 31.53 (-CH_2Th). **EI-HRMS** calcd for [$C_{16}H_{14}Br_2S_3$] 61.8624; found 461.8622.

Synthesis of 3,3''-di(2-[*N*,*N*,*N*-trimethylammonium]ethyl)-2, 2':5', 2''-terthiophene **3.61**

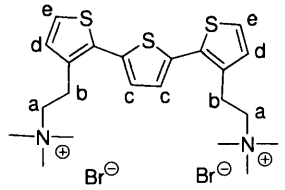

To 0.2 g (0.43 mmol) of 3,3''-di(2-bromoethyl)-2,2':5',5''-terthiophene **3.69** was added an excess of a 20 % solution of trimethylamine in ethanol (20 cm^3) and a catalytic amount of KI. The product precipitated during the reaction and was filtered and washed several times with ethanol to afford the pure ammonium salt in 68 % yield.

^{1}H-NMR (400 MHz, D_2O): δ(ppm): 7.32 (d, *J* = 5.2 Hz, 1H, e), 7.12 (s, 2H, c), 7.04 (d, *J* = 5.2 Hz, 2H, e), 3.39 (m, 4H, a), 3.18 (t, *J* = 7.6 Hz, 4H, b), 3.03 (s, 18H, -NCH_3). **^{13}C-NMR (126 MHz, D_2O): δ(ppm):** 135.45, 132.45, 132.10, 130.19, 128.10, 126.68 (thiophene *C*), 65.2 (-CH_2Th), 53.25(-CH_2N), 22.88 (–NCH_3). **ES-HRMS** calcd for $[C_{22}H_{32}N_2S_3]^+$ 420.1728; found 420.1736.

Synthesis of 3,3'''-di(2-hydroxyethyl)-2,2':5',2'':5'':2'''-quaterthiophene **3.71**

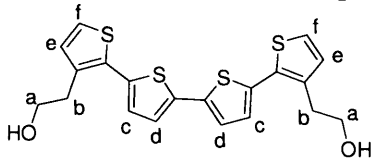

The synthesis was carried out analogous to the synthesis of terthiophene **3.68**. A mixture of 0.49 g (0.24 mmol) of 2-bromo-3-(2-hydroxy-ethyl)thiophene and 0.05 g (0.11 mmol) of

2,2'-bithiophene-5,5'-diboronic acid bis(pinacol) ester in 6 cm^3 toluene / methanol (1: 1) in the presence of 0.021 g (0.155 mmoles) of K_2CO_3 and a catalytic amount of PEPPSI-iPr was subjected to microwave irradiation at 80 °C for 10 min, at 100 W fixed power. The product was purified by column chromatography using silica gel and dichloromethane / ethyl acetate (2: 1) as eluent to afford a yellow-orange fluorescent solid in 87% yield.

^{1}H-NMR (400 MHz, $CDCl_3$): δ(ppm): 7.14 (d, *J* = 5.0 Hz, 2H, f), 7.03 (d, *J* = 4.0 Hz 2H, d), 6.97 (d, *J* = 4.0 Hz, 2H, c), 6.91 (d, *J* = 5.4 Hz, 2H, e), 3.82 (t, *J* = 6.5 Hz, 4H, a), 2.78 (t, *J* = 6.5 Hz, 4H, b), 1.47 (s, 2H, -OH). **^{13}C-NMR (126 MHz, $CDCl_3$): δ(ppm):** 137.06, 135.39, 134.76, 132.10, 130.11, 127.15, 124.58, 124.10, (thiophene *C*), 62.86 (-CH_2OH), 32.48 (-CH_2Th). **EI-HRMS** calcd for [$C_{20}H_{18}O_2S_4$] 418.0190; found 418.0177

Synthesis of 3,3'''-di(2-bromoethyl)-2,2':5',2'':5'':2'''-quaterthiophene **3.72**

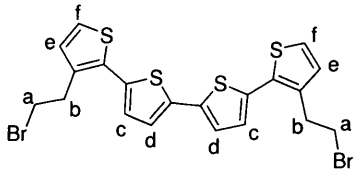

The synthesis was carried out analogous to the synthesis of terthiophene **3.69**, using 0.2 g (0.49 mmol) of quaterthiophene **3.71**, CBr_4 (0.40g, 1.22 mmol) and PPh_3 (0.32g, 1.22 mmol) in 40 cm^3 dry DCM. The product was purified by column chromatography using hexane / ethyl acetate (9:1) as eluent, providing the title compound in 80 % yield.

^{1}H-NMR (500 MHz, $CDCl_3$): δ(ppm): 7.14 (d, *J* = 5.0 Hz, 2H, f), 7.05 (d, *J* = 3.5 Hz, 2H, d), 6.95 (d, *J* = 4.0 Hz, 2H, c), 6.92 (d, *J* = 5.0 Hz, 2H, e), 3.48 (t, *J* = 8 Hz, 4H, a), 3.27(t, *J* =8 Hz, 4H, b), 1.47. **^{13}C-NMR (500 MHz, $CDCl_3$): δ(ppm):** 137.17, 135.71, 134.39, 132.26, 129.68, 127.19, 124.28, 124.30, (thiophene *C*), 32.66 (-CH_2Br), 31.53 (-CH_2Th). **EI-HRMS** calcd for [$C_{20}H_{16}Br_2S_4$] 543.8481; found 541.8513.

Synthesis of 3,3'''-di(2-[*N*,*N*,*N*-trimethylammonium]ethyl)- 2,2':5',2'':5'':2'''-quaterthiophene dibromide **3.62**

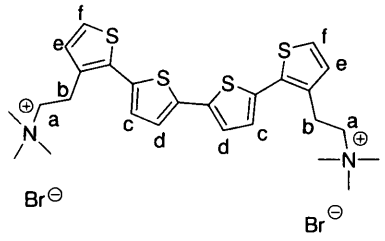

The synthesis was carried out analogous to the synthesis of **3.60.** Quaterthiophene **3.72** (0.2 g, 0.36 mmol), an excess of a 20 % solution of trimethylamine in ethanol (20 cm^3) and a catalytic amount of KI were reacted at room temperature, shielded from light. The product precipitated during the reaction and was filtered and washed several time with ethanol to afford the pure ammonium salt in 72 % yield.

^{1}H-NMR (500 MHz, D_2O): δ(ppm): 7.15 (d, *J* = 5.0 Hz, 2H, f), 6.92 (d, *J*= 5.0 Hz, 2H, d), 6.89 (d, *J* = 3.5 Hz, 2H, c), 6.77 (d, *J* = 3.5 Hz, 2H, e), 3.25 (t, *J* =8.5 Hz, 4H, a), 2.99 (t, *J* = 8.5 Hz, 4H, b), 2.94 (s, 18H, -NCH_3). **^{13}C-NMR (126 MHz, D_2O): δ(ppm):** 136.86, 133.91, 132.63, 131.84, 127.68, 126.27, 125.24 (thiophene *C*), 65.80 (-CH_2Th), 53.26 (-CH_2N), 22.89 (–NCH_3). **ES-HRMS** calcd for $[C_{26}H_{33}N_2S_4]^+$ 501.1527; found 501.1520.

References

1. Mishra, A.; Ma, C. Q.; Bäuerle, P., *Chem. Rev.* **2009,** *109* (3), 1141-1276.
2. Negishi, E.; Zeng, X.; Tan, Z.; Qian, M.; Hu, Q.; Huang In, Z., *Metal-Catalyzed Cross-Coupling Reactions* **2010.**
3. Müllen, K., Wegner, G. *Electronic Materials: the Oligomer Approach; Wiley: Weinheim* **2006.**
4. Barbarella, G.; Zambianchi, M.; Bongini, A.; Antolini, L., *J. Org. Chem.* **1996,** *61* (14), 4708-4715.
5. Barbarella, G.; Zambianchi, M.; Pudova, O.; Paladini, V.; Ventola, A.; Cipriani, F.; Gigli, G.; Cingolani, R.; Citro, G., *J. Am. Chem. Soc.* **2001,** *123* (47), 11600-11607.
6. Ewbank, P. C.; Nuding, G.; Suenaga, H.; McCullough, R. D.; Shinkai, S., *Tetrahedron Lett.* **2001,** *42* (2), 155-157.
7. Bidan, G.; De Nicola, A.; Enee, V.; Guillerez, S., *Chem. Mat.* **1998,** *10* (4), 1052-1058.

8. Kirschbaum, T.; Azumi, R.; Mena-Osteritz, E.; Bauerle, P., *New J. Chem.* **1999,** *23* (2), 241-250.
9. Cremer, J.; Mena-Osteritz, E. M.; Pschierer, N. G.; Müllen, K.; Bäuerle, P., *Org. Biomol. Chem.* **2005,** *3* (6), 985-995.
10. Nilsson, K. P. R.; Olsson, J. D. M.; Konradsson, P.; Inganas, O., *Macromolecules* **2004,** *37* (17), 6316-6321.
11. Wong, M. S.; Zhang, X. L., *Tetrahedron Lett.* **2001,** *42* (24), 4087-4089.
12. Yoshida, H.; Yamaryo, Y.; Ohshita, J.; Kunai, A., *Tetrahedron Lett.* **2003,** *44* (8), 1541-1544.
13. Singh, B. K.; Kaval, N.; Tomar, S.; Van der Eycken, E.; Parmar, V. S., *Org. Proced. Res. Dev.* **2008,** *12* (3), 468-474.
14. Nilsson, P.; Ofsson, K.; Larhed, M., Microwave Methods in Organic Synthesis. Springer-Verlag Berlin: Berlin, 2006; Vol. 266, pp 103-144.
15. Schiedel, M. S.; Briehn, C. A.; Bäuerle, P., *J. Organomet. Chem.* **2002,** *653* (1-2), 200-208.
16. Knapp, D. M.; Gillis, E. P.; Burke, M. D., *J. Am. Chem. Soc.* **2009,** *131* (20), 6961-6963.
17. Gillis, E. P.; Burke, M. D., *J. Am. Chem. Soc.* **2007,** *129* (21), 6716-6717.
18. Kirschbaum, T.; Briehn, C. A.; Bäuerle, P., *J. Chem. Soc.-Perkin Trans. 1* **2000,** (8), 1211-1216.
19. Sotgiu, G.; Zambianchi, M.; Barbarella, G.; Botta, C., *Tetrahedron* **2002,** *58* (11), 2245-2251.
20. Tierney, S.; Heeney, M.; McCulloch, I., *Synth. Met.* **2005,** *148*, 195-198.
21. Marion, N.; Nolan, S. P., *Accounts Chem. Res.* **2008,** *41* (11), 1440-1449.
22. Aslund, A.; Herland, A.; Hammarstrom, P.; Nilsson, K. P. R.; Jonsson, B. H.; Inganas, O.; Konradsson, P., *Bioconjugate Chem.* **2007,** *18*, 1860-1868.
23. Melucci, M.; Barbarella, G.; Sotgiu, G., *J. Org. Chem.* **2002,** *67* (25), 8877-8884.
24. Alesi, S.; Di Maria, F.; Melucci, M.; Macquarrie, D. J.; Luque, R.; Barbarella, G., *Green Chem.* **2008,** *10* (5), 517-523.
25. Sato, M.; Shimizu, T.; Yamauchi, A., *Synth. Met.* **1991,** *41* (1-2), 551-554.
26. Sato, M. A.; Morii, H., *Macromolecules* **1991,** *24* (5), 1196-1200.
27. McCarley, T. D.; Noble, C. O.; DuBois, C. J.; McCarley, R. L., *Macromolecules* **2001,** *34* (23), 7999-8004.
28. Chayer, M.; Faid, K.; Leclerc, M., *Chem. Mat.* **1997,** *9* (12), 2902-2905.
29. Bäuerle, P.; Fischer, T.; Bidlingmeier, B.; Stabel, A.; Rabe, J. P., *Angew. Chem. Int. Edit. Engl.* **1995,** *34* (3), 303-307.
30. Pascal S. *Regioselectivity of lithiation of selected heteroaromatics*; Cardiff University: 2008.
31. Appel, R., *Angew. Chem. Int. Edit. Engl.* **1975,** *14* (12), 801-811.

Chapter 4

AGGREGATION OF CATIONIC OLIGOHETEROAROMATICS IN AQUEOUS SOLUTION

Abstract: *This chapter describes the correlation between aggregation, polymer conformation and optical properties of conjugated materials in solution. The chapter gives a short review regarding the self-organisation of oligo-and polythiophenes in aqueous media, with a focus on supramolecular assemblies before discussing the mode of self aggregation of cationic oligoheteroaromatics. All synthesised oligoheteroaromatics show diverse self aggregation behaviour in aqueous solution. The aggregation mode changes from non-cooperative self aggregation to cooperative self aggregation and formation of micellar aggregates. Different mathematical models are also used to quantify the modes of self aggregation for cationic oligoheteroaromatics.*

4. 1. Aggregation sensitive optical properties: overview

Advances in the synthesis and structural variability of π-conjugated systems in combination with their semiconducting properties offers much potential within these systems by increasing the number of applications such as field-effect transistors (OFETs), electro-luminescent devices and solar cells.[1,2] A requirement for high-performance optoelectronic devices is efficient control over the self organisation of π-conjugated systems through noncovalent interactions. The self organisation of conjugated oligomers and polymers in both the solid state and in solution derives from intermolecular aggregation driven mainly by π-π stacking interactions. For example, π-π stacking interactions, in combination with hydrogen bonds, enabled the self assembly of substituted oligothiophenes into fibers on a graphite surface.[3] In other examples, oligo[4,5] or polythiophenes[6,7] monolayers were self assembled using Langmuir-Blodgett or layer-by-layer techniques.[8] Changes in the electronic structure and in the chain conformation affect the electronic properties of conjugated polymers and oligomers. Therefore, the transition between disordered polymer chains and aggregated arranged chains can result in changes in optoelectronic properties such as colour. A red shift of the absorption maximum can be also observed through inter-chain processes due to self aggregation.[9] Not surprisingly, therefore, polythiophenes exhibit thermochromic,[10,11] solvatochromic,[12-14] ionochromic and piezochromic properties.[15] Moreover, the fluorescence intensity and the fluorescence quantum yield depend on the separation or aggregation of polymer chains. Polythiophenes show weaker fluorescence intensities if they aggregate compared to the single chains. In other examples, the absorption and fluorescence spectra of poly(phenylene-

ethynylene)s (PPE) are red shifted as a consequence of their strongly aggregated state.[16] Also, the low fluorescence intensities observed for cationic poly(fluorene)s are believed to correspond to a tight aggregated state presumably formed by π-π interchain hydrophobic interactions.[17] Moreover, conformational changes of conjugated polymers are affected by order-disorder transitions of side chains. Changes in thermal motion of lateral chains will cause changes in repulsion between the chains, modifying the planarisation of the polymer backbone and concomitant changes to its electronic structure. Other studies on polymer chain aggregation point out that increasing the number of substituents can prevent π-stacking interactions between the main chains and, as a consequence, the polymer will adopt a wormlike cylindrical conformation.[18] By decreasing the number of substituents, the polymer chain can become more planar resulting in a lamellar arrangement. Chiral polythiophene **4.1** shows handed helical induction associated with π-π* transitions when chiral substituents are introduced on the polythiophene chain (Figure 4.1).[9] Strong optical activity is obtained if the polymer backbone is in its aggregated state, *i.e.*, in poor solvents and at low temperatures. In contrast, in good solvents or at high temperature, no optical activity can be observed.

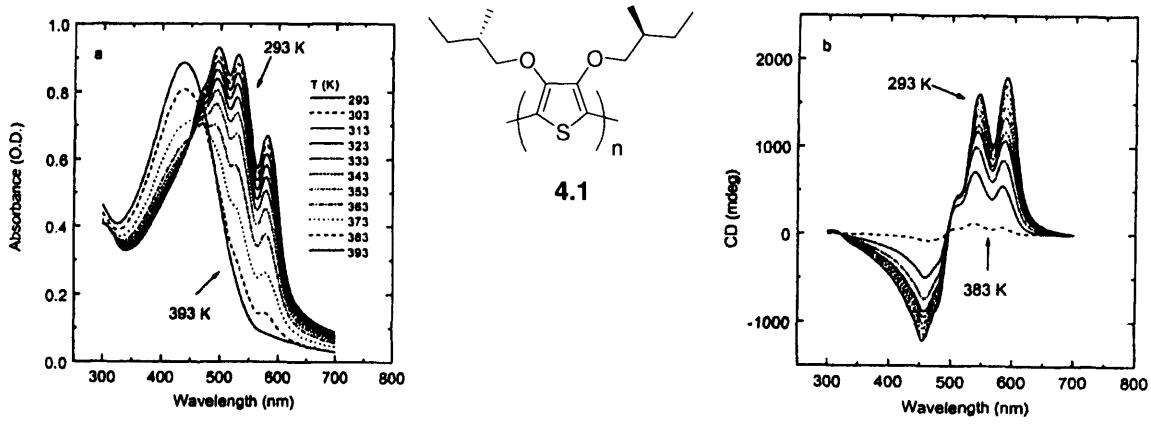

Figure 4.1 UV-Vis absorption and CD spectra of chiral polythiophenes **4.1** in decanol at different temperatures. Picture taken from reference 9.

4.2. Self organisation of conjugated polymers and oligomers in aqueous media

Conducting polymers can be used as highly sensitive optical components for biosensors (Section 1.2). For biosensor applications, water-soluble polymers are required and aqueous solubility can be ensured by introducing a charged moiety along the polymer backbone. Due to their amphiphilic structure (hydrophobic backbone and hydrophilic side groups), conducting polymers carrying ionic side groups show a tendency to self aggregate in aqueous solution, even at low concentration. In water, hydrophobic interactions cause the stacking of aromatic molecules. Additionally, solvophobic interactions also contribute to the stacking contrary to stacking in organic solvents where the solvent-solvent interactions are weak.[18] Hunter and Sanders developed a simple model which explains the geometrical requirements for interactions between aromatic molecules.[19] In addition, hydrogen bonding interactions, electrostatic interactions and London dispersion interactions contribute to the formation of stable aggregates in solution and, hence, to the formation of supramolecular structures.

The most studied supramolecular architectures formed by aggregation in aqueous media are spherical micelles, wormlike micelles, vesicle, bilayers and inverted micelles (Figure 4.2).[20]

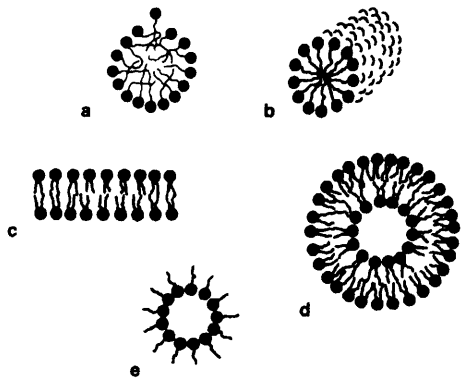

Figure 4.2 Aggregate morphologies obtained by self-assembly in aqueous solution; spherical micelle (a), wormlike micelle (b), bilayer fragment (c), vesicle (d) and inverted micelle (e). Picture taken from reference 20.

In 1997 Mc. Cullough and co-workers reported the aggregation behaviour of a regioregular HT-2,5-poly(thiophene-3-propionic acid) and its deprotonated form in aqueous solution.[21] Both forms generate protein-like hydrophobic assemblies driven by inter-and intramolecular hydrogen bond stabilisation and π-π stacking interactions. Just one year later, the same authors showed that an alternating sequence of hydrophobic ($-C_{12}H_{25}$) and hydrophilic (propioniccarboxylate) substituents on polythiophenes result in a lamellar structures at the air/water interface and in Langmuir-Blodgett multilayers (Figure 4.3)[22].

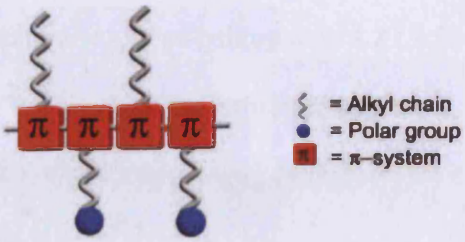

Figure 4.3 Schematic orientation of propionic carboxylate substituent at the air-water interface.[23]

Nilsson *et al.* showed that the aggregation of a 3-substituted polythiophene carrying an amino-acid group in buffer is pH dependent because of the protonation and deprotonation of the zwitterionic group.[24] At low pH the polymer adopts a planar non-aggregated conformation, where the chains are separated one from another. At pH 5-6, this conformation changes to a helical non-planar conformation but the polymer is still in a non-aggregated state. In contrast, at high pH the polymer returns to a planar conformation, while showing agglomeration of the backbone chains. Further evidence of aggregation has been observed for substituted poly(fluorene)s and fluorene-containing copolymers,[25-27] poly-(arylene-ethynylene)s,[28, 29] poly (p-phenylenevinylene)s or poly(propylene imine) dendrimers modified with oligo(p-phenylenevinylene)s carrying either cationic or anionic side groups.[30] All these examples show how the interplay between electrostatic interactions and the hydrophobic nature of the polymeric chains provides varying driving forces for the aggregation of these polymers in aqueous solution.

Researchers have also discovered conjugated materials that are present as a single species in solution. In this context, the work done in Meijer's group[31] regarding the synthesis of non-ionic polythiophenes containing oligoethylene glycol side chains needs to be mentioned.

Investigating the thermal denaturation of polythiophene **4.2** (Scheme 4.1), the authors showed that this polymer folds into a non-aggregating structure in water.

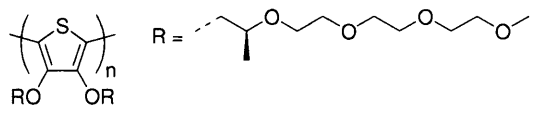

4. 2

Scheme 4.1

There are only a few studies into the self assembly of oligothiophenes in aqueous solutions and most of these studies do not refer to the self assembly of oligothiophenes containing charged substituents. Fortunately, other charged or neutral oligoaromatics have been developed, which provide useful reference structures for our work on the self assembly of ionic oligothiophenes. Aggregation of cationic oligo(phenylene-1,2,3-triazole)s using circular dichroism spectroscopy and dynamic light scattering revealed different conformations varying from random-coil in methanol to large size helical aggregates in water.[32] In other examples, amphiphilic perylenes,[33] oligo- and poly(*p*-phenylenevinylene)s,[34] dendronised oligo-aromatics,[18] *etc.* are known to self assemble in aqueous solution *via* hydrophobic π-π stacking interactions. Advincula *et al.*[35, 36] designed a bolaform amphiphilic sexithiophene bearing ammonium groups at both ends that shows different self aggregation modes in different water-THF mixtures. In 100% water, for example, dicationic sexithiophene **4.3** (Scheme 4.2) self aggregates into a lamellar structure, while upon addition of THF these large aggregates break down into small aggregates.

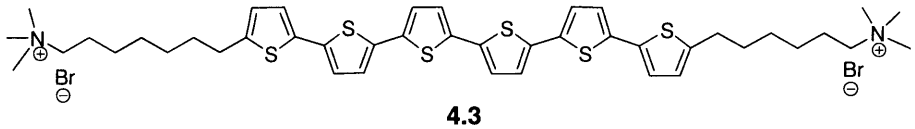

4.3

Scheme 4.2

Studies using UV-visible and fluorescence spectroscopy showed that oligothiophenes **4.4** (Scheme 4.3) form H-type aggregates, in water/butanol, at low temperature.[37] The large blue shift observed in the UV-visible spectrum suggests strong exciton coupling which was attributed to a tightly packed structure.

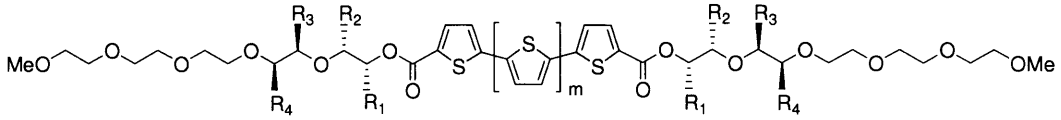

m = 3 - 5

R_1,R_2, R_3, R_4 = -H or -CH_3

4.4

Scheme 4.3

Amphiphilic sexithiophene **4.5** (Scheme 4.4) containing amides groups shows a higher tendency to aggregate in aprotic solvents and on a silica surface compared to the corresponding ester derivatives **4.4**.[38] In this case, hydrogen bond interactions in addition to hydrophobic interactions contribute to the formation of dense and stable stacks in aqueous solution.

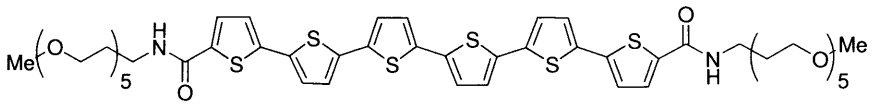

4.5

Scheme 4.4

Introducing an ammonium substituent in the structure of **4.5**, the same authors showed that the new derivative form complexes with chiral polyanions in aqueous media in which the thiophene moieties aggregate in a meta-stable helical manner with a preferred handed orientation.

Shorter oligothiophenes form more dynamic and smaller water-soluble aggregates. Surprisingly, attaching only one oligo(ethyleneoxide) chain to the α-position of quaterthiophene led to formation of vesicles.[39] Further, ordered lamellar films could be obtained by casting the oligothiophenes solution onto a glass surface. Tsai and co-workers observed that peptides segments form β-sheet structures can be used to stimulate chirality in π-conjugated systems.[40] As a result of such stimulation of chirality, terthiophene peptide lipid **4.6** self assembles into one-dimensional helical nanofibers. Furthermore, spectrophotometric investigations confirmed that double- and triple- stranded nanostructures can be formed due to the formation of *J*-aggregates between the fibers.

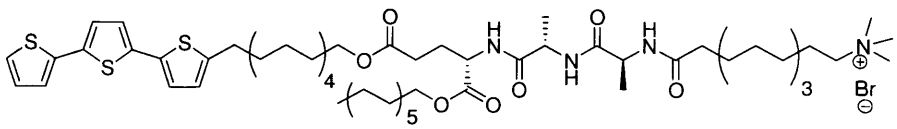

4.6

Scheme 4.5

Chiral aggregates were also formed by self assembly of carbohydrate-functionalised oligothiophenes **4.7** and **4.8** in an aqueous environment (Scheme 4.6).[41] The stereochemistry of the carbohydrates determines the helicity of the aggregates. The free –OH groups present

on the carbohydrates are able to form intermolecular hydrogen bonds, driving the π-system into well-ordered helical structure.

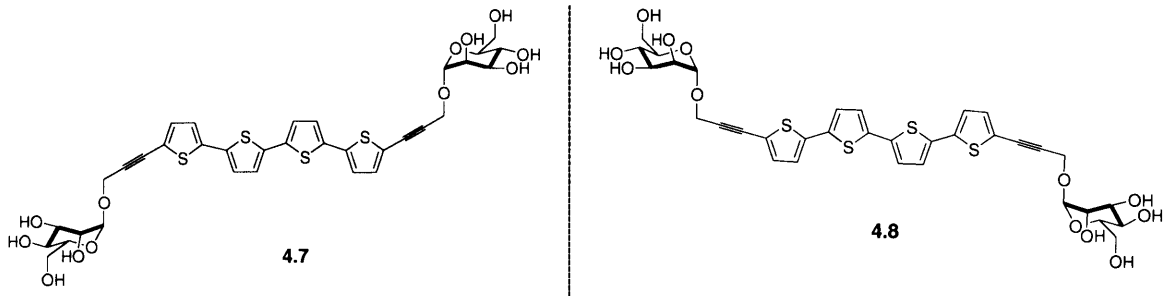

4.7 **4.8**

Scheme 4.6

Van Esch and co-workers[42] synthesised amphipilic conjugated terthiophenes (Scheme 4.7) that aggregate into micelles in water. Studies based on dynamic light scattering and cryo-transmission electron microscopy indicate that isomer **4.9** shows spherical micellar morphology with a diameter of 6 ± 2 nm while isomer **4.10** forms cylindrical micelles with a diameter of 21 ± 5 nm. These micelles can host hydrophobic chromophores such as tetraphenylporphyrin or Nile Red, forming new antenna systems by self assembly.

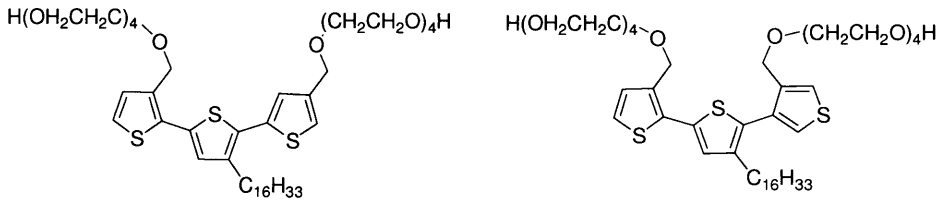

4.9 **4.10**

Scheme 4.7

4.3 Results and discussions

π-Conjugated aromatic molecules such as oligothiophenes, polythiophenes as well as the fluorescent dye Hoechst 33258[43] self aggregate in solution *via* π-π stacking interactions (Section 4.1). Self aggregation should be taken into account when studying the thermodynamics and modes of interactions of conjugated oligoaromatics with nucleic acids. The key issue with ligand self aggregation phenomena is that self aggregation competes with the DNA binding. Understanding and quantifying the self aggregation of conjugated oligoaromatics in aqueous solution is crucial. Our aims here are, therefore, to determine the mode of self aggregation and to quantify the thermodynamics of self association of a series of cationic oligoheteroaromatics in aqueous solution using a variety of complementary techniques, *viz.* ^{1}H-NMR, pulsed gradient spin echo NMR (PGSE NMR), isothermal titration calorimetry (ITC), and small angle neutron scattering (SANS). The molecules investigated are summarised in Scheme 4.8.

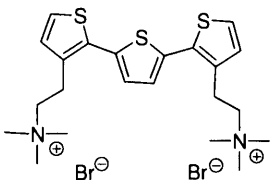

4.11

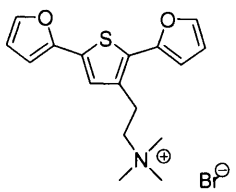

4.12

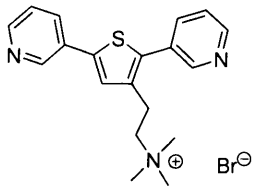

4.13

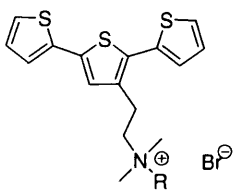

4.14 R=CH_3
4.15 R= CH_2CH_2OH
4.16 R=$CH_2CH_2OCH_2CH_2OH$

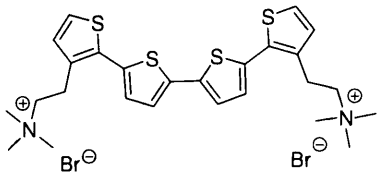

4.17

Scheme 4.8

4.3.1 Non-cooperative self association. Isodesmic self aggregation *vs* dimerisation

4.3.1.1 Self association of dicationic terthiophenes 4.11

^{1}H-NMR

In order to determine if dicationic terthiophene **4.11** self aggregates in aqueous solution, a series of ^{1}H-NMR spectra of **4.11** in D_2O at 25 °C were recorded as a function of concentration.

The chemical shifts for two selected protons were highly shifted with increasing concentration of **4.11** (Figure 4.4).

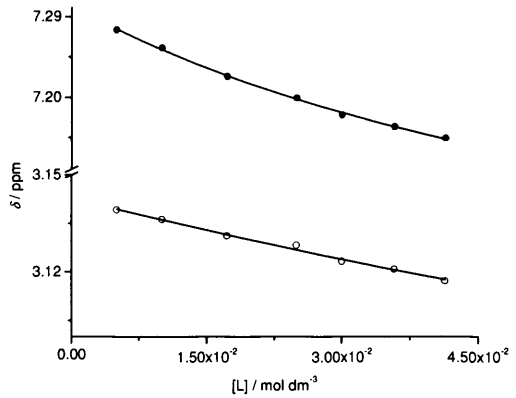

Figure 4.4 Concentration dependence of chemical shifts for $-N^+(CH_3)_3$ (o) and –CH(Th) (•) protons of **4.11** in D_2O, at 25 °C. Black lines represent (identical) fits to stepwise self aggregation and dimerisation models.

Figure 4.4 reveals a monotonous decrease in chemical shift with increasing concentration indicating that **4.11** self aggregates non-cooperatively in the studied concentration range. In order to estimate the association constant that characterises the aggregation process, the experimental results have been analysed using an indefinite non-cooperative models (Section 2.3).

The red lines in Figure 4.4 show the fits to both isodesmic and stepwise self aggregation models described by equations (2.31) and (2.32) in Section 2.4.1. Both models provide identical fits and the values of K_{agg} and K_{dim} (Table 4.1) are identical apart of a factor of two, as anticipated from their mathematical relationship. Table 4.1 shows the association constants for **4.11** in terms of both stepwise aggregation and dimerisation models. The small values found for the association constants suggest that dicationic terthiophene **4.4** self aggregates weakly. The predicted chemical shifts for monomers (δ_{mon}) and aggregates (δ_{agg}) are also summarised in Table 4.1.

Table 4.1 The calculated chemical shifts and equilibrium constants for **4.11** in D_2O at 25 °C

Isodesmic self aggregation			
Proton	δ_{mon}(ppm)	δ_{agg}(ppm)	K_{agg}/ M^{-1}
-Ar	7.3±0. 1	6.6±0.1	7.8±1.657
$-CH_3$	3.1±0. 1	3.0±0. 2	
Dimerisation			
Proton	δ_{mon}(ppm)	δ_{dim} (ppm)	K_{dim}/ M^{-1}
-Ar	7.3±0. 1	6.6±0.1	4.0±1.1
$-CH_3$	3.1±0. 2	2.7±0.1	

Diffusion NMR (PGSE NMR)

To confirm the self aggregation of **4.11**, its diffusion coefficient was measured as a function of concentration using PGSE NMR (Figure 4.5).

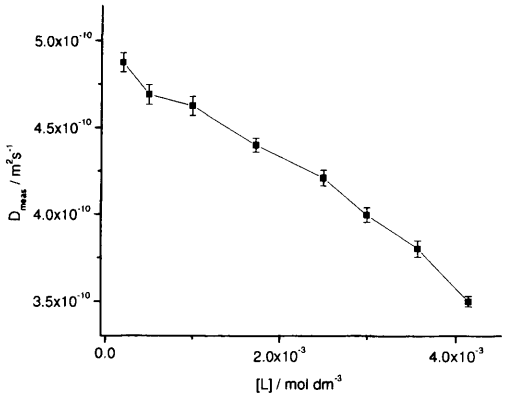

Figure 4.5 Variations of the self diffusion coefficient (■) with concentration for **4.11** in D_2O at 25 °C.

Figure 4.5 illustrates a monotonous decrease of the self diffusion coefficient of dicationic terthiophene **4.11** with increasing concentration. The absence of sigmoidal behaviour indicates that **4.11** self aggregates non-cooperatively in aqueous solution in the studied concentration range.

Isothermal titration calorimetry (ITC)

Self association of dicationic terthiophene **4.11** in aqueous solution was further studied using ITC. A concentrated solution of **4.11** in H_2O was injected into the calorimeter cell and the heat effects of breaking up of the aggregates were measure after each injection (Figure 4.6).

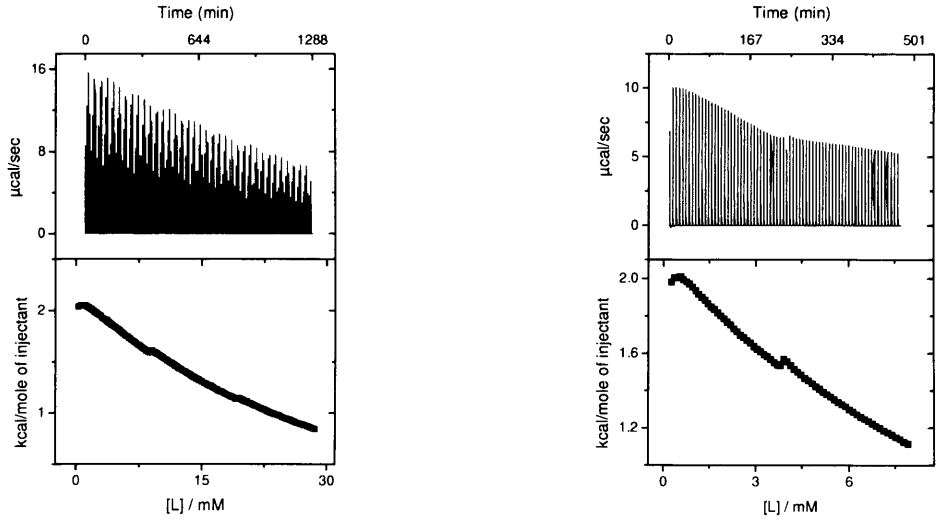

Figure 4.6 Heats of dilution of 43.0 mM solution of **4.11** in H_2O (left) and 23.6 mM of **4.11** at pH 7.0, in 25 mM MOPS, 50 mM NaCl and 1 mM EDTA (right), both at 25°C.

Figure 4.6 shows a non-constant monotonously decreasing heat of dilution without sigmoidal behaviour for **4.11** in H_2O as a function of ligand concentration in the cell. The absence of sigmoidal behaviour suggests that **4.11** self aggregates non-cooperatively in H_2O up to a concentration of 16.6 mM. The data agrees with the ^{1}H-NMR data and PGSE NMR. Similarly, heats of dilution for **4.11** in salt-containing buffer do not show sigmoidal behaviour (Figure 4.6). The lack of sigmoidal behaviour indicates that **4.11** does not aggregate cooperatively, even in the presence of added salt. We analysed the calorimetric data

for dicationic terthiophene **4.11** using stepwise self aggregation and dimerisation models (Figure 4.7).

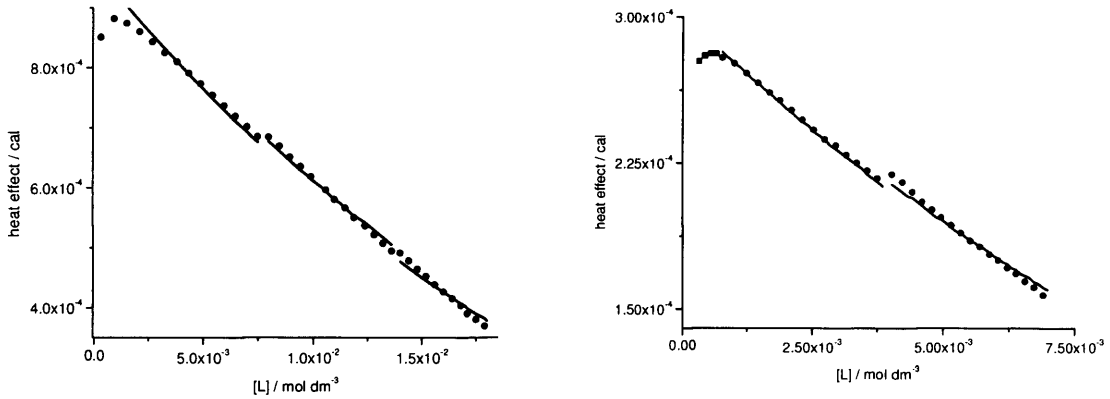

Figure 4.7 Integrated heat effects for dilution of 40.3 mM solution of **4.11** in H_2O (left) and 23.6 mM of **4.11** at pH 7, in 25 mM MOPS, 50 mM NaCl and 1 mM EDTA (right) at 25 °C. The solid black lines represent the fits to stepwise self aggregation and dimerisation models.

Figure 4.7 shows the fits to stepwise self aggregation and dimerisation models for dilution of **4.11** in H_2O and MOPS buffer at 25°C. The dilution curves for self aggregated **4.11** in both H_2O and MOPS buffer at 25°C do not display pronounced curvature, suggesting weak self aggregation and making quantification of the thermodynamic parameters difficult. The thermodynamic parameters for stepwise self aggregation and dimerisation in both H_2O and MOPS buffer together with $\{\Sigma dev^2/dof\}^{1/2}$ are summarised in Table 4.2.

Table 4.2 Thermodynamic parameters describing stepwise self aggregation and n-merisation model of 43.0 mM solution in water and 23.6 mM in MOPS buffer of **4.11**, at 25°C

	Stepwise self aggregation				
	K_{agg} (M^{-1})	ΔH_{agg} (kcal mol^{-1})	ΔG_{agg} (kcal mol^{-1})	$-T\times\Delta S_{agg}$ (kcal mol^{-1})	$\{\Sigma dev^2/dof\}^{½}$ (μcal)
MOPS, pH7.0	2.6	-29.4(-34.3; -8.7)[a]	[b]	[b]	2.7
H_2O	1.1	-45.3[c]	[b]	[b]	9.6
	Dimerisation				
	K_{dim} (M^{-1})	ΔH_{dim} (kcal mol^{-1})	ΔG_{dim} (kcal mol^{-1})	$-T\times\Delta S_{dim}$ (kcal mol^{-1})	$\{\Sigma dev^2/dof\}^{½}$ (μcal)
MOPS, pH7.0	1.0	-76.2(-85.7; -33.1)[a]	[b]	[b]	2.5
H_2O	1.0	-50.1(-60.6; -20.9)[a]	[b]	[b]	10.8

a) The reported range given within the brackets corresponds to fits for which the normalized $\Sigma dev^2/dof < 2$.
b) No value reported for ΔG and ΔS because K and ΔH are not well defined.
c) No error margins or variable range reported because global minimum does not appear to have been found (See appendix).

Analysis of the dilution data of **4.11** in H_2O in terms of dimerisation and stepwise self aggregation models show high values for $\{\Sigma dev^2/dof\}^{½}$, but these values are still on the limit of the model's suitability. However, analysis of dilution data of **4.11** in MOPS buffer resulted in fits that better reproduce the experimental data. Unfortunately, K_{agg} and K_{dim} are not sufficiently defined to obtain Gibbs energy changes and therefore entropy changes. Plots of $\Sigma dev^2/dof$ as a function of optimisable parameters showed that errors margins are typically large (See Appendix).

Summary

^{1}H-NMR and ITC show weak non-cooperative self aggregation for dicationic terthiophene **4.11** in the studied concentration range. PGSE-NMR also confirms that **4.11** does not self aggregate cooperatively in the studied concentration range.

4.3.1.2. Self association of cationic furan-thiophene derivatives 4.12

^{1}H-NMR

The mode of self aggregation of furan-thiophene derivative **4.12** was first determined using ^{1}H-NMR spectroscopy. A series of ^{1}H-NMR spectra of **4.12** was recorded as a function of concentration (Figure 4.8).

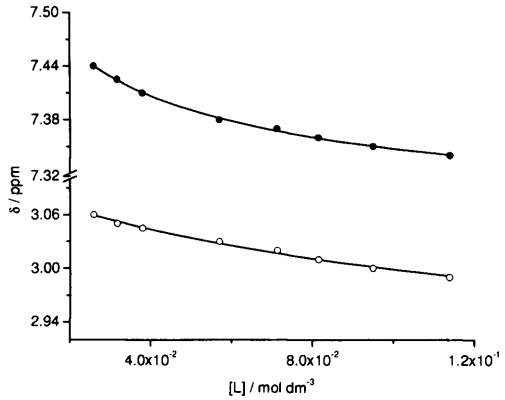

Figure 4.8 Concentration dependence of chemical shifts for $-N^+(CH_3)_3$ (o) and –CHTh (•) protons of **4.12** in D_2O, at 25 °C. The black lines are (identical) fits to stepwise self aggregation and dimerisation models.

The chemical shifts for two chosen protons in Figure 4.8 are shifted with increasing concentration. This indicates that **4.12** self aggregates in aqueous solution. The non-sigmoidal decrease of the chemical shifts with concentration indicates a non-cooperative process for self aggregation of **4.12**. Additionally, Figure 4.8 shows fits to both stepwise self aggregation and dimerisation models for dilution of **4.12** in D_2O at 25°C. Both models provide identical fits.

The association constants resulting from the fitting of stepwise self aggregation and dimerisation models to the experimental ^{1}H-NMR data are presented in Table 4.3.

Again, the association constants for analysis in term of both aggregation models are different by a factor of two. Moreover, these values are small suggesting that mono-cationic **4.12** self aggregates weakly. The predicted chemical shifts for monomers (δ_{mon}) and aggregates (δ_{agg}) are also summarised in Table 4.3.

Table 4.3 The calculated self association parameters for **4.12** in D_2O at 25 °C

Isodesmic self aggregation			
Proton	δ_m(ppm)	δ_{agg}(ppm)	K_{agg}/ M^{-1}
-Ar	7.7±0.1	7.2±0.01	112.2±85.2
$-CH_3$	3.2±0.3	2.9±0.05	
Dimerisation			
Proton	δ_m(ppm)	δ_d(ppm)	K_{dim}/ M^{-1}
-Ar	7.7±0.1	7.2±0.01	56.1±42.6
$-CH_3$	3.2±0.3	2.9±0.05	

Diffusion NMR (PGSE NMR)

In order to confirm the mode of self aggregation of **4.12** in aqueous solution, we carried out PGSE-NMR experiments. The diffusion coefficient of **4.12** in D_2O at 25 °C was measured as a function of the concentration (Figure 4.9). The solutions used for this experiment were prepared by dilution of 36.7 mM solution of **4.12**. The experiments were set-up over one week.

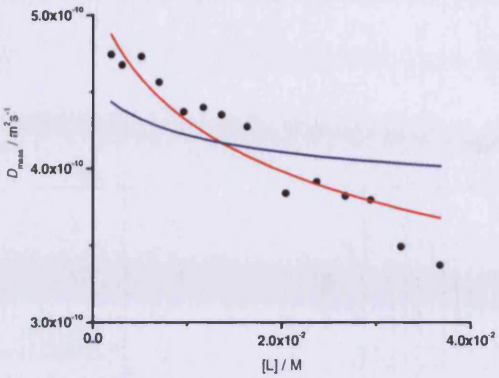

Figure 4.9 Diffusion coefficients for **4.12** in D_2O, at 25 °C as a function of concentration. Coloured lines represent fitted diffusion coefficients assuming stepwise aggregation (red) or dimerisation (blue) models.

Figure 4.9 shows a monotonous decrease in the diffusion coefficient with increasing concentration. The non-sigmoidal curve is analogous to that observed for the ^{1}H-NMR spectra, confirming that **4.12** self aggregates non-cooperatively in aqueous solution. Unfortunately, **4.12** degrades over time *(vide infra)* and this probably explains the significant scatter in Figure 4.9. Nevertheless, fitting the diffusion data using models assuming dimerisation or stepwise aggregation (Section 2.4.2) confirms stepwise self aggregation as mode of self aggregation for **4.12**.

Isothermal titration calorimetry (ITC)

The thermodynamics of self aggregation of **4.12** in aqueous solution was further analysed using isothermal titration calorimetry. A dilution experiment in D_2O, at 25 °C was carried out using 13.8 mM stock solution of **4.12**. The solution was kept in dark, at room temperature over 8 months. The dilution in MOPS buffer was run using a fresh solution of **4.12**.

The ITC data for both dilutions of **4.12** into D_2O and MOPS buffer at pH 7.0 and at 25 °C are presented in Figure 4.10.

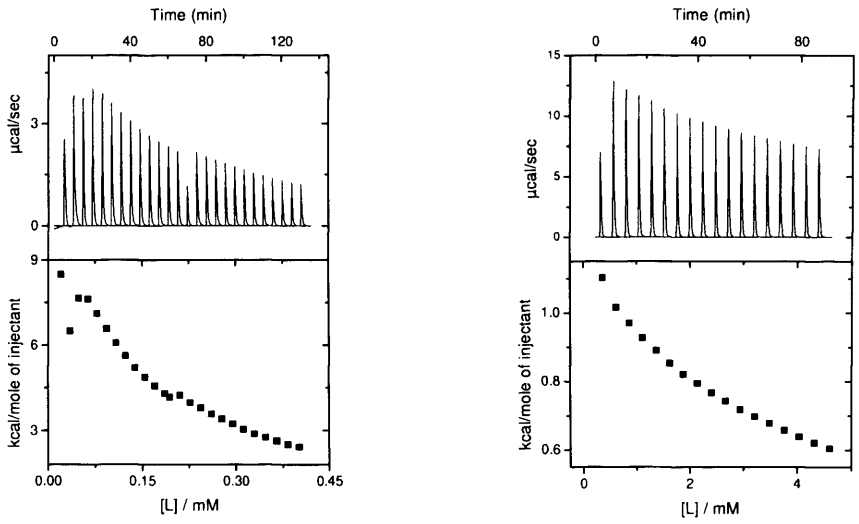

Figure 4.10 Heats of dilution for 13.80 mM solution of **4.12** in D_2O (left) and 20.1 mM of **4.12** at pH 7.0, in 25 mM MOPS, 50 mM NaCl and 1 mM EDTA, at 25°C.

Figure 4.10 shows non-constant heat effects without sigmoidal behaviour for dilution of **4.12** as a function of ligand concentration in the calorimeter cell. The absence of sigmoidal behaviour suggests that the ligand self aggregates non-cooperatively in the studied concentration range. Also in the presence of salt-containing buffer, heats of dilution for **4.12** do not show sigmoidal behaviour indicating that **4.12** does not aggregate cooperatively. Ligand dilution experiments were analysed using stepwise aggregation and dimerisation models (Figure 4.11).

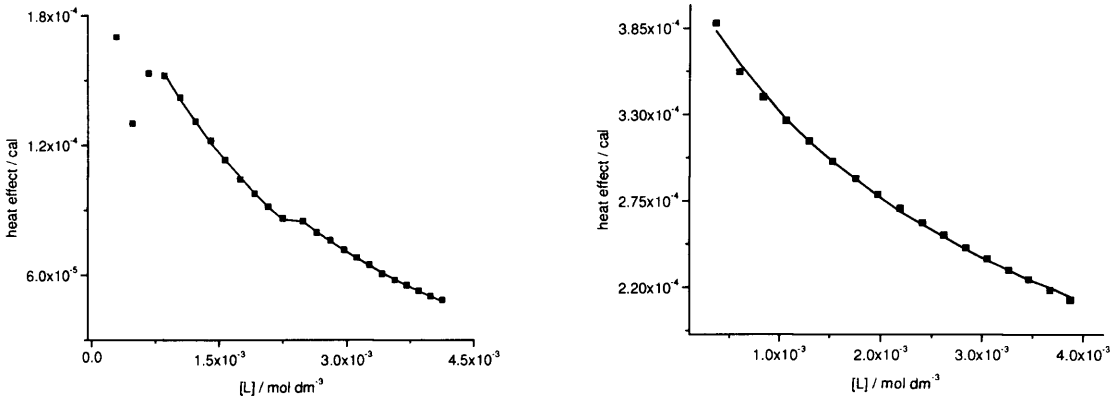

Figure 4.11 Integrated heat effects for dilution of 13.80 mM solution of **4.12** in D_2O and 20.1 mM solution of **4.12** in 25 mM MOPS, 50 mM NaCl and 1 mM EDTA, pH 7.0, both at 25 °C. The solid black lines represent the fits to stepwise self aggregation and dimerisation models.

Figure 4.11 shows that the dimerisation and stepwise self aggregation models provide identical fits and that both models accurately reproduce the ITC dilution data for **4.12**. The thermodynamic parameters obtained from fitting the stepwise self aggregation and dimerisation models to the observed heats of dilution for **4.12** in D_2O and in MOPS buffer, at pH 7.0 are summarised in Table 4.4. Also $\{\Sigma dev^2/dof\}^{1/2}$ are presented in Table 4.4.

Table 4.4 Thermodynamic parameters describing stepwise self aggregation and dimerisation of **4.12** in MOPS buffer[a,b] and in D_2O

Stepwise self aggregation

		K_{agg} (M^{-1})	ΔH_{agg} (kcal mol^{-1})	ΔG_{agg} (kcal mol^{-1})	$-T\times\Delta S_{agg}$ (kcal mol^{-1})	$\{\Sigma dev^2/dof\}^{1/2}$ (μcal)
10 °C						
D_2O	32.2 mM[a]	18.1 (13.7; 20.7)[f]	-3.9 (-4.8; -3.7)[f]	-1.6 (-1.7; -1.4)[f]	2.3 (2.3; 3.1)[f]	1.0
	15.3 mM[b]	158.6 (65.5; 276.3)[f]	-1.3±0.2	-2.8±0.3	-1.5±0.1	1.3
25°C						
MOPS[c]	20.1 mM[e]	92.7± 5.4	-1.7±0.8	-2.7±0.3	-1.0±0.5	2.2
MOPS[d]	26.8 mM[a]	1.8	-29.9 (-57.9; -10.9)[f]	[g]	[g]	1.5
D_2O	13.8 mM[b]	120±30	-1.7±0.2	-2.8±0.1	-1.1±0.1	0.5
	32.2 mM[a]	14.7 (11.7; 16.8)[f]	-4.8±(-5.6; -4.3)[f]	-1.6 (-1.7;-1.4)[f]	3.2 (2.9; 3.9)[f]	1.0

Dimerisation

		K_{dim} (M^{-1})	ΔH_{dim} (kcal mol^{-1})	ΔG_{dim} (kcal mol^{-1})	$-T\times\Delta S_{dim}$ (kcal mol^{-1})	$\{\Sigma dev^2/dof\}^{1/2}$ (μcal)
10°C						
D_2O	32.2 mM[a]	9.8 (7.1; 13.1)[f]	-7.6±1.8	-1.3±0.2	6.3±1.6	0.9
	15.3 mM[b]	79.2 (47.7; 139.6)[f]	-2.60±0.5	-2.3 ±0.3	0.2±0.2	1.3
25°C						
MOPS[c]	20.1 mM[d]	43.9±30.2	-3.3±0.6	-2.2±0.3	1.1±0.3	2.2
MOPS[d]	26.8 mM[a]	1.0	-54.3	[g]	[g]	1.5
D_2O	13.8 mM[b]	59.7±12.2	-3.5±0.2	-2.4±0.1	1.1±0.1	0.50
	32.2 mM[a]	7.3 (5.7; 8.3)[f]	-9.75 (-11.4; -8.9)[f]	-1.1±0.1	8.6(7.9; 11.2)[f]	1.0

a) Solutions 2months old.
b) Solutions 8 months old.
c) Solutions in deutered 25mM MOPS, 50 mMNaCl and 1mM EDTA, pH 7.0.
d) Solutions in 25 mM MOPS, 50 mMNaCl and 1 mM EDTA, pH 7.0.
e) Solutions 1day old.
f) The reported range given within brackets corresponds to fits for which the normalised $\Sigma dev^2/dof<2$ (See Appendix)
g) No value reported for ΔG and ΔS because K and ΔH are not well defined.

Despite the good fits obtained for stepwise self aggregation and dimerisation models (See Appendix), thermodynamic parameters for dilution of **4.12** under identical conditions are not reproducible. Table 4.4 shows discrepancies between the thermodynamic parameters for dilution experiments run at different concentrations, in the same solvent and temperature. For example, the self aggregation of 32.2 mM solution of **4.12** in D_2O at 10°C is characterised by negative entropy changes, while positive entropy changes characterise the dilution of a 15mM solution of **4.12** in D_2O, at the same temperature. These discrepancies for the thermodynamic parameters can be explained by degradation of **4.12** in time. The stability of **4.12** in time was studied by UV-Vis spectroscopy. A series of UV-Vis spectra were recorded for solutions of **4.12** in Table 4.4 (Figure 4.12).

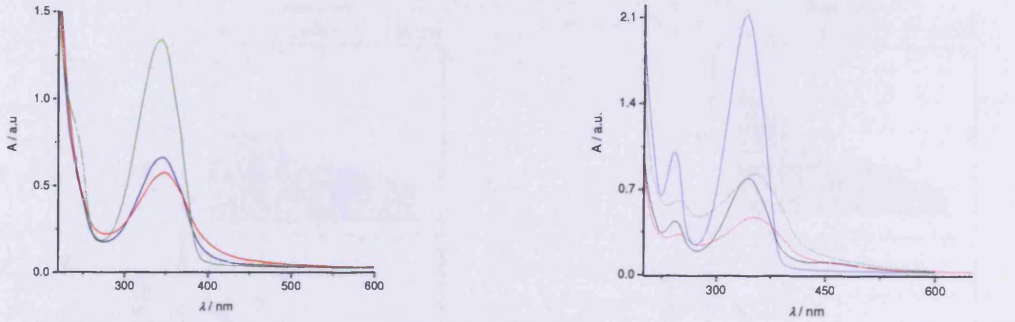

a **b**

Figure 4.12 UV-visible spectra for **4.12** in MOPS buffer **(a)**: fresh stock solution-one day old (green line) ; 26.8 mM solution obtained by dilution of fresh solution (red line) and 20.1 mM solution (blue line). UV-visible spectra for **4.12** in D_2O **(b)**: fresh stock solution-one day old (blue line); 32.2 mM solution obtained by dilution of a fresh stock solution (black line); 15.38 mM (red line); 13.8 mM (green line).

Figure 4.12 shows how the UV-Vis spectra of **4.12** in MOPS buffer and D_2O changes with the time. A slow increase in the absorption of **4.12** in both MOPS buffer and D_2O at long wavelengths was observed suggesting that **4.12** slowly polymerises.

Summary

Cationic furan derivative **4.12** shows non-cooperative self aggregation according to dilution studied using ^{1}H-NMR, PGSE-NMR and ITC. The thermodynamic parameters could not be quantified because **4.12** slowly degrades in aqueous solution.

4.3.1.3 Preliminary studies of self association of cationic pyridine derivative 4.13

Isothermal titration calorimetry

To further study the thermodynamics and the mode of self aggregation of cationic pyridine **4.13**, dilution experiments were carried out using isothermal titration calorimetry (Figure 4.13).

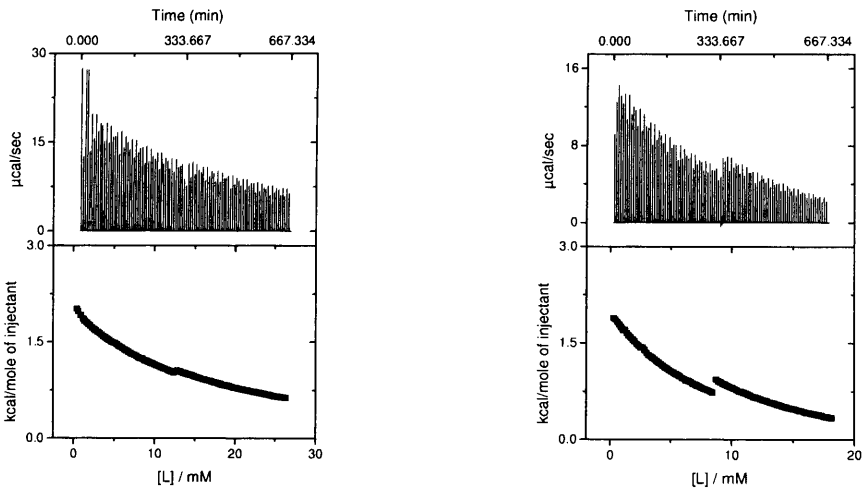

Figure 4.13 Heats of dilution of 64.82 mM solution of **4.13** in H_2O (left) and 45.5 mM of **4.13** at pH 7.0, in 25 mM MOPS, 50 mM NaCl and 1 mM EDTA, at 25 °C (right). Both data sets consist of two consecutive titrations.

Figure 4.13 shows a monotonous decrease without sigmoidal behaviour for cationic pyridine derivative **4.13**. The absence of sigmoidal behaviour suggests that **4.13** does not self aggregate cooperatively in aqueous solution in concentration range studied. Dimerisation and stepwise self aggregation models were used to analyse the ITC data for **4.13** in H_2O at 25°C.

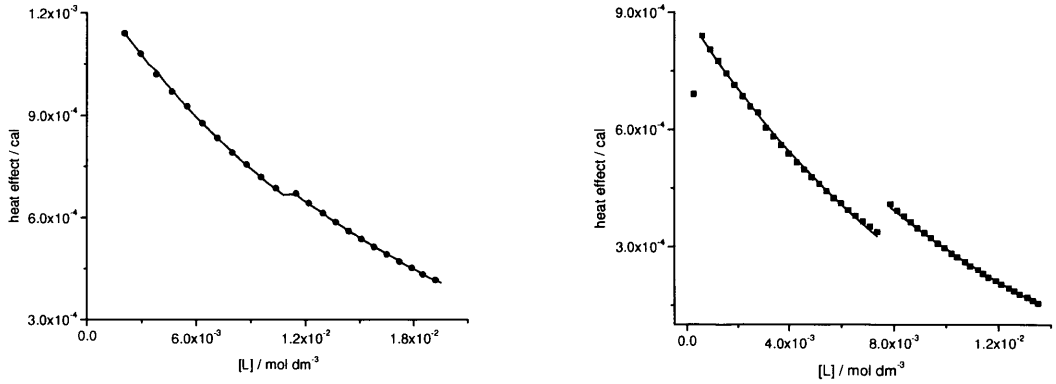

Figure **4.13** Integrated heat effects for dilution of a 64.4 mM solution of **4.13** in H_2O and 45.5 mM of **4.13** at pH 7.0, in 25 mM MOPS, 50 mM NaCl and 1 mM EDTA at 25 °C. The solid black lines represent the fits to stepwise self aggregation and dimerisation models.

Figure 4.13 shows that the dimerisation and stepwise self aggregation models provide identical fits and both models accurately reproduce the ITC dilution data. Identical fits were also obtained for dilution of **4.3** at pH 7.0, in 25 mM MOPS, 50 mM NaCl and 1 mM EDTA, at 25°C (Appendix). The thermodynamic parameters for the dilution of cationic pyridine **4.13** in H_2O and in MOPS buffer, at 25 °C are shown in Table 4.5.

Table 4.5 Thermodynamic parameters for stepwise self aggregation and dimerisation of **4.13** in MOPS buffer[a] and H_2O at **25°C**

Stepwise self aggregation

	K_{agg} (M^{-1})	ΔH_{agg} (kcal mol^{-1})	ΔG_{agg} (kcal mol^{-1})	$-T\times\Delta S_{agg}$ (kcal mol^{-1})	$\{\Sigma dev^2/dof\}^{1/2}$ (μcal)
MOPS, pH7.0	11.6±3.8	-9.6±2.3	-1.4±0.2	8.2±2.1	4.7
D_2O	8.8±2.0	-7.0±1.1	-1.2±0.1	5.8±1.0	2.9

Dimerisation

	K_{dim} (M^{-1})	ΔH_{dim} (kcal mol^{-1})	ΔG_{dim} (kcal mol^{-1})	$-T\times\Delta S_{dim}$ (kcal mol^{-1})	$\{\Sigma dev^2/dof\}^{1/2}$ (μcal)
MOPS, pH7.0	5.8±2.0	-19.3±5.8	-1.0±0.2	18.3±5.6	4.7
D_2O	4.4±1.0	-13.9±2.2	-0.9±0.1	13.0±2.1	2.9

a) 25 mM MOPS, 50 mM NaCl and 1 mM EDTA.
b) For errors see Appendix

Table **4.5** indicates that all thermodynamic parameters change from water to buffer. In particular, self aggregation constant K_{dim} and K_{agg} are higher in MOPS buffer, suggesting that the aggregation of **4.13** is induced by one (or more) of the buffer components. The most likely candidate is NaCl which could shield the electrostatic repulsions between molecules of **4.13**. However, K_{agg} and K_{dim} are small, indicating a small tendency of this surfactant molecule to self aggregate in aqueous solution. Dimerisation and stepwise self aggregation are exothermic processes with negative entropy changes.

This weak aggregation for **4.13** in aqueous solution can be associated with protonation and deprotonation of the pyridines. The values for $\{\Sigma dev^2/dof\}^{1/2}$ obtained for the dilution of **4.13** in terms of dimerisation and stepwise self aggregation are small, suggesting that the calculated data reproduce well the experimental data. Equilibrium contants (*e.g.* K_{agg} and K_{dim}) are sufficiently defined to obtain Gibbs energy changes (ΔG_{agg} and ΔG_{dim}) and therefore entropy changes ($-T\Delta S_{agg}$ and $-T\Delta S_{dim}$). Error margins are distributed symmetrically around the optimisable parameters (See Appendix).

Summary

In conclusion diffusion ^{1}H-NMR and ITC data show that the cationic pyridine derivative **4.13** weakly self aggregates non-cooperatively in aqueous solution pH 7.0. The self aggregation might be associated with protonation and deprotonation of the pyridine ring.

4.3.2 Cooperative self association in aqueous solution

4.3.2.1 Self aggregation of cationic terthiophenes 4.14-4.16

^{1}H-NMR

The mode of self aggregation of **4.14-4.16** in aqueous solution was studied using ^{1}H-NMR. A series of ^{1}H-NMR spectra for **4.14** and **4.16** were recorded in D_2O, at 25 °C as a function of concentration (Figure 4.14).

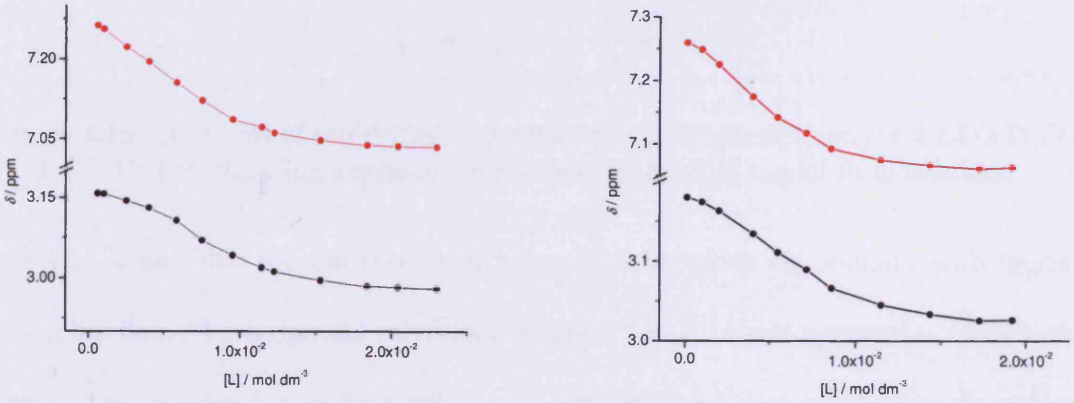

Figure 4.14 Concentration dependence of chemical shifts for $-N^+(CH_3)_3$ protons (●) and –CHTh (●) of **4.14** (left) and **4.16** (right) in D_2O, at 25 °C.

Figure 4.14 shows a sigmoidal decrease in the chemical shifts for two selected protons with increasing concentration, indicating that **4.14** and **4.16** self aggregate cooperatively in the

studied concentration range. The similarity in the data for **4.14** and **4.16** shows that the introduction of short substituents, *e.g.*, oligoethyleneglycol, on the ammonium group does not change the mode of self aggregation.

Diffusion NMR (PGSE NMR)

We investigated the self aggregation of cationic terthiophenes **4.14-4.16** using PGSE NMR. The diffusion coefficient of **4.14** in D_2O at 25 °C was measured as a function of concentration (Figure 4.15).

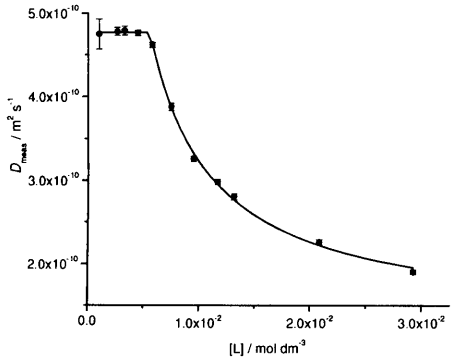

Figure 4.15 Variations of self diffusion coefficient with concentration for **4.14** in D_2O at 25 °C. The black line represents the two-state mobility model fit to the data.

Figure 4.15 shows that the diffusion coefficient of **4.14** varies sigmoidally with increasing the concentration. The sigmoidal behaviour suggests that **4.14** self aggregates cooperatively. Assuming that at equilibrium both spherical aggregates and free monomers are present in solution, the diffusion data in Figure 4.15 was analysed using the two-state mobility model (Section 2.4.2). The obtained value for the critical micelle concentration is 5.6 mM, in good agreement with the value obtained from surface tension and isothermal titration calorimetry experiments *(vide infra)*. The self diffusion coefficient of micelles estimated through the two-

state mobility model was found to be $D_{micelle}$= (1.28 ± 0.04)×10^{-10}. Using the Stoke-Einstein equation, we found a hydrodynamic radiusof 16.1 Å. This value is in agreement with the radius of 16 Å found from SANS experiments *(vide infra)*. Using equation 2.41 (Section 2.4.2), the volume of micelles is 17.5×10^3 (Å)^3 while the volume of the monomers was calculated from the crystal structure of **4.14** to be 456.7 Å. Therefore, from the ratio between the volume of micelles and the volume of monomers we found an aggregation number of 38.2. Unfortunately, this aggregation number is not in agreement with the aggregation number determined by ITC *(vide infra)*.

Surface tension

In order to confirm the critical micelle concentration, we carried out surface tension measurements as a function of concentration for **4.14** in aqueous solutions, at 25 °C. Figure **4.16** shows the plot of the surface tension for **4.14** in H_2O, at 25 °C against the natural logarithm of the concentration (Figure 4.16).

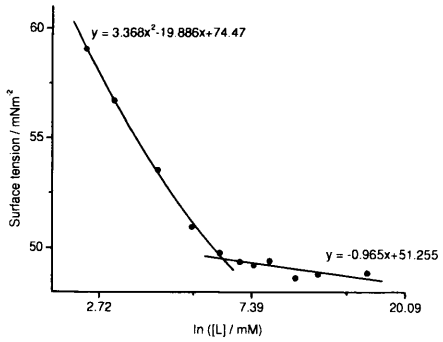

Figure 4.16 Variations of surface tension with concentration for **4.14** in H_2O, at 25 °C. The black lines represent fits to polynomial and linear expressions.

The data in Figure 4.16 depicts that the surface tension of **4.14** in H_2O at 25 °C shows an inflection point at concentration 6.1 mM. This behaviour suggests that **4.14** forms micelles in H_2O at 25 °C when it reaches a concentration of 6.1 mM. Moreover, the surface tension curve presents no minimum around the critical micelle concentration, indicating a good purity of the surfactant. Similarly, the surface tension of **4.14** was measured as a function of concentration in MOPS buffer, pH 7.0, at 25 °C (Figure 4.17).

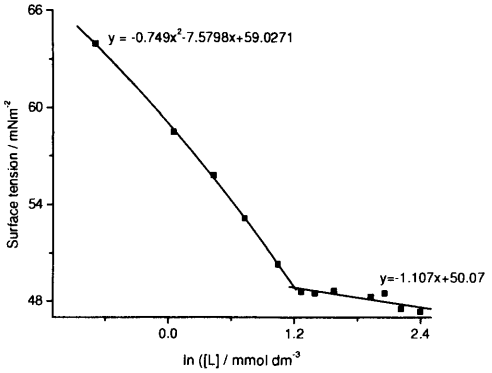

Figure 4.17 Variations of surface tension with concentration for **4.14** in MOPS buffer, pH 7.0, at 25 °C. The black lines represent fits to polynomial and linear expressions.

The surface tension data in MOPS buffer, pH 7.0, at 25 °C shows an inflection point at 3.3 mM, which suggests that **4.14** form micelles in the buffer as well. The cmc decreases in MOPS buffer compared to H_2O, suggesting that aggregation of **4.14** is facilitated by one (or more) of the buffer components. Most likely, this is the result of increased screening of electrostatic repulsion between monomers, at higher concentrations of NaCl. This is in perfect agreement with the data observed by ITC *(vide infra)*.

Isothermal titration calorimetry

To further study in detail the self association of cationic terthiophene **4.14**, we used isothermal titration calorimetry. Dilution experiments were carried out by injecting a concentrated solution of **4.14** in H_2O into a calorimeter cell containing the same solvent (Figure 4.18).

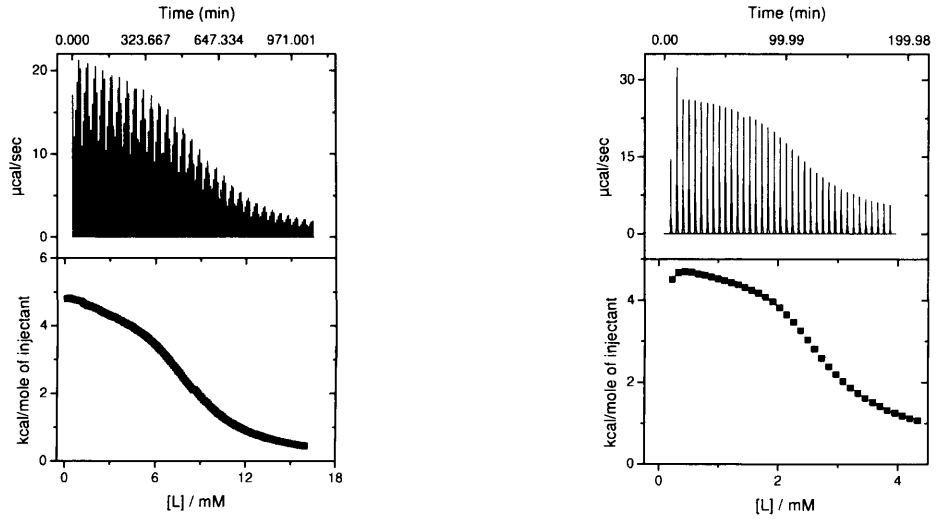

Figure 4.18 Heats of dilution of a 41.7 mM solution of **4.14** in H_2O (left) and 22.3 mM solution of **4.14** at pH 7.0, in 25 mM MOPS, 50 mM NaCl and 1 mM EDTA (right), both at 25 °C.

Figure 4.18 shows a non-constant heat of dilution with sigmoidal behaviour for **4.14** as a function of ligand concentration in the calorimeter cell. The sigmoidal behaviour indicates that **4.14** self aggregate cooperatively in H_2O in the studied concentration range. Heats of dilution for **4.14** in 25 mM MOPS, 50 mM NaCl and 1 mM EDTA, at 25 °C show also sigmoidal behaviour (Figure 4.18).

The same sigmoidal behaviour was observed for **4.15** and **4.16** suggesting that **4.15** and **4.16** also self aggregate cooperatively at pH 7.0, in 25 mM MOPS, 50 mM NaCl and 1 mM EDTA (Figure 4.19).

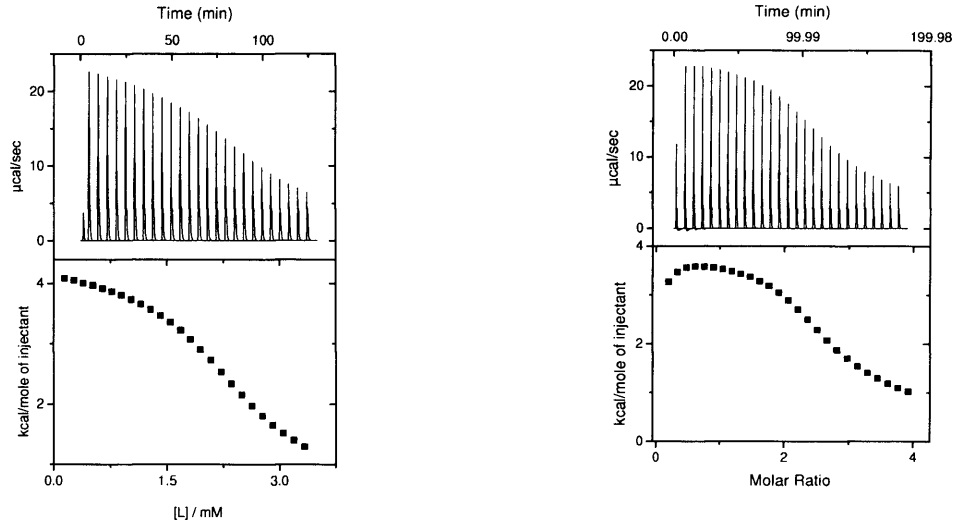

Figure 4.19 Heats of dilution of a 17.7mM solution of **4.15** (left) and 19.8 mM of **4.16** (right) at pH 7.0, in 25 mM MOPS, 50 mM NaCl and 1 mM EDTA, at 25 °C.

The mode of self aggregation does not change if the substituent on the amine group is replaced by longer alkyl substituents. Critical micelle concentrations for **4.14-4.16** at pH 7.0, in 25 mM MOPS, 50 mM NaCl and 1 mM EDTA at 25 °C, were determined by plotting the derivative of the heat effect of dilution against the concentration of the ligand in the calorimeter cell (Figure 4. 20).

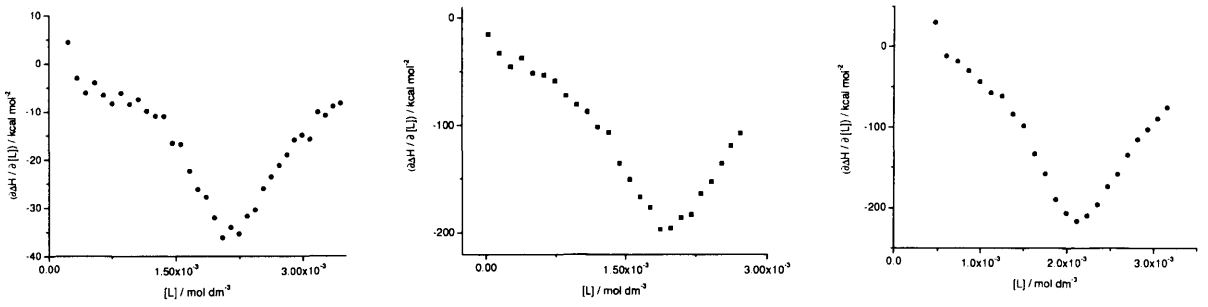

4.14 **4.15** **4.16**

Figure 4.20 Derivative of the molar heat effect as a function of ligand concentration in the calorimeter cell for the dilution of a 22.3 mM solution of **4.14**, 17.7 mM solution of **4.15** and 19.7 mM solution of **4.16** into MOPS buffer, pH 7.0, at 25 °C.

The derivatives of the dilution curves in Figure 4.20 display a minimum, which is indicative of the critical micelle concentration and the formation of micelles. Similarly, the critical micelle concentration for **4.14** was determined in H_2O at 10 °C, 25 °C and 40 °C (See Appendix). The critical micelle concentrations obtained from ITC dilution of **4.14-4.16** in aqueous solutions, at 10 °C, 20 °C and 40 °C are summarised in Table 4.6.

Table 4.6 Critical micelle concentrations (in mM) for **4.14-4.16** in aqueous solutions, at 10°C, 25°C and 40 °C.

	10 °C	25°C	40°C
4.14			
MOPS, pH7.0	1.2	2.14	3.9
D_2O	-	6.34	>7.5
water	-	6.37	>8.2
4.15			
MOPS, pH7.0	-	1.95	-
4.16			
MOPS, pH7.0	-	2.11	-

a) 25 mM MOPS, 50 mM NaCl and 1 mM EDTA.

Clearly the cmc values obtained for **4.14-4.16** in MOPS buffer, at 25 °C are comparable, suggesting that replacing the substituent on the ammonium group does not affect the self aggregation. Smaller values for cmcs were found for **4.14** in MOPS buffer compared to

water. This suggests a higher tendency for **4.14** to self aggregate in MOPS buffer. This is attributed to NaCl salt present in MOPS buffer which increase screening of electrostatic repulsions between the monomers. If the temperature increases, the cmc increases as well while at low temperature a decrease in cmc could be observed.

Isothermal titration calorimetry - quantifying aggregation of 4.14-4.16 in H_2O and D_2O

To quantify the thermodynamic parameters of micellisation for **4.14-4.16**, we analysed the calorimetric data in terms of different cooperative self aggregation models (Section 2.6.2).

Figure 4.21 shows fits to *n*-merisation and Kegeles' models for dilution of **4.14** in H_2O, at 25 °C.

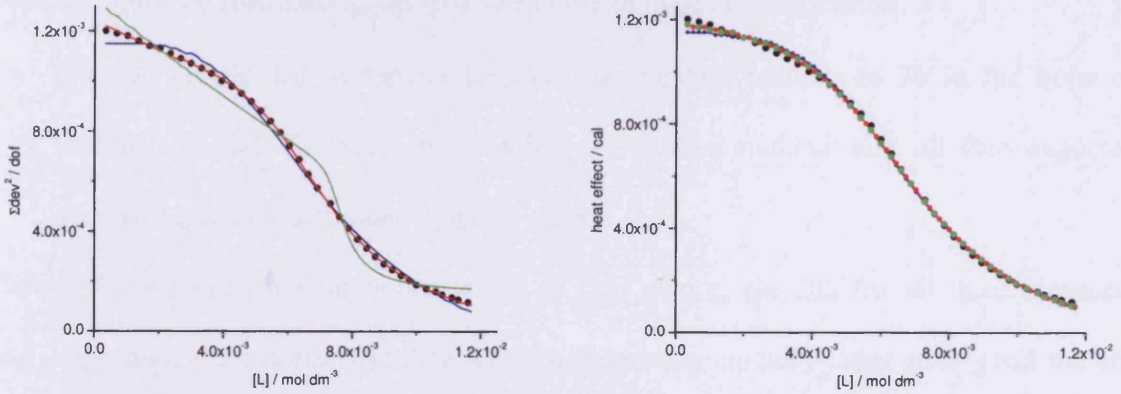

a **b**

Figure 4.21 Fits of the heat of dilution of 41.7 mM solution of **4.14** in H_2O, at 25 °C for a) n-merisation model involving: n-merisation (blue line), n-merisation and pre-micellar aggregation (red line), *n*-merisation and aggregation number n_{keg} fixed at 38 (green line); b) Kegeles' model involving: f_{keg} fixed at 0.01 (-●-), f_{keg} and aggregation number variable n_{keg} (-●-), f_{keg}variable and n_{keg} fixed at 76 (●).

We analysed calorimetric data in term of a cooperative *n*-merisation model without including the formation of pre-micellar aggregates. The fit to *n*-merisation model in Figure 4.21 does

not accurately reproduce the experimental data, especially at the beginning of the dilution curve. This occurs because *n*-merisation model does not include the formation of pre-micellar aggregates. A better fit can be obtained if the *n*-merisation model is combined with stepwise self aggregation model, accounting for the formation of pre-micellar aggregates.

To be in line with the molar distribution functions according to Kegeles' model, in case of *n*-merisation model we restricted the aggregation number to 38. Unfortunately, in this case the *n*-merisation model does not fit well to the experimental data.

For Kegeles' model we decided to test three situations and to compare the fits in all these cases.

- Firstly, the factor f_{keg} and Kegeles' aggregation number n_{keg} were variable.
- Secondly we restricted f_{keg} to 0.01 according to literature suggestion.[44]
- Finally, we decided to restrict Kegeles' aggregation number to 76 in the hope of finding a model for which the median aggregation number was 38 (the expected average aggregation number equals ½ n_{keg}).

All these fits are presented in Figure 4.21. At first glance, the fits for all three Kegeles' models reproduce the calorimetric data well. In order to accurately judge how good the fits are, we compared the values for $\{\Sigma dev^2/dof\}^{1/2}$ (Table 4.7). Table 4.7 shows relatively small values for $\{\Sigma dev^2/dof\}^{1/2}$ for analysis of dilution data of **4.14** in H_2O in terms of the *n*-merisation model with pre-micellar aggregation included compared to the *n*-merisation model without the isodesmic self aggregation model and the model where the aggregation number is restricted to 38. Also, the values for $\{\Sigma dev^2/dof\}^{1/2}$ are smaller for both Kegeles' models which

have f_{keg}variable, compare to the model where f_{keg} is restricted to 0.01. Analysis of $\Sigma dev^2/dof$ as a function of different variable shows for both *n*-merisation and Kegeles' models that error margins are large (See Appendix).

Table 4.7 also gives the aggregation numbers, equilibrium constants and interaction enthalpies for dilution of **4.14** in H_2O, at 25 °C analysed in terms of cooperative self aggregation models. ΔH_{mic} calculated using n-merisation model is negative, indicating that micellisation of **4.14** in H_2O is exothermic. ΔH_{mic} is found to be less negative if the *n*-merisation model is used in conjunction with isodesmic self aggregation model to allow for expression of premicellar aggregates. The negative values of ΔS_{mic} suggest that micellisation is mainly driven by π-π stacking interactions. Aggregation numbers for **4.14** in H_2O at 25°C are 8 according to the n-merisation model in combination with isodesmic self aggregation model and 4.9 without accounting the pre-micellar aggregates. These values are not in agreement with the aggregation number of 38 obtained from SANS and PGSE NMR data. Moreover, the differences in the aggregation number found here in comparison with SANS and PGSE-NMR cast doubt on whether *n*-merisation model is appropriate for the analysis of calorimetric data.

Table 4.7 Thermodynamic parameters for dilution of **4.14** in D_2O at 25 °C

***n*-merisation**

K_{agg} (M^{-1})	ΔH_{agg} (kcal mol^{-1})	K_{mic} (M^{-1})	ΔH_{mic} (kcalmol^{-1})	$-T\times\Delta S_{mic}$ (kcal mol^{-1})	n_{mic}	$\{\Sigma dev^2/dof\}^{1/2}$ (μcal)
-	-	59.2[a]	-10.1[a]	7.6[a]	4.9[a]	24

***n*-merisation and stepwise self aggregation**

K_{agg} (M^{-1})	ΔH_{agg} (kcal mol^{-1})	K_{mic} (M^{-1})	ΔH_{mic} (kcalmol^{-1})	$-T\times\Delta S_{mic}$ (kcal mol^{-1})	n_{mic}	$\{\Sigma dev^2/dof\}^{1/2}$ (μcal)
1.0[a]	-8.5(-132.4;-6.3)[b]	76.4[a]	-7.3 (-6.9;-7.9)[b]	4.8[a]	8.1(7.3;10.1)[b]	4.2
1.0[a]	-20.3[a]	109.6[a]	-5.5[a]	[c]	38[d]	49.1

Kegeles model

$K_{keg}/10^2$ (M^{-1})	ΔH_{keg} (kcal mol^{-1})	$-T\times\Delta S_{keg}$ (kcal mol^{-1})	n_{keg}	$10^2 f_{var}$	$\{\Sigma dev^2/dof\}^{1/2}$ (μcal)
2.3[a]	-7.7[a]	4.5[a]	12.0[a]	1.0[e]	19.6
1.3 (1.2; 1.6)[b]	-6.4 (-7.3;-6.1)[b]	3.5 (3.3; 4.0)[b]	250.0[b]	6.4 (2.8; 8.8)[b]	11.7
1.4±0.1	-6.8 (-7.9;-6.0)[b]	(3.1; 4.9)[f]	76[d]	5.5 (3.0; 8.3)[b]	12.8

a) No error margins or variable range reported because global minimum does not appear to have been found (See Appendix).

b)The reported range given within brackets corresponds to fits for which the normalised $\Sigma dev^2/dof < 2$ (See Appendix).

c) Error margins or variable range not reported because K_{mic} and ΔH_{mic} are not well defined

d) Aggregation number was restricted to 76 for Kegeles' model and 38 for *n*-merisation model.

e) f_{keg} was restricted to 0.01 and not optimised.

f) Variable range reported because global minimum does not appear to have found for ΔG_{keg} and ΔS_{keg} respectively.

Our next attempt at data analysis was to use Kegeles' model. Surprisingly, for the Kegeles' model when we left the cooperativity parameter f_{keg} and aggregation number variable, we obtained an aggregation number of 250. This value is higher than the value of 76 obtained from SANS and PGSE NMR. In this fit, the cooperativity parameter f_{keg} was optimised to a value of 6.4×10^{-2}. Unfortunately, leaving n_{keg} and f_{keg} unrestricted leads to fits showing strong parameter correlation for n_{keg} and f_{keg} (Figure 4.22).

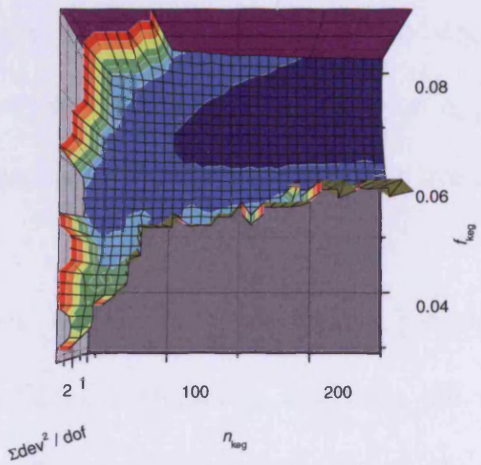

Figure 4.22 Normalised dev^2/dof as a function of values of n_{keg} and f_{keg}. Aggregation number n_{keg} is limited to a value smaller than 250 for computational reasons.

Although f_{keg} is not determined well because of the "tail" at low values of n_{keg} it is likely to be between 0.02 and 0.08. Nevertheless, as a result of covariance, Kegeles' model does not allow us to determine aggregation number. When we restricted the cooperativity parameter f_{keg} to 1×10^{-2} and we obtained an aggregation number n_{keg} of 12. In addition, we tried to estimate a reasonable value for f_{keg}, by restricting the aggregation number to 76, which was expected to lead to an average aggregation number of 38. In this case we obtained

a value for f_{keg} of 5.5×10^{-2}. The two values for cooperativity parameter factor obtained when f_{keg} was variable suggest that f_{keg} needs to be higher than 1×10^{-2}. This was also suggested by Kruif and coworkers when they studied the micellisation of bovine β-casein[45]. In contrast, Kegeles suggested that the value for f_{keg} should be lower, *viz.* approximately 10^{-4} for β-casein, a value estimated from the dependence of the apparent molecular mass of micelles on protein concentration at constant temperature.[46] We plotted the distribution of aggregation number when n_{keg} is 12, 250 and 78 using Wolfram Mathematica software (Figure 4.23). Figure 4.23 shows a maximum aggregation number of 10 when we set n_{keg} to 12. Surprisingly, the same maximum could be observed when we set n_{keg} to 250. Even when we set n_{keg} to 76, the parameters manage to find values, so that the average aggregation number is still 10.

For all three versions of Kegeles' model, the thermodynamic parameters K_{keg}, ΔH_{keg}, ΔG_{keg} and $-T\Delta S_{keg}$ do not vary significantly, suggesting that these are well-defined regardless of the covariance between n_{keg} and f_{keg}. Moreover, analysing the dilution of **4.14** using Kegeles' model we found negative values for ΔH_{Keg} in agreement with analysis in terms of *n*-merisation model. The entropy of micellisation is also negative as found for n-merisation models.

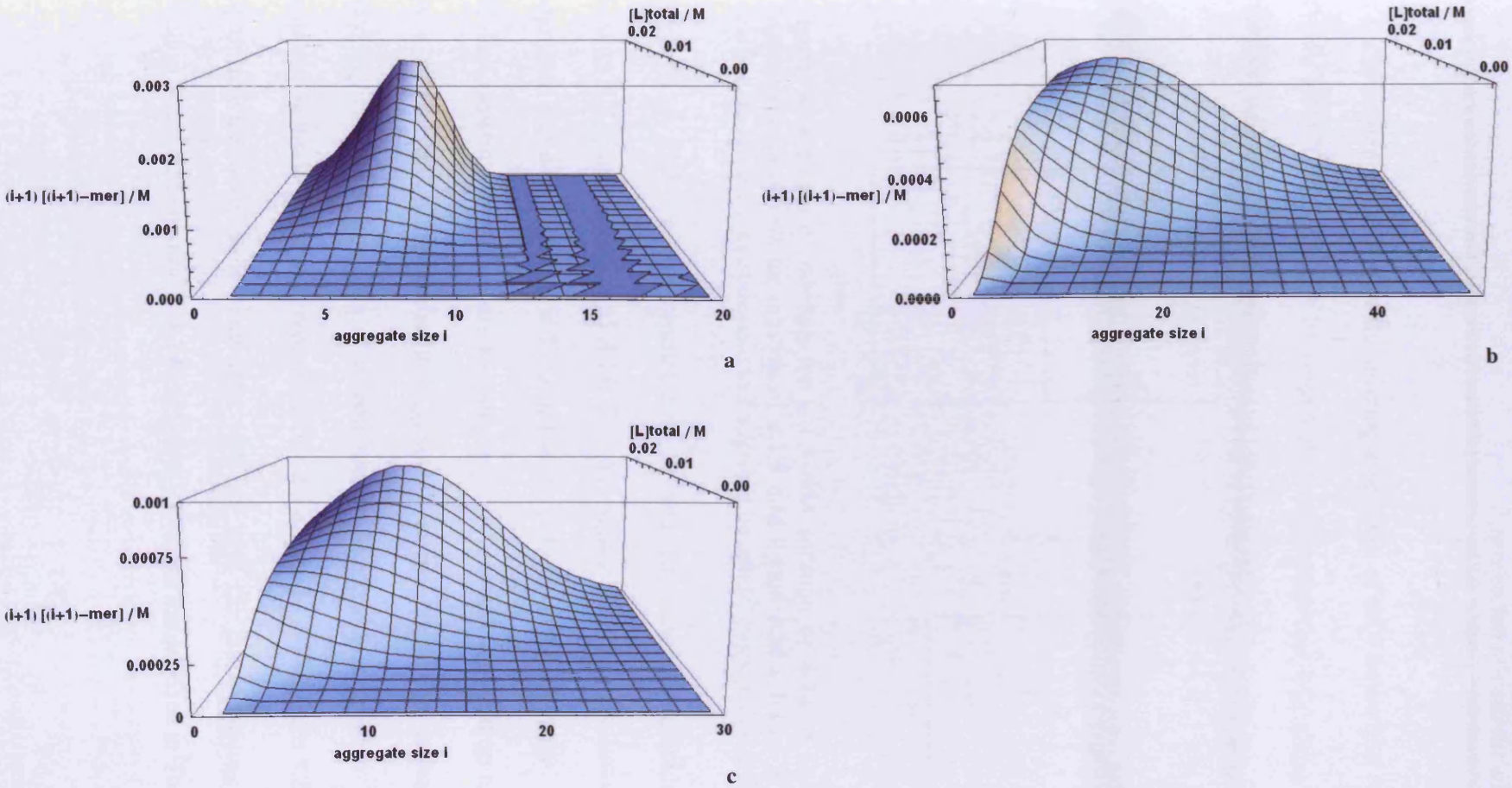

Figure 4.23 Average of aggregation number for n_{keg} 12 (a), n_{keg} 250 (b), n_{keg} 76 (c)

We also carried out experiments, diluting a solution of **4.14** below the cmc in D_2O at 25°C (Figure 4.24).

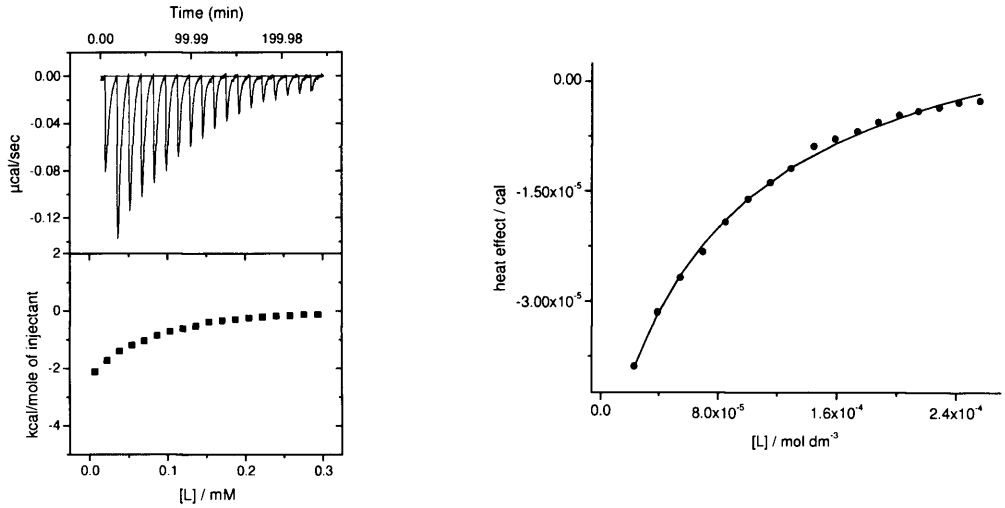

Figure 4.24 Heats of dilution for a 1.5 mM solution of **4.14** in D_2O, at 25 °C (left). Integrated heat effects for dilution of a 1.5 mM ligand **4.14** solution in D_2O, at 25 °C (•) analysed in terms of an isodesmic self aggregation model (solid black line).

Figure 4.24 shows a non-constant heat of dilution with non-sigmoidal behaviour when diluting a 1.5 mM solution of **4.14**. The non-sigmoidal behaviour indicates that **4.14** self aggregate non-cooperatively in D_2O in the studied concentration range. In this case, ligand dilution experiments were analysed using an isodesmic self aggregation model, characterised by a single equilibrium constant K_{agg}, and a single interaction enthalpy ΔH_{agg}, for the successive addition processes of a monomer to an existing aggregate. The isodesmic self aggregation model accurately reproduces the experimental data (Figure 4.24).

Optimised thermodynamic parameters together with the corresponding $\{\Sigma dev^2/dof\}^{1/2}$ for dilution of 1.5 mM solution of **4.14** in D_2O, at 25 °C are summarised in Table 4.8.

Table 4.8 Thermodynamic parameters for isodesmic self aggregation of 1.5 mM solution of **4.14** in D_2O at 25 °C

	Isodesmic self aggregation				
	$K_{agg}/10^3$ (M^{-1})	ΔH_{agg} (kcal mol^{-1})	ΔG_{agg} (kcal mol^{-1})	$-T\times\Delta S_{agg}$ (kcal mol^{-1})	$\{\Sigma dev^2/dof\}^{1/2}$ (μcal)
D_2O	4.4±(3.0-6.6)	3.8±(3.6-4.2)	-4.9±0.2[a]	-1.1±(-1.6-0.5)	0.6

a) For error margins see appendix.

Table 4.8 shows that aggregation of 1.5 mM of **4.14** in D_2O, at 25 °C is driven by entropy and enthalpy opposed. Small value for $\{\Sigma dev^2/dof\}^{1/2}$ has been obtained for analysis of dilution of **4.14** below the cmc. Moreover, plots of $\Sigma dev^2/dof$ as a function of optimisable parameters (*e.g.*K_{agg}, ΔH_{agg}, etc.) are well defined (See Appendix). This suggests that the isodesmic self aggregation model is suitable for the analysis of calorimetric dilution data of **4.14** below the cmc.

Isothermal titration calorimetry – quantifying aggregation of 4.14-4.16 in buffer solutions

Thermodynamic parameters for *n*-merisation and Kegeles' model shave been also obtained analysing the dilution of **4.14-4.16** above the cmc in salt containing buffers (25 mM MOPS, 50 mMNaCl and 1 mM EDTA, pH 7.0) at 25°C (Figure 4.25).

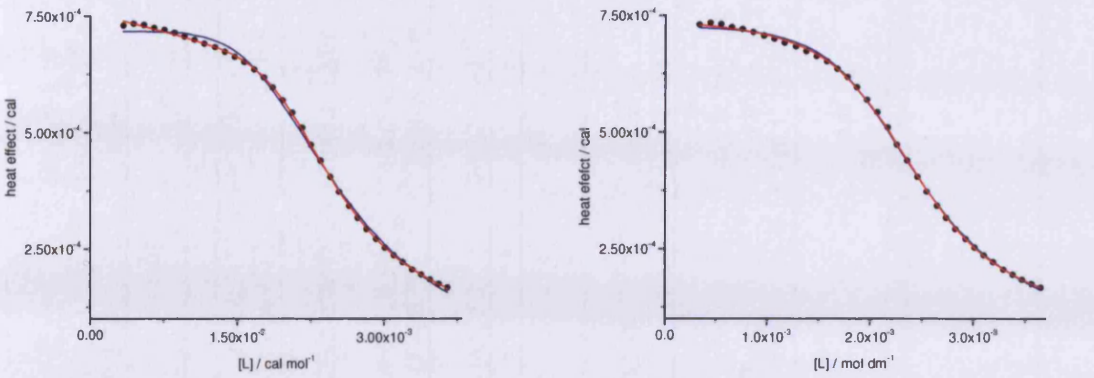

Figure 4.25 Fits of the heat of dilution of a 22.3 mM solution of **4.14** in MOPS buffer, at 25 °C for a) model involving *n*-merisation in combination with stepwise self aggregation (red line); *n*-merisation model without pre-micellisation model (blue line); b) Kegeles' model with f_{keg} fixed to 0.01 (blue line) and f_{keg} variable (red line).

Figure 4.25 shows the fits to n-merisation models and Kegeles' models for dilution of **4.14** in 25 mM MOPS, 50 mM NaCl and 1 mM EDTA, pH 7.0, at 25 °C. Again, analysis of calorimetric data for dilution of **4.14-4.16** in MOPS buffer (25 mM MOPS, 50 mM NaCl and 1 mM EDTA), pH 7.0, at 25 °C in terms of cooperative self-aggregation models yields to aggregation numbers, equilibrium constants and interaction enthalpies. Fits to the *n*-merisation model reproduces the experimental data better if the model includes the formation of pre-micellar aggregates, as before. In case of Kegeles' model, both fits reproducethe ITC dilution data for **4.14** in MOPS buffer, at 25°C, well. The goodness of the fits to both n-merisation and Kegeles' models was quantified through the values of $\{\Sigma dev^2/dof\}^{1/2}$ in Table 4.9.

Table 4.9 Thermodynamic parameters for stepwise self aggregation and dimerisation of **4.1** in MOPS buffer

n-merisation

	K_{agg} (M^{-1})	ΔH_{agg} (kcal mol^{-1})	K_{mic} ($10^2 M^{-1}$)	ΔH_{mic} (kcal mol^{-1})	$-T\times\Delta S_{mic}$ (kcal mol^{-1})	n_{mic}	$\{\Sigma dev^2/dof\}^{1/2}$ (μcal)
25°C							
4.14	-	-	1.2(0.6-2.3)[a]	-13.6 (-20.3; -6.1)[a]	10.7 (3.6; 17.1)[a]	4.4 (3.2; 8.1)[a]	5.0[b]
4.15	-	-	1.2[c]	-12.4[c]	9.4[c]	4.0 (2.4; 5.4)[d]	7.1
4.16	-	-	2.1±0.3	-5.6 (-6.9; -4.7)[d]	2.5 (1.7; 3.7)[d]	6.5±1.2	4.6
40°C							
4.14	-	-	0.9 (0.8; 1.27)	-10.1[b]	7.2[b]	5.2[b]	14.8

n-merisation and stepwise self aggregation

	K_{agg} (M^{-1})	ΔH_{agg} (kcal mol^{-1})	K_{mic} ($10^2 M^{-1}$)	ΔH_{mic} (kcal mol^{-1})	$-T\times\Delta S_{mic}$ (kcal mol^{-1})	n_{mic}	$\{\Sigma dev^2/dof\}^{1/2}$ (μcal)
25 °C							
4.1a	2.4 (1.2;13.6)[a]	-57.9(244.4; 5.6)[a]	1.9(1.5; 4.4)[a]	-6.5 (-10.8; -5.1)[a]	3.3 (2.1; 7.1)[a]	7.9(5.1; 12.9)[a]	1.9[b]
4.1b	1.4[b]	-146.9 (247.6-10.0)[d]	2.1 (1.7-3.2)[d]	-6.3 (-7.9; -5.4)[d]	3.4 (2.4; 4.5)[d]	6.2 (5.4; 7.6)[d]	2.0
4.1c	1.0[b]	-78.9 (-136.7; 0.7)[d]	2.3 (2.17; 2.9)[d]	-5.1 (-5.6; -4.6)[d]	(1.4; 2.3)[e]	7.5 (6.3; 9.7)[d]	3.1
40°C							
4.1a	1.0[a]	-152.9 (-175.4; 12.2)[d]	1.2±0.8	-7.8±0.4	4.8 (4.5; 5.2)[d]	7.9 (7.1; 9.1)[d]	3.2

Kegeles' model

	K_{keg} ($10^2 M^{-1}$)	ΔH_{keg} (kcal mol^{-1})	$-T\times\Delta S_{keg}$ (kcal mol^{-1})	n_{keg}	$10^2 f_{keg}$	$\{\Sigma dev^2/dof\}^{1/2}$ (μcal)
25 °C						
4.1a	5.6 (4.4; 8.8)[a]	-8.3 (-9.9; - 4.0)[a]	4.6 (0.4; 5.8)[a]	12.0 (8.8; 53.1)[a]	1.0[f]	5.1[b]
	3.6 (3.0; 5.4)[a]	-6.0 (-8.1; -4.5)[a]	2.4 (1.1; 4.3)[a]	250[c]	4.2 (1.1; 13.1)[a]	2.5[b]
4.1b	8.2 (7.3; 9.0)[d]	-6.3 (-7.4; -5.0)[d]	2.3 (1.1; 3.4)[d]	9.0[c]	1.0[f]	7.0
	4.3 (4.2; 5.0)	-4.9 (-7.3; -4.5)	1.3 (1.0; 3.6)	250[c]	7.4 (2.8; 9.0)[d]	2.7
4.1c	5.7±0.2	-4.4±0.3	0.6± 0.2	24.0±7	1.0[f]	2.1
	6.5 (5.5; 9.5)	-4.6 (-5.2; -4.5)	(0.7; 1.2)[e]	17.0[c]	6.3 (0.1; 12.2)[d]	2.6
40°C						
4.1a	3.6 (3.1; 3.8)[d]	-7.9 (-8.4; -7.1)[d]	(3.5; 4.7)[e]	14.0[c]	1.0[f]	9.6
	2.3 (2.2; 2.8)	-6.4 (7.4; -6.1)	3.0 (2.9; 3.9)	250[c]	(2.4; 6.5)[d]	4.4

a) The reported range given within brackets corresponds to fits for which the normalised $\Sigma dev^2/dof < 2$(See Appendix). The range is estimated from combined plots of normalised $\Sigma dev^2/dof$ for three independent titrations.

b) $\{\Sigma dev^2/dof\}^{1/2}$ is an average of three independent titrations.

c) No error margins or variable range reported because global minimum does not appear to have been found (See Appendix).

d) The reported range given within brackets corresponds to fits for which the normalised $\Sigma dev^2/dof < 2$ (See Appendix).

e) Variable range reported because ΔG_{keg} is not well defined to obtain therefore ΔS_{keg}. f) f_{keg} was restricted to 0.01 and not optimised

If the data analysis model includes both n-merisation and formation of pre-micellar aggregates, small values for $\{\Sigma dev^2/dof\}^{1/2}$ are observed for analysis of dilution data of **4.14** in H_2O. This is not the case if data is analysed in term of n-merisation alone, suggesting that an *n*-merisation model is not complete if it does not take in account the formation of pre-micellar aggregates. Kegeles' model reproduces calorimetric data for dilution of **4.14** in MOPS buffer at 25 °C well, regardless of whether cooperativity parameter f_{keg} is variable or not.

Comparison of Table 4.7 and Table 4.9 shows that the thermodynamic parameters for self aggregation of **4.14** change from water to MOPS buffer. In particular, changes could be observed for K_{mic} and K_{keg} are clear, indicating that aggregation is facilitates by one of the buffer components (most likely NaCl as before). The micellisation constants K_{mic} and K_{keg} decrease as the temperature increases from 25 °C to 40 °C. Accordingly, ΔH_{mic} and ΔH_{keg} are negative; micellisation of **4.14-4.16** in MOPS buffer is exothermic as it is in water. Equilibrium constants and enthalpy changes are similar for all terthiophenes **4.14-4.16**. With increasing temperature ΔH_{mic} becomes more negative, whereas ΔH_{keg} shows only small changes. Self aggregation of **4.14-4.16** in MOPS buffer is characterised by negative entropy changes which do not change significantly from **4.14** to **4.16**. Table 4.9 shows that aggregation numbers for all data analysis models are in agreement with the aggregation numbers obtained in water, in the absence of counterion effects. Aggregation numbers remain practically constant over the entire series of terthiophenes **4.14-4.16**. This suggests that **4.14-4.16** form comparable micelles in aqueous solution. This hypothesis is further supported by the observation that replacing the substituent on the ammonium group does not affect the self aggregation of **4.14-4.16** in aqueous solutions according to other techniques, *e.g.* ^{1}H-NMR.

Small- angle neutron scattering (SANS)

To confirm the mode of self aggregation and the shape of the aggregates for **4.14** in aqueous solution we used small-angle neutron scattering. Small-angle neutron scattering data and corresponding fits for **4.14** in D_2O, at 25 °C are present in Figure 4.26.

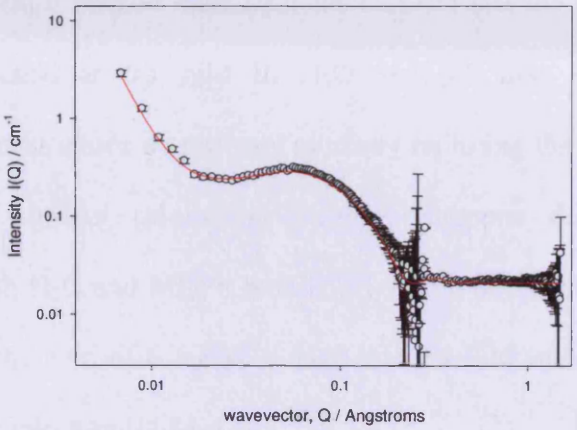

Figure 4.26 SANS data and fit to a solid sphere model for **4.14** in D_2O at 25 °C

Our first attempts to analyse SANS data for 29.2 mM solution of **4.14** in D_2O at 25 °C was to fit a solid charged sphere model to the data (Section 2.4.3). An upturn in the low Q region corresponds to a Q^{-4} term that describes the scattering from some large scatters. The charged sphere model allowed us to determine the hydrodynamic radius and, therefore, volume of micelle. We found a hydrodynamic radius of 16 Å, which corresponds to an aggregation number of 38. The hydrodynamic radius is in agreement with the number determined using PGSE-NMR. Experiments using **4.14** in D_2O at 37 °C, show that the hydrodynamic radius (and therefore the aggregation number) increases with temperature. At 37 °C in D_2O, cationic terthiophene **4.14** forms micelles with a radius of 18 Å corresponding to an aggregation number of 53.

Summary

We successfully demonstrated that cationic conjugated terthiophenes **4.14-4.16** aggregate into micellar type assemblies. ^{1}H-NMR and diffusion NMR confirm cooperative self-aggregation for **4.14-4.16** and provide estimates of aggregation numbers of **4.16** (in D_2O at 25 °C) of 38 and a cmc of 5.6 mM. Surface tension measurements confirm that the critical micelle concentrations for **4.16** were reached at 6.1 mM in H_2O and 3.3 mM in MOPS buffer at 25 °C. Critical micelle concentrations do not vary much by replacing the substituent on the ammonium group. Isothermal titration calorimetry strongly supports that **4.14-4.16** self aggregate cooperatively in both H_2O and MOPS buffer, pH 7.0, at temperatures range from 25 to 40 °C. ITC data confirms the cmc of 6.1 mM in H_2O and 2.4 mM in MOPS buffer, pH 7.0, both at 25 °C for cationic terthiophenes**4.14-4.16**.

We used different mathematical models (*e.g. n*-merisation and Kegeles' models) to analyse ITC dilution data for **4.14-4.16**. Unfortunately ITC data does not currently allow us to determine the aggregation numbers.

4.3.2.2 Self aggregation of cationic quaterthiophenes 4.17

^{1}H-NMR

The mode of self aggregation of dicationic quaterthiophene **4.17** in aqueous solution was determined using ^{1}H-NMR. A series of ^{1}H-NMR spectra for **4.15** were recorded in D_2O, at 25 °C as a function of concentration (Figure 4.27).

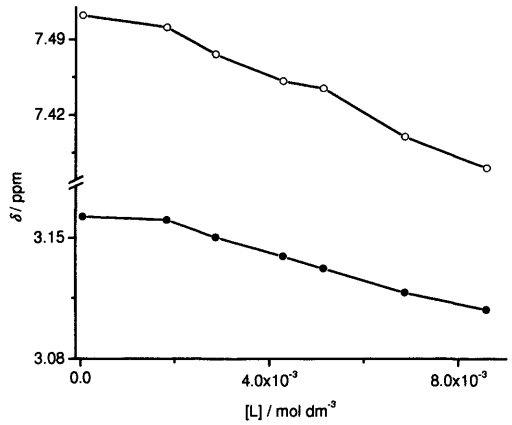

Figure 4.27 Concentration dependence of chemical shifts for $-N^{+}(CH_3)_3$ protons (•) and -Ar protons (o) of **4.17** in D_2O, at 25 °C. The black lines are drawn to guide the eye.

Figure 4.27 shows a sigmoidal decrease in the chemical shifts for two selected protons with increasing concentration, indicating that cationic quaterthiophene **4.17** self aggregate cooperatively in the studied concentration range.

Diffusion NMR (PGSE NMR)

We investigated the self aggregation of cationic quaterthiophene **4.17** further using PGSE-NMR. The diffusion coefficient of **4.17** in D_2O at25 °C was measured as a function of concentration (Figure 4.28).

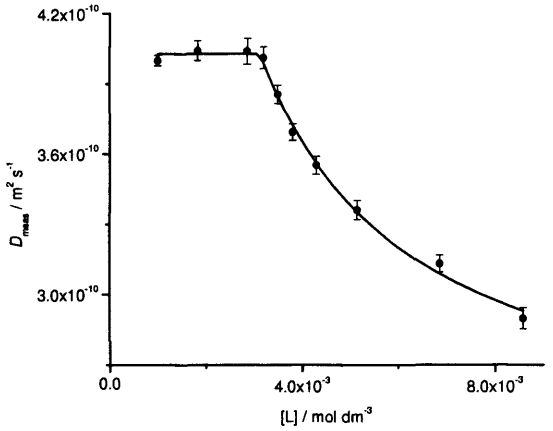

Figure 4.28 Variations of self diffusion coefficient with concentration for **4.17** in D_2O at 25 °C. The black line represents the two-state mobility model fits to the data.

Figure 4.28 shows that the diffusion coefficient of **4.17** varies sigmoidally with increasing concentration. The sigmoidal behaviour suggests that **4.17** self aggregates cooperatively. Measured diffusion coefficients were analysed using a two-state mobility model. The critical micelle concentration is 5.6 mM, value in good agreement with the value obtained from surface tension and isothermal titration calorimetry experiments *(vide infra)*. The self diffusion coefficient of micelles estimated through the two-state mobility model was found to be $D_{micelle} = (2.3\pm0.04)10^{-10}$. From the extracted micellar diffusion coefficient, and assuming Stokes-Einstein equation we estimated a radius of 8.3 Å for the micelles. Using equation 2.41 (Section 2.4.2) we found a micellar volume of 2393.8 $Å^3$. The molar volume of monomers of **4.17** was calculated by Dr. Larry Goldman using Gaussian 03, at the B3LYP/6-31+G(d) level of theory. The molar volume of **4.15** is 447.9 cm^3/mol, which corresponds to 743.6 $Å^3$ $molecule^{-1}$. Calculating the ratio between the volume of micelles and

the monomer volume led to an aggregation number of 3.2. This aggregation number is in agreement with the aggregation number determined by ITC *(vide infra)*.

Surface tension

In order to confirm the critical micelle concentration, we carried out surface tension measurements as a function of concentration for **4.17** in H_2O and in MOPS buffer, at 25 °C (Figure 4.29)

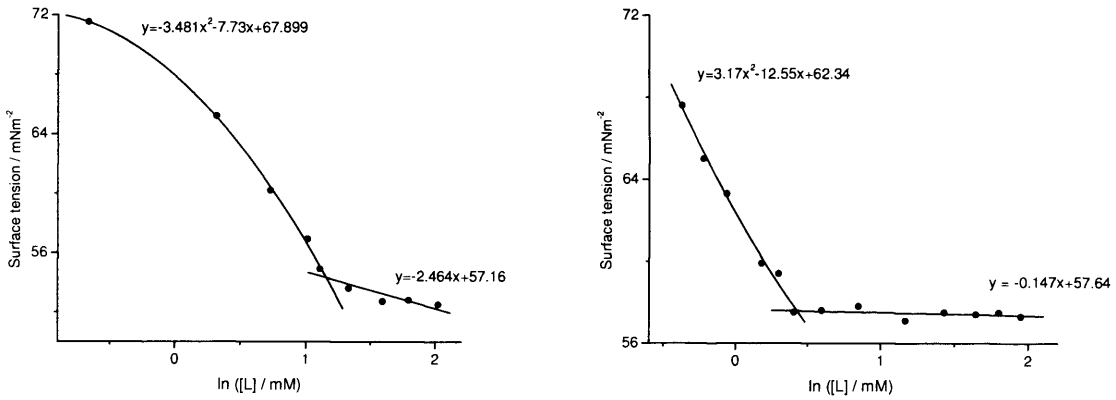

Figure 4.29 Variation of surface tension with concentration for **4.17** in H_2O, at 25 °C (left) and MOPS buffer, pH 7.0, at 25 °C (right). The black lines represent the fits to polynomial and linear expressions.

Figure 4.29 shows that the surface tension of **4.17** in H_2O at 25 °C varies strongly with concentration below the inflection point, while above this point the surface tension remains almost constant. This suggests that **4.17** forms micelles in H_2O, at 25 °C, when it reaches 3.1 mM concentration. Moreover, the surface tension curve presents no minimum around the critical micelle concentration, indicating a good purity of the surfactant. Similarly, the surface tension of **4.17** in MOPS buffer, pH 7.0, at 25 °C shows an inflection point around 1.5 mM (Figure 4.29 right), suggesting formation of micelles. Critical micelle concentration decreases

from H_2O to MOPS buffer, suggesting that the aggregation of **4.17** is facilitated by one(or more) of the buffer components (NaCl).

Isothermal titration calorimetry

To further study in detail the self association of cationic terthiophene**4.17**in MOPS buffer at 25 °C we used isothermal titration calorimetry. Dilution experiments were carried out by injecting a concentrated ligand solution of **4.17** in MOPS buffer into the calorimeter cell containing the same solvent (Figure 4.30).

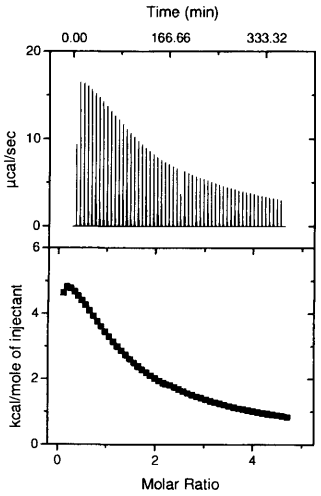

Figure 4.30 Heats of dilution of 10.9 mM solution of **4.17** in 25 mM MOPS, 50 mM NaCl and 1 mM EDTA at pH 7.0 at 25 °C.

Figure 4.30 shows a non-constant heat of dilution with sigmoidal behaviour for **4**.17 as a function of ligand concentration in the calorimeter cell. The sigmoidal behaviour indicates that **4.17** self aggregates cooperatively in MOPS buffer in the studied concentration range. Critical micelle concentrations for **4.17** at pH 7, in 25 mM MOPS, 50 mM NaCl and 1 mM

EDTA at 25 °C were determined by plotting the derivative of the heat effect of dilution against the concentration of the ligand in the calorimeter cell (Figure 4.31).

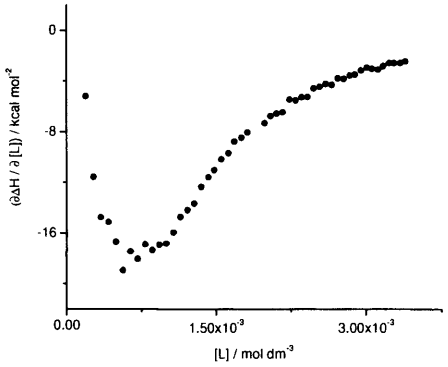

Figure 4.31 Derivative of the molar heat effect of dilution of 10.9 mM solution of **4.17**, into 25 mM MOPS, 50 mM NaCl and 1 mM EDTA, at pH 7, at 25°C.

The derivative of the dilution curves in Figure 4.31 displays a minimum, suggesting that **4.17** forms micelles when its concentration reaches 7.0×10^{-4} M. This critical micelle concentration is smaller than the value found for cationic terthiophene **4.14** in MOPS buffer, at 25 °C, suggesting that **4.17** is more hydrophobic, despite its double positive charge. To quantify the thermodynamic parameters of micellisation for **4.17** we analysed the calorimetric data in terms of different cooperative self aggregation models (Section 2.6.2). Figure 4.31 shows fits to *n*-merisation and Kegeles' models for dilution of **4.17** in MOPS buffer, pH 7.0, at 25 °C. Table 4.10 summarises the thermodynamic parameters which best reproduce experimental data.

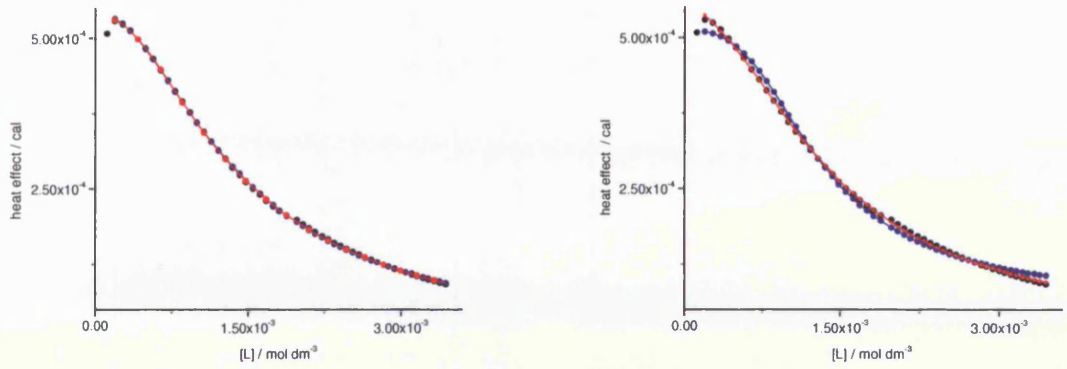

Figure 4.31 Fits of the heat of dilution of 10.9 mM solution of **4.17** in MOPS buffer, at 25 °C for a) model involving n-merisation model and pre-micellar aggregation (-●-); model involving n-merisation model, aggregation not included (-●-); b) Kegeles' model with f_{keg} fixed to 0.01 (-●-) ; Kegeles' model, with f_{keg} variable (-●-).

Surprisingly, Figure 4.31 shows that both versions of *n*-merisation model reproduce well the experimental data well. Kegeles' model fits better to the experimental data if the cooperativity parameter f_{keg} is variable (Figure 4.31b). The values for $\{\Sigma dev^2/dof\}^{½}$ for both fits (Table 4.10) confirm the results from visual inspection. Values of $\{\Sigma dev^2/dof\}^{½}$ for n-merisation, n-merisation including stepwise self aggregation, and the fully optimisable Kegeles model are around 2 μcal. Kegeles' model with f_{keg} restricted to 0.01 results in a statistically unacceptable fit with $\{\Sigma dev^2/dof\}^{½}$ of 9.6 μcal.

Table 4.10 Thermodynamic parameters for dilution of **4.17** in MOPS buffer at **25 °C**

n-merisation

K_{agg} (M^{-1})	ΔH_{agg} (cal mol^{-1})	$10^{-2}K_{mic}$ (M^{-1})	ΔH_{mic} (kcalmol^{-1})	$-T\times\Delta S_{mic}$ (kcal mol^{-1})	n_{mic}	$\{\Sigma dev^2/dof\}^{1/2}$ (μcal)
-	-	2.1±0.2	-10.0±1	6.9±0.7	3.0±0.2	1.6

n-merisation and stepwise self aggregation

$10^{-2}K_{agg}$ (M^{-1})	ΔH_{agg} (cal mol^{-1})	$10^{-2}K_{mic}$ (M^{-1})	ΔH_{mic} (kcalmol^{-1})	$-T\times\Delta S_{mic}$ (kcal mol^{-1})	n_{mic}	$\{\Sigma dev^2/dof\}^{1/2}$ (μcal)
1.3	-1.0	3.3 (1.9; 4.5)[a]	-12.6 (-18.0; -9.5)[a]	(6.1, 14.4)[b]	3.6 (2.8; 4.5)[a]	1.4

Kegeles' model

$10^{-3}K_{keg}$ (M^{-1})	ΔH_{keg} (10^3cal mol^{-1})	$-T\times\Delta S_{keg}$ (kcal mol^{-1})	n_{keg}	$10^2 f_{keg}$	$\{\Sigma dev^2/dof\}^{1/2}$ (μcal)
2.1 (1.6; 2.3)[a]	-6.4 (-6.9; -5.5)[a]	1.9 (1.1; 2.5)[a]	5.0[b]	1.0[c]	9.6
1.1 (0.6; 1.4)[a]	-8.7 (-9.5; -7.1)[a]	4.6 (3.1; 5.2)[a]	4.0[b]	9.0 (0.4; 18.0)[a]	2.2

a) The reported range given within brackets corresponds to fits for which the normalised $\Sigma dev^2/dof < 2$ (See Appendix).
b) No error margins or variable range reported because global minimum does not appear to have been found (See Appendix).
c) f was set up to 0.01 and not variable.

Thermodynamic parameters resulting from the fitting of micellisation models to the heats of dilution of **4.17** in MOPS buffer at 25 °C (Table 4.10) show that ΔH_{mic} and ΔH_{keg} from the different models are all negative, indicating that the micellisation of **4.17** in MOPS buffer, at 25 °C is exothermic. K_{agg} is small and, therefore, does not play an important role. A negative change in the entropy indicates that micellisation is mainly driven by π-π stacking interactions. Surprisingly, aggregation numbers according to different models are similar. The aggregation number for **4.17** in MOPS buffer at 25°C is 3 according to the n-merisation model, regardless of whether pre-micellar aggregation is included or not. Kegeles' model gives similar values for the aggregation number, *e.g.* 5 and 4 for f_{keg} fixed and f_{keg} optimisable, respectively.

Summary

We have demonstrated by ^{1}H-NMR, PGSE-NMR and ITC that dicationic quaterthiophene **4.17** self aggregates cooperatively in 25 mM MOPS, 50 mM NaCl and 1 mM EDTA, at pH 7.0 and at 25°C. Using PGSE-NMR we found **4.17** forms micelles with a radius of 8.5 Å, which corresponds to an aggregation number of 3.3. Surface tension experiments confirmed that **4.17** forms micelles above a concentration of 7.0×10^{-4} M. Titration calorimetry revealed that self aggregation of **4.17** in MOPS buffer at 25°C is exothermic, with a negative entropy change. Analysis of heats of dilution of **4.17** in MOPS buffer at 25°C using both n-merisation and Kegeles' model suggest aggregation number of approximately 3 in good agreement with PGSE-NMR data. This contradicts the disagreement in aggregation numbers found for dilutions of cationic terthiophene **4.14**

in H_2O and MOPS buffer, at 25 °C. Addition of a thiophene ring in the series of terthiophenes increases the hydrophobic character of the molecule as suggested by the decreased cmc compared to terthiophenes **4.14-4.16**.

4.3.2.3 Validation of ITC models

In order to verify whether our micellisation models are useful, in combination with experiments where binding events are studied to provide reliable output, we performed some ITC experiments involving one of our compounds in a 1:1 host-guest system.

We have chosen β-cyclodextrin (β-CD) as a host. As a guest we have opted for monocationic terthiophene **4.14**. Binding experiments were carried out by injecting an 8.5 mM solution of cationic terthiophene **4.14** into a 1.0 mM solution of β-CD in H_2O at 25 °C (Figure 4.32 left). For this particular system, we can avoid the problems caused by self aggregation by performing a reverse titration *i.e.* injecting an 18.0 mM solution of β-CD in H_2O into a 1mM solution of cationic terthiophene **4.14** (below the cmc) in the calorimeter cell (Figure 4 right).

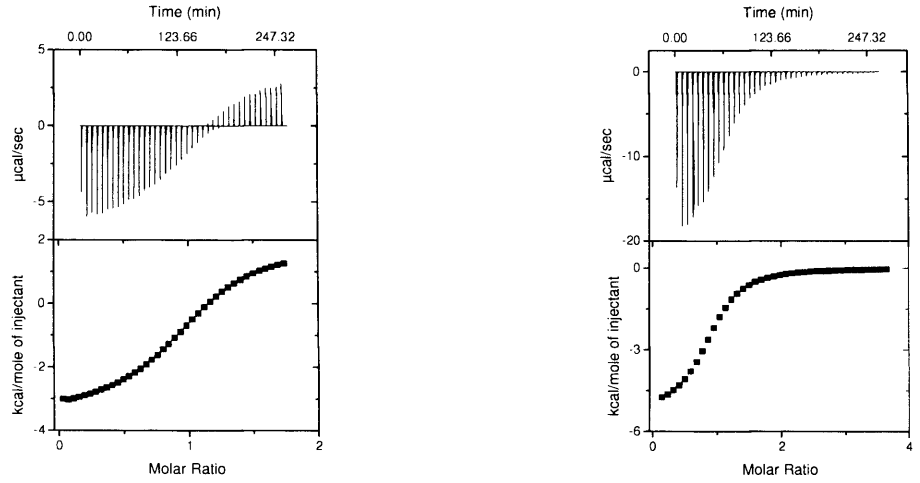

Figure 4.32 Titration of 8.5 mM solution of **4.14** into a 1.0 mM solution β-CD (left). Titration of 18.0 mM solution of β-CD into1.0 mM solution of **4.14** (right). Both experiments in H_2O at 25 °C.

Figure 4.32 shows a non-constant heat for **4.14** interacting with β-CD, which suggests that **4.14** forms a complex with β-CD. The heat of binding becomes lower with each injection due to less β-CD being available to accommodate molecules of cationic terthiophene **4.14**. The heats are exothermic which means that binding of **4.14** to β-CD is highly exothermic because the heat effects include the endothermic breaking up of ligand aggregates. Within this range of molar ratios studied here, only one binding event is apparent as the final molar heats effects resemble those for ligand dilution. The binding stoichiometry is 1:1. The reverse titration (Figure 4.32) shows a non-constant heat for interaction of β-CD with cationic terthiophene **4.14**, which also corresponds to a 1:1 binding mode. The binding data were analysed in terms of a model involving one binding mode, *viz.* equilibrium A1

(Scheme 4.8). The analysis also includes various micellisation models which describe ligand self aggregation.

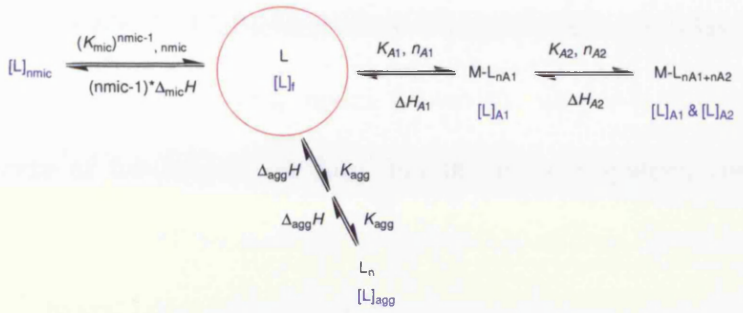

Scheme 4.8. L refers to ligand 5.14 and M refers to β-CD.

To minimize the number of optimisable parameters, ligand self aggregation parameters were restricted to the best fit values in Table 4.7. The analysis resulted in fits that reproduce the experimental data well (Table 4.11).

Table 4.11 Thermodynamic parameters for binding of **4.14** to β-CD, in H_2O at 25 °C

no corrections for self aggregation

$10^{-4}K_{A1}$ (M^{-1})	ΔH_{A1} (10^3cal mol^{-1})	$-T\times\Delta S_{A1}$ (cal mol^{-1})	n_{A1}	{Σdev²/dof}^{½} (μcal)
1.1±0.1	-5.3±0.1	2±0.05	1.1±0.1	0.6

n-merisation model and stepwise self aggregation[b]

$10^{-4}K_{A1}$ (M^{-1})	ΔH_{A1} (10^3cal mol^{-1})	$-T\times\Delta S_{A1}$ (cal mol^{-1})	n_{A1}	n_{mic}	{Σdev²/dof}^{½} (μcal)
1.1±	-5.5±0.1	3.0±0.07	1.1±0.01	8.1	0.5
-	-	-	-	38	-

Kegeles' model[c]

$10^{-4}K_{A1}$ (M^{-1})	ΔH_{A1} (10^3cal mol^{-1})	$-T\times\Delta S_{A1}$ (cal mol^{-1})	n_{A1}	n_{keg}	$10^2 f$	{Σdev²/dof}^{½} (μcal)
1.1±0.1	-5.5±0.5	1.0±0.1	1.08±0.1	12	1.0	0.6
1.1±0.1	-5.4±0.1	1.1±0.1	1.09±0.1	250	6.4	0.5

reverse titration

$10^{-4}K_{A1}$ (M^{-1})	ΔH_{A1} (10^3cal mol^{-1})	$-T\times\Delta S_{A1}$ (10^3cal mol^{-1})	n_{A1}	{Σdev²/dof}^{½} (μcal)
1.1±0.1	-4.9±0.1	-0.6±0.1	1.0±0.1	0.6

a),b),c) Parameter values restricted to best fit values as reported in Table 4.7

The values for $\{\Sigma dev^2/dof\}^{1/2}$ are small and very similar suggesting there is not much difference in goodness of the fits. Table 4.11 shows that similar binding constants, thermodynamic parameters and stoichiometries were obtained regardless of whether self aggregation is included in the binding model. Moreover, similar binding parameters could be observed in case of the reverse titration. For the present system, corrections for self aggregation are not important because the concentration of free ligand in the calorimeter cell remains far below the critical micelle concentrations during the experiment. Nerveless, the models including self aggregation correctly identify the endothermic process at higher molar ratios as micellar dissociation, whereas models not including micellisation report a remarkably endothermic ligand dilution event or even suggest a second binding event. According to Table 4.11 the binding of **4.14** to β-CD is exothermic, with a negative entropy change. This thermodynamic signature is characteristic for flat molecules binding to concave molecules. The interaction of β-CD and cationic terthiophene **4.14** shows a molar ratio of 1:1, suggesting that one molecule of **4.14** is accommodated in the cavity of β-CD.

Summary

Binding experiments of cationic terthiophene **4.14** to β-CD were designed in order to study the use of different aggregation models in combination with a well-defined binding event. For this system with a 1:1 binding mode and in the range of molar ratios studied, corrections for self aggregationare not important, because the concentration of the free ligand in the calorimeter cell remains below the cmc.

4.3 Conclusions

All synthesised cationic conjugated oligoheteroaromatics **4.11-4.17** self aggregate in aqueous solution *via* π-π stack interactions in combination with hydrophobic interactions. The results show mainly two modes characteristic for self assembly of cationic oligoheteroaromatics in aqueous solution: non-cooperative self aggregation and cooperative self aggregation. Cationic terthiophenes **4.14-4.17** self aggregate with formation of small micelles. Surprisingly introducing a second positive charge on the terthiophene skeleton improves the solubility, showing a very weak stepwise self aggregation. In this case we were able to quantify the binding of **4.11** to DNA without taking in to account the ligand self aggregation (Section 5.3). Replacing the thiophene rings in the series of terthiophenes, switches the self aggregation mode. For example, cationic furan derivative **4.12** and cationic pyridine derivative **4.13** self aggregate non-cooperatively in aqueous solution. To quantify self aggregation is quite a difficult process, especially when using isothermal titration calorimetry. There is a continuous interest in our group to implement different mathematical models in order to quantify the self aggregation of cationic oligoheteroaromatics and therefore the binding of these compounds to DNA. In this sense, we analysed ITC data for dilution of **4.14-4.17** in aqueous solution using different mathematical models. Non-cooperative self aggregation can be described using dimerisation or stepwise self aggregation while two models were used to describe cooperative self aggregation: n-merisation and Kegeles' models. The last two models treat our ligands as micelle-forming surfactants. Despite the fact that micellisation models give similar thermodynamic parameters, the aggregation numbers are different. In this context, we verified whether

parameters are physically meaningful, *i.e.* whether our models are appropriate. Diffusion NMR confirms non-cooperative self aggregation for **4.11-4.13** and micellisation for **4.14-4.17**, providing in the last case estimates of aggregation numbers. Surface tension also confirms that **4.14-4.17** form micellar aggregates in aqueous solution. We found an aggregation number of 38 for monocationic terthiophene. Therefore to validate this aggregation number and the assumption that aggregates are roughly spherical, we used SANS. A preliminary SANS experiment shows that this is viable. Although we found a good correlation between the results of these two techniques, when we restricted the aggregation number in ITC to 76 in the case of the Kegeles' model, the precise meaning and expected values for cooperative factor f_{keg} remain to be determined. Restricting the aggregation number to 38, the n-merisation model did not reproduce the ITC data well, suggesting that this model is not a suitable model to describe the micellisation in aqueous solution. Also, the n-merisation model is not complete because it does not take in account the formation of pre-micellar aggregates.

4.4 Materials and methods

4.4.1 Chemicals

All the compounds**4.11-4.17** were synthesised according to the procedures described in Chapter 3. β-cyclodextrin was purchased either from Sigma-Aldrich. Experiments were performed in H_2O, D_2O and MOPS buffer. MOPS buffer was made mixing 25 mM MOPS, 50mMNaCl and 1 mM EDTA in demineralised water. The components of MOPS buffer,

e.g. EDTA, MOPS, NaCl and NaOH were also obtained from Sigma-Aldrich. Deuterated water was procured from Sigma-Aldrich. Then, MOPS buffer was titrated with aqueous solution of NaOH to pH 7.0. Water was purified using an ELGA option-R 7BP water purifier. The pH of aqueous solutions was determined with a Hanna Instruments pH 210 pH meter equipped with a VWR 662-1759 glass electrode.

4.4.2 ^{1}H-NMR

Concentrated stock solutions of oligoheteroaromatics **4.11-4.17** were prepared in deuterated water. The concentrations of these solutions were quantified spectrophotometrically based on their extinction coefficients (See Appendix). These stock solutions were diluted from 1 to 11 times in order to obtain solutions of **4.11-4.17** at different concentration. Measurements were carried out in standard NMR tubes, using a minimum volume of 0.5 ml solution of **4.11-4.17**, at 25 °C. ^{1}H-NMR spectra were recorded at 400 MHz on a Bruker B-ACS-6. All spectra are referenced to residual proton solvent. The chemical shift of the residual HDO is temperature-dependent and it was corrected using equation 4.1[47]

$$\delta = 5.060 - 0.0122T + (2.11x10^{-5})T^2$$

Prior to every ^{1}H-NMR measurements, we recorded ^{13}C-NMR spectra in order to assure that the sample reaches 25 °C. The temperature for every measurement varies within maximum ±0.2 °C shifts as a function of the concentration were extracted from ^{1}H-NMR spectra and analysed in terms of self aggregation models (Section 2.3) using Origin 7.5.

4.4.3 PGSE-NMR

Pulsed-gradient spin-echo NMR experiments were conducted on a Bruker AMX360 NMR spectrometer operating at 369 Hz which uses a simulated echo sequence. A Bruker gradient spectroscopy accessory unit was also attached to spectrometer. Experiments were carried out using the same solutions as for ^{1}H-NMR. All experiments were measured at 25 °C.

The temperature stability was kept to an accuracy of 0.3 °C by a standard air heating/ cooling system. First, the integral for a certain peak has been calculated and the diffusion coefficient was extracted by fitting these integrals to equation 2.37 (Section 2.4.2) using Sigma Plot 10.

4.4.4 Surface tension

Stock solutions were prepared in water or in MOPS buffer (pH 7.0) and concentrations were determined spectrophotometrically. To prepare different ligand concentrations, serial dilutions were carried out and 1.0 ml of each solution was added to a small glass vial. The surface tension for every solution was measured using a bubble pressure tensiometer (SITA Online t60) which was calibrated using water. All measurements were made at 25 °C ± 0.3.

4.4.5 Isothermal titration calorimetry(ITC)

Calorimetric dilution experiments were carried out in the temperature range 25-40 °C on a Microcal VP ITC microcalorimeter. The instrument was functioned in high-gain mode, applying a reference power of 10-15 μcal s^{-1} while stirring the sample cell contents at 350 rpm. The set up of each ligand dilution experiments provided injections of 5-15 μl of ligands

4.1-4.15 (depending on how concentrated is the ligand stock solution) from the syringe into a known volume (1.6-1.8μl) of water or D_2O. The time interval between the injections was 350 sec. The same dilution experiments we recorded in MOPS buffer, pH 7.0. Before injecting the solution in the sample cell and syringe they were degassed using a thermo-vacuum machine. Some dilution experiments were carried out in two or three stages by refilling the syringe with the same ligand concentration, without mixing the contents of the calorimeter cell. This results in small jumps between subdatasets. These titrations were typically analysed so every subdataset received individual dilution enthalpy. Titrations involving β-CD were carried out by injecting 7 μl concentrated solutions of **4.14** into calorimeter cell containing1.7 μl solution of β-CD. A reverse titration was performed injecting this time 7 μl concentrated solutions of β-CD into calorimeter cell containing 1.7 μl solution of **4.14**. At the end of each titration, a file containing total concentrations of all the compounds in both syringe and cell for every injection has been written using custom-written software. Then, integrated heat effects per injection (dh) or molar heat effects per injection (ndh) were generated using Origin 7.0. These values were copied in a file having dh as extension, which together with the file containing total concentrations and ligand volume for every injections, served as input for IC ITC software (Section 2.6.2).

4.4.6 Small angle neutron scattering (SANS)

SANS experiments were carried out using a time-off flight LOQ diffractometer at the ISIS Spallation Neutron Source, Rutherford Appleton Laboratory, Didcot, UK. Stock solutions of cationic terthiophene **4.14** were freshly prepared and 600 μl of these

stocks solutions were added in 2 mm path length, quartz cuvettes. The cuvettes were placed in aluminum holder on an enclosed, sample compartment. The temperature was maintained using a thermostated circulating bath pumping fluid through the base of the sample compartment, accomplishing a temperature stability of ±0.2 °C. Experimental measuring times were approximately 30-40 min. The obtained scatters were background corrected using a quartz cell filled with D_2O. Using an instrument specific software package, the scatters were normalised for the sample transmission and corrected for linearity and efficiency of the detector response.

Acknowledgements

I am grateful to Dr. Peter Griffiths and Dr. Alison Paul for providing me the support and equipments I have needed to study the self aggregation of oligoheteroaromatics in aqueous solution. I thank Craig James for his help on recording and analysing PGSE-NMR data.

I thank to Dr. Niek Buurma, for his patience and guidance which he provided me for analysis of ITC data using IC ITC software.

References

1. Facchetti, A., *Mater. Today* **2007,** *10* (3), 28-37.
2. Skotheim, T. A.; Reynolds, J. R., *Taylor & Francis Group* **2009.**
3. Mena-Osteritz, E., *Adv. Mater.* **2002,** *14* (8), 609-616.
4. Leclere, P.; Surin, M.; Viville, P.; Lazzaroni, R.; Kilbinger, A. F. M.; Henze, O.; Feast, W. J.; Cavallini, M.; Biscarini, F.; Schenning, A.; Meijer, E. W., *Chem. Mat.* **2004,** *16* (23), 4452-4466.
5. Park, M. K.; Advincula, R.; Kidowaki, M.; Ichimura, K., *Macromol. Symp.* **2000,** *154*, 149-161.
6. Hassenkam, T.; Greve, D. R.; Bjornholm, T., *Adv. Mater.* **2001,** *13* (9), 631-634.

7. Sgobba, V.; Troeger, A.; Cagnoli, R.; Mateo-Alonso, A.; Prato, M.; Parenti, F.; Mucci, A.; Schenetti, L.; Guldi, D. M., *J. Mater. Chem.* **2009,** *19* (25), 4319-4324.
8. Voegel, J. C.; Decher, G.; Schaaf, P., *Actualite Chimique* **2003,** (11-12), 30-38.
9. Langeveld-Voss, B. M. W.; Janssen, R. A. J.; Meijer, E. W., *J. Mol. Struct.* **2000,** *521*, 285-301.
10. Dufresne, G.; Bouchard, J.; Belletete, M.; Durocher, G.; Leclerc, M., *Macromolecules* **2000,** *33* (22), 8252-8257.
11. Kawano, S.; Fujita, N.; Shinkai, S., *Chem.-Eur. J.* **2005,** *11* (16), 4735-4742.
12. Lanzi, M.; Della-Casa, C.; Costa-Bizzarri, P.; Bertinelli, F., *Macromol. Chem. Phys.* **2001,** *202* (9), 1917-1923.
13. Bolognesi, A.; Schieroni, A. G.; Botta, C.; Marinelli, M.; Mendichi, R.; Rolandi, R.; Relini, A.; Inganas, O.; Theandher, M., *Synth. Met.* **2003,** *139* (2), 303-310.
14. Leclerc, M.; Frechette, M.; Bergeron, J. Y.; Ranger, M.; Levesque, I.; Faid, K., *Macromol. Chem. Phys.* **1996,** *197* (7), 2077-2087.
15. Perepichka, I. F.; Besbes, M.; Levillain, E.; Salle, M.; Roncali, J., *Chem. Mat.* **2002,** *14* (1), 449-457.
16. Kaur, P.; Yue, H. J.; Wu, M. Y.; Liu, M.; Treece, J.; Waldeck, D. H.; Xue, C. H.; Liu, H. Y., *J. Phys. Chem. B* **2007,** *111* (29), 8589-8596.
17. Jiang, H.; Taranekar, P.; Reynolds, J. R.; Schanze, K. S., *Angew. Chem. Int. Ed.* **2009,** *48* (24), 4300-4316.
18. Hoeben, F. J. M.; Jonkheijm, P.; Meijer, E. W.; Schenning, A. P. H. J., *Chem. Rev.* **2005,** *105* (4), 1491-1546.
19. Hunter, C. A.; Sanders, J. K. M., *J. Am. Chem. Soc.* **1990,** *112* (14), 5525-5534.
20. Buwalda, R. T. Molecular Aggregation in Water.The interplay of Hydrophobic and Electrostatic Interactions, Ph. D Thesis. University of Groningen, 2001.
21. McCullough, R. D.; Ewbank, P. C.; Loewe, R. S., *J. Am. Chem. Soc.* **1997,** *119* (3), 633-634.
22. Bjornholm, T.; Greve, D. R.; Reitzel, N.; Hassenkam, T.; Kjaer, K.; Howes, P. B.; Larsen, N. B.; BÃ¸gelund, J.; Jayaraman, M.; Ewbank, P. C.; McCullough, R. D., *J. Am. Chem. Soc.* **1998,** *120* (30), 7643-7644.
23. Norgaard, K.; Bjornholm, T., *Chem. Commun.* **2005,** (14), 1812-1823.
24. Nilsson, K. P. R.; Andersson, M. R.; Inganäs, O., *J. Phys.: Condens. Matter* **2002,** *14* (42), 10011-10020.
25. Wagberg, T.; Liu, B.; Oradd, G.; Eliasson, B.; Edman, L., *Eur. Polym. J.* **2009,** *45* (11), 3228-3233.
26. Knaapila, M.; Almasy, L.; Garamus, V. M.; Pearson, C.; Pradhan, S.; Petty, M. C.; Scherf, U.; Burrows, H. D.; Monkman, A. P., *J. Phys. Chem. B* **2006,** *110* (21), 10248-10257.
27. Burrows, H. D.; Lobo, V. M. M.; Pina, J.; Ramos, M. L.; Seixas de Melo, J.; Valente, A. J. M.; Tapia, M. J.; Pradhan, S.; Scherf, U., *Macromolecules* **2004,** *37* (20), 7425-7427.
28. Tan, C.; Atas, E.; MÃ¼ller, J. r. G.; Pinto, M. R.; Kleiman, V. D.; Schanze, K. S., *J. Am. Chem. Soc.* **2004,** *126* (42), 13685-13694.

29. Pinto, M. R.; Kristal, B. M.; Schanze, K. S., *Langmuir* **2003,** *19* (16), 6523-6533.
30. Schenning, A. P. H. J.; Jonkheijm, P.; Hofkens, J.; De Feyter, S.; Asavei, T.; Cotlet, M.; De Schryver, F. C.; Meijer, E. W., *Chem. Commun.* **2002,** (12), 1264-1265.
31. Matthews, J. R.; Goldoni, F.; Schenning, A.; Meijer, E. W., *Chem. Commun.* **2005,** (44), 5503-5505.
32. Wang, Y.; Li, F.; Han, Y. M.; Wang, F. Y.; Jiang, H., *Chem.-Eur. J.* **2009,** *15* (37), 9424-9433.
33. Arnaud, A.; Belleney, J.; Boue, F.; Bouteiller, L.; Carrot, G.; Wintgens, W., *Angew. Chem. Int. Ed.* **2004,** *43* (13), 1718-1721.
34. Gu, Z.; Bao, Y. J.; Zhang, Y.; Wang, M.; Shen, Q. D., *Macromolecules* **2006,** *39* (9), 3125-3131.
35. Locklin, J.; Youk, J. H.; Xia, C.; Park, M.-K.; Fan, X.; Advincula, R. C., *Langmuir* **2002,** *18* (3), 877-883.
36. Xia, C.; Locklin, J.; Youk, J. H.; Fulghum, T.; Advincula, R. C., *Langmuir* **2001,** *18* (3), 955-957.
37. Henze, O.; Feast, W. J.; Gardebien, F.; Jonkheijm, P.; Lazzaroni, R.; Leclere, P.; Meijer, E. W.; Schenning, A., *J. Am. Chem. Soc.* **2006,** *128*, 5923-5929.
38. Brustolin, F.; Surin, M.; Lemaur, V.; Romanazzi, G.; Sun, Q.; Cornil, J.; Lazzaroni, R.; Sommerdijk, N.; Leclere, P.; Meijer, E. W., *Bull. Chem. Soc. Jpn.* **2007,** *80*, 1703-1715.
39. Jiang, L.; Hughes, R. C.; Sasaki, D. Y., *Chem. Commun.* **2004,** (8), 1028-1029.
40. Tsai, W. W.; Li, L. S.; Cui, H. G.; Jiang, H. Z.; Stupp, S. I., *Tetrahedron* **2008,** *64* (36), 8504-8514.
41. Schmid, S.; Mena-Osteritz, E.; Kopyshev, A.; Bauerle, P., *Org Lett* **2009,** *11* (22), 5098-101.
42. Van Rijn, P.; Savenije, T. J.; Stuart, M. C. A.; Van Esch, J. H., *Chem. Commun.* **2009,** (16), 2163-2165.
43. Buurma, N. J.; Haq, I., *J. Mol. Biol.* **2008,** *381* (3), 607-621.
44. Kegeles, G., *J. Phys. Chem.* **1979,** *83* (13), 1728-1732.
45. Mikheeva, L. M.; Grinberg, N. V.; Grinberg, V. Y.; Khokhlov, A. R.; de Kruif, C. G., *Langmuir* **2003,** *19* (7), 2913-2921.
46. Tai, M. S.; Kegeles, G., *Biophys. Chem.* **1984,** *20* (1-2), 81-87.
47. Gottlieb, H. E.; Kotlyar, V.; Nudelman, A., *J. Org. Chem.* **1997,** *62* (21), 7512-7515.

Chapter 5

DNA BINDING STUDIES

Abstract: *In this chapter we studied the interactions of cationic oligoheteroaromatics with double-stranded DNA using a combination of molecular docking studies, spectroscopy, viscosity and calorimetry. All synthesised cationic oligothiophenes bind moderately strongly to duplex DNA and binding is accompanied by a change in optoelectronic properties. Surprisingly, cationic oligoheteroaromatics bind to duplex DNA through different binding modes varying from minor-groove binding to intercalation to side-by-side binding in the minor groove.*

5.1. Introduction

Our aims in this chapter are to determine the mode of interactions and to quantify the thermodynamics of binding to DNA of a series of cationic oligoheteroaromatics **5.1-5.6** using a variety of complementary techniques, *viz.* UV-visible spectroscopy, circular dichroism spectroscopy (CD), Job plots, viscosity, as well as isothermal titration calorimetry (ITC). All structures investigated are summarised in Scheme 5.1.

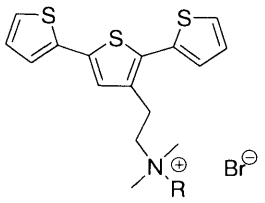

5.1 R=CH_3
5.2 R= CH_2CH_2OH
5.3 R=$CH_2CH_2OCH_2CH_2OH$

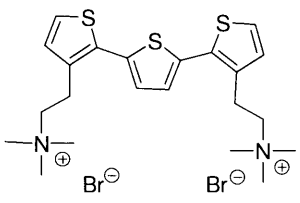

5.4

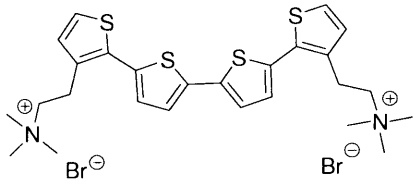

5.5

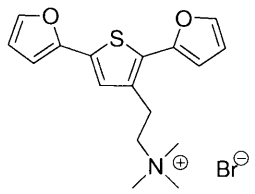

5.6

Scheme 5.1

5.2 Cationic terthiophenes 5.1, 5.2 and 5.3 binding to DNA

UV-visible spectroscopy

The interactions of cationic terthiophenes **5.1-5.3** to fish sperm DNA and calf thymus DNA were studied by UV-visible spectroscopy, at concentrations where self aggregation is negligible. The changes in absorption of **5.1** upon addition of DNA were measured in 25 mM

MOPS, 50 mM NaCl and 1 mM EDTA at 25 °C. Figure 5.1 shows that the binding of cationic oligothiophenes **5.1** to DNA is accompanied by a red shift in the UV-visible absorption.

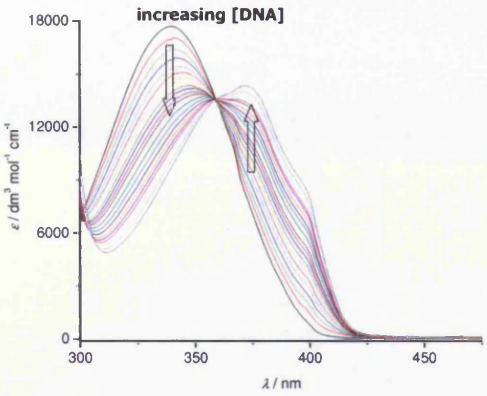

Figure 5.1 UV-visible spectra for 4.58×10^{-2} mM cationic terthiophene **5.1** upon addition of 0 – 2.36 mM calf thymus DNA in 25 mM MOPS, 50 mM NaCl and 1 mM EDTA, pH 7.0, at 25 °C.

Similar red shifts were observed for terthiophenes **5.1** and **5.2** (See Appendix). This red shift suggests an increase in effective conjugation length, which we attribute to an increase in planarity of the oligomer upon interaction with DNA. The isosbestic point in Figure 5.1 indicates that only two forms of the DNA binder are involved in the titration, *viz.* the free and bound ligand. Titration curves in Figure 5.2 were extracted from the UV-visible data and all show that saturation of the binding sites has been reached.

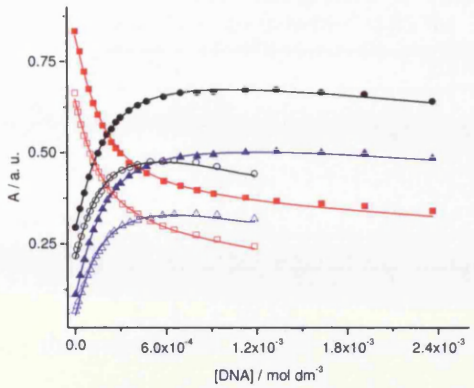

Figure 5.2 A solution of **5.1** (4.58×10^{-2} mM) was titrated with 0 – 2.36 mM calf thymus DNA, in 25 mM MOPS, 50 mM NaCl and 1 mM EDTA, pH 7.0, at 25 °C (black symbols). A second solution of **5.1** (3.62×10^{-2} mM) was titrated with 0 – 1.18 mM calf thymus DNA in the same buffer, pH 7, at 25 °C (open symbols). Absorbances at wavelengths 336 nm (■ and □), 380 nm (● and ○) and 397 nm (▲ and Δ) are plotted against DNA concentration and the solid lines represent a global fit to a multiple independent sites model.

The binding constants (K) and binding site sizes (n) were obtained by analysis of the titration curves in terms of a multiple independent binding sites model correcting for dilution of the DNA-binders (See Section 2.5.1). Binding parameters for **5.1-5.3** are summarised in Table 5.1. Monocationic terthiophenes **5.1-5.3** bind to fish sperm DNA and calf thymus DNA with a moderate binding constant in the order of 10^4 M^{-1}. The binding site size for the interactions of these ligands with DNA is 3 base pairs, which is in good agreement with molecular docking and Job plot data *(vide infra)*. A slightly higher affinity, but the same binding site size, was found for **5.1** and **5.3** binding to calf thymus DNA compared to binding to fish sperm DNA. Whereas the difference in binding constants is outside error margins, we believe that the difference is not such that it warrants further interpretation.

Table 5.1 Binding constants *K* and binding site sizes *n* for **5.1-5.3** with FS DNA and CT DNA in buffer[a] at 25 °C.

	FS DNA		CT DNA	
	K /10^4 M^{-1}	n / bp	K /10^4 M^{-1}	n / bp
5.1	1.8 ±0.2	3.3±0.2	2.9±0.2	3.1±0.2
5.2	1.9±0.4	3.3±0.3	-	-
5.3	1.8±0.8	3.1±0.5	2.2±0.3	3.2±0.3

a) 25 mM MOPS, 50 mM NaCl and 1 mM EDTA, pH 7

Table 5.1 shows that replacing the substituent on the ammonium group does not significantly affect the DNA affinity or the binding site size, suggesting it performs its role as solubilising group without interfering with DNA. The absence of the substituent effects on binding of **5.1-5.3** to DNA thus suggests that hydrophobic interactions of the π-conjugated frameworks in combination with the electrostatic interactions between the ammonium group and the negatively charged DNA are the driving forces responsible for the formation of ligand-DNA complexes. Cationic terthiophene **5.1** was also titrated with single-stranded polydA in 25 mM MOPS pH 7.0, 50 mM NaCl and 1 mM EDTA at 25 °C (Figure 5.3).

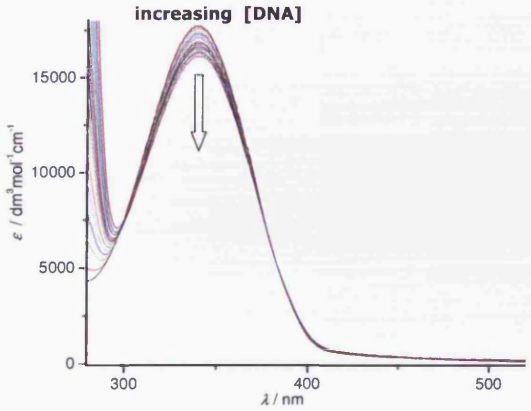

Figure 5.3 UV-visible spectra for 7.64 ×10^{-3} mM cationic terthiophene **5.1** upon addition of 0 – 0.25 mM poly dA in 25 mM MOPS pH 7.0, 50 mM NaCl and 1 mM EDTA, at 25 °C.

A slight decrease in the ligand absorption upon addition of polydA in addition to ligand dilution could be observed, suggesting that **5.1** interacts with single-stranded DNA. The titration curves in Figure 5.4 reveal that the binding sites are not saturated upon addition of 0.25 mM polydA.

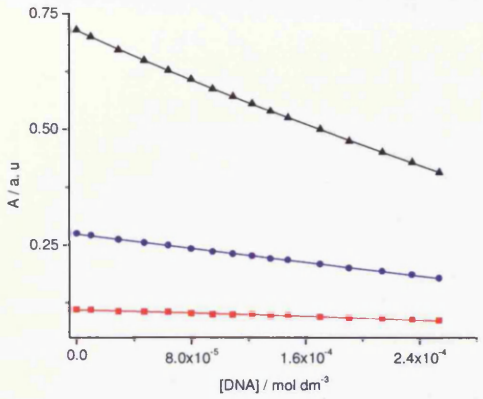

Figure 5.4 UV-visible titration of 7.64×10^{-3} mM cationic terthiophene **5.1** upon addition of 0 – 0.25 mM polydA in 25 mM MOPS pH 7.0, 50 mM NaCl and 1 mM EDTA, at 25 °C. Absorbances at wavelengths 339 nm (▲), 380 nm (●) and 397 nm (■) are plotted against polydA concentration and the solid lines represent a global fit to a multiple independent sites model.

The limited decrease of the signal at 339 nm together, with the limited extent of binding indicated by Figure 5.4, suggests that cationic terthiophenes interact only weakly with single-stranded DNA. The observation that interactions of cationic oligothiophenes with single-stranded DNA are weaker than with double-stranded DNA is in agreement with the use of cationic polythiophenes as component of systems sequence-selectively detecting single stranded DNA through hybridisation detection.

Continuous variation analysis (UV Vis Job plot)

Binding site sizes were confirmed by the construction of Job plots (See section 2.5.3). Figure 5.5 shows the Job plot for the interaction of 5.1 with calf thymus DNA.

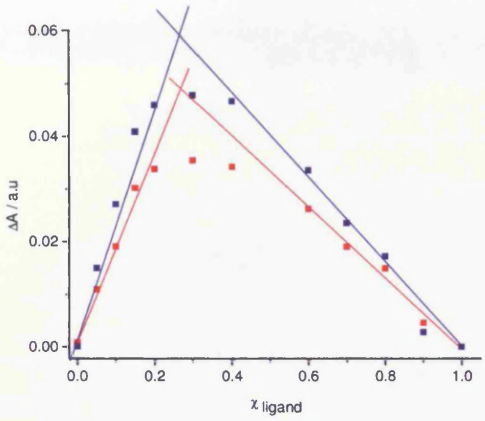

Figure 5.5 UV-visible Job plot for **5.1** interacting with CT-DNA, in buffer (25 mM MOPS, 50 mM NaCl and 1 mM EDTA, pH 7.0) at 25 °C. The changes in the absorbance at 395 (■) and 405 (■) nm are plotted against the mole fraction of the ligand χ_{ligand}.

The intersection points in the Job plots were found at mole fractions of 0.26 and 0.27. These values are equivalent to a stoichiometry of one ligand per three base pairs.

Molecular docking studies

The feasibility of a minor-groove binding mode for **5.1** with DNA was explored through a docking study using GOLD docking software[1] with $d(CGCAAATTTGCG)_2$[2] as the double-stranded DNA target (docking studies have been conducted by Dr. Marina Cioffi from Prof. Hunter's group at the University of Sheffield).

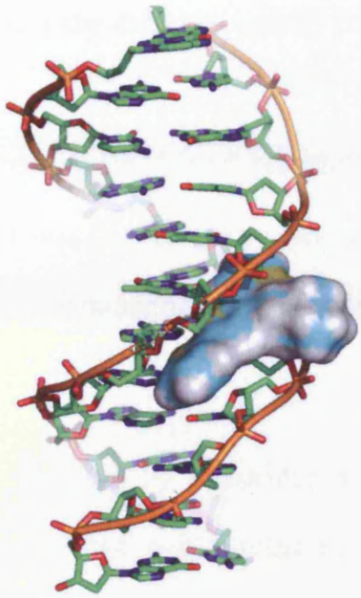

Figure 5.6 Top ranked pose for **5.1** docked with d(CGCAAATTTGCG)$_2$

The molecular docking studies showed that minor groove binding is possible for **5.1**. We observed that the hydrophobic part of the molecule preferred the hydrophobic environment of the minor groove and the cationic charges are oriented to the phosphate anions along the DNA sugar backbone. The complex structure in Figure 5.6 is in agreement with the results of binding studies for **5.1-5.3.** Substituents on the ammonium group are orientated away from the DNA and therefore do not affect binding.

In contrast, López Navarrete and coworkers[3] found that intercalation between the base pairs is a feasible mode of interaction of unsubstituted terthiophene with DNA. Unfortunately, in this example the rigid macromolecule structure, which includes a pre-formed intercalation site, effectively acts a bias in order to support the intercalation mode. A cavity was created in the DNA structure by removing an intercalated organic aromatic molecule from a crystal structure of a DNA-intercalator complex. During the docking studies terthiophene prefers the pre-formed

cavity in the DNA structure, because the energetic penalty for the creation of the intercalation site is not accounted for.

Our molecular docking studies are similarly biased because the DNA structure was also kept rigid and only one molecule of **5.1** was docked. As a result, effects resulting from 2:1 binding, potential intercalation and flexibility in minor groove were not taken into account.

Circular dichroism

To confirm the binding mode proposed by molecular docking studies *(vide supra)*, the interaction of **5.1** with calf thymus DNA was studied by circular dichroism spectroscopy. Induced circular dichroism (ICD) spectra for **5.1** were recorded over a range of $[ligand]_{bound}$ / [DNA] ratios (Figure 5.7).

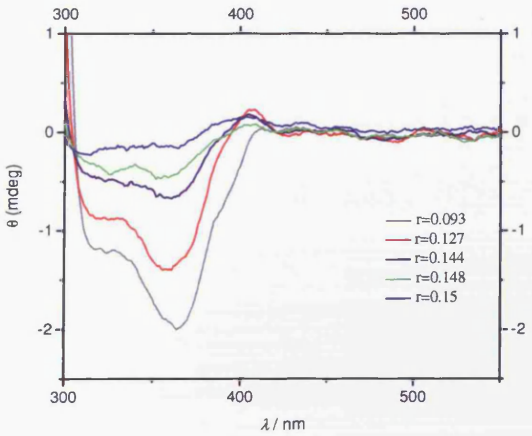

Figure 5.7 Induced circular dichroism spectra for **5.1** interacting with calf thymus DNA at different $[ligand]_{bound}$ / [DNA] ratios (r) in 25 mM MOPS pH 7.0, 50 mM NaCl, 1mM EDTA, at 25 °C.

Figure 5.7 shows typical ICD profiles for the interaction of **5.1** with calf thymus DNA, in 25 mM MOPS, 50 mM NaCl, 1 mM EDTA, pH 7.0 at 25 °C. The buffer absorption was subtracted

and no circular dichroism signal was observed for DNA in the wavelength range of interest. We can identify several ICD bands in the ICD spectra for **5.1** binding to calf thymus DNA. A negative band at 364 nm is observed and this band increases in intensity upon addition of DNA. The magnitude and negative sign of this ICD band suggests that **5.1** intercalates between the base pairs of DNA.[4] There is also a weak positive band over the range of 367-422 nm. This band appears but then decreases in intensity upon addition of DNA, up to a $[ligand]_{bound}$ / [DNA] ratio of 0.17. Upon continued addition of DNA, a sharp band starts to grow at 405 nm. This band disappears completely at high DNA concentration. These observations suggest more than one binding mode for interaction of **5.1** with calf thymus DNA.

Viscosity

The mode of interaction of **5.1** with double-stranded DNA was further studied using viscometry. In order to determine whether **5.1** is a minor groove binder, the viscosity of a DNA solution upon addition of **5.1** was compared with the viscosity for two known DNA binders which act either as an intercalator (ethidium bromide) or as a minor groove binder (Hoechst H33258). Figure 5.8 shows the relative viscosity for three DNA binders, including cationic terthiophene **5.1** in 25mM MOPS pH 7.0, 50 mM NaCl, 1 mM EDTA at 25 °C.

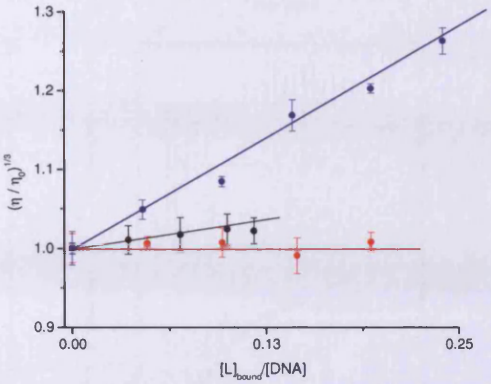

Figure 5.8 Relative viscosity of a 0.5 mM CT DNA solution upon addition of **5.1** (●), H33258 (●) and ethidium bromide (●) at 25 °C in 25 mM MOPS pH 7.0, 50 mM NaCl, 1mM EDTA.

The small increase in viscosity upon addition of **5.1** suggests a minor groove binding as the predominant binding mode, but some extent of intercalation of **5.1** between the base pairs is not excluded considering the slight increase in viscosity.

Isothermal titration calorimetry (ITC)

To further explore the binding of cationic terthiophenes **5.1-5.3** with fish sperm and calf thymus DNA we used isothermal titration calorimetry (ITC). Figure 5.9 shows typical enthalpograms obtained by adding **5.1, 5.2** and **5.3** to fish sperm DNA and calf thymus DNA, in 25 mM MOPS, 50 mM NaCl and 1 mM EDTA, pH 7.0 at 25 °C.

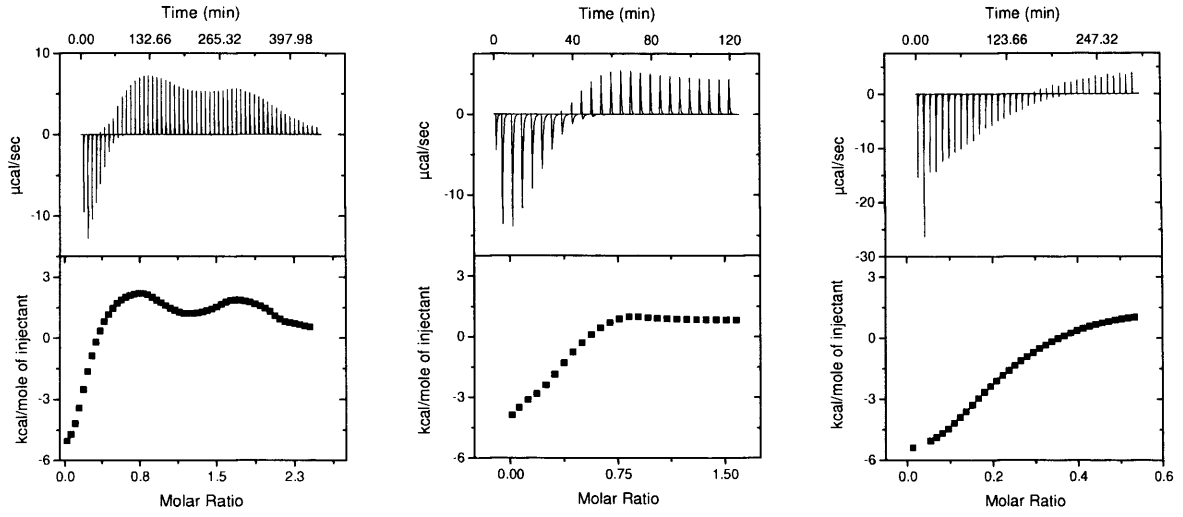

a **b** **c**

Figure 5.9 Titrating a 19.38 mM solution of **5.1** into a 1.6 mM solution of CT DNA (a), titrating a 19.80 mM solution of **5.2** into a 2.0 mM solution of FS DNA (b), titrating a 19.7 mM solution of **5.3** into a 5 mM solution of CT DNA (c), all in buffer (25 mM MOPS, 50 mM NaCl and 1 mM EDTA, pH 7.0 at 25 °C.

The interaction of **5.1** with CT DNA indicates more than one binding event. This is supported by the observation that during the titration a precipitate is formed, which suggests that, in the presence of excess of ligand, aggregates of ligand-DNA complexes are formed. This behaviour is reminiscent from the two DNA binding modes found for minor-groove binder Hoechst H33258.[5] The observation of more than one binding mode is in agreement with ICD data that showed complex behaviour for interaction of **5.1** with CT DNA. In contrast, the titration of **5.2** with calf thymus DNA suggests only one binding event. Similarly, cationic terthiophene **5.3** does not show a complex binding mode for the interaction with calf thymus DNA, but it should be noted that this titration only reaches a ligand : base pairs molar ratio of 0.55. The simpler enthalpogram suggests that, the oligoethyleneglycol chains act as solubilising groups and prevent precipitation of DNA-ligand complexes, a problem commonly encountered

in the study of interactions involving DNA and cationic ligands.[6-9] According to Figure 5.9, interactions of **5.1**, **5.2** and **5.3** with DNA are exothermic. The binding of the ligand to DNA is highly exothermic because the observed heat effects include the endothermic break-up of ligand aggregates, which must accompany the DNA binding. Because DNA-ligand complexes precipitate at high ligand concentration, the interactions of **5.1** with CT DNA cannot be analysed. Therefore, we performed a partial titration for **5.1** with CT DNA up to a maximum molar ratio [ligand]/[DNA] of 0.55 in order to avoid precipitation (See Appendix). We used our IC-ITC software to analyse the ITC data for the titrations of **5.1**, **5.2** and **5.3** with FS or CT DNA. Thermodynamic parameters are corrected for ligand self aggregation using both n-merisation and Kegeles' models but subsequent binding events are not included. As a result, binding constants are relative binding constants, *i.e.*, they represent lower limits. Correspondingly values for $-T\Delta S_{A1}$ are upper limits. Table 5.1 summarises the thermodynamic characteristics for binding of **5.1**, **5.2** and **5.3** to DNA.

Table 5.2 Thermodynamic parameters for binding of **5.1**, **5.2** and **5.3** to CT-DNA, 25 mM MOPS, 50 mM NaCl and 1 mM EDTA, pH 7, at 25 °C

n-merisation model[a]

	K_{A1} ($10^3 M^{-1}$)	ΔH_{A1} (kcal mol^{-1})	$-T\Delta S_{A1}$ (kcal mol^{-1})	$1/n_{A1}$	n_{mic}	$\{\Sigma dev^2/dof\}^{1/2}$ (μcal)
5.1	3.5±0.8	-10.0±1.0	5.2±0.8	3.7±0.3	8.1	0.5
5.2	2.6[b]	-9.3[b]	[c]	2.2[b]	6.2	31.2
5.3	2.6±0.8	-11.2±2.3	6.6±2.1	4.2±0.2	7.5	3.5

Kegeles' model[b]

	K_{A1} ($10^3 M^{-1}$)	ΔH_{A1} (kcal mol^{-1})	$-T\Delta S_{A1}$ (cal mol^{-1})	$1/n_{A1}$	n_{keg}	$10^2 f$	$\{\Sigma dev^2/dof\}^{1/2}$ (μcal)
5.1	3.3±1.1	-10.4±0.8	5.2±0.6	3.7±0.2	12	1.0	4.8
5.2	0.5±	-43.7	[c]	4.6	9	1.0	29.8
5.3	2.7±0.6	-10.0 (-12.2; -9.1)[d]	5.4 (-7.4; -4.6)[d]	4.3 (4; 4.5)[d]	24	1.0	3.3

a) Parameter values restricted to best fit values as reported in Table 4.7

b) No error margins or variable range reported because global minimum does not appear to have been found (See Appendix).

c) Variable range not reported for ΔS_{keg} because ΔG_{keg} is not well defined.

d) The reported range given within brackets corresponds to fits for which the normalised $\Sigma dev^2/dof < 2$(See Appendix).

In Table 5.2 we observe that thermodynamic parameters have similar values for binding models incorporating ligand aggregation in terms of n-merisation and Kegeles' models. This suggests that the binding models are in good agreement. The values for $\{\Sigma dev^2/dof\}^{½}$ are small, except for ligand **5.2** which shows large values for $\{\Sigma dev^2/dof\}^{½}$. This suggests that analysis of data for **5.1** and **5.3** binding to FS DNA and CT DNA, respectively, resulted in fits that reproduce the experimental data well. However, analysis of the error margins showed that errors are typically large. The binding constants are smaller than from the UV-visible titrations because it is relative to the next equilibrium binding process. Binding of **5.1**, **5.2** and **5.3** to FS DNA and CT DNA is accompanied by a negative enthalpy change and a negative entropy change suggesting an intercalation as a mode of binding.[10] The binding site size is 4 base pairs in reasonable agreement with binding site size obtained from UV-Vis titrations.

Binding mode for 5.1-5.3 interacting with DNA

Docking studies confirm that minor groove binding is possible, but do not exclude intercalation. Circular dichroism suggests intercalation, but minor groove binding mode could still occur. It may be possible that the ICD spectroscopy is very sensitive to intercalation, so the ICD signal being big covers the band characteristic for minor groove binding mode. Viscosity suggest mainly groove binding but does not exclude an extent of intercalation. Calf thymus DNA contains mixed sequences of A-T and G-C base pairs and, as a result, the ligand can bind to one sequence in the minor groove while intercalates between the base pairs in the other sequence. ITC suggests that first binding mode is intercalation.

Summary

Monocationic terthiophenes **5.1-5.3** bind to FS and CT DNA with a moderate binding affinity of ~10^4 M^{-1} along 3 or 4 base pairs. Docking studies suggests that minor-groove binding is indeed a favourable mode of binding, but intercalation is not excluded. Viscosity studies reveal that monocationic terthiophenes **5.1** interact with DNA through a mixed binding mode. In addition, ICD spectroscopy seems to be more sensitive to intercalation between the base pairs, suggesting intercalation at high ligand concentration but with some evidence of minor groove binding mode when DNA is in large excess. Isothermal titration calorimetry confirms three modes of binding for cationic terthiophene **5.1** while **5.2** and **5.3** show a simple one binding mode in the concentration range studied. Analysis of partially titration for **5.1** with FS DNA and **5.2** and **5.3** with CT DNA suggests intercalation of the ligands between the base pairs. Several binding modes are apparent from ITC experiments used natural DNA, and these may occur in competition. Different techniques have different sensitivities towards different binding modes, hence the seemingly contradictory results. Working with homogeneous DNA such as polydA·polydT, *etc.* could identify specific binding modes for specific sequences.

5.3 Dicationic terthiophene 5.4 binding to DNA

UV-visible spectroscopy

The interactions of dicationic terthiophene **5.4** with calf thymus DNA were studied by UV-visible spectroscopy. The changes in absorption of **5.4** upon addition of DNA were measured in 25 mM MOPS, 50 mM NaCl and 1 mM EDTA at 25 °C (Figure 5.10).

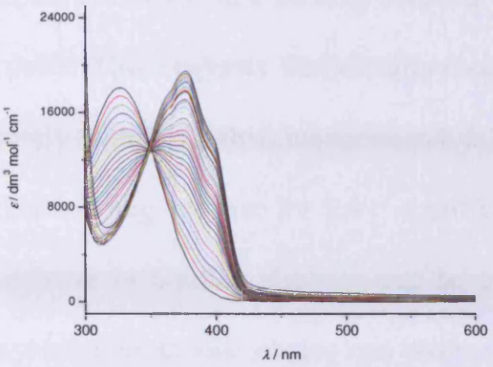

Figure 5.10 UV-visible spectra for 3.31×10^{-2} mM dicationic terthiophene **5.4** upon addition of 0 – 1.63 mM calf thymus DNA in 25 mM MOPS, 50 mM NaCl and 1 mM EDTA, pH 7.0, at 25 °C.

Figure 5.10 shows that interaction of **5.4** with DNA produces a bathochromic shift in the UV-Vis spectrum. We attribute the bathochromic shift to changes in effective conjugation length of the ligand. Titration curves were extracted from the data in Figure 5.10 and these were analysed in terms of a multiple independent binding sites model (Figure 5.11).

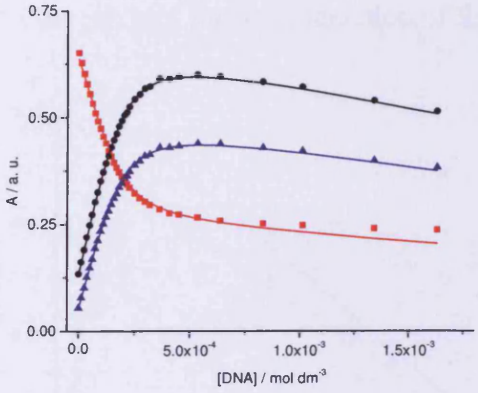

Figure 5.11 UV-visible titration of 3.31×10^{-2} mM dicationic terthiophene **5.4** with 0 – 1.63 mM calf thymus DNA, in 25 mM MOPS, 50 mM NaCl and 1 mM EDTA, pH 7, at 25 °C. Absorbances at wavelengths 330 nm (■), 380 nm (●) and 400 nm (▲) are plotted against DNA concentration and the solid lines represent a global fit to a multiple independent sites model (Figure 5.11).

Dicationic terthiophene **5.4** binds to DNA with a binding constant of $(21.0\pm1.5)\times10^4$ M^{-1} and a binding site size of 6 base pairs. This suggests that dicationic terthiophene **5.4** interacts an order of magnitude more strongly with DNA than monocationic **5.1**, suggesting the importance of electrostatic interactions. The binding site-size for **5.4** is significantly larger than the binding site sizes for **5.1-5.3**. The increase in binding site size can be attributed to one or more of several factors. First, the ethylammonium side chains can cover supplementary base pairs on both sides of the binding site of the conjugated oligothiophene framework. Second, sequence selectivity can result in certain sequence being excluded from interaction with **5.4**. Third, the binding mode of **5.4** *(vide infra)* appears to be significantly different from that of **5.1-5.3**, making comparison complicated.

Job Plot

The stoichiometry found from the UV-visible titration was confirmed by constructing a UV-vis Job plot. Figure 5.12 shows the job plot for the interaction of **5.4** with calf thymus DNA.

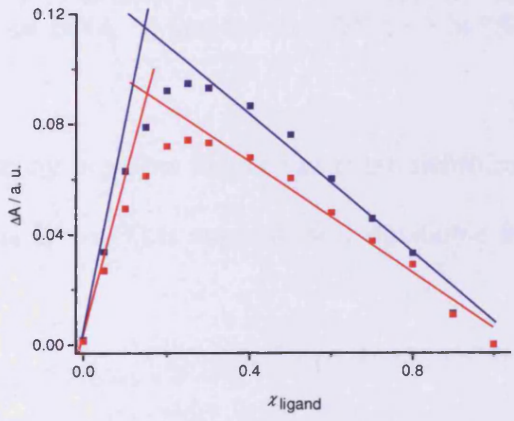

Figure 5.12 UV-visible Job plot for **5.4** interacting with CT-DNA, in buffer (25 mM MOPS, 50 mM NaCl and 1 mM EDTA), pH 7.0, at 25 °C. The changes in the absorbance at 380 (■) and 400 (■) nm wavelength are plotted against the mole fraction of the ligand χ_{ligand}.

The inflection points at mole fractions of 0.14 and 0.15 indicate a stoichiometry of 6 base pairs per ligand.

Circular dichroism

We investigated the binding mode for the interaction of **5.4** with calf thymus DNA using circular dichroism spectroscopy. Induced circular dichroism spectra for **5.4** were recorded at ratio $[ligand]_{bound}$ / [DNA] of 0.14 (Figure 5.13) in 25mM MOPS, 50 mM NaCl, 1 mM EDTA, pH 7.0 at 25 °C.

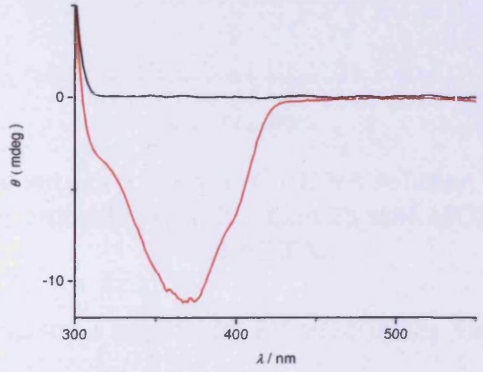

Figure 5.13 Induced circular dichroism spectra for a 1.15×10^{-4} M solution of **5.4** interacting with 4.96×10^{-4} M calf thymus DNA (-) and for free DNA (-) in 25 mM MOPS buffer, pH 7.0, 50 mM NaCl, 1mM EDTA.

Figure 5.13 shows that a strong negative induced circular dichroism signal is observed for **5.4** interacting with calf thymus DNA. This suggests that dicationic terthiophene **5.4** intercalates between the base pairs.[4]

Viscosity

To confirm intercalation as a binding mode for **5.4** with calf thymus DNA, we determined the relative viscosity of a DNA solution in the presence of different concentration of **5.4** in MOPS buffer, pH 7.0 (25mM MOPS 50 mM NaCl, 1mM EDTA) at 25 °C (Figure 5.14).

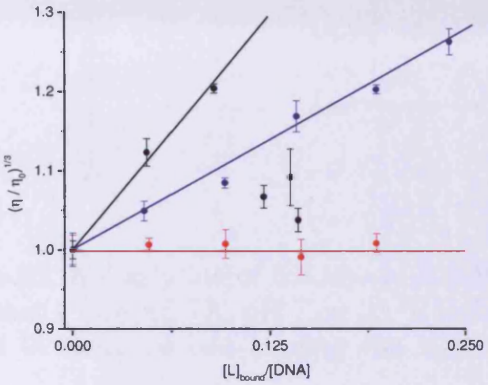

Figure 5.14 Relative viscosity of a 0.5 mM CT DNA solution upon addition of **5.4** (●), H33258 (●) and ethidium bromide (●) at 25 °C in 25 mM MOPS pH 7.0, 50 mM NaCl, 1mM EDTA.

Figure 5.14 shows that **5.4** causes a significant increase in the viscosity of the DNA solution, comparable to the increase observed by ethidium bromide, indicating that **5.4** interacts with calf thymus DNA through intercalation. Upon addition of ligand, the DNA solution became opalescent and a decrease in the viscosity was observed. We attribute these observations to precipitation of DNA-ligand complexes.

Isothermal titration calorimetry

The interaction of dicationic terthiophene **5.4** with calf thymus DNA was further investigated using isothermal titration calorimetry (ITC). Figure 5.15 (left) shows a typical titration of **5.4** with calf thymus DNA, in 25 mM MOPS, 50 mM NaCl and 1 mM EDTA, pH 7 at 25 °C.

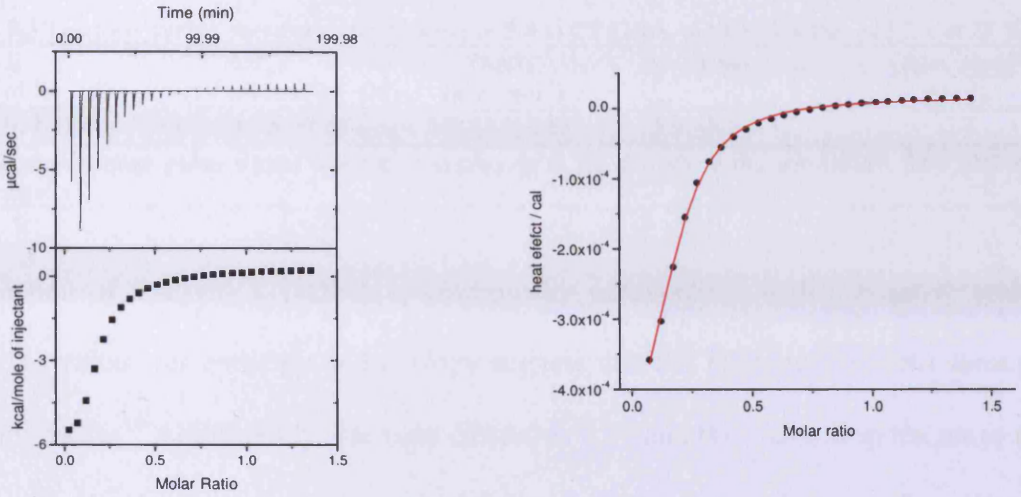

Figure 5.15 Titration of a 6.85 mM solution of **5.4** into a1.0 mM solution of CT DNA in 25 mM MOPS, 50 mM NaCl and 1 mM EDTA, pH 7, at 25 °C (left). Integrated heat effects for the same titration analysed in terms of one binding site size model with aggregation not included.

The calorimetric titration involving **5.4** and CT DNA clearly indicates one binding event. The calorimetric data was analysed in terms of the one binding model (Section 2.6.7). We did not take into account the self aggregation of **5.4** in the binding studies, because we worked with a low concentration of ligand in the syringe (6.85 mM) and at this concentration dicationic terthiophene **5.4** does not show strong self aggregation (Section 4.3.1.1). The fit to the one-binding site model shows that this binding model reproduces the experimental data well. The thermodynamic parameters for the interaction of dicationic terthiophene **5.4** with CT DNA in 25 mM MOPS, 50 mM NaCl and 1 mM EDTA, pH 7.0, at 25 °C are summarised in Table 5.3.

Table 5.3 Thermodynamic parameters for binding of **5.4** to CT-DNA, in MOPS buffer, pH 7.0, at 25 °C

K_{A1} ($10^4 M^{-1}$)	ΔH_{A1} (10^3cal mol^{-1})	$-T\times\Delta S_{A1}$ (kcal mol^{-1})	$1/n_{A1}$	$\{\Sigma dev^2/dof\}^{1/2}$ (μcal)
1.6; (1.0; 2.3)[a]	-8.7; (-11.3; -7.3)[a]	3.0; (1.4; 6.8)[a]	5.9; (5.5-7.1)[a]	3.7

a) The reported range given within brackets corresponds to fits for which the normalised $\Sigma dev^2/dof < 2$ (See Appendix).

The interaction of **5.4** with CT-DNA is entropically unfavorable, with a negative enthalpy. The negative values for enthalpy and entropy suggest that **5.4** binds to CT DNA through an intercalation mode.[10] Additionally, the ratio $\Delta H/\Delta G$ is 1.52 and this value is in the range (0.83-1.97) typically found for a ligand intercalating between the base pairs.[10] The binding site size is 6 base pairs in agreement with binding site size obtained from UV-Vis titrations.

Binding mode for 5.4 interacting with CT DNA

Circular dichroism, viscometry and ITC suggest mainly intercalation as mode of binding for **5.4** to DNA.

Summary

In our series of cationic oligoheteroaromatics, dicationic terthiophene **5.4** is the strongest DNA binder $(21.0\pm1.5)\times10^4$ M^{-1}. The ligand binds along 6 base pairs. CD spectroscopy reveals a negative ICD signal when **5.4** binds to DNA, suggesting an intercalation as a mode of binding. The intercalation mode is confirmed by the increasing viscosity of DNA solutions upon addition of **5.4**. The binding is characterised by negative enthalpy and entropy, further confirming that **5.4** acts as an intercalator.

5.4 Dicationic quaterthiophene 5.5 binding to DNA

UV-visible spectroscopy

We first studied the interactions of dicationic quaterthiophene **5.5** with calf thymus DNA by UV-visible spectroscopy, in the concentration range where self aggregation is negligible. The changes in absorption of **5.5** upon addition of DNA were measured in 25 mM MOPS, pH 7.0, 50 mM NaCl and 1 mM EDTA at 25 °C (Figure 5.16).

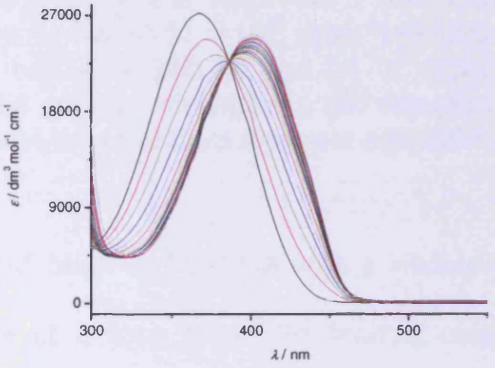

Figure 5.16 UV-visible spectra for 3.52×10^{-2} mM cationic quaterthiophene **5.5** upon addition of 0 – 0.90 mM calf thymus DNA in 25 mM MOPS, 50 mM NaCl and 1 mM EDTA, pH 7.0 at 25 °C.

Figure 5.16 shows a red-shift in the absorption spectrum of cationic quaterthiophene **5.5** upon addition of DNA, with a good isosbestic point, suggesting that only two species are involved in the titration, *viz.* free and bound ligand. Because of the region in which the spectroscopic changes take place in combination with the extent of the shift in λ_{max}, the spectroscopic changes can be observed as colour changes by the naked eye: a solution of **5.5** changes colour from yellow to green upon addition of DNA. Titration curves in Figure 5.17 were analysed in terms of a multiple independent binding sites model (Figure 5.17).

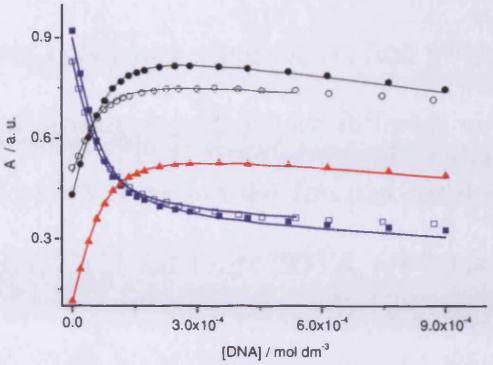

Figure 5.17 UV-visible titration of 3.02×10^{-2} mM solution of **5.5** with 0 – 0.87 mM calf thymus DNA in 25 mM MOPS, 50 mM NaCl and 1 mM EDTA, pH 7, at 25 °C (black symbols). A second solution of **5.5** (3.52×10^{-2} mM) was titrated with 0 – 0.90 mM calf thymus DNA in the same buffer, at pH 7.0 and 25 °C (open symbols). Absorbances at wavelengths 355 nm (■), 360 nm (□), 400 nm (○), 407 nm (●) and 430 nm (▲) are plotted against DNA concentration and the solid lines represent a global fit to independent binding site model.

Dicationic quaterthiophene **5.5** binds to CT-DNA with a binding constant of $(11.4 \pm 0.2) \times 10^4$ M^{-1} and a binding site size of 2 base pairs. The binding constant is higher than for the terthiophenes **5.1-5.3**. It is likely that both increased hydrophobicity and increased positive charge play a role. The smaller binding site size suggests that cationic quaterthiophene **5.5** binds in a "side-by-side" fashion, where two of the ligand molecules bind next to each other in the minor groove, with two ligands together covering four base pairs. The same small stoichiometry has been observed for Dervan *et al.*[11, 12] Compared to the dicationic terthiophene **5.4,** the binding constant for dicationic quaterthiophene **5.5** is smaller. This could be a result of a variety of factors including: increased crowding in the minor groove as a result of side by side binding; curvature mismatch for the longer oligothiophene; or different binding modes for oligothiophenes **5.4** and **5.5.**

Job plot

The binding stoichiometry was confirmed using the method of continuous variation. Changes in UV-visible absorption of **5.5** were monitored for different mole fractions and at specific wavelength (Figure 5.18). Figure 5.18 shows the Job plot for the interaction of **5.5** with CT DNA, in 25 mM MOPS, 50 mM NaCl and 1 mM EDTA, pH 7.0 at 25 °C.

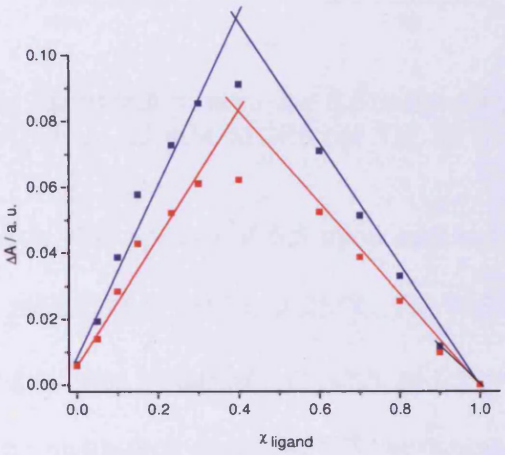

Figure 5.18 UV-visible Job plot for **5.5** interacting with CT-DNA, in buffer (25 mM MOPS, 50 mM NaCl and 1 mM EDTA), pH 7.0 at 25 °C. The changes in the absorbance at 410 (■) and 430 (■) nm wavelengths are plotted against the mole fraction of the ligand χ_{ligand}

The inflection points at 0.37 in Figure 5.18 correspond to a stoichiometry (binding site size) of 1.7 base pairs per molecule of ligand. This stoichiometry is in agreement with the stoichiometry from analysis of UV-visible titrations (*vide supra*).

Circular dichroism

To investigate the binding mode of **5.5** interacting with calf thymus DNA we used circular dichroism spectroscopy. As for **5.1-5.4**, ICD spectra for **5.5** were recorded at different $[ligand]_{bound}$ / [DNA] ratios (Figure 5.19).

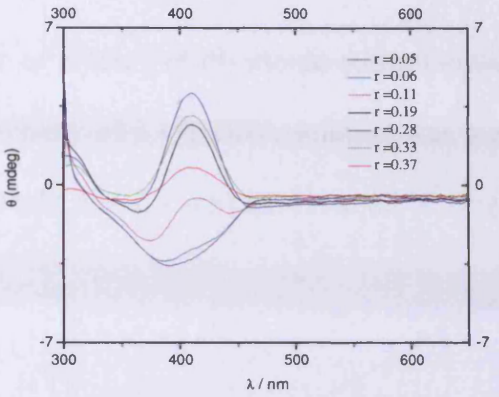

Figure 5.19 Induced circular dichroism spectra for **5.5** interacting with calf thymus DNA at different $[ligand]_{bound}$ / [DNA] (r) in 25 mM MOPS pH 7.0, 50 mM NaCl, 1mM EDTA at 25 °C.

Figure 5.19 presents changes in ICD spectra of **5.5** upon addition of calf thymus DNA, in 25 mM MOPS, 50 mM NaCl, 1 mM EDTA, pH 7.0 at 25 °C. The buffer absorption was subtracted and no circular dichroism signal was observed for DNA in the wavelength range of interest. Figure 5.19 shows more than one binding mode for **5.5** interacting with CT DNA. There is an increase in the positive ICD signal at 409 nm upon addition of CT DNA, which is attributed to the formation of DNA-ligand complexes. The positive sign of this ICD signal suggests that **5.5** binds in the minor groove of DNA.[4] At a ratio $[ligand]_{bound}$ / [DNA] of 0.19 this band decreases and eventually a negative band appears, at the same wavelength. This negative band may be induced by a second event involving intercalation of dicationic quaterthiophene **5.5** between the base pairs. These observations suggest that binding of dicationic terthiophene **5.5** with calf thymus DNA occurs by a mixed binding mode, *viz.* minor groove binding with a "side-by-side" fashion at low DNA concentration and intercalation between the base pairs at high DNA concentration. Isothermal titration calorimetry (ITC) also demonstrates more than one mode of interactions for **5.5** interacting with CT DNA *(vide infra).*

Viscosity

To further confirm the mode of binding of dicationic quaterthiophene **5.5** to CT DNA we used viscometry. The relative viscosity of a CT DNA solution was measured upon addition of **5.5** in 25 mM MOPS pH 7.0, 50 mM NaCl, 1 mM EDTA at 25 °C (Figure 5.20).

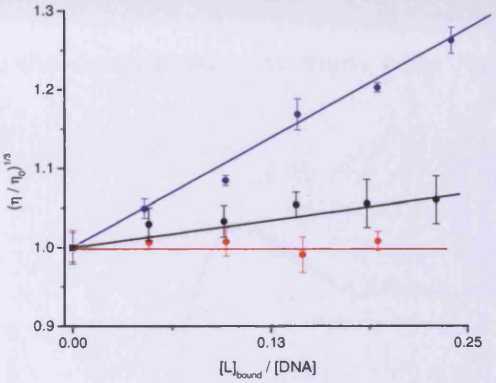

Figure 5.20 Relative viscosity of a 0.5 mM CT DNA solution upon addition of **5.5** (●), H33258 (●) and ethidium bromide (●) at 25 °C in 25 mM MOPS pH 7.0, 50 mM NaCl, 1mM EDTA.

Figure 5.20 shows the relative viscosity for Hoechst H33258, ethidium bromide and dicationic quaterthiophene **5.5** at different $[ligand]_{bound}/[DNA]$ ratios. Dicationic quaterthiophene **5.5** causes a relative small increase in viscosity of a DNA solution, comparable with the effect caused by a known minor-grove binder H33258. This observation is in agreement with the hypothesis that dicationic quaterthiophene **5.5** binds mainly "side-by-side", in the minor groove. Intercalation of **5.5** between the base pairs is not excluded, considering there is a second binding event *(vide supra)*.

Isothermal titration calorimetry

To further explore the binding of cationic terthiophenes **5.5** with DNA we used isothermal titration calorimetry (ITC). The heats and integrated heat effects for two consecutive calorimetric titrations with cell remixing (See Appendix) involving **5.4** and calf thymus DNA were measured in 25 mM MOPS, 50 mM NaCl and 1 mM EDTA, pH 7.0, at 25 °C. Integrated heat effects corresponding to these consecutive titrations were combined using IC ITC (Figure 5.21).

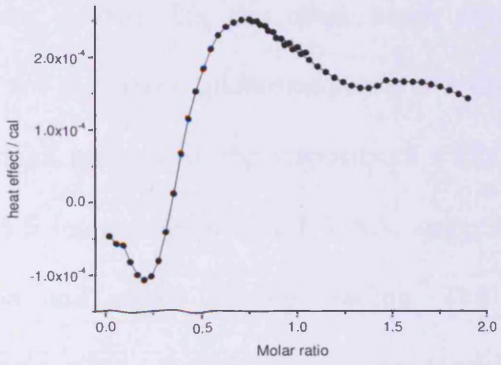

Figure 5.21 Combined heat effects for a series of two ITC experiments involving dicationic quaterthiophene **5.5** and CT-DNA in 25 mM MOPS, 50 mM NaCl and 1 mM EDTA, pH 7.0 at 25 °C.

The enthalpogram for binding of **5.5** to CT-DNA in Figure 5.21 clearly suggests three binding modes. The data is too complicated to be analysed by IC ITC.

Binding mode for 5.5 interacting with DNA

Circular dichroism suggests (at least) two binding modes for interaction of **5.5** with CT DNA, *e.g*, minor groove binding in a "side-by-side" fashion and intercalation. We note the binding mode can be influenced by DNA sequence and **5.5** may shows different modes of binding for

different DNA sequences. Viscosity studies suggest mainly a minor groove binding, but intercalation can be attributed to the second binding mode. Compared to ICD, ITC suggests at least three binding modes, all binding modes may occur in competition.

Summary

Dicationic quaterthiophene **5.5** binds with a binding constant of $(11.4 \pm 0.2)\times10^4$ and a binding site size of 2 base pairs. At high ligand concentration the interaction of dicationic quaterthiophene **5.5** with CT DNA results in a positive ICD signal, suggesting "side-by-side" binding of **5.5** in the minor groove. On the other hand, at low ligand concentration a negative signal is observed for dicationic quaterthiophene **5.5** suggesting that **5.5** intercalates between the base pairs. A small increase in the viscosity of a DNA solution was observed for dicationic quaterthiophene **5.5** interacting with CT DNA, suggesting a mixed binding mode, involving both intercalation and minor groove binding. The complex binding mode is supported by ITC, which shows at least three binding modes for **5.5** interacting with DNA.

5.5 Cationic furan derivative 5.6 binding to DNA

UV-visible spectroscopy

The binding of **5.6** with calf thymus DNA was studied by UV-visible spectroscopy in the concentration range where self aggregation is negligible. We monitored changes in absorption of **5.6** upon addition of fish sperm DNA in 25 mM MOPS, 50 mM NaCl and 1 mM EDTA, at 25 °C (Figure 5.22).

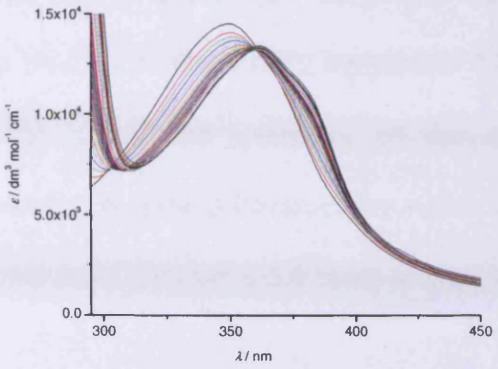

Figure 5.22 UV-visible spectra for 6.08×10^{-2} mM cationic furan derivative **5.6** upon addition of 0-1.25 mM calf thymus DNA in 25 mM MOPS, 50 mM NaCl and 1 mM EDTA, pH 7.0 at 25 °C.

Figure 5.22 shows that increasing the DNA concentration, the absorption at 345 nm (characteristic for the free ligand) decreases and a new absorption appears at 384 nm as a result of **5.6** binding to DNA. This red shift suggests an increase in effective conjugation length. Titration curves were extracted from the data in Figure 5.22 and were analysed in terms of multiple independent binding site model (Figure 5.23).

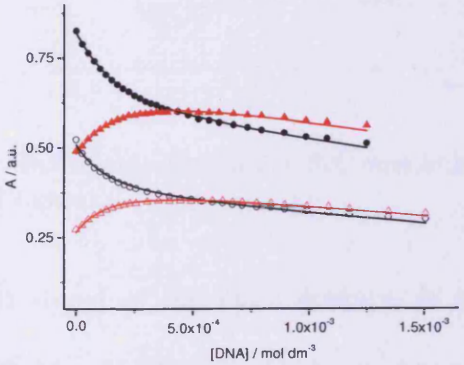

Figure 5.23 UV-visible titration of 6.08×10^{-2} mM solution of **5.6** with 0 – 1.25 mM fish sperm DNA in 25 mM MOPS, 50 mM NaCl and 1 mM EDTA, pH 7, at 25 °C (black symbols). A second solution of **5.6** (3.79×10^{-2} mM) was titrated with 0 – 1.51 mM fish sperm DNA in the same buffer, at pH 7.0 and 25 °C (open symbols). Absorbances at wavelengths 333 nm (● and ○), 384 nm (▲ and △) are plotted against DNA concentration and the solid lines represent a global fit to a multiple independent binding site model.

Cationic furan-thiophene-furan derivative **5.6** binds marginally more strongly than the cationic terthiophenes **5.1-5.3**, with a binding constant of $(2.4\pm0.6)\times10^4$ M^{-1}. The difference might be explained by changes in the shape and geometry of the molecules but also in the hydrophobicity. We note, however, that the differences are within error margins on the binding constants. Surprisingly, cationic furan derivative **5.6** binds along 2 base pairs.

Circular dichroism

To further investigate the binding mode of **5.6** with calf thymus DNA we used circular dichroism spectroscopy. As for other ligands, ICD spectra for **5.6** were recorded at different $[ligand]_{bound}$ / [DNA] ratios (Figure 5.24).

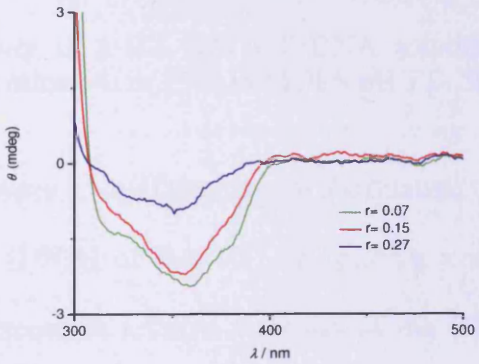

Figure 5.24 Induced circular dichroism spectra for **5.6** interacting with calf thymus DNA at different $[ligand]_{bound}$ / [DNA] ratios.

Figure 5.24 presents the ICD signal of **5.6** upon addition of calf thymus DNA, in 25mM MOPS, 50 mM NaCl, 1mM EDTA, pH 7.0 at 25 °C. A broad negative signal grows in intensity and shifts to the red with increasing the concentration of CT DNA. The negative ICD spectra of **5.6** binding to calf thymus DNA are attributed to intercalation of **5.6** between the base pairs of DNA.[4]

Viscosity

The binding mode of **5.6** to calf thymus DNA was further studied using viscosity. The relative viscosity of a CT DNA solution was measured at different $[ligand]_{bound}/[DNA]$ ratios, in 25 mM MOPS, pH 7.0, 50 mM NaCl, 1 mM EDTA at 25 °C (Figure 5.25).

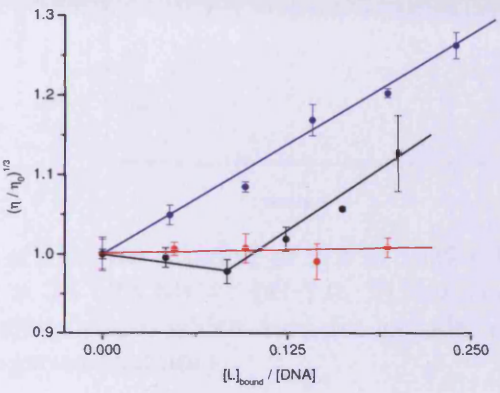

Figure 5.25 Relative viscosity of a 0.5 mM CT DNA solution upon addition of **5.5** (●), H33258 (●) and ethidium bromide (●) in 25 mM MOPS pH 7.0, 50 mM NaCl, 1 mM EDTA, at 25 °C

Figure 5.25 shows that **5.6** causes a small decrease in the relative viscosity of CT DNA solution up to a ratio $[ligand]_{bound}$ / [DNA] of $8.8x10^{-2}$, suggesting a minor groove binding mode. Above this ratio, a large increase in relative viscosity of the CT DNA solution, comparable with the effect of ethidium bromide, could be observed. This suggests that at higher $[ligand]_{bound}$ / [DNA] ratios **5.6** intercalates between the base pairs.

Isothermal titration calorimetry (ITC)

To probe thermodynamic details of the interaction of **5.6** with calf thymus DNA we used isothermal titration calorimetry (ITC). For this experiment we used 20.1 mM stock solution (5 days old) for which we previously studied the self aggregation (Section 4.3.1.2).

Figure 5.15 shows integrated heats for a typical titration of **5.6** with calf thymus DNA, in 25 mM MOPS, 50 mM NaCl and 1 mM EDTA, pH 7.0 at 25 °C.

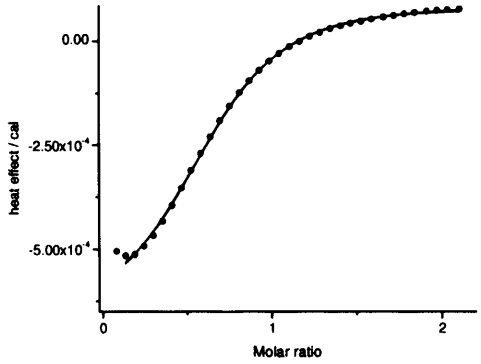

Figure 5.26 Integrated heat effects for titration of a 20.1 mM solution of **5.6** into a 2.0 mM of fish sperm DNA solution in 25 mM MOPS pH 7.0, 50 mM NaCl, 1 mM EDTA, at 25 °C. The data is fitted using a binding model which does not include self aggregation (blue line) or includes isodesmic self aggregation (red line).

Figure 5.26 indicates one type of interaction for monocationic furan derivative **5.6** binding to fish sperm DNA. Heat effects are exothermic, indicating that binding is highly exothermic because the observed heat effects include the endothermic effect of deaggregation of the ligand. First, ITC data was analysed using a model describing one binding event, A1 (Scheme 2.1 in Section 2.6.2), in which ligand self aggregation was not taken into account. A second model describing the same binding was also used, but this time the model incorporates ligand isodesmic self-aggregation $[L]_{agg}$ (Section 2.6.2). Analysis using both models resulted in fits that reproduce the experimental data well (Table 5.5). Thermodynamic parameters from analysis of data for a reverse titration are also summarised in Table 5.5.

Table 5.5 Thermodynamic parameters for interaction of **5.6** with FS-DNA, in MOPS buffer, pH 7.0, at **25 °C**

aggregation not included

$[L]_{syringe}$ (mM)	$[DNA]_{cell}$ (mM)	K_{A1} ($10^3 M^{-1}$)	ΔH_{A1} (10^3cal mol^{-1})	$-T\times\Delta S_{A1}$ (cal mol^{-1})	$1/n_{A1}$	$\{\Sigma dev^2/dof\}^{1/2}$ (µcal)
20.1	2.0	4.8±1.0	-5.1 ±0.3	72.0±20.2	1.5±0.1	3.8

isodesmic self aggregation[a]

$[L]_{syringe}$ (mM)	$[DNA]_{cell}$ (mM)	K_{A1} ($10^3 M^{-1}$)	ΔH_{A1} (10^3cal mol^{-1})	$-T\times\Delta S_{A1}$ (cal mol^{-1})	$1/n_{A1}$	$\{\Sigma dev^2/dof\}^{1/2}$ (µcal)
20.1	2.0	3.7±1.1	-5.8±0.5	92.4±0.4	1.4±0.7	5.4

reverse titration

$[L]_{cell}$ (mM)	$[DNA]_{syringe}$	K_{A1} ($10^3 M^{-1}$)	ΔH_{A1} (10^3cal mol^{-1})	$-T\times\Delta S_{A1}$ (10^3cal mol^{-1})	$1/n_{A1}$	$\{\Sigma dev^2/dof\}^{1/2}$ (µcal)
6.5×10^{-1}	6.3	2.7; (0.5; 5.4)[b]	–6.1; (–8.8; 4.9)[b]	1.4; (1.3; 3.8)[b]	1.5	1.5

a) Parameter values restricted to best fit values as reported in Table 4.4.

b) The reported range given within brackets corresponds to fits for which the normalised $\Sigma dev^2/dof < 2$ (See Appendix).

c) For error margins see Appendix

According to Table 5.5 calorimetric parameters obtained from analysis using a one binding site model without ligand self aggregation and a model including isodesmic aggregation and analysis of the data from the reverse titration are all similar because **5.6** self aggregates weakly (Section 4.3.1). Table 5.5 shows that cationic furan derivative **5.6** binds to FS DNA with an affinity of ~10^3 M^{-1}. This affinity is lower than that obtained from the UV-visible titration. The potential problem here is that there is a weak second binding event. Such a weak event can affect the observed binding constants from UV-Vis and ITC differently. The binding site size is 1.5 in reasonable agreement with the binding site size obtained from UV-vis titrations. Binding is further characterised by a negative enthalpy change, as well as a negative entropy change. These values for enthalpy and entropy are in between the values characteristic for minor groove binders and intercalators and as a consequence do not allow distinguishing clearly between the two binding modes.[10]

Binding mode for interaction of 5.6 with DNA

As for monocationic terthiophenes **5.1-5.3**, different techniques have different sensitivities towards different binding modes, yielding confusing results.

Circular dichroism suggests intercalation as mode of binding for **5.6** with DNA, but minor groove binding mode could still occur if we consider that CD is more sensitive to intercalation (a negative band characteristic for intercalation can cover a positive ICD band).

Viscosity suggests minor groove binding and intercalation, while the ITC data do not allow distinguishing between the two binding modes.

Summary

Cationic furan derivative **5.6** binds to fish sperm DNA with a binding constant of $(2.4\pm0.6)\times10^4$ M^{-1} and a binding site size of 2 base pairs determined by UV-visible spectroscopy. The ligand causes a significant increase in the viscosity above a ratio $[ligand]_{bound}/[DNA]$ of 8.8×10^{-2}, indicating that **5.6** intercalates between the base pairs. Below this ratio, a decrease in the viscosity of CT DNA solution was observed. A negative induced circular dichroism spectrum was observed for **5.6,** suggesting intercalation as a binding mode. The interaction of **5.6** with DNA is accompanied by a negative enthalpy contribution and unfavourable entropy.

5.7 Conclusions

All synthesised cationic oligoheteroaromatics **5.1-5.6** bind to duplex DNA and binding is accompanied by a change in optoelectronic properties as clear from the fact that binding of cationic oligoheteroaromatics **5.1-5.6** to DNA is accompanied by a red-shift in the UV-visible absorption. This red shift suggests an increase in effective conjugation, *i.e.*, an increase in planarity of the oligomer upon interaction with DNA. The driving force for **5.1-5.6** binding to DNA is provided by interaction between the conjugated framework of the oligothiophene and DNA, either when intercalated or bound in the minor groove, in combination with electrostatic interactions between the ammonium group and the negatively charged DNA. Binding constants have been summarised in Figure 5.32.

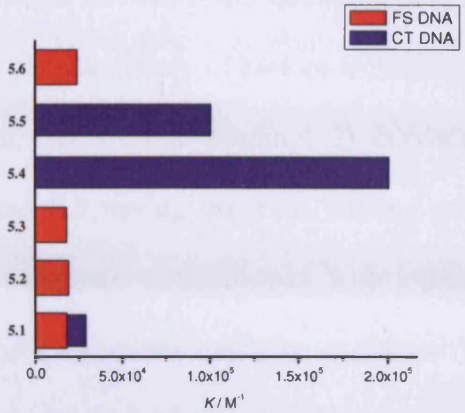

Figure 5.32 Binding constants by UV-Vis titration for ligands **5.1-5.6** with FS DNA (—) and CT DNA (—) in buffer (25 mM MOPS, 50 mM NaCl and 1 mM EDTA, pH 7.0) at 25 °C.

Monocationic terthiophenes **5.1-5.3** bind to fish sperm DNA with a moderate binding constant in the order of 10^4 M^{-1} and a binding site size of 3 base pairs. Binding to single-stranded DNA is too weak to quantify. On the other hand, dicationic terthiophene **5.4** interacts an order of magnitude more strongly with DNA, indicating the importance of electrostatic interactions. Moreover, it appears as if the introduction of additional pendant group carrying a cationic charge reduces flexibility of the thiophene scaffold and produces steric hindrances, making groove binding unfavourable leading to intercalation instead. As a result, the binding site size for **5.4** is 6 base pairs, significantly larger than the binding site sizes for all the other oligoheteroaromatics. This is an intriguing result for an intercalator, but a similarly large binding site was found for a dicationic biarylpyrimidine which binds selectively to poly(dA)•poly(rU) through intercalation.[13] Dicationic quaterthiophene **5.5** binds to calf thymus DNA with a binding site size of 2 base pairs per ligand. This binding site size is smaller than for all other oligoheteroaromatics, suggesting quarterthiophene **5.5** can bind in the minor groove in a "side-by-side" fashion, reminiscent of many other minor groove binders.

The decrease in binding constant for dicationic quaterthiophene **5.5** compared to dicationic terthiophene **5.4** could result from a variety of factors including 1) increased crowding in the minor groove as a result of side by-side binding; 2) curvature mismatch for the longer oligothiophene and 3) **5.4** and **5.5** having different binding modes. Replacing the terminal thiophene rings in the monocationic terthiophenes with other heteroaromatics varies the binding affinity to DNA. These variations might be explained by changes in the shape and geometry of the molecules but also in the hydrophobicity. For example, replacing the terminal thiophenes with furan rings, results in a slight difference in the angle between the rings and these changes affect the curvature of **5.6** compared to **5.1**. Modifications of the curvature may affect the selectivity of **5.6** for minor groove of DNA. In addition to hydrophobic interactions, oxygen atoms can form hydrogen bonds with DNA base pairs which might affect the affinity of **5.6** for DNA.The binding site size is smaller than for corresponding monocationic terthiophenes **5.1-5.3**. The mode of interaction of interaction of **5.1-5.6** with double-stranded DNA was studied using viscometry and the results are summarised in Figure 5.33.

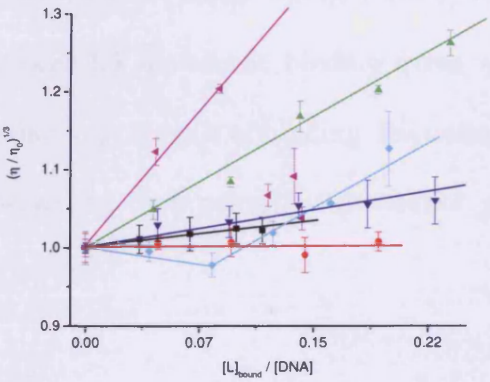

Figure 5.33 Relative viscosity of a 0.5 mM CT DNA solution upon addition of **5.1** (■), **5.4** (◄), **5.5** (▼), **5.6** (●), H33258 (●) and ethidium bromide (▲) at 25 °C in 25 mM MOPS pH 7.0, 50 mM NaCl, 1mM EDTA.

Compounds **5.1** and **5.5** cause a relatively small increase in viscosity, comparable with the effect of known minor-groove binder H33258. In combination with the docking study (and the well-known preference of flat aromatic molecules to bind in the minor groove rather than in the major groove), we interpret the minor increase in viscosity as indicative of predominant binding in the minor groove. However, compound **5.4** causes a significant increase in viscosity, comparable with ethidium bromide, indicating that **5.4** intercalates between the base pairs. In addition to a small decrease in viscosity at low DNA concentration, **5.6** shows a significant increase in viscosity suggesting intercalation of **5.6** between the base pairs of DNA. Circular dichroism spectra for **5.1-5.6** interacting with DNA show a negative induced circular dichroism spectrum for **5.4** and **5.6**, confirming intercalation as a binding mode. Positive and negative signals are found for **5.1** and **5.5**, suggesting complex binding modes involving minor groove binding and intercalation. Isothermal titration calorimetry confirms three binding modes for **5.1** binding to FS DNA, while **5.2** and **5.3** show only one binding mode. Precipitation was observed at the end of the titration of **5.1** with FS DNA, suggesting that DNA-ligand complexes stick together in solution.[5, 14] Dicationic quaterthiophene **5.5** also shows (at least) three binding modes. Compound **5.4** shows one binding event with thermodynamic binding parameters suggesting intercalation as a mode of binding. In contrast the binding of **5.6** to DNA occurs by intercalation between the base pairs, but the minor groove binding mode is not excluded.

Acknowledgements

Dr. Verónica González González is acknowledged for helpful discussions about DNA binders. Dr. Marina Cioffi is thanked for performing docking studies. Prof. Rudolf Allemann is thanked for access to circular dichroism equipment.

5.8 Materials and Methods

5.8.1 DNA preparation

All the compounds investigated in these chapters were synthesised as described in Chapter 3. All experiments were carried out in buffer (25 mM MOPS, 50mM NaCl and 1 mM EDTA) titrated with aqueous NaOH to pH 7.0. Buffer components were procured from Acros or Sigma-Aldrich. The pH of aqueous solutions was determined with a Hanna Instruments pH 210 pH meter equipped with a VWR 662-1759 glass electrode. Water was purified using an ELGA option-R 7BP water purifier. Fish sperm DNA was procured from Acros and calf thymus DNA was obtained from Sigma-Aldrich as a lyophilised solid sodium salt. Fish sperm DNA solutions were prepared by dissolution in buffer. Calf thymus DNA was suspended in the buffer and subjected to sonication for a total of 30 min. All DNA solutions were dialysed extensively against buffer using a 3.5 kDa MW cut-off dialysis membrane. DNA concentrations were determined spectrophotometrically using ε_{260nm} = 12800 $M(bp)^{-1}$ cm^{-1} for fish sperm DNA and ε_{260nm} = 12824 $M(bp)^{-1}$ cm^{-1} for calf thymus DNA[15]. Purity of DNA solutions was checked by UV-visible spectroscopy from the ratio $A_{260\ nm}$ / $A_{280\ nm}$, which was found to be 1.92 for calf thymus DNA and 1.89 for fish sperm DNA, suggesting that both solutions are essentially free of protein.

5.8.2 Spectroscopic studies

UV-visible spectra were recorded using a Jasco V-630Bio or Jasco V-650 UV-visible spectrophotometer coupled with a Peltier temperature controller at 25 °C. Circular dichroism spectra were recorded on a Chirascan CD Spectrophotometer.

Concentrated stock solutions of oligothiophenes **5.1-5.6** in buffer were freshly prepared and volumes of these stock solutions was added into 2500 µl of buffer as required in a 1.00 cm pathlength cuvette. The absorption in the range 0.6-0.9 a.u. was measured spectrophotometrically and the concentration was quantified using the extinction coefficients of **5.1-5.6** (See Appendix). UV-visible titrations were carried out by adding aliquots of a concentrated stock solution of DNA in buffer to the ligand solution in the cuvette (typically starting with 5 µl additions of DNA solution followed by 10 µl additions). UV-visible spectra in the range 200-600 nm were recorded after each addition of DNA. Absorptions at selected wavelengths as a function of DNA and DNA-binder concentrations were extracted from the UV-visible spectra and analysed globally in terms of a multiple independent binding sites model (Section 2.5.1) using Origin 7.5. For the construction of Job plots, stock solutions of ligand and DNA, each at a concentration of 1 mM in buffer were prepared. Different volumes of these solutions were mixed with buffer in such way that the molar fraction of the ligand varied from 1 to 0 at a total summed concentration [DNA] + [DNA binder] of 0.5 mM. The absorption of 300 µl of the resulting solution in a 1 mm pathlength cuvette was measured spectrophotometrically and the changes in the absorption were plotted against the molar fraction of the component.

5.8.3 Viscometry

Viscosity studies were carried out using a Cannon-Fenske routine viscometer placed in a temperature-controlled circulated water bath, maintained at 25 ± 0.3 °C. The viscometer was filled with 14 ml of a 0.5 mM solution of calf thymus DNA and small volumes of a concentrated stock solution of ligand were added. The flow time was measured several times after each addition and the results were averaged. The relative viscosity was calculated and plotted as a function of the ratio $[\text{DNA binder}]_{bound}$ / [DNA], where $[\text{DNA binder}]_{bound}$ was calculated using the binding parameters from UV-visible spectroscopy.

5.8.4 Isothermal titration calorimetry

All ligand solutions were prepared in buffer, pH 7.0 (25 mM MOPS, 50 mM NaCl and 1 mM EDTA) and concentrations were determined by UV-Vis spectroscopy, based on the extinction coefficients. Calorimetric binding experiments were carried out at 25 °C on a Microcal VP ITC microcalorimeter. The instrument was used in high-gain mode, applying a reference power of 10-15 μcal s^{-1} while stirring the sample cell contents at 307 rpm. Titrations were carried out using different concentrations of CT DNA or FS DNA (typically in the range of 1.0-4.0 mM). The sample cell was filled with a known volume (approximately 1.9 ml) of a solution containing FS DNA or CT DNA. For each experiment, the syringe was loaded with a concentrated ligand solution (usually 12 fold higher than the DNA concentration). This solution was added in 27 injections of 10 μl each into the sample cell, every 500 seconds, at 25 °C. Data were treated in Origin (Microcal, Inc) to calculate heat effects per injection (dh). These integrated heat effects were analysed using IC ITC.[5]

References

1. Jones, G.; Willett, P.; Glen, R. C.; Leach, A. R.; Taylor, R., *J. Mol. Biol.* **1997,** *267* (3), 727-748.
2. Woods, K. K.; Maehigashi, T.; Howerton, S. B.; Sines, C. C.; Tannenbaum, S.; Williams, L. D., *J. Am. Chem. Soc.* **2004,** *126* (47), 15330-15331.
3. Navarrete, J. T. L.; Casado, J.; Ramirez, F. J., *J. Mol. Struct.* **2007,** *834*, 176-181.
4. Garbett, N. C.; Ragazzon, P. A.; Chaires, J. B., *Nat. Protoc* **2007,** *2* (12), 3166-3172.
5. Buurma, N. J.; Haq, I., *J. Mol. Biol.* **2008,** *381* (3), 607-621.
6. Loontiens, F. G.; Regenfuss, P.; Zechel, A.; Dumortier, L.; Clegg, R. M., *Biochemistry* **1990,** *29* (38), 9029-9039.
7. Adhikary, A.; Buschmann, V.; Muller, C.; Sauer, M., *Nucleic Acids Res.* **2003,** *31* (8), 2178-2186.
8. Saito, M.; Kobayashi, M.; Iwabuchi, S. I.; Morita, Y.; Takamura, Y.; Tamiya, E., *J. Biochem.* **2004,** *136* (6), 813-823.
9. Kobayashi, M.; Takashi, K. B.; Saito, M.; Kaji, S.; Oomura, M.; Iwabuchi, S.; Morita, Y.; Hasan, Q.; Tamiya, E., *Electrochem. Commun.* **2004,** *6* (4), 337-343.
10. Chaires, J. B., *Arch. Biochem. Biophys.* **2006,** *453* (1), 26-31.
11. Dervan, P. B.; Edelson, B. S., *Curr Opin Chem Biol* **2003,** *13* (3), 284-299.
12. Heckel, A.; Dervan, P. B., *Chem.-Eur. J.* **2003,** *9* (14), 3353-3366.
13. Wheelhouse, R. T.; Garbett, N. C.; Buurma, N. J.; Chaires, J. B., *Angew. Chem. Int. Ed.* **2010,** *49* (18), 3207-3210.
14. Buurma, N. J.; Haq, I., *Methods* **2007,** *42* (2), 162-172.
15. Ren, J. S.; Chaires, J. B., *Biochemistry* **1999,** *38* (49), 16067-16075.

Chapter 6

EPILOGUE

Abstract: *Preliminary synthetic studies towards extended cationic oligoheteroaromatics; DNA binding studies of* ***6.10-6.11****; and structural selectivity studies of cationic oligothiophenes are presented. General conclusions on the development and use of conjugated oligoheteroaromatics as optoelectronically active DNA binders as well as outlook on future challenges finish the chapter.*

6.1 Introduction

In addition to the work described in previous chapters, several projects of more exploratory character were started. The preliminary results of these projects are presented here, together with general conclusions from the work and an outlook suggesting future work.

6.2 Preliminary synthetic studies

6.2.1 Extended quaterthiophene derivative 6.11 based on benzene and thiophene

A new extended conjugated cationic oligoheteroaromatic has been synthesised starting from the usual commercially available 3-(2-hydroxyethyl)thiophene. The 3-(2-hydroxyethyl) thiophene was protected and brominated with 1 eq. of NBS according to the procedure described in Section 3.2.1. Protected 2-bromo-3-(2-hydroxyethyl)thiophene was first coupled with phenylboronic acid by a Suzuki cross-coupling reaction then brominated with NBS to give bromide **6.4** (Scheme 6.2). Lithiation of **6.4** followed by quenching with 2-isopropoxy-4,4,5,5-tetramethyl-1,3,2-dioxo-borolane led to intermediate **6.5.**

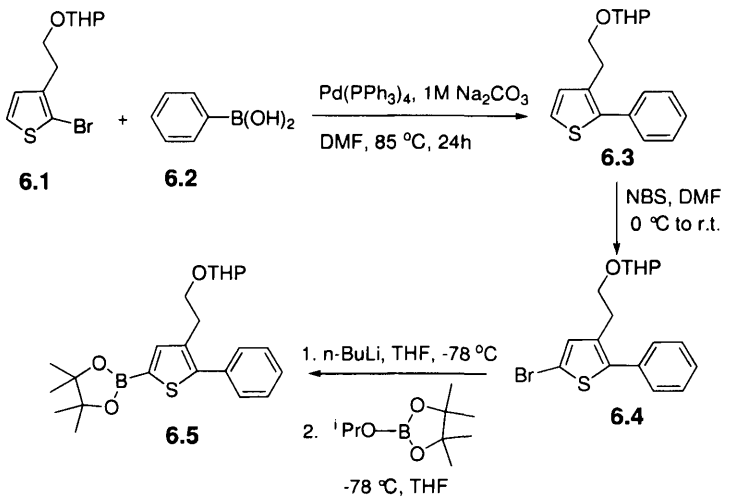

Scheme 6.1

Intermediate **6.5** was coupled with bromide **6.4** by a microwave-assisted Suzuki cross-coupling reaction to obtain quaterthiophene derivative **6.6** in 58% yield (Scheme 6.2). Future plans involve removing the THP protecting group of **6.6** by treatment with a solution of 0.2 M HCl and synthesis of ammonium salt **6.9** using procedures analogous to those used for monocationic terthiophene (Section 3.2.1).

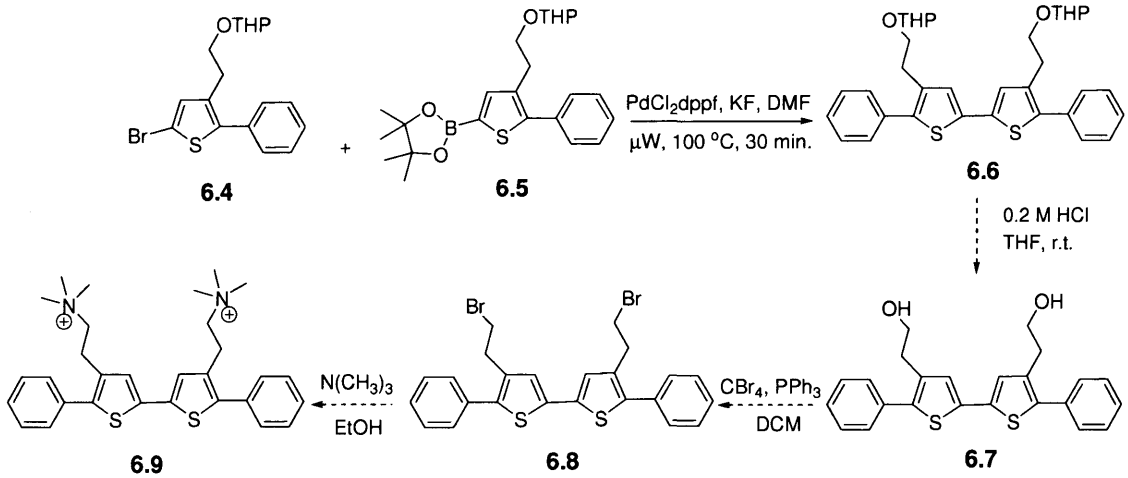

Scheme 6.2

6.3 Preliminary binding studies

The structures investigated in this Section are summarised in Scheme 6.3.

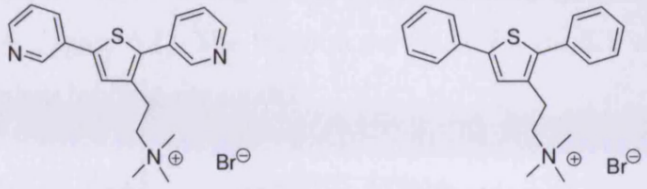

6.10 **6.11**

Scheme 6.3

6.3.1 Preliminary studies of pyridine derivative 6.10 binding to DNA

UV-Visible spectroscopy

The interactions of cationic terthiophene **6.10** with calf thymus DNA were studied by Uv-visible spectroscopy. We monitored changes in absorption of **6.10** upon addition of fish sperm DNA in 25 mM MOPS, 50 mM NaCl and 1 mM EDTA, at 25 °C (Figure 6.1).

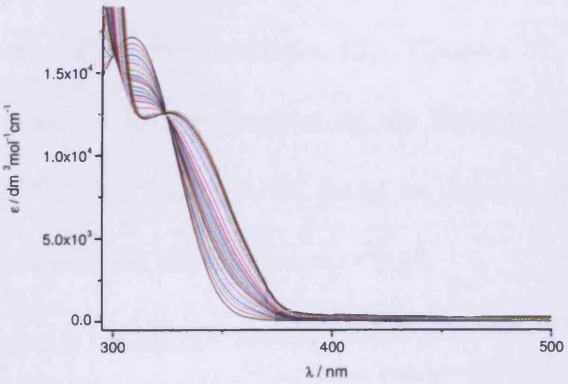

Figure 6.1 UV-visible spectra for 4.64×10^{-2} mM cationic pyridine derivative **5.10** upon addition of 0–4.46 mM fish sperm DNA in 25 mM MOPS, 50 mM NaCl and 1 mM EDTA, pH 7, at 25 °C.

Figure 5.29 shows that interaction of **6.10** with fish sperm DNA produces a bathochromic shift in the UV-Vis, indicating that **6.10** binds to DNA. In order to determine the binding constant and the stoichiometry, binding curves were extracted from the UV-visible titration of **6.10** with FS DNA (Figure 6.1). The titration curves in Figure 6.1 were analysed in terms of a multiple independent binding site model.

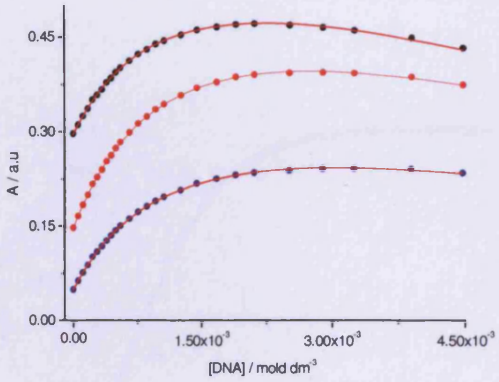

Figure **6.1** UV-visible titration of 4.64×10^{-2} mM solution of **6.10** with 0–4.46 mM fish sperm DNA in 25 mM MOPS, 50 mM NaCl and 1 mM EDTA, pH 7, at 25 °C. Absorbances at wavelengths 339 nm (●), 350 nm (●) and 360 nm (●) are plotted against DNA concentration and the solid lines represent a global fit to a multiple independent sites model.

The affinity of cationic pyridine derivative **6.10** for fish sperm DNA is smaller than the affinities observed for other oligoheteroaromatics (See Chapter 5). The binding constant is $(2.4\pm0.2)\text{x}10^3$ M^{-1} and it was calculated restricting the binding site size to 3 base pairs. This low affinity of **6.10** for fish sperm DNA could be caused by a high polarity of the pyridine ring and by protonation and deprotonation of **6.10.**

Isothermal titration calorimetry

To further investigate the binding of cationic pyridine derivative **6.10** with fish sperm DNA we used isothermal titration calorimetry (ITC). Figure 6.2 shows typical enthalpograms obtained by titrating **6.10** into fish sperm DNA, in 25 mM MOPS, 50 mM NaCl and 1 mM EDTA, pH 7.0, at 25 °C.

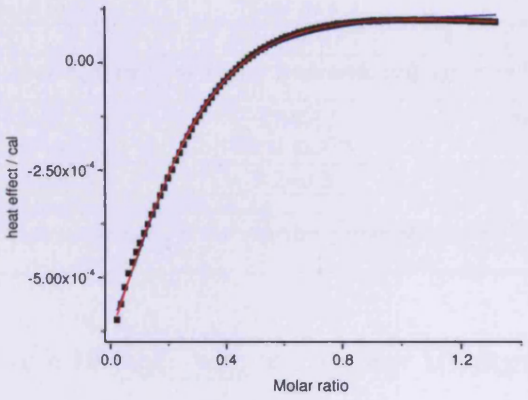

Figure 6.2 Integrated heat effects for titration of a 45.5 mM solution of **6.10** into 7.3 mM of FS DNA solution in 25 mM MOPS pH 7.0, 50 mM NaCl, 1mM EDTA, at 25 °C. The data is analysed using a binding model with isodesmic self-aggregation included (red line) and a binding model with aggregation not included (blue line).

Figure 6.2 shows one mode of binding for the interaction of **6.10** with FS DNA in 25 mM MOPS pH 7.0, 50 mM NaCl, 1mM EDTA, at 25 °C. The interaction of **6.10** with FS DNA indicates one binding event. First, ITC data was analysed using a model describing one binding event (Section 2.6) for which ligand self-aggregation was not taken into account. We also used a binding model which includes isodesmic self-aggregation of **6.10**. Figure 6.2 shows that the binding model including self-aggregation reproduces the calorimetric data for **6.10** binding to FS DNA better than the model without self-aggregation terms.

Differences between the fits are also apparent when comparing the values of $\{\Sigma dev^2/dof\}^{½}$ for the two analyses in Table 6.1. In this case the necessity to include ligand self-aggregation when studying the binding of π-conjugated molecules to DNA is clear.

Table 6.1 Thermodynamic parameters for interaction of **6.10** with FS-DNA, in MOPS buffer, pH 7.0 at **25 °C**

binding model not including aggregation[a]				
K_{A1} ($10^3 M^{-1}$)	ΔH_{A1} (kcal mol^{-1})	$-T\times\Delta S_{A1}$ (kcal mol^{-1})	$1/n_{A1}$	$\{\Sigma dev^2/dof\}^{½}$ (μcal)
1.4; (1.0; 2.1)[b]	-7.7; (-11.1; -6.0)[b]	3.4 (1.9-6.6)[b]	4.6; (1.5; 3.5)[b]	9.8
binding model including isodesmic self aggregation[a]				
K_{A1} ($10^3 M^{-1}$)	ΔH_{A1} (kcal mol^{-1})	$-T\times\Delta S_{A1}$ (kcal mol^{-1})	$1/n_{A1}$	$\{\Sigma dev^2/dof\}^{½}$ (μcal)
0.7±0.2	-12.0±0.5	8.2±0.3	4.1; (3.7; 5.2)	5.7

a) Parameter values restricted to best fit values as reported in Table 4.5
b) The reported range given within brackets corresponds to fits for which the normalised $\Sigma dev^2/dof < 2$ (See Appendix).
c) For error margins see Appendix

Cationic pyridine derivative **6.10** binds with much lower affinity to FS DNA compared to other oligoheteroaromatics, with a binding site size of 4 base pairs. The negative values of both enthalpy and entropy preliminarily suggest that **6.10** binds as an intercalator.

Summary

Preliminary Uv-Vis studies of interactions of cationic pyridine derivative **6.10** to FS DNA show that the affinity of **6.10** to FS DNA is low ($2.4\times10^3\ M^{-1}$). This value was calculated for a restricted binding site size of 3 base pairs using. ITC suggests intercalation as a binding mode.

6.3.2 *Preliminary studies of monocationic benzene derivative 6.11 binding to DNA*

UV-Vis spectroscopy

The binding of cationic benzene-thiophene derivative **6.11** with fish sperm DNA was monitored by UV-visible spectroscopy, in the concentration range where self-aggregation of **6.11** is negligible. Changes in absorption of **6.11** were recorded upon addition of fish sperm DNA in 25 mM MOPS, 50 mM NaCl and 1 mM EDTA, at 25 °C (Figure 6.3).

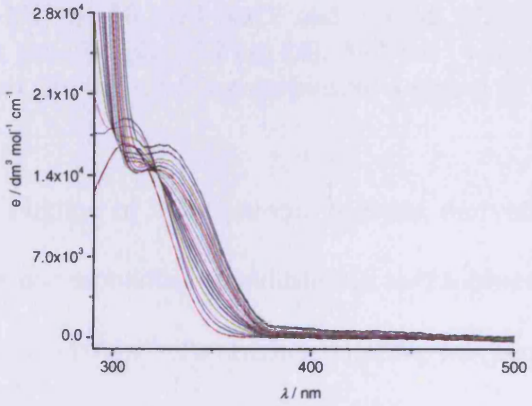

Figure 6.3 UV-visible spectra for 2.88×10^{-2} mM cationic benzene derivative **6.11** upon addition of 0–1.75 mM fish sperm DNA in 25 mM MOPS, 50 mM NaCl and 1 mM EDTA, pH 7, at 25 °C.

Figure 6.3 shows that interaction of **6.11** with DNA produces a red-shift in the absorption of **6.11**. We attribute the red-shift to changes in effective conjugation length of the ligand. In order to determine the binding constant and stoichiometry of interaction, titration curves are extracted from the data in Figure 6.3 and analysed in terms of a multiple independent binding sites model (Figure 6.4).

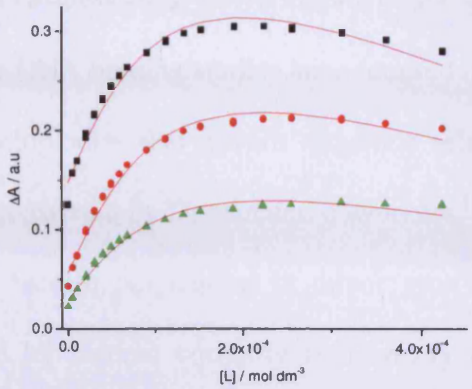

Figure 6.4 UV-visible titration of 2.88×10^{-2} mM solution of **6.11** with 0–1.75 mM fish sperm DNA in 25 mM MOPS, 50 mM NaCl and 1 mM EDTA, pH 7, at 25 °C (black symbols). Absorbances at wavelengths 339 nm (■), 350 nm (●) and 360 (▲) nm are plotted against DNA concentration and the solid lines represent a global fit to a multiple independent sites model.

Data analysis shows that binding of monocationic benzene derivative **6.11** with FS DNA is stronger compared to the corresponding monocationic terthiophenes, with an equilibrium / binding constant of $(5.1\pm1.5)\times10^4$ M^{-1}. To obtain a good fit, we restricted the binding site size to 3 base pairs. Changes in the ligand geometry as a result of introducing two benzene rings, a flat surface together with an increase in the hydrophobicity probably contribute towards this higher affinity to DNA.

Summary

Preliminary investigations using UV-Vis spectroscopy reveal that benzene derivative **6.10** binds to FS DNA.

6.4 Competition dialyses of cationic conjugated oligoheteroaromatics

In the last two decades, drug-DNA binding studies have focused mainly on characterisation of sequence selectivity to develop rules that govern sequence selectivity of drugs binding to DNA. This was already demonstrated by Dervan and coworkers,[1, 2] who developed the recognition code for binding of hairpin polyamides in minor groove of DNA (Section 1.4.3). The set of rules developed by Dervan currently finds many applications allowing small molecules to be designed to selectively target sequences that control the expression of particular genes. To explore the sequence and structural selectivities of cationic oligothiophenes in Scheme 6.3 competition dialysis[3] was employed for different polynucleotide sequences.

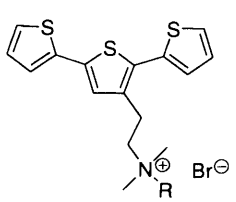

6.12

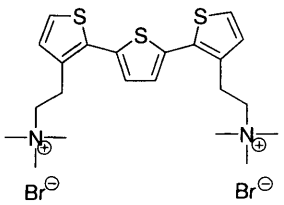

6. 13

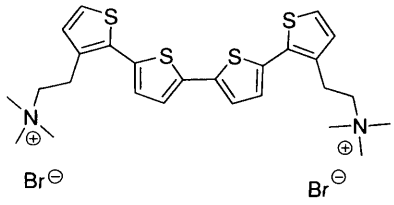

6. 14

Scheme 6.3

Different nucleic acid sequences in separate containers were dialysed against a common ligand solution. When the solution reached equilibrium, the amount of ligand bound to each sequence was measured using either fluorescence or UV-visible spectroscopy. First, competition dialysis tests were performed for monocationic terthiophene **6.12** with single-stranded, duplex, triplex and quadruplex forming nucleic acid targets in KPEK buffer

pH 7.0 (2 mM KH_2PO_4, 6 mM K_2HPO_4, 1 mM EDTA, 185 mM KCl, for a total K^+ concentration of 199 mM) (Figure 6.5).

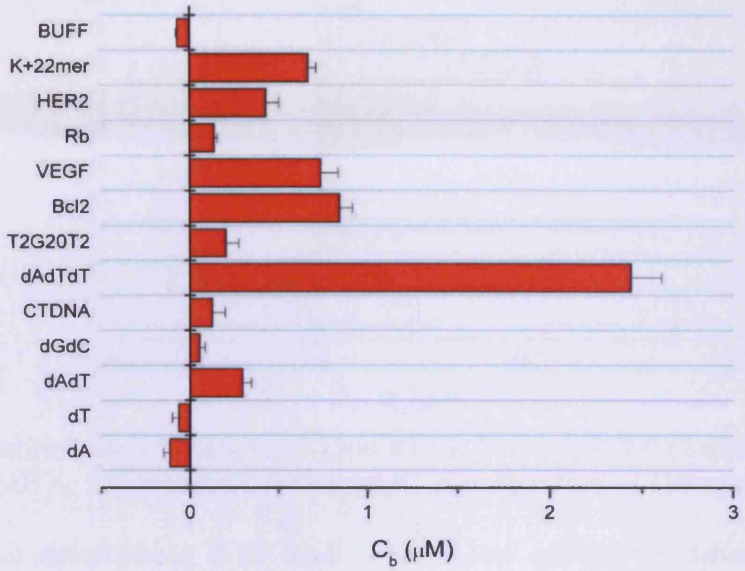

Figure 6.5 Competition dialysis data for **6.12** in KPEK buffer pH 7.0 (2 mM KH_2PO_4, 6 mM K_2HPO_4, 1 mM EDTA, 185 mM KCl, for a total K^+ concentration of 199 mM).

Surprisingly, Figure 6.5 shows that monocationic terthiophene **6.12** binds preferentially to AT-rich triplex DNA structures. A preference for A·T base pairs is also observed for cationic terthiophene **6.12** interacting with duplex DNA. The competition dialysis assay shows no appreciable binding to single-stranded DNA. This is in perfect agreement with the results from our UV-visible titration for **6.12** interacting with polydA (Section 5.2). Cationic terthiophene **6.12** also display binding to quadruplex DNA with preferences for human Bcl2 promoter sequence and VEGF (a promoter sequence of tumour angiogenesis).

Similarly, the selectivity of dicationic terthiophene **6.13** binding towards different sequences of nucleic acids was investigated in KPEK buffer pH 7.0 (Figure 6.6).

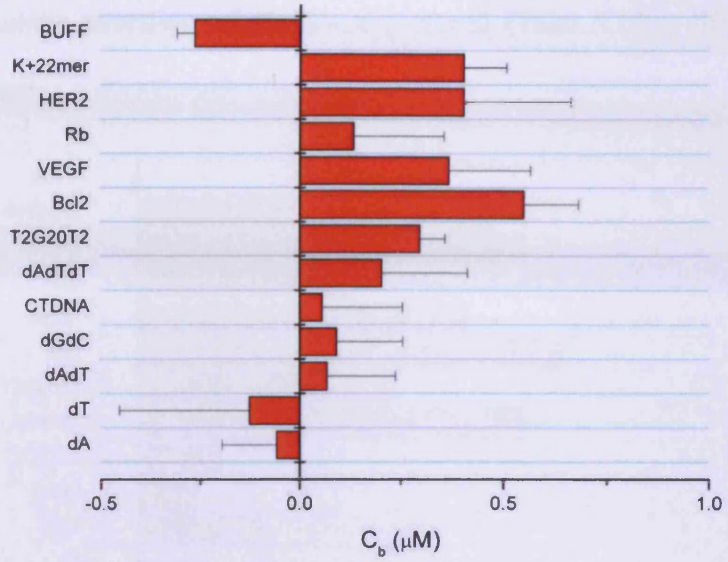

Figure 6.6 Competition dialysis data for **6.13** in KPEK buffer, pH 7.0 (2 mM KH_2PO_4, 6 mM K_2HPO_4, 1 mM EDTA, 185 mM KCl, for a total K^+ concentration of 199 mM).

Overall, dicationic terthiophene **6.13** binds with a low affinity to different nucleotides. This finding contradicts the results obtained in Section 5.3, in which it showed the highest affinity for ds-DNA out of the series of oligioheteroaromatics **6.12–6.14**. We attribute the discrepancy to the hypothesis that the binding affinity is strongly dependent on salt concentration, especially given that terthiophene **6.13** has two charges while **6.12** carries only one.

Dicationic terthiophene **6.13** shows some preferences for G·C base pairs and over A·T base pairs. This is strongly supported by a low affinity to both the dAdTdT triplex DNA and to the dAdT duplex DNA. This finding is also promising as intercalation tends to be strongest in G·C base pairs, while minor groove binding is often stronger at A·T rich sequences. The preference for polydGdC over polydAdT, therefore, appears to confirm our earlier conclusions that **6.13** is an intercalator.

We also investigated the selectivity of dicationic quaterthiophene **6.14** to different nucleotides sequences (Figure 6.7).

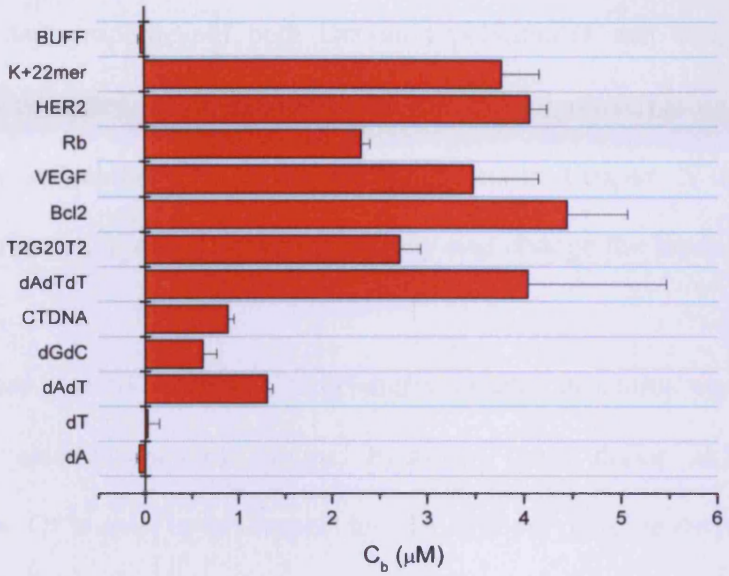

Figure 6.7 Competition dialysis data for **6.14** in KPEK buffer, pH 7.0 (2 mM KH_2PO_4, 6 mM K_2HPO_4, 1 mM EDTA, 185 mM KCl, for a total K^+ concentration of 199 mM).

Figure 6.7 clearly shows a high preference of dicationic quaterthiophene **6.14** for G-quadruplex and triplex DNA. In the series of oligothiophenes, dicationic quaterthiophene **6.13** shows higher affinity for triplex and G-quadruplex DNA than **6.12** and **6.13**. Dicationic quaterthiophene **6.14** also binds with preference to AT base pairs. There was no appreciable binding to single-stranded DNA.

6.5 Conclusions and Outlook

The question underlying the work described in this thesis is whether we can design molecules those posses the best properties of both Dervan's polyamides and conjugated polymers. The present thesis describes a first generation of cationic oligoheteroaromatics that address both opportunities and challenges. It was demonstrated in Chapter 5 of this thesis that variation of ligand structure can improve the affinity and change the mode of binding to ds-DNA.

In view of this, we plan to synthesise oligoheteroaromatic structures containing electron-withdrawing and electron-donating groups; hydrogen bond donor and acceptors; and solubilising groups. Of interest in this respect are our cationic pyridine derivatives binding to ds-DNA. In addition to the 3-pyridine isomer we will synthesise other pyridine derivatives (*e.g.* 2- and 4-pyridines). The affinity and binding mode of these compounds to ds-DNA will be compared and studied at different pH conditions. Because fluorinated organic molecules in medicinal chemistry are well known as antiviral and antitumor agents, the effects of fluorine substituents on DNA binding are also of interest.

Based on our results for cationic oligoheteroaromatics interacting with ds-DNA, extending the conjugation along the oligoheteroaromatic chain is expected to increase the affinity of our binders for ds-DNA, selectively targeting the minor groove. Longer substituted oligoheteroaromatics will provide new thermodynamic data on the importance of electron-richness of minor groove binders and on the effects of hydrogen bonding. The affinity of cationic oligoheteroaromatics for ds-DNA seems indicates their suitability for use as building blocks for sequence-selective cationic conjugated polymers.

Identifying building blocks with high selectivity for short DNA sequences should allow the construction of polyheteroaromatics for the recognition of longer DNA sequences with high affinity.

Chapter 6 offers evidence that cationic oligoheteroaromatics involving conjugated systems and a variety of mixed heteroaromatics are required in order to obtain some sequence recognition of DNA. Regarding the sequence selectivity for ds-DNA, it appears that **6.12** and **6.14** prefer A·T base pairs, while **6.13** shows specificity towards G·C base pairs. Binding experiments performed with homogeneous DNA such as polydA·polydT or polydGpolydC could help to establish binding modes more clearly for specific DNA sequences.

Interestingly, competition dialysis studies showed that cationic conjugated oligothiophenes **6.12–6.14** prefer higher-order DNA structures (*e.g.* triplex and G-quadruplex DNA) over double-stranded DNA. Additional studies on selectivity of these oligothiophenes for higher order DNA structures will be very interesting.

Regarding the self aggregation of conjugated oligoheteroaromatics in aqueous solution, efforts will be made to determine the aggregation number and the thermodynamic parameters of self aggregation. As an alternative, structural variation and introduction of supplementary cationic charges will facilitate the solubility, avoiding self aggregation.

Acknowledgements

Prof. Brad Chaires and Nichola Garbett (University of Louisville, US) are thanked for competition dialysis experiments.

6.6 Experimental

6.6.1 Synthesis

2-phenyl-3-[2-(tetrahydropyranyloxy)ethyl] thiophene **6.3**

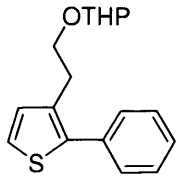

A mixture of protected 2-bromo-3-(2-hydroxyethyl)thiophene (2.5 g, 8.5 mmol) and phenylboronic acid (2.2 g, 12.7 mmol) in DMF (20 ml) was degassed (freeze-pump-thaw, 3 cycles) and 1 mol % $Pd(PPh_3)_4$ was added to the reaction mixture, under N_2 atmosphere. The mixture was then stirred at 85 °C for 24h, in the dark. The reaction was cooled to room temperature, quenched with water (100 ml) and extracted with dichloromethane (3 × 100ml). The combined organic layers were dried over $MgSO_4$, concentrated under reduced pressure. The residue was purified by flash column chromatography eluting with petrol: diethyl ether (8:2) to give **6.3** in 70% yield.

^{1}H-NMR (500 MHz, CH_3Cl): δ(ppm): 7.41 (d, 2H, J=8.2, *o*-C_6H_5), 7.32 (t, 2H, J=7.6, m-C_6H_5), 7.25 (t, 1H, J=6.0, p-C_6H_5), 7.15 (t, J=5.8, 1H, -SCH**CH**), 6.97 (d,J=5.3, 1H, -S**CH**CH) 4.50 (t, 1H, J=3.6, O-CH-O), 3.85 (m, 1H, Th-CH_2-CH_a**H_b**), 3.67 (m, 1H, CH-$(CH_2)_3$-CH_a**H_b**), 3.51 (m, 1H, Th-CH_2-**CH_a**H_b), 3.40 (m, 2H, CH-$(CH_2)_3$-**CH_a**H_b), 2.82 (t, 2H, J=6.8, -CH_2Th), 1.62 (m, $1H_{THP}$), 1.73(m, $1H_{THP}$), 1.48 (m, $4H_{THP}$). **^{13}C-NMR (126 MHz, CH_3Cl): δ(ppm):** 139.10, 134.31, 134.09, 129.54, 129.34, 128.6, 127.62, 125.79, 124.26, 97.5, 66.0, 60.9, 29.3, 28.0 24.4, 18.1 ES-HRMS calcd for [$C_{17}H_{20}O_2S$] 288.1180, found 288.1184

5-bromo-2-phenyl-3-[2-(tetrahydropyranyloxy)ethyl] thiophene **6.4**

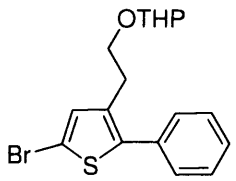

A solution of *N*-bromosuccinimide (0.6 g, 3.5 mmol) in DMF (10 ml) was added dropwise over 20 min. to a solution of **6.3** (1 g, 3.4 mmol) in DMF at 0 °C. The mixture was stirred for 30 min. at 0 °C then for 2 days at room temperature in the dark. The reaction mixture was poured into Na_2CO_3 (aq.) (150 ml) and extracted with ether (3 × 50mL). The combined organic layers were washed with water (3 × 100mL), dried over $MgSO_4$ and concentrated under reduced pressure. The residue was purified by flash column chromatography eluting with hexane / diethyl ether (8:2) to give **6.4** in 81 % yield.

^{1}H-NMR (500 MHz, CH_3Cl): δ(ppm): 7.23-7.41 (m, 5H, *o,p,m*-C_6H_5), 76.94 (s, $1H_{Th}$), 4.50 (t, 1H, J=3.6, O-CH-O), 3.85 (m, 1H, Th-CH_2-$CH_a\mathbf{H_b}$), 3.67 (m, 1H, CH-$(CH_2)_3$-$CH_a\mathbf{H_b}$), 3.51 (m, 1H, Th-CH_2-$C\mathbf{H_a}H_b$), 3.40 (m, 2H, CH-$(CH_2)_3$-$C\mathbf{H_a}H_b$), 2.82 (t, 2H, J=6.8, -CH_2Th), 1.62 (m, $1H_{THP}$), 1.73(m, $1H_{THP}$), 1.48 (m, $4H_{THP}$). **^{13}C-NMR (126 MHz, CH_3Cl): δ(ppm):** ES-HRMS calcd for [$C_{17}H_{19}BrO_2S$] 366.0289, found 366.0291

Borolane intermediate **6.5**

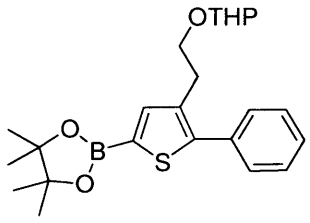

In a 25 mL round bottom flask were added 0.5 g (1.4 mmol) of bromide **6.4** dissolved in 10 mL dry THF. 2 eq. of ^{n}BuLi (1.0 ml, 1.5 mmol) were added drop wise to the solution at -78 °C. After stirring for 2 hours, 2 eq. of 2-isopropoxy-4,4,5,5-tetramethyl-1,3,2-dioxo-borolane

(0.6 ml, 2.8 mmol) was added at -78 °C by syringe. The reaction mixture was stirred at this temperature for additional 1 hour and then it was gradually warmed to RT and stirred overnight. The mixture was washed with an aqueous $NaHCO_3$ solution (50 mL) and the aqueous layer was extracted with Et_2O (2 × 50 mL). The combined THF and Et_2O were washed with 50 ml saturated NaCl solution and dried with $MgSO_4$ and the solvent were evaporated under reduced pressure to give light yellow oil. The residue was purified by flash column chromatography eluting with hexane:diethyl ether (8:2) to give borolane **6.5** in 69% yield.

^{1}H-NMR (500 MHz, CH_3Cl): δ(ppm): 7.39-7.47 (m, 4H, *o*-C_6H_5), 7.31-7.38 (m, 4H, *m*C_6H_5), 7.22-7.29 (m, 2H, *p*C_6H_5), 7.06 (s, 2H_{Th}), 4.58 (t, 2H, J=3.4, O-CH-O), 3.91 (m, 2H, Th-CH_2-CH_a**H_b**), 3.71 (m, 2H, CH-$(CH_2)_3$-CH_a**H_b**), 3.57 (m, 2H, Th-CH_2-**CH_a**H_b), 3.40 (m, 2H, CH-$(CH_2)_3$-**CH_a**H_b), 2.88 (t, 4H, J=6.9, -CH_2Th), 1.62 (m, 2H_{THP}), 1.73(m, 2H_{THP}), 1.48 (m, 8H_{THP}). **^{13}C-NMR (126 MHz, CH_3Cl): δ(ppm):** 137.0, 136.9, 134.9, 134.3, 134.0, 133.1, 128.9, 127.8, 126.3, 125.5, 97.5, 66.0, 60.9, 29.3, 28.0 24.4, 18.1. ES-HRMS calcd for [$C_{23}H_{31}BO_4S_2$] 415.2114 found 414.2134

Protected quaterthiophene derivative **6.6**

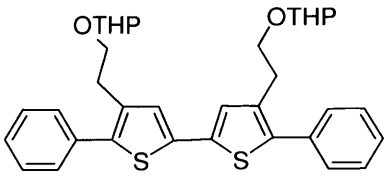

A mixture of **6.4** (5.7×10^{-2} g, 1.5×10^{-1} mmol) and **6.5** (7.7×10^{-2} g, 1.8×10^{-1} mmol) in DMF (7 ml) was degassed (freeze-pump-thaw, 3 cycles), KF (2.5×10^{-2} g, 4.5×10^{-1} mmol) and a catalytic amount of $PdCl_2$(dppdf) was added to the reaction mixture, under N_2 atmosphere, in a glove bag. The mixture was then irradiated at 80 °C for 10min at a fixed power (100 W). The reaction mixture was cooled to room temperature and concentrated by reduced pressure.

The residue was purified by flash column chromatography eluting with hexane : diethyl ether (7:3) to give **6.7** in 58% yield.

^{1}H-NMR (500 MHz, CH_3Cl): δ(ppm): 7.39-7.47 (m, 4H, *o*-C_6H_5), 7.31-7.38 (m, 4H, *m*C_6H_5), 7.22-7.29 (m, 2H, *p*C_6H_5), 7.06 (s, $2H_{Th}$), 4.58 (t, 2H, J=3.4, O-CH-O), 3.91 (m, 2H, Th-CH_2-$CH_a\mathbf{H_b}$), 3.71 (m, 2H, CH-$(CH_2)_3$-$CH_a\mathbf{H_b}$), 3.57 (m, 2H, Th-CH_2-$\mathbf{CH_a}H_b$), 3.40 (m, 2H, CH-$(CH_2)_3$-$\mathbf{CH_a}H_b$), 2.88 (t, 4H, J=6.9, -CH_2Th), 1.62 (m, $2H_{THP}$), 1.73(m, $2H_{THP}$), 1.48 (m, $8H_{THP}$). **^{13}C-NMR (126 MHz, CH_3Cl): δ(ppm):** 137.0, 136.9, 134.9, 134.3, 134.0, 133.1, 128.9, 127.8, 126.3, 125.5, 97.5, 66.0, 60.9, 29.3, 28.0 24.4, 18.1. ES-HRMS calcd for [$C_{34}H_{38}O_4S_2$] 574.2212 found 574.2220

6.4.2 Binding studies

Binding assays were performed following similar protocols as in Section 5.9.

References

1. Poulin-Kerstien, A. T.; Dervan, P. B., *J. Am. Chem. Soc.* **2003,** *125* (51), 15811-15821.
2. Heckel, A.; Dervan, P. B., *Chem.-Eur. J.* **2003,** *9* (14), 3353-3366.
3. Holt, P. A.; Ragazzon, P.; Strekowski, L.; Chaires, J. B.; Trent, J. O., *Nucleic Acids Res.* **2009,** *37* (4), 1280-1287.

A1 Dicationic terthiophene 4.11

1.1 Extinction coefficient

A stock solution of **4.11** (43.0 mM) in water was prepared. A total volume of 9 μl of this solution was added in two aliquots to 2500 μl of buffer in a 1.00 cm pathlength cuvette (○). A further 4.5 μl of the same stock solution was added in three aliquots to 2500 μl buffer in a 1.00 cm cuvette (■). In a 1.00 mm pathlength cuvette containing 300 μl buffer, a total volume of 6.0 μl of the stock solution in water was added in four aliquots (□). Ligand absorbance at λ_{max} 327 nm was plotted against ligand concentration and a linear fit (black line) was applied to obtain the extinction coefficient of (18.8±0.2) × 10^3 dm^3 mol^{-1} cm^{-1} (Figure A11).

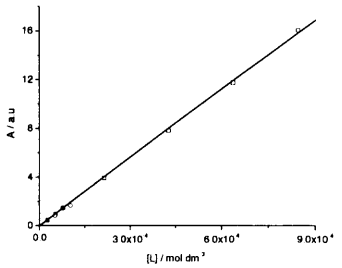

Figure A1 Absorbance for **4.11** as a function of concentration

1.2 Normalised Σdev²/dof for dilution parameters of 4.11

*Dilution of 43.0 mM solution of **4.11** in H_2O, at 25 °C*

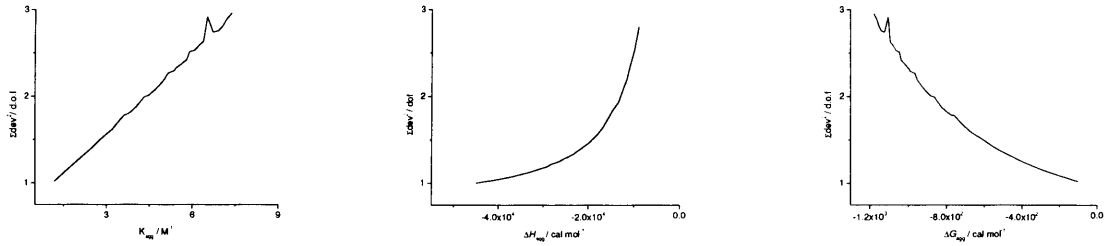

Figure A2 Normalised Σdev²/dof for dilution parameters. Error margins are calculated from the fitting to stepwise self aggregation model.

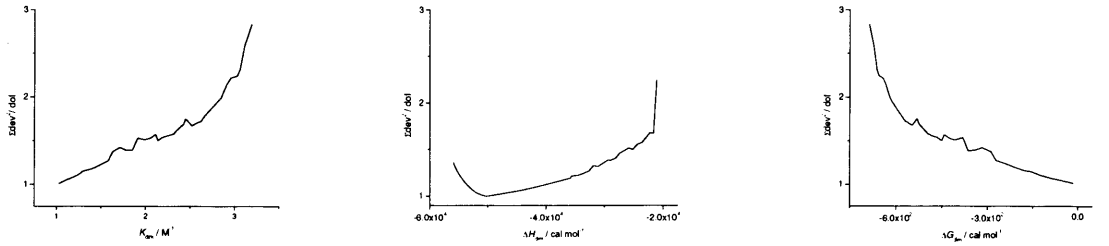

Figure A3 Normalised Σdev²/dof for dilution parameters. Error margins are calculated from the fitting to dimerisation model.

Dilution of 23.6 mM solution of ***4.11*** *in MOPS buffer, pH 7.0, , at 25 °C*

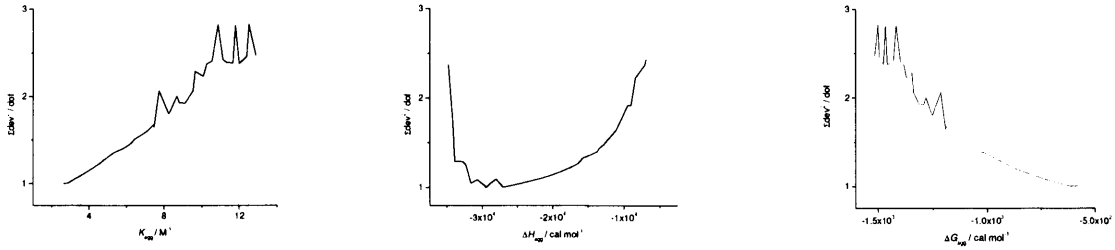

Figure A4 Normalised $\Sigma dev^2/dof$ for dilution parameters. Error margins are calculated from the fitting to stepwise self aggregation model.

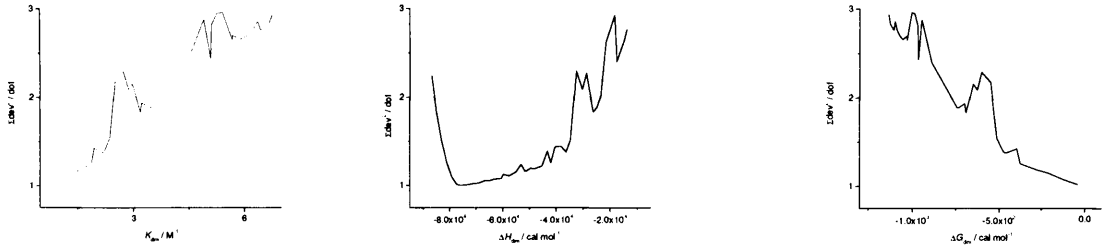

Figure A5 Normalised $\Sigma dev^2/dof$ for dilution parameters. Error margins are calculated from the fitting to stepwise self aggregation model.

A2 Monocationic thiophene-furan-thiophene derivative

Dilution of 15.3 mM solution of ***4.12*** *in H_2O, at 10 °C*

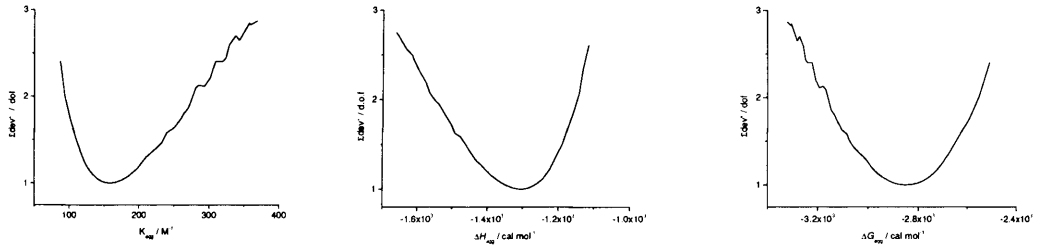

Figure A6 Normalised $\Sigma dev^2/dof$ for dilution parameters. Error margins are calculated from the fitting to stepwise self aggregation model.

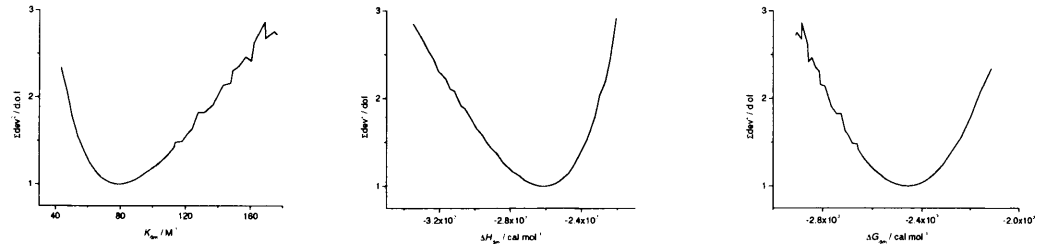

Figure A7 Normalised $\Sigma dev^2/dof$ for dilution parameters. Error margins are calculated from the fitting to dimerisation model.

Dilution of 26.8mM *solution of* ***4.12*** *in MOPS buffer, at 25 °C*

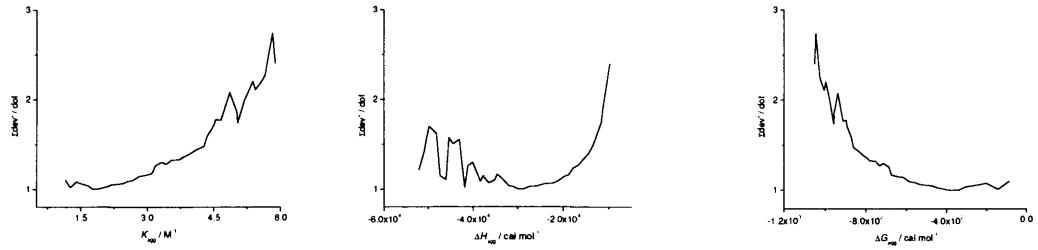

Figure A8 Normalised $\Sigma dev^2/dof$ for dilution parameters. Error margins are calculated from the fitting to stepwise self aggregation model.

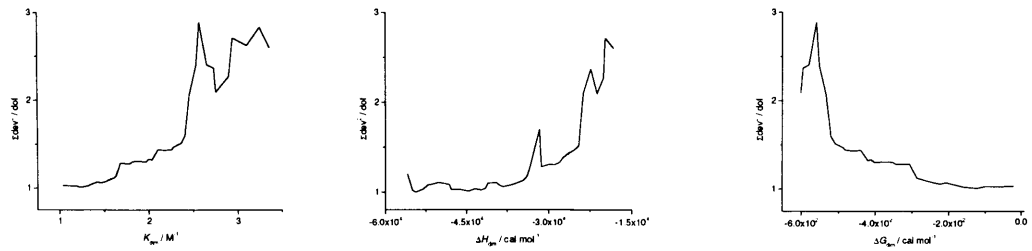

Figure A9 Normalised $\Sigma dev^2/dof$ for dilution parameters. Error margins are calculated from the fitting to dimerisation model.

Dilution of 13.8 mM solution of ***4.12*** *in* D_2O*, at 25 °C*

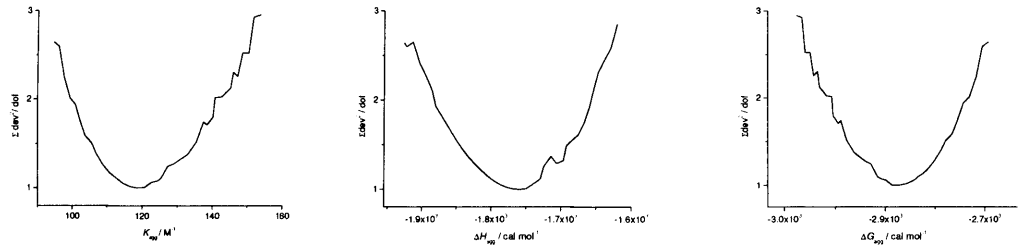

Figure A10 Normalised $\Sigma dev^2/dof$ for dilution parameters. Error margins are calculated from the fitting to stepwise self aggregation model.

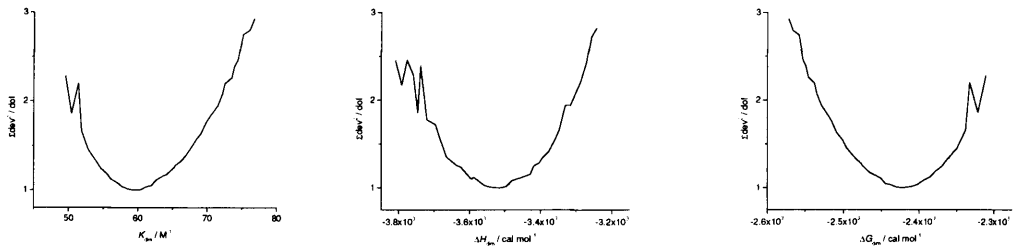

Figure A11 Normalised $\Sigma dev^2/dof$ for dilution parameters. Error margins are calculated from the fitting to dimerisation model.

Dilution of 32.2 mM solution of ***4.12*** *in D_2O, at 25 °C*

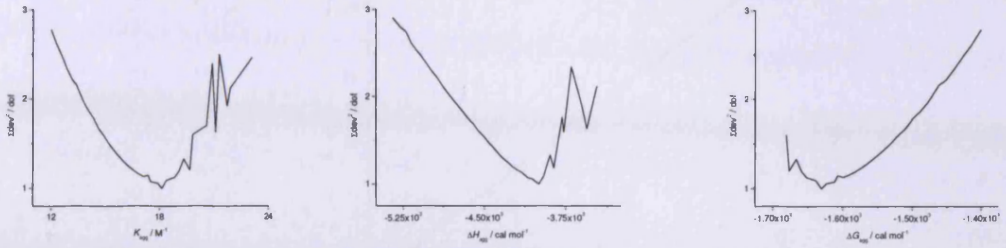

Figure A12 Normalised $\Sigma dev^2/dof$ for dilution parameters. Error margins are calculated from the fitting to stepwise self aggregation model.

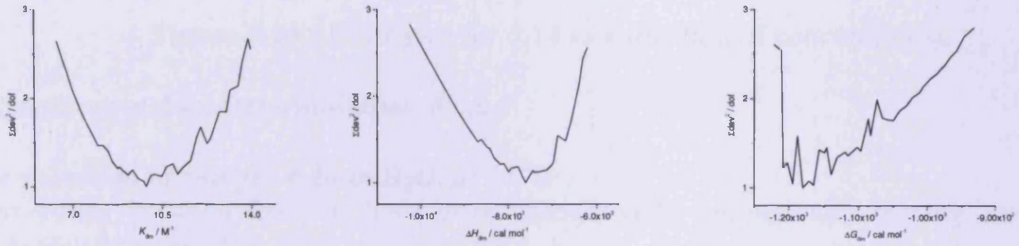

Figure A13 Normalised $\Sigma dev^2/dof$ for dilution parameters. Error margins are calculated from the fitting to dimerisation model.

A3. Monocationic terthiophene 4.14

3.1 Extinction coefficient

A total volume of 23 µl of a solution of **4.14** in buffer (16.69 mM) was added in five steps to 2500 µl of buffer in a 1.00 cm pathlength cuvette (●). A further 15µl of the same stock solution of **4.14** was added in three aliquots to 250 µl of buffer in a 1.00 mm pathlength cuvette (■). A second solution of **4.14** in water (10.2 mM) was prepared separately and 20 µl of this solution was added in three aliquots to 2500 µl of water in a 1.00 cm pathlength cuvette (○). In a 2.00 mm pathlength cuvette containing 600 µl of water, a total volume of 14 µl of the same stock solution in water was added in four aliquots (□). Ligand absorbance at λ_{max} 339 nm was plotted against ligand concentration and a linear fit (black line) was applied to obtain an extinction coefficient of (17.8±0.2) × 10^3 dm^3 mol^{-1} cm^{-1} (Figure A1).

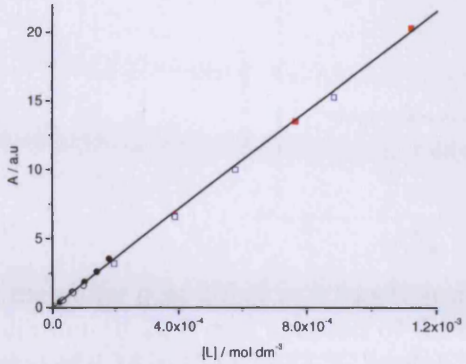

Figure A14 Absorbance for **4.14** as a function of concentration.

3.2 Surface tension. Determination of cmc

Determination of cmc for 4.14 in H_2O, at 25 °C

Intersections between the two lines were calculated by numerically solving the quadratic equations (Equation A1).

$$3.36x^2 - 19.88x + 74.4 = -0.96x + 51.25 \qquad \text{(A1)}$$

Equation A1 gives two solutions: x_1=1.81 and x_2=3.80, respectively.

The solution x_2=3.80 corresponding to the intersection point in the graphical representation was chosen and used to evaluate the exponential.

Determination of cmc for 4.14 in MOPS buffer, pH 7.0, at 25 °C

Similarly, solving equation A2, we also found two solutions (x_1= -9.95 and x_2=1.2). The solution x_2=1.2 was chosen to evaluate the exponential.

$$-0.74x^2 - 7.57x + 59.02 = -1.01x + 50.07 \qquad \text{(A2)}$$

3.3 Isothermal titration calorimetry. Critical micelle concentration

Figure A15 Derivative of the molar heat effect as a function of ligand concentration in the calorimeter cell for dilution of 20.85 mM solution of **4.14** into D_2O (left) and 41.7 mM solution of **4.14** into H_2O (right), at 25°**C.**

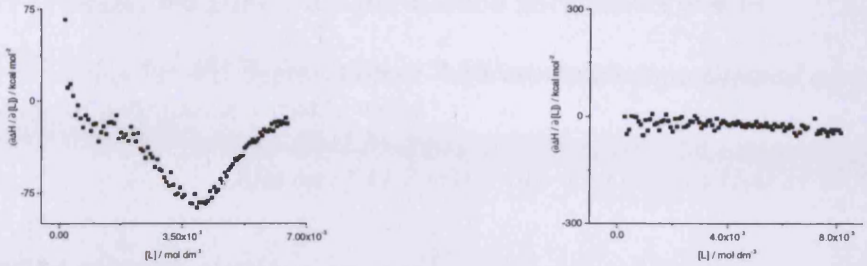

Figure A16 Derivative of the molar heat effect as a function of ligand concentration in the calorimeter cell for dilution of 22.3 mM solution of **4.14** into MOPS buffer at 40 °C (left), 41.7 mM solution of **4.14** in H_2O, at 37 °C (right).

3.4 Fits to n-merisation and Kegeles' model for 4.14 in MOPS buffer, 25 °C

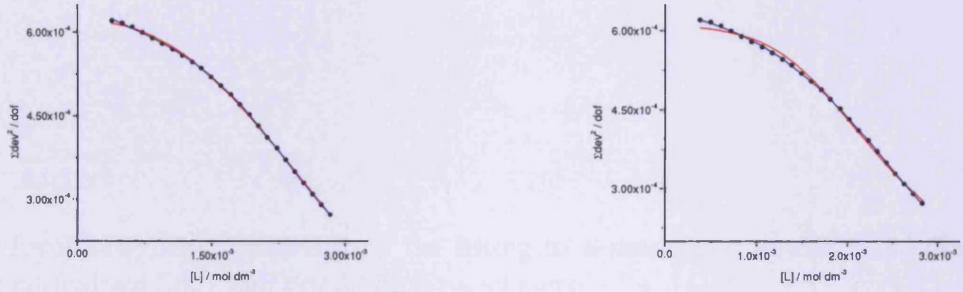

a **b**

Figure A17 Fits of the heat of dilution of 17.1 mM solution of **4.14** in MOPS buffer, at 25°C for: a) n-merisation model (red line), n-merisation model including stepwise self aggregation (blue line); b) Kegeles' model, f_{keg} fixed at 0.01 (red line), Kegeles' model, f_{keg} variable.

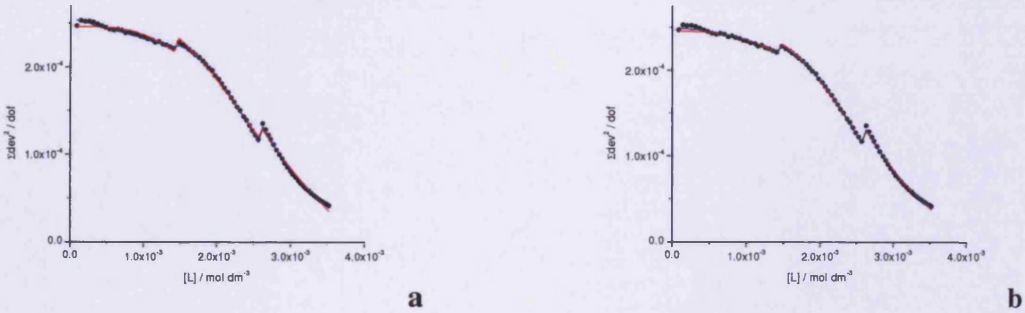

a **b**

Figure A18 Fits of the heat of dilution of 8.6 mM solution of **4.14** in MOPS buffer, at 25°C: a) n-merisation (red line), n-merisation model with self aggregation included (blue line); b) Kegeles' model, *f* fixed at 0.01; d) Kegeles' model, *f*-variable.

3.5 Normalised Σdev^2 / dof for dilution parameters of 4.14

Error margins for self aggregation of **4.14** estimated from plots of normalised $\Sigma dev^2/dof$ as a function of optimisable variable value.

Dilution of 41.7 mM solution of 4.14 in H_2O at 25°C

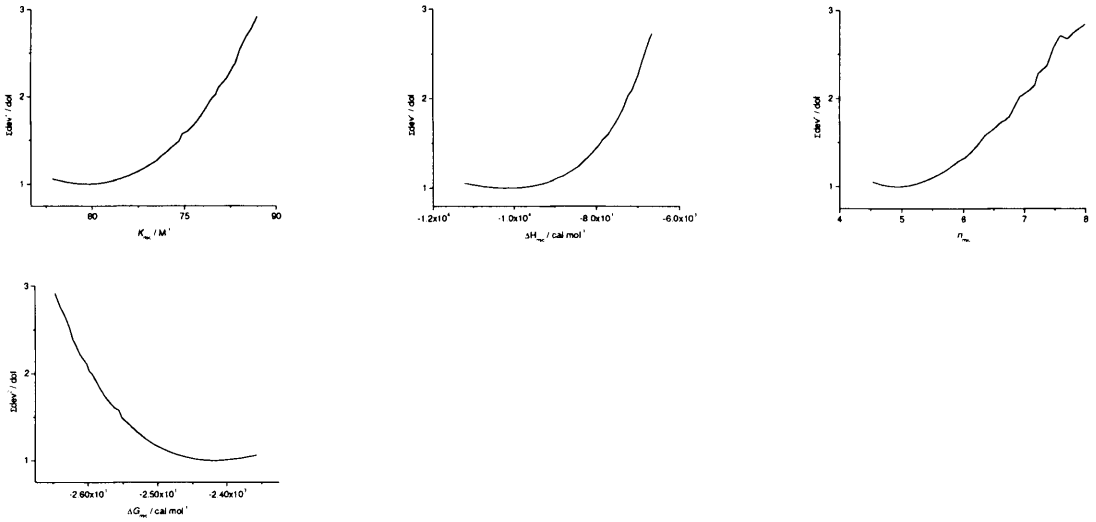

Figure A19 Error margins calculated from the fitting to n-merisation model. Black lines represent the normalised $\Sigma dev^2/dof$ for dilution parameters.

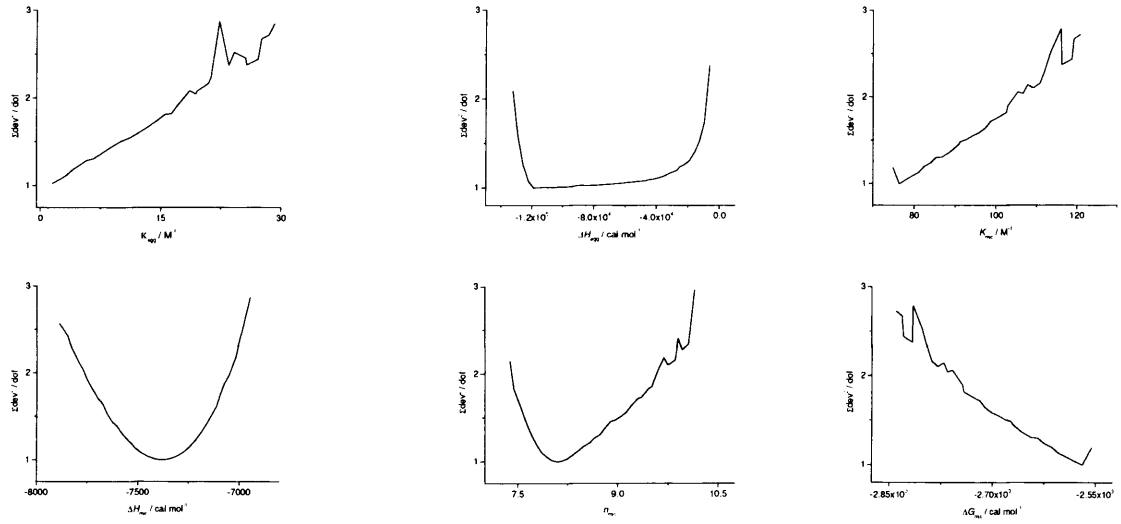

Figure A20 Error margins calculated from the fitting to n-merisation and stepwise self aggregation models. Black lines represent the normalised $\Sigma dev^2/dof$ for dilution parameters.

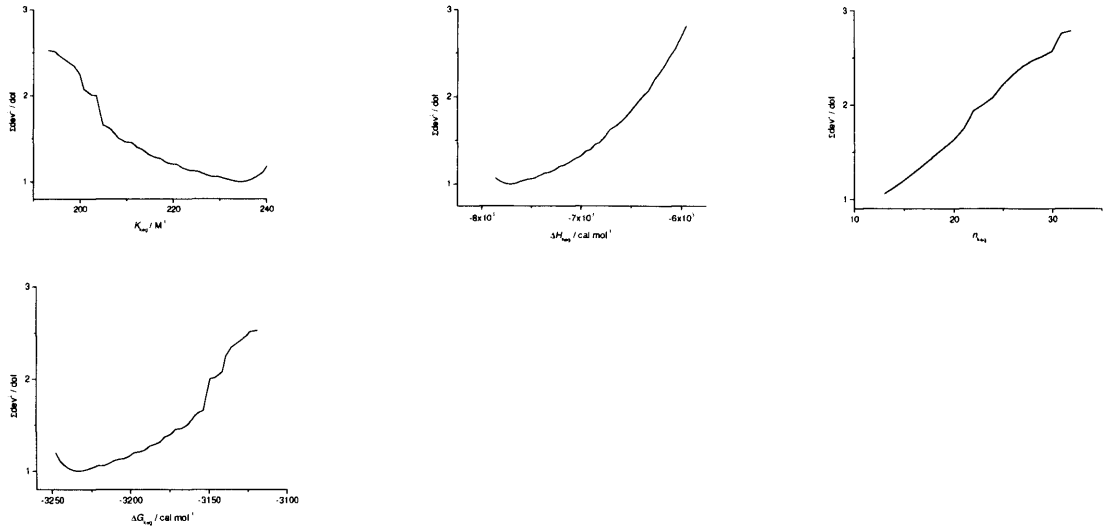

Figure A21 Error margins calculated from the fitting to Kegeles model with f_{keg} fixed to 0.01. Black lines represent the normalised $\Sigma dev^2/dof$ for dilution parameters

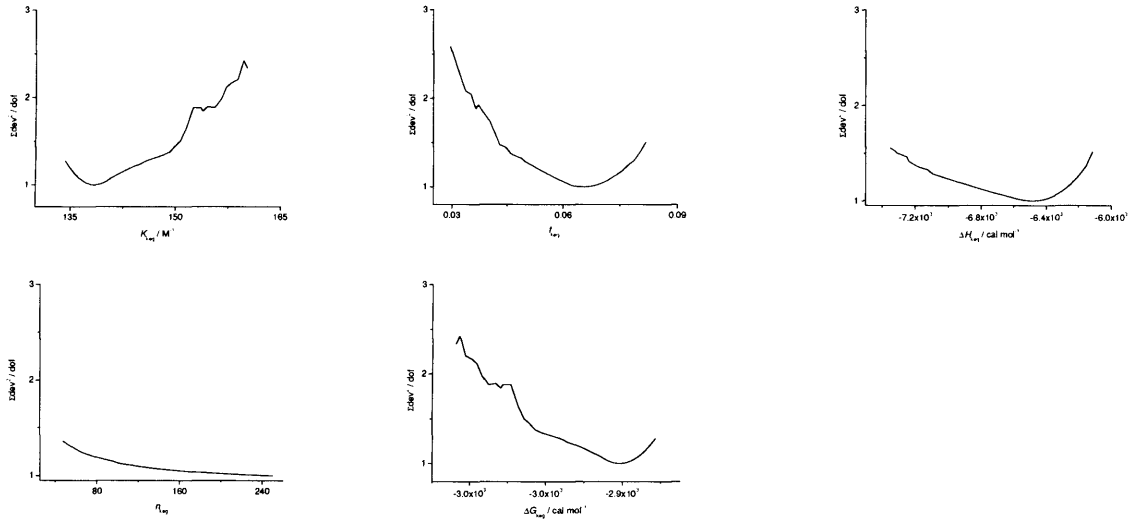

Figure A22 Error margins calculated from the fitting to Kegeles model with f_{keg} variable. Black line represents the normalised $\Sigma dev^2/dof$ for dilution parameters.

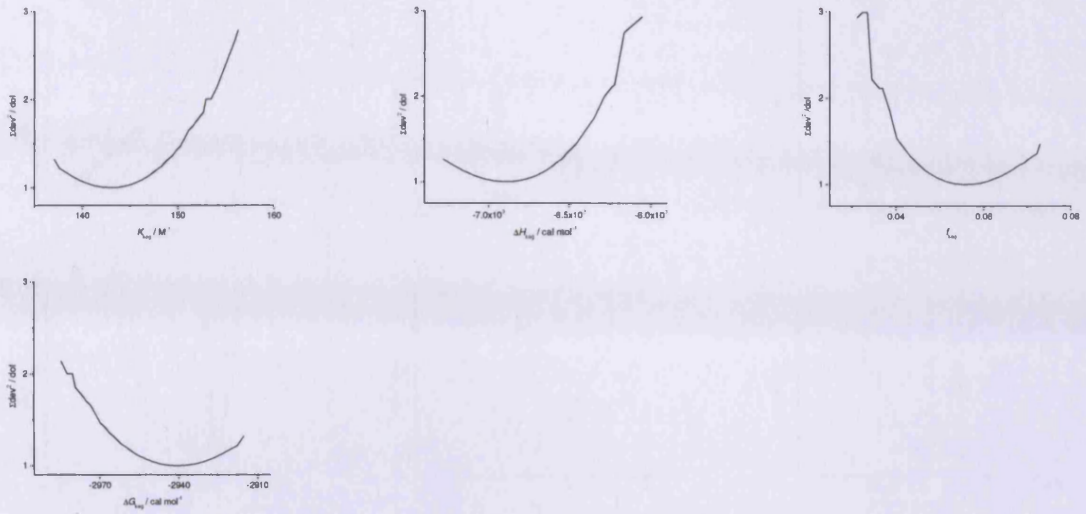

Figure A23 Error margins calculated from the fitting Kegeles model with *f* variable and n_{keg} fixed to 76. Red line represents the normalised $\Sigma dev^2/dof$ for dilution of 41.7 mM parameters.

Dilution of 17.1 mM, 8.6 mM and 22.3 mM solution of 4.14 in MOPS buffer, 25 °C

Black, red and blue lines are normalised $\Sigma dev^2/dof$ for three individual titrations. Unfortunately, the three sets of data do not provide enough overlap in data in order to estimate the average of $\Sigma dev^2/dof$.

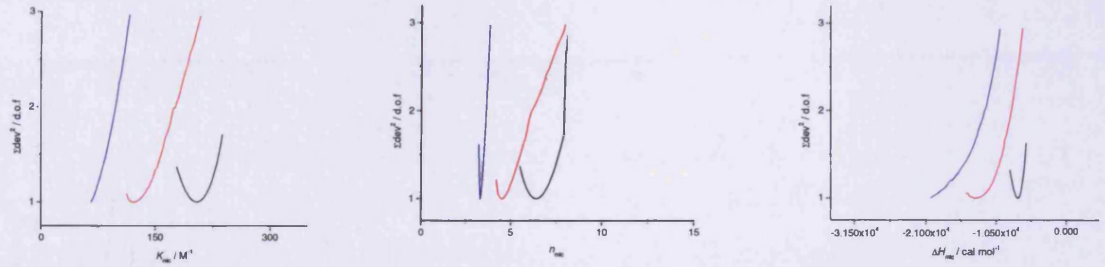

Figure A24 Error margins calculated from the fitting to n-merisation model. Blue, red and black lines represent the normalised $\Sigma dev^2/dof$ for dilution parameters.

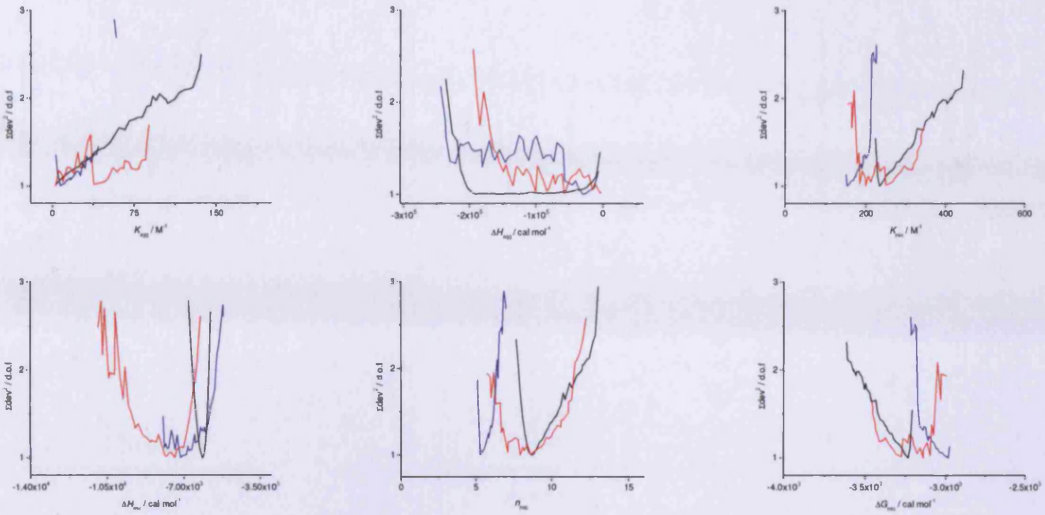

Figure **A25** Error margins calculated from the fitting to n-merisation and stepwise self aggregation models. Blue, red and black lines represent the normalised $\Sigma dev^2/dof$ for dilution of 17.1 mM, 8.6 mM respective 22.3 mM solution of **4.14** in MOPS buffer, at 25°C.

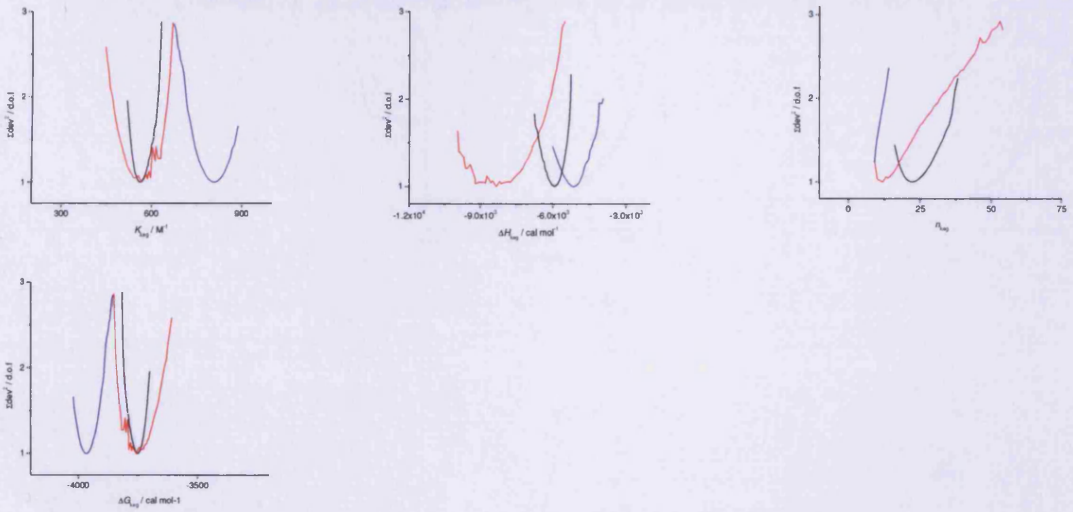

Figure A26 Error margins calculated from the fitting to Kegeles model with *f* fixed to 0.01. Blue, red and black lines represent the normalised $\Sigma dev^2/dof$ for dilution of 17.1 mM, 8.6 mM respective 22.3 mM solution of **4.14** in MOPS buffer, at 25°C.

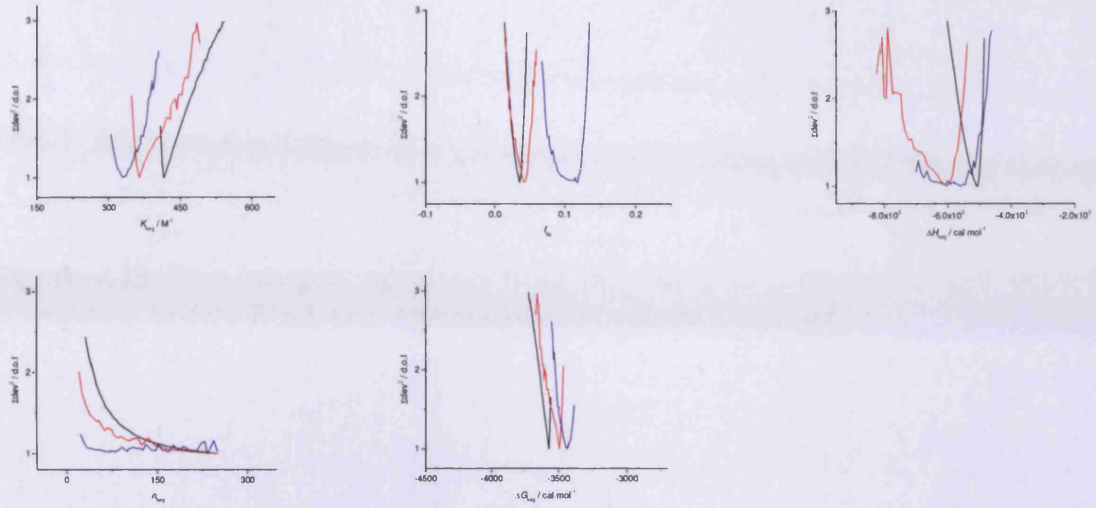

Figure A27 Error margins calculated from the fitting to Kegeles model with *f*-var. Blue, red and black lines represent the normalised $\Sigma dev^2/dof$ for dilution of 17.1 mM, 8.6 mM respective 22.3 mM solution of **4.14** in MOPS buffer, at 25°C.

*Dilution of 22.3 mM solution of **4.14** in MOPS buffer, at 40°C*

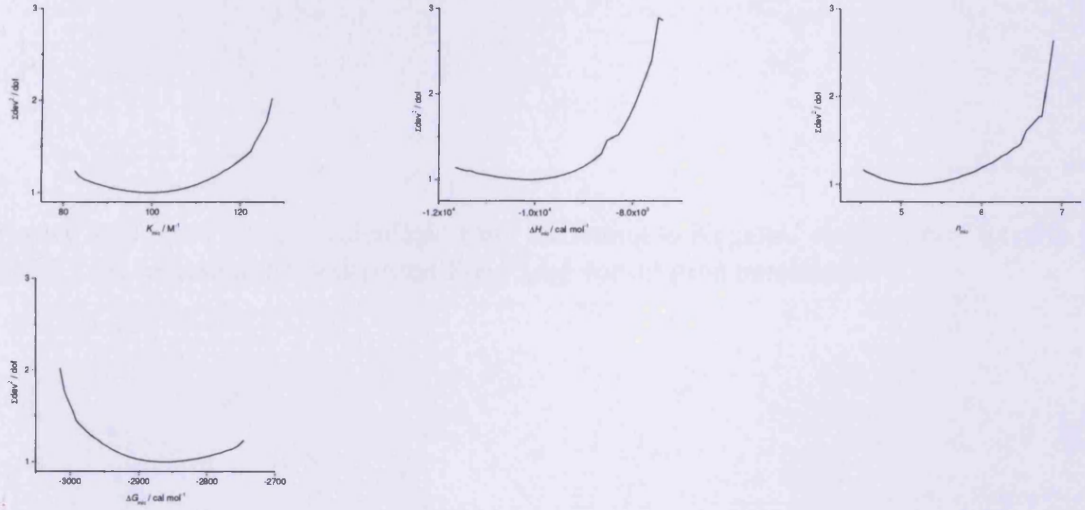

Figure A28 Error margins calculated from the fitting to n-merisation model. Black lines represent the normalised $\Sigma dev^2/dof$ for dilution of

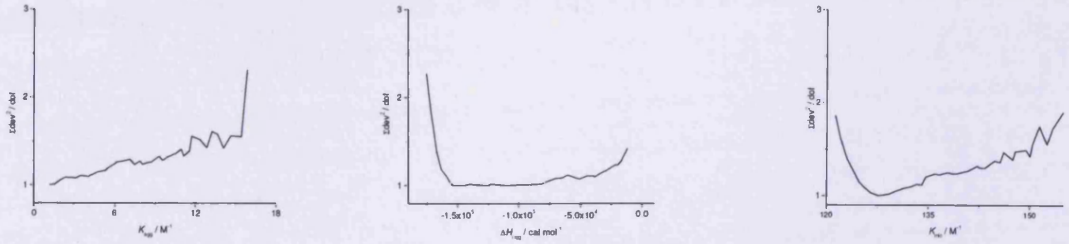

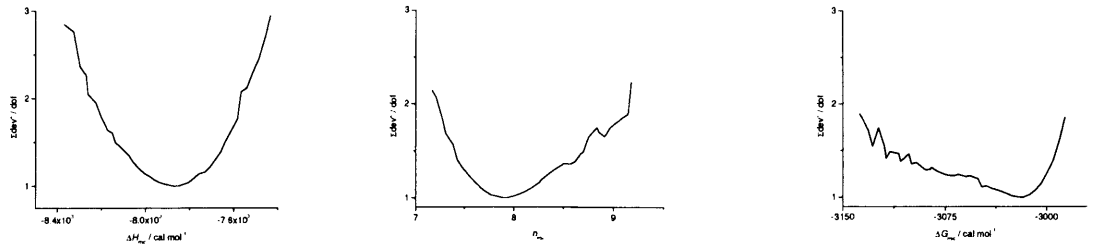

Figure A29 Error margins calculated from the fitting to n-merisation and stepwise self aggregation models. Black lines represent the normalised $\Sigma dev^2/dof$.

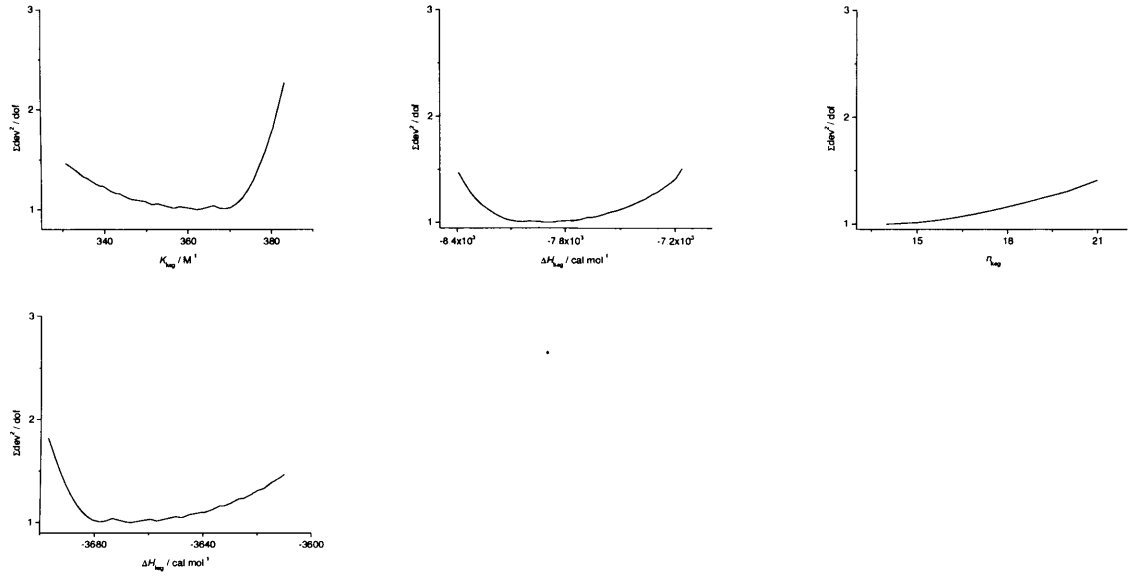

Figure A30 Error margins calculated from the fitting to Kegeles' model with *f* fixed to 0.01. Black lines represent the normalised $\Sigma dev^2/dof$ for dilution parameters.

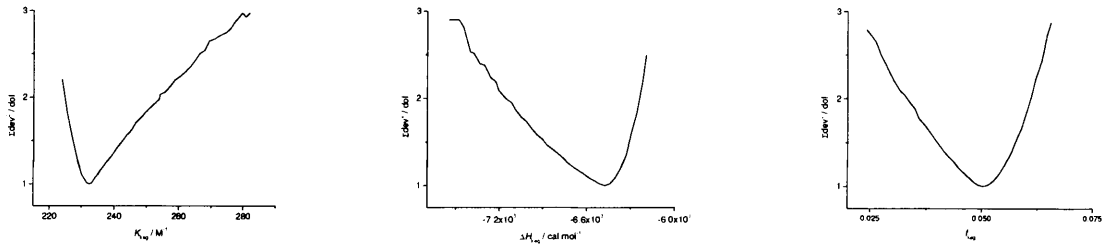

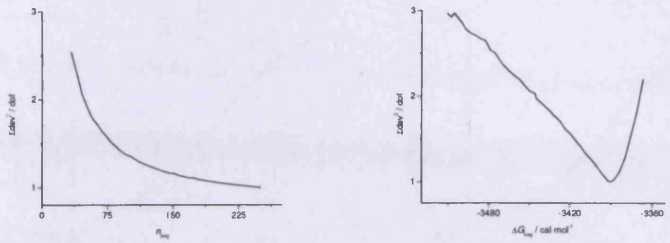

Figure A32 Error margins calculated from the fitting to Kegeles' model with *f* variable. Black lines represent the normalised $\Sigma dev^2/dof$ for dilution parameters.

Dilution of 1.5 mM solution of 4.14 in D_2O

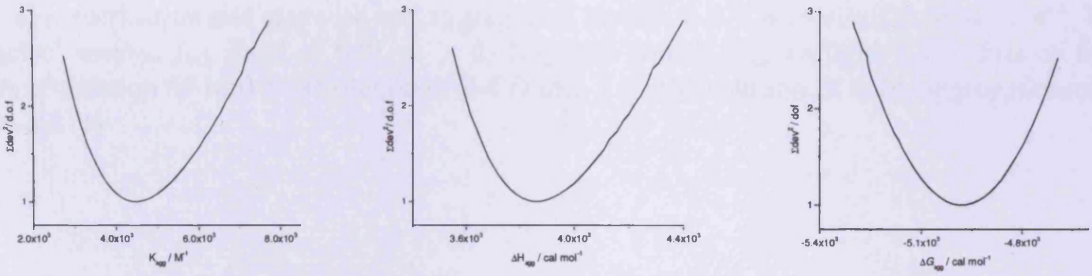

Figure A33 Error margins calculated from the fitting to stepwise self aggregation model. Black lines represent normalised $\Sigma dev^2/dof$ for dilution parameter.

3.6 Fits to n-merisation and Kegeles' models for 4.14 in MOPS buffer, 40 °C

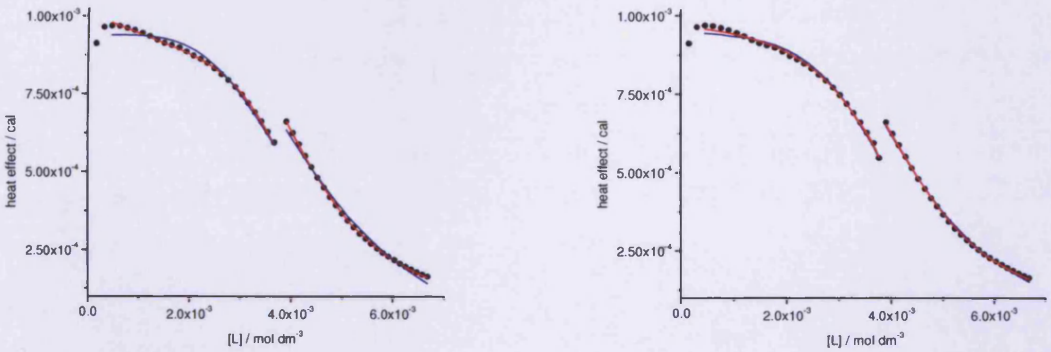

Figure A34 Fits of the heat of dilution of 22.3 mM solution of **4.14** in MOPS buffer, at 40°C for: a) n-merisation model (red line), n-merisation model with stepwise self aggregation included (blue line); b) Kegeles' model, *f* fixed at 0.01 (red line), Kegeles' model, *f* variable

3.7 Binding of 4.14 interacting with β-CD, in H_2O, at 25 °C

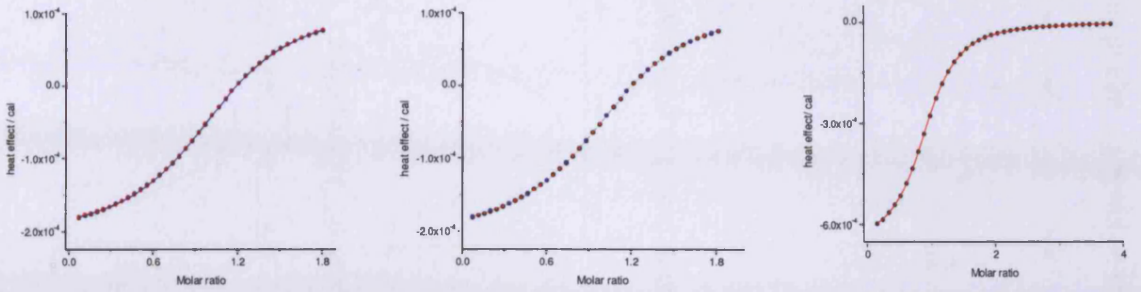

a b c

Figure A35 Fits of the heats of titration of 8.5 mM solution of **4.14** into 1.0 mM solution β-CD: a) *n*-merisation and stepwise self aggregation models (-●-), *n*-merisation model (-●-); b) Kegeles' model, f_{keg} fixed at 0.01(-●-); d) Kegeles' model, f_{keg} variable (-●-). Fits of the heats of titration of 18.0 mM solution of β-CD into 1.0 mM solution of **4.14**, aggregation not included (c)

Titration of a 8.65 mM solution of 4.14 into 1.0 mM solution of β-CD, in H_2O, at 25 °C

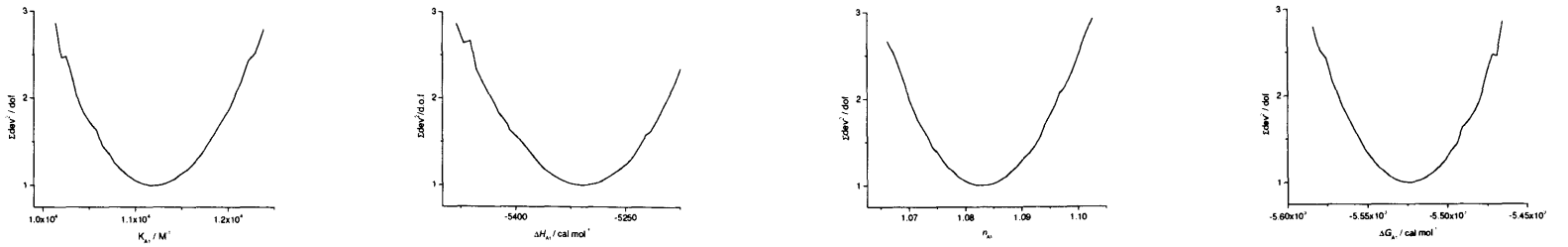

Figure A35 Normalised $\Sigma dev^2/dof$ for binding parameters The binding model does not include ligand self aggregation.

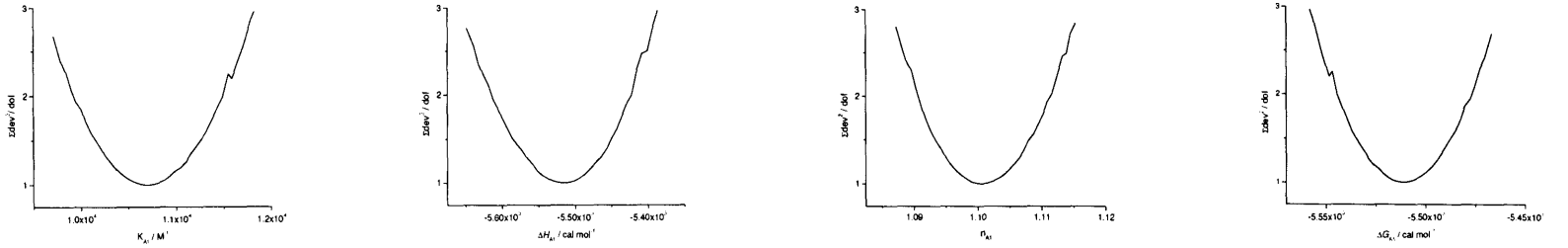

Figure A36 Normalised $\Sigma dev^2/dof$ for binding parameters. The binding model includes n-merisation model in combination with stepwise model for ligand self aggregation.

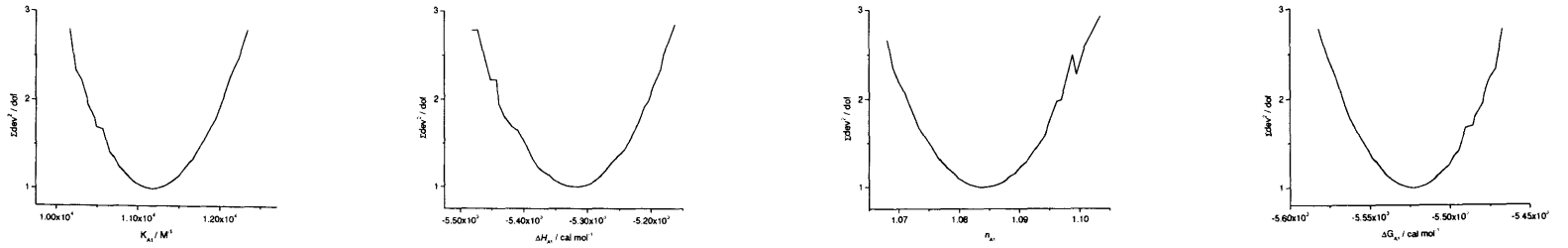

Figure A37 Normalised $\Sigma dev^2/dof$ for binding parameters. The binding model includes Kegeles' model as mode for ligand self aggregation, with f_{keg} fixed to 0.01 and n_{keg} fixed to 12.

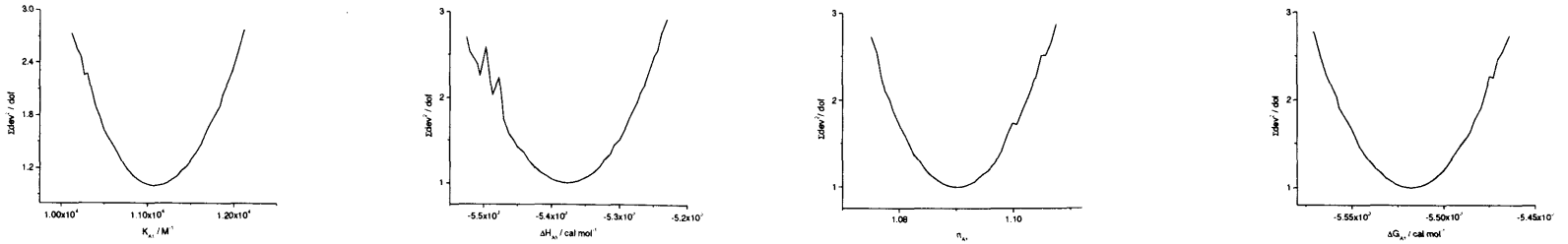

Figure A38 Normalised $\Sigma dev^2/dof$ for binding parameters. The binding model includes Kegeles' model as mode for ligand self aggregation, with f_{keg} fixed to 0.06 and n_{keg} fixed to 250.

Titration of 18.0 mM solution of β-CD into 1.0 mM in H_2O, at 25 °C

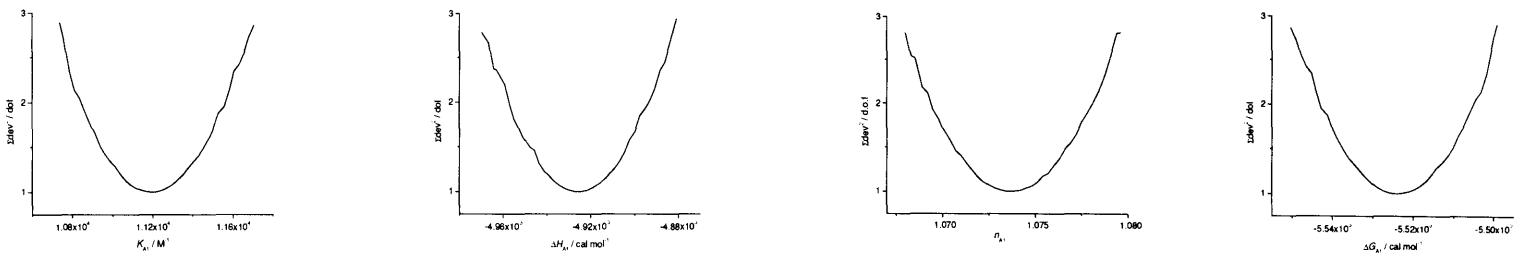

Figure A39 Titration of Normalised $\Sigma dev^2/dof$ for binding parameters

A4 Monocationic terthiophene 4.15

4.1 Extinction coefficient

The molar extinction coefficient of stock solution of **4.15** in buffer was determined through point checks. A volume of 10 µl of this solution in buffer was added to 2000 µl buffer in a 1.00 cm pathlength cuvette. A further 5 µl of the same solution was added to 200 µl buffer in a 1.00 mm pathlength cuvette. Ligand absorbance was measured at λ_{max} 339 nm and the molar extinction coefficient was extracted from the linear fit to give a value of $(17.6\pm0.2) \times 10^3$ dm^3 mol^{-1} cm^{-1}, which is very similar to oligothiophenes **4.15** and **4.16.**

4.2 Fits to n-merisation and Kegeles' model for dilution of 4.15 in MOPS buffer, at 25°C

Titration of 17.7 mM solution of 4.15 in MOPS buffer, at 25°C.

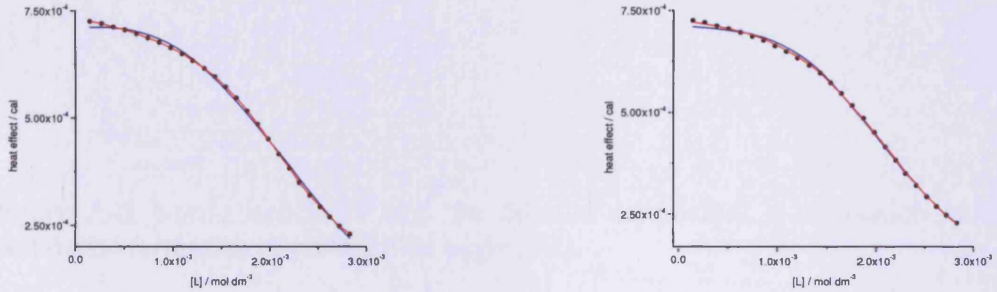

Figure A40 Fits to: a) n-merisation model, aggregation not included (blue line), n-merisation model, aggregation included (red line); b) Kegeles' model , f_{keg} fixed at 0.01. (blue line), Kegeles' model, f_{keg} variable.

4.3 Normalised $\Sigma dev^2/dof$ for dilution parameters of 4.15

*Dilution of 17.7 mM solution of **4.15** in MOPS buffer, at 25 °C*

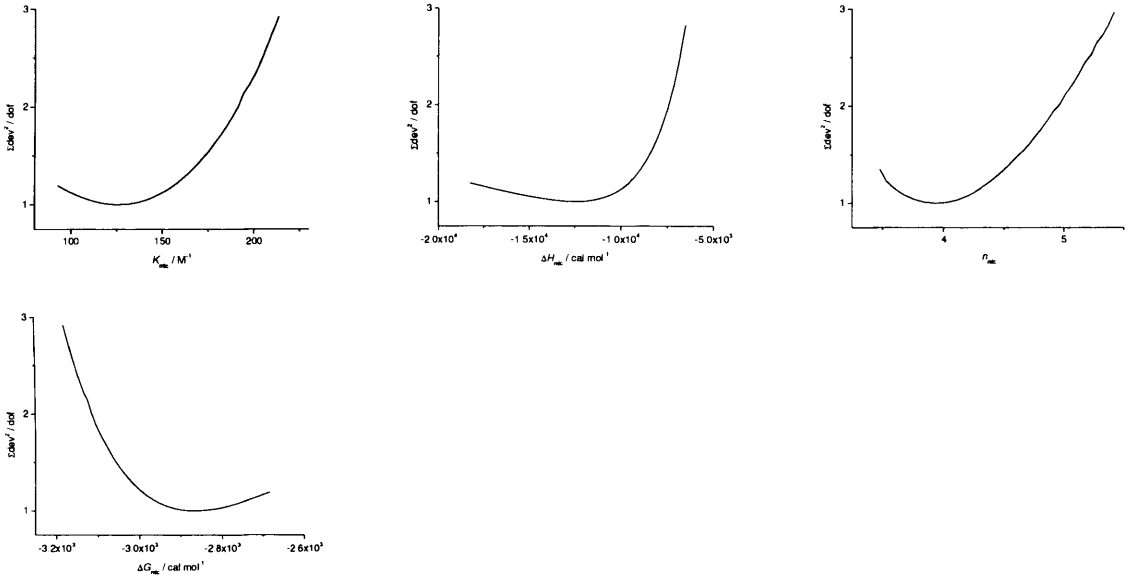

Figure A41 Normalised $\Sigma dev^2/dof$ for dilution parameters. *n*-merisation model does not include the formation of pre-micellar aggregates.

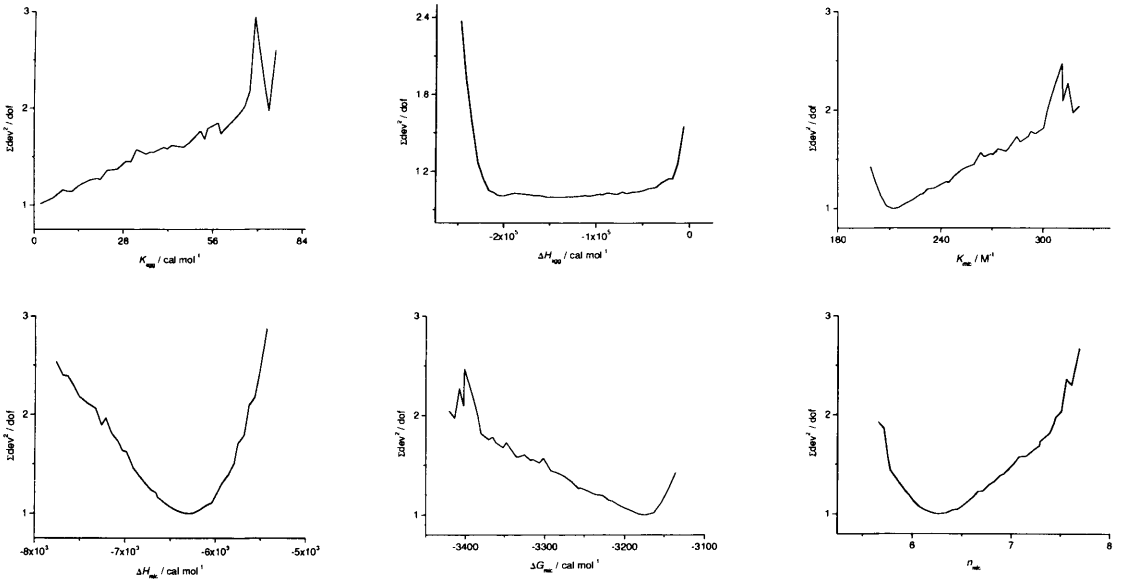

Figure A42 Normalised $\Sigma dev^2/dof$ for dilutionparameters. *n*-merisation model includes isodesmic self aggregation.

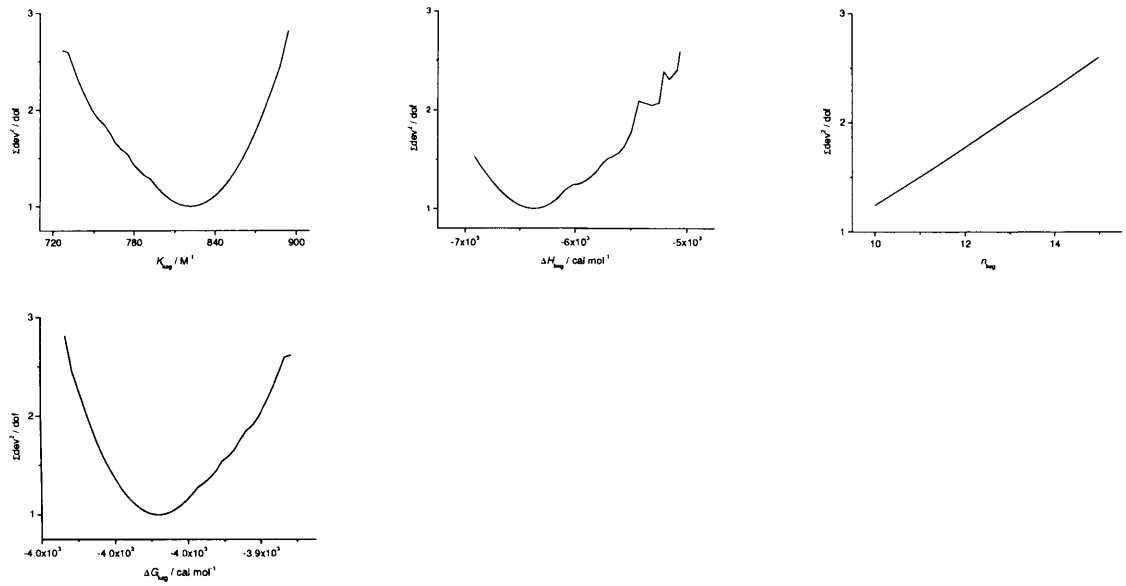

Figure A43 Normalised $\Sigma dev^2/dof$ for dilution parameters. Errors are calculated from the fiting to Kegeles' model, f_{keg} fixed to 0.01.

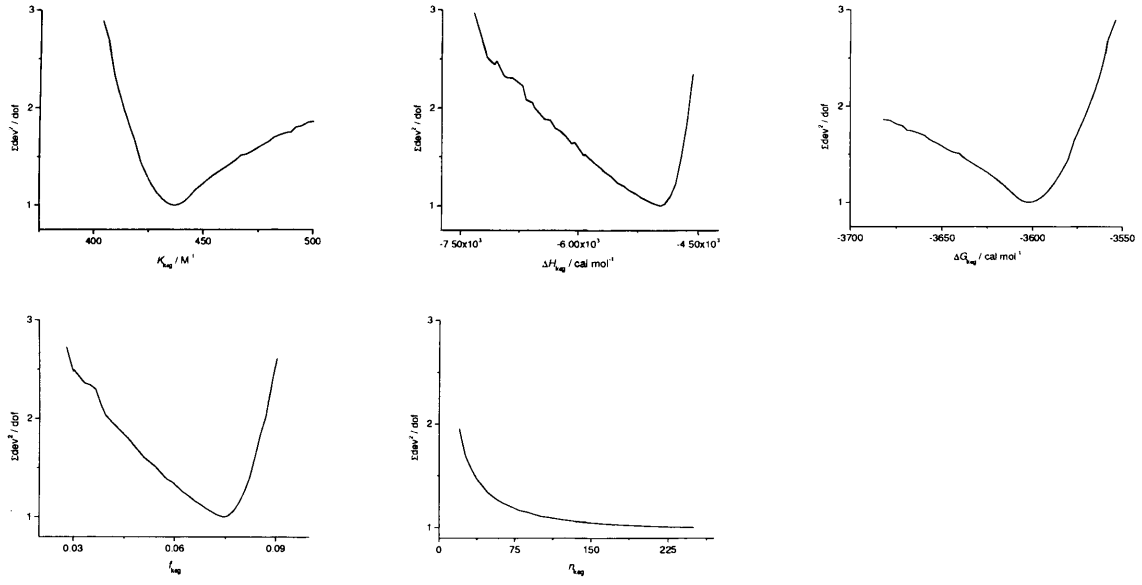

Figure A44 Normalised $\Sigma dev^2/dof$ for dilution parameters. Error margins are obtained from the fitting to Kegeles' model with both f_{keg} and n_{keg} variable.

A5 Monocationic terthiophene 4.16

4.1 Fits to n-merisation and Kegeles' model

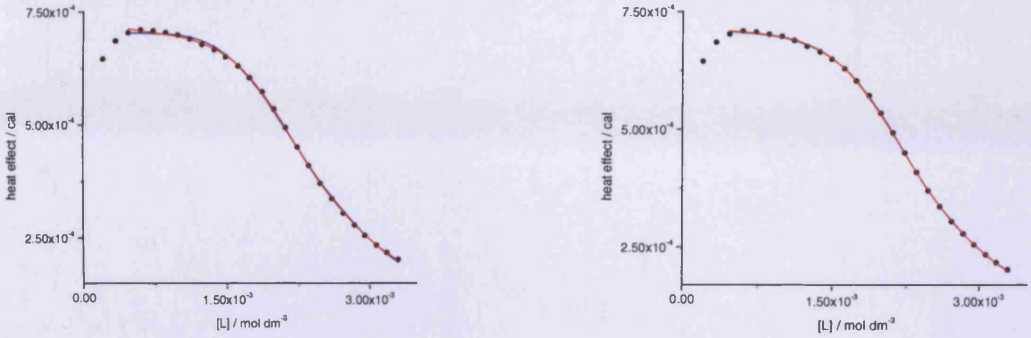

Figure **A45** Fits to: a) n-merisation model, aggregation not included (blue line), n-merisation model, aggregation included (red line); b) Kegeles' model , f_{keg} fixed *at 0.01* (blue line), Kegeles' model, f_{keg} variable (red line) for 19.8 mM solution of **4.1c** in MOPS buffer, at 25°C.

4.2 Normalised $\Sigma dev^2/dof$ for dilution of 4.16

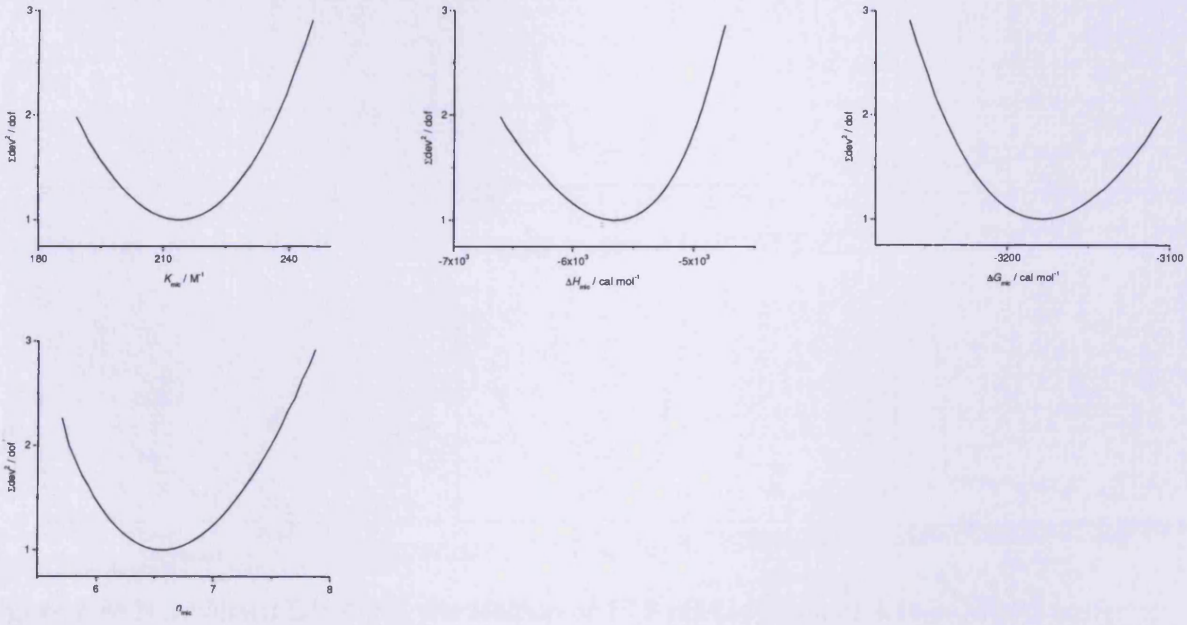

Figure A46 Normalised $\Sigma dev^2/dof$ for dilution of 19.8 mM solution of **4.16** in MOPS buffer, at 25°C.The error margins calculated from the fitting to n-merisation model with premicellar aggregates not included.

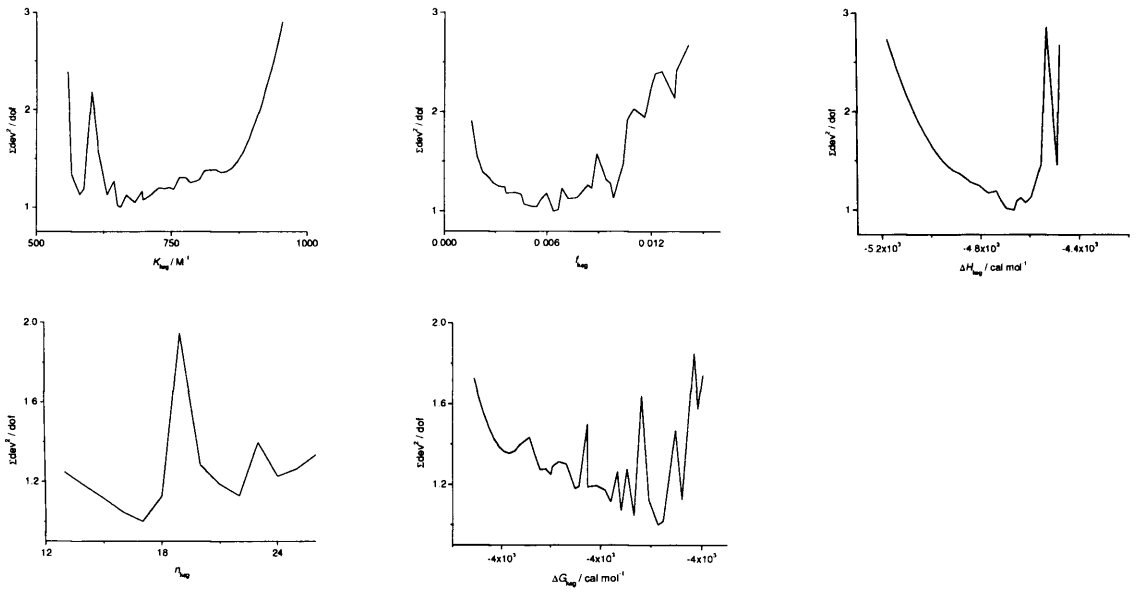

Figure A47 Normalised $\Sigma dev^2/dof$ for dilution of 19.8 mM solution of **4.16** in MOPS buffer, at 25°C. The error margins calculated from the fitting Kegeles model with f_{keg} variable

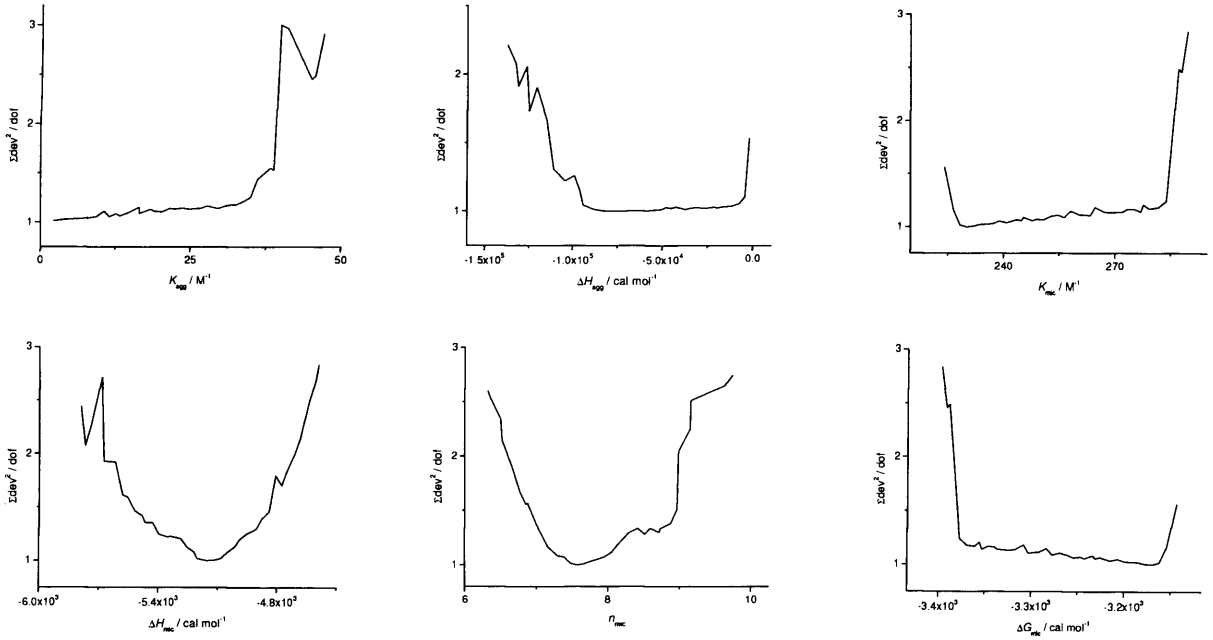

Figure A48 Normalised $\Sigma dev^2/dof$ for dilution of 19.8 mM solution of **4.16** in MOPS buffer, at 25°C.The error margins calculated from the fitting to n-merisation model with premicellar aggregates included.

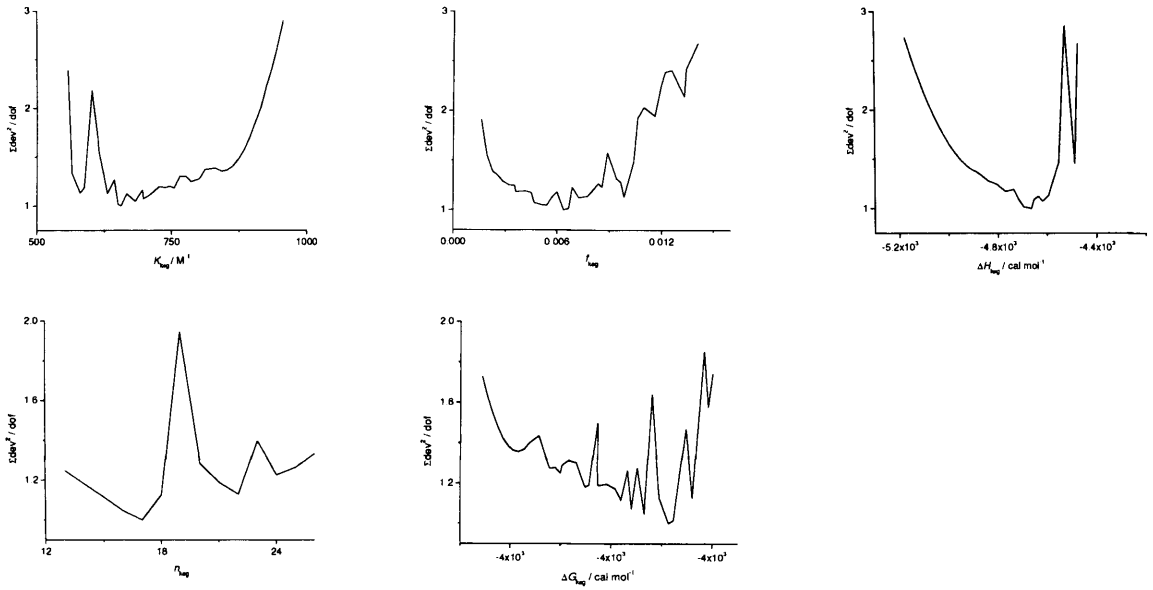

Figure 49 Normalised $\Sigma dev^2/dof$ for dilution of 19.8 mM solution of **4.16** in MOPS buffer, at 25°C.The error margins calculated from the fitting Kegeles model with f_{keg}-variable.

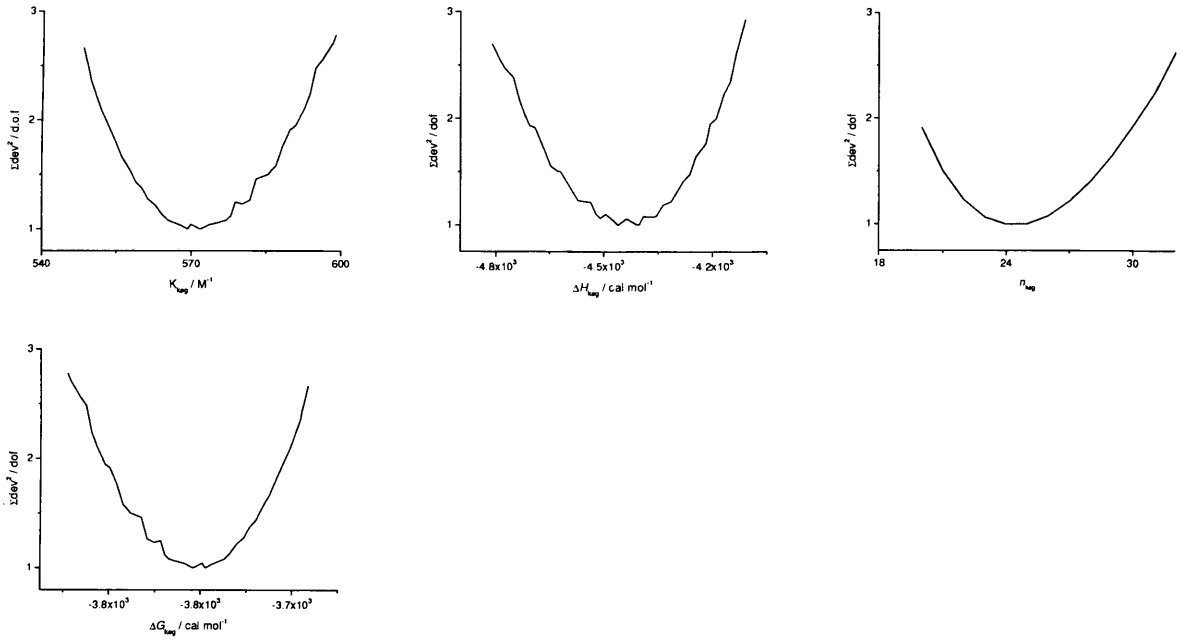

Figure A50 Normalised $\Sigma dev^2/dof$ for dilution of 19.8 mM solution of **4.16** in MOPS buffer, at 25°C.The error margins calculated from the fitting Kegeles model with $f\,keg$ fixed to 0.01.

A5 Dicationic quaterthiophene 4.17

5.1 Normalised $\Sigma dev^2/dof$ for dilution of 4.17

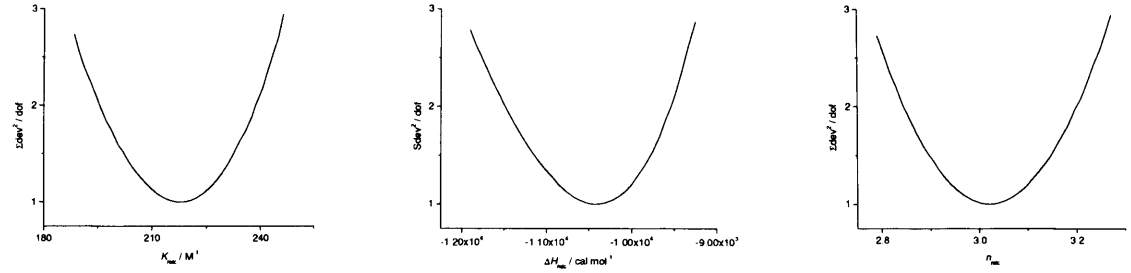

Figure A51 Normalised $\Sigma dev^2/dof$ for dilution of 10.9 mM solution of **4.17** in MOPS buffer Error margins are calculated from the fitting to n-merisation model, aggregation included.

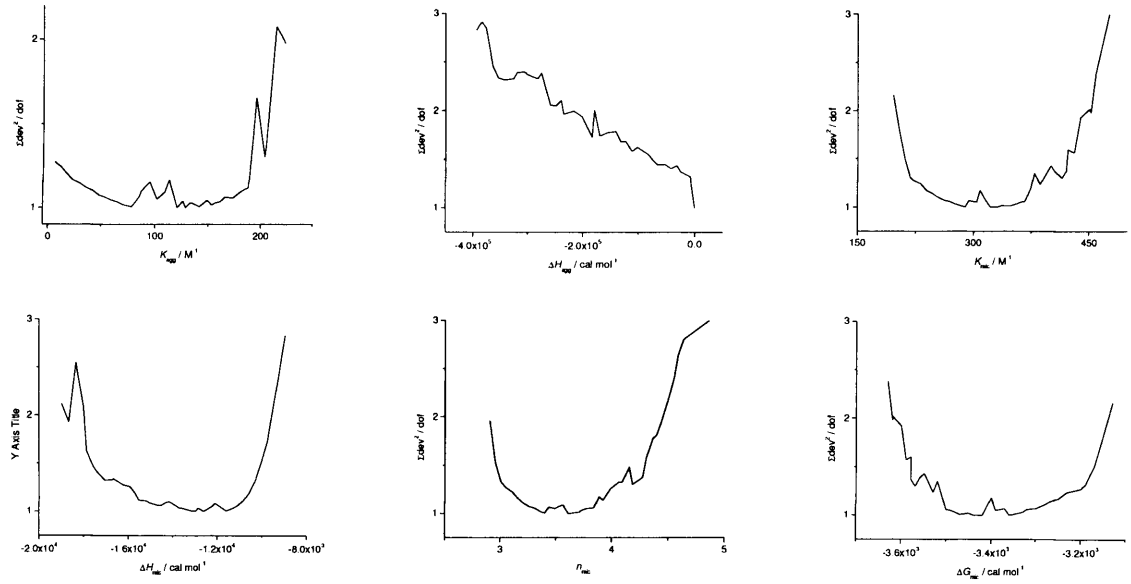

Figure A52 Normalised $\Sigma dev^2/dof$ for dilution of 10.9 mM solution of **4.17** in MOPS buffer Error margins are calculated from the fitting to *n*-merisation model in combination with stepwise self aggregation model.

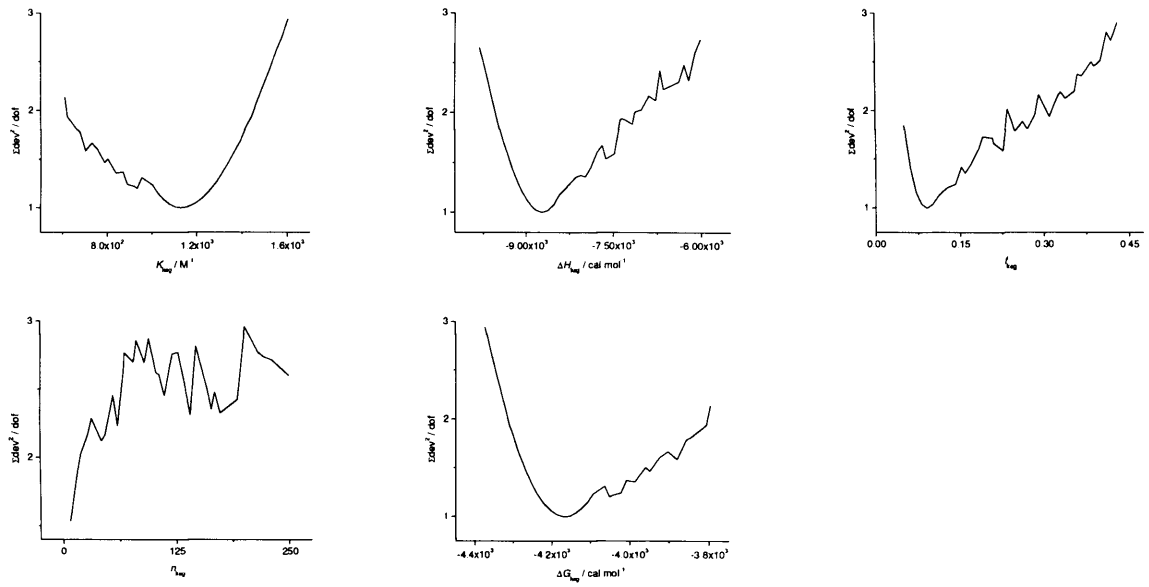

Figure A53 Normalised $\Sigma dev^2/dof$ for dilution of 10.9 mM solution of **4.17** in MOPS buffer Error margins are calculated from the fitting to Kegeles' model, f_{keg} variable.

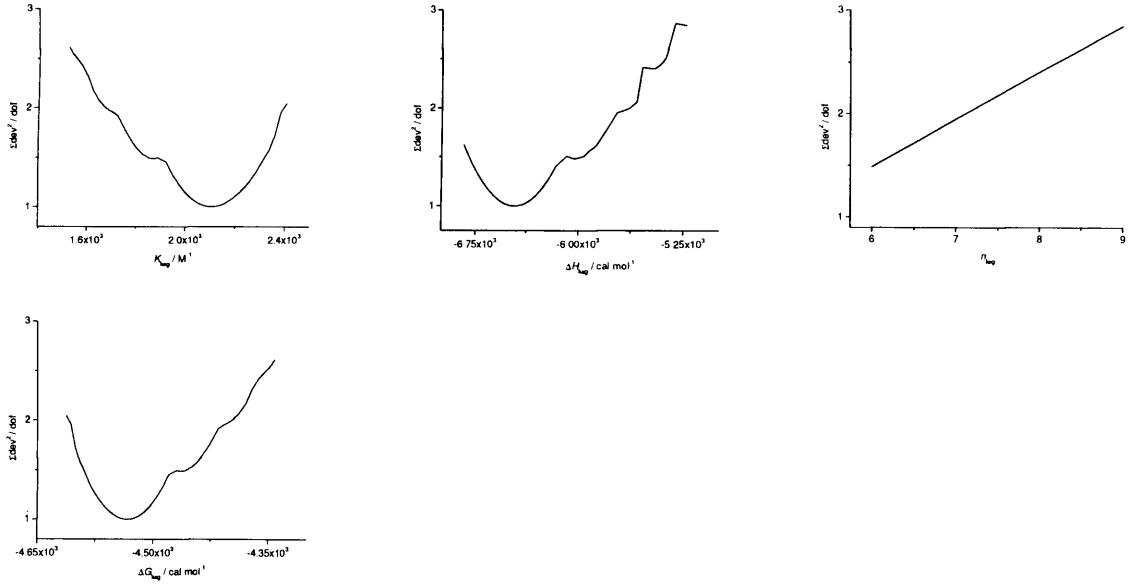

Figure A54 Normalised $\Sigma dev^2/dof$ for dilution of 10.9 mM solution of **4.17** in MOPS buffer Error margins are calculated from the fitting to Kegeles' model, f_{keg} fixed at 0.01.

A6 Monocationic terthiophene 5.1 binding to DNA

6.1 Isothermal titration calorimetry

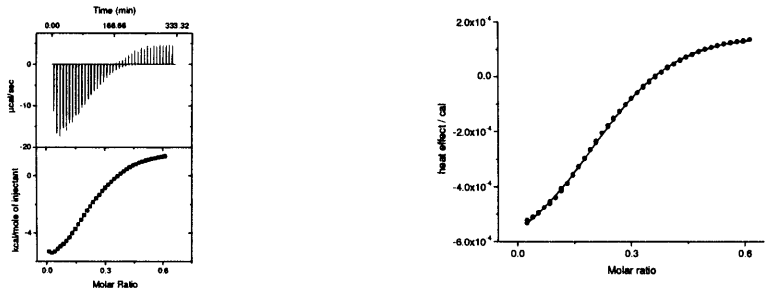

Figure A55 Heats of injection of 19.38 mM solution of **5.1,** titrated into 4.5 mM solution of CT DNA, in 25 mM MOPS, 50 mM NaCl and 1 mM EDTA, pH 7.0, at 25^{0}C (left).Fits to one binding site model and n-merisation model(blue line) or Kegeles' model (red line)

6.2 Error margins

Titration of 19.8 mM solution of **5.1** into 4.5 mM solution of CT DNA, at 25°C

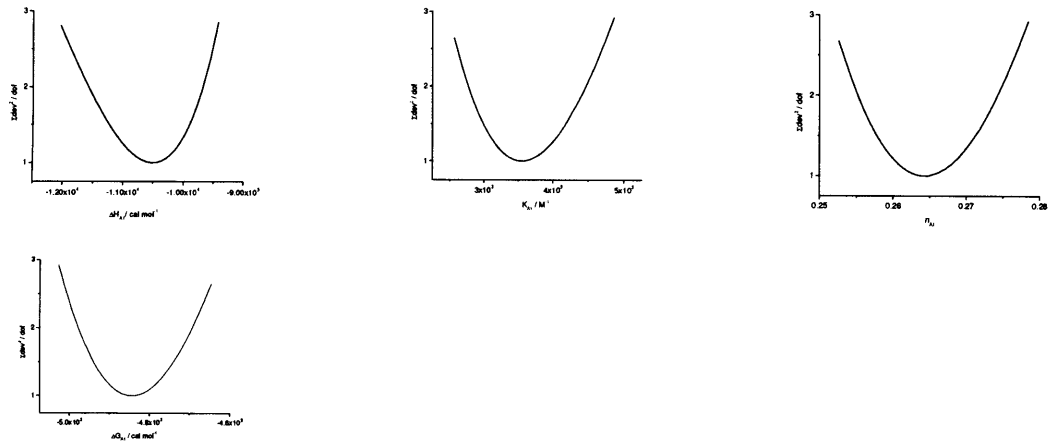

Figure A56 Normalised $\Sigma dev^2/dof$ for binding parameters. Error margins calculated from the fitting to a binding model which includes n-merisation model as model for self aggregation.

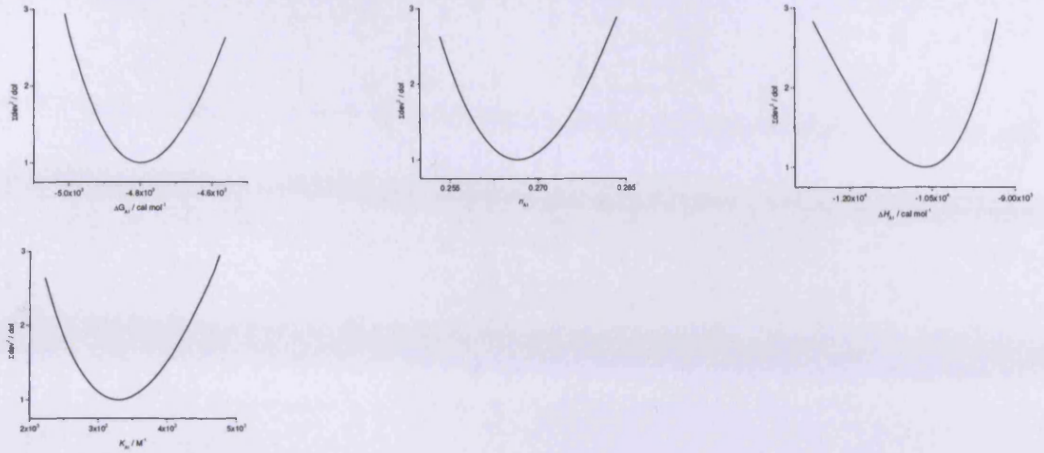

Figure A57 Normalised $\Sigma dev^2/dof$ for binding parameters. Error margins calculated from the fitting to a binding model which includes kegeles' model as model for self aggregation of 5.1.

A7 Monocationic terthiophene 5.2 binding to DNA

7.1 UV-Vis titrations

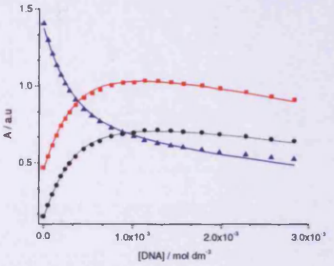

Figure A58 UV-visible titration of 7.94×10^{-2} mM cationic terthiophene **5.2** with 0 – 2.83 mM fish sperm DNA in 25 mM MOPS, 50 mM NaCl and 1 mM EDTA, pH 7.0, at 25 °C. Absorbances at wavelengths 336 nm (▲), 380 nm (●) and 397 nm (■) are plotted against DNA concentration and the solid lines represent a global fit to a multiple independent sites model.

7.2 Isothermal titration calorimetry

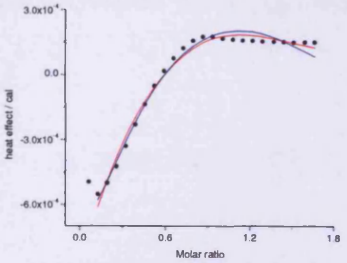

Figure A59 Titration of 17.8 mM solution of 5.2 into 2.0 mM solution of FS DNA. Fits to one binding site model with ligand self aggregation included: *n*-merisation model (blue fit), Kegeles' model (red-fit)

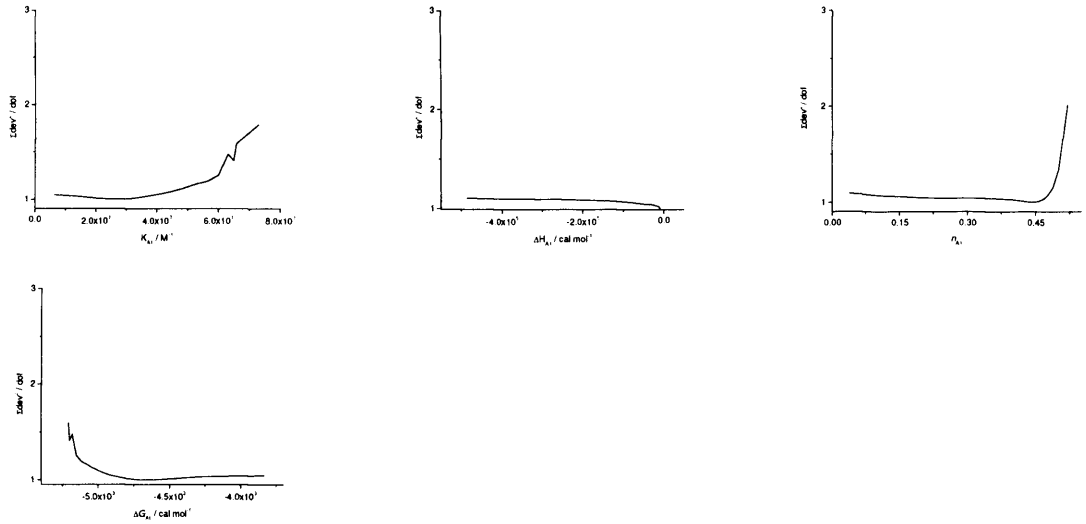

Figure A60 Normalised $\Sigma dev^2/dof$ for binding parameters. Errors are calculated from the fitting to one binding site model and n-merisation model.

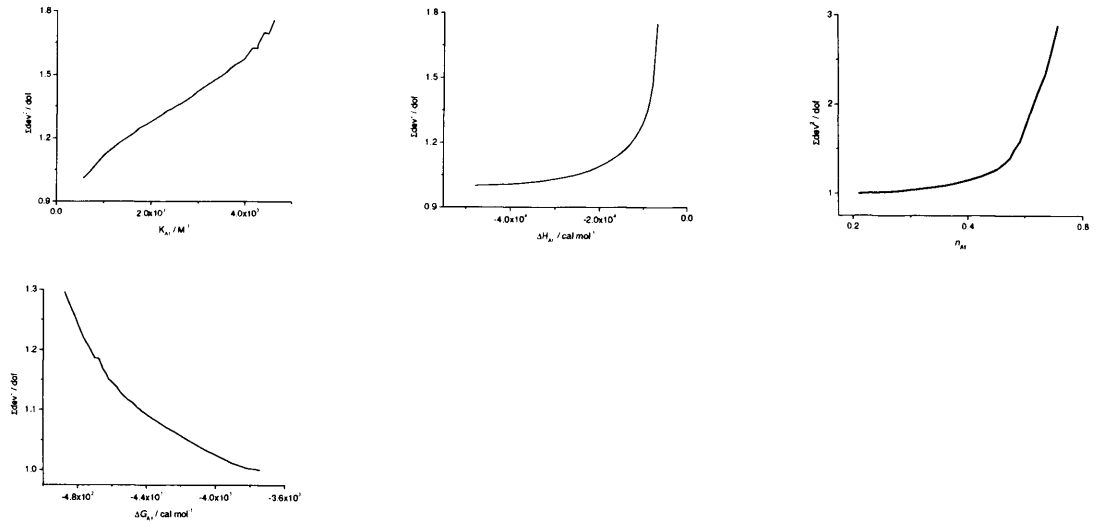

Figure A61 Normalised $\Sigma dev^2/dof$ for binding parameters. Errors are calculated from the fitting to one binding site model and Kegeles' model, f_{keg} fixed to 0.01.

A8 Monocationic terthiophene binding to DNA

8.1 UV-Vis titration

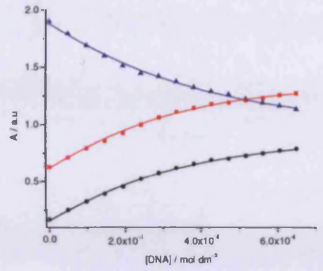

Figure A62 UV-visible titration of 1.02×10^{-1} mM cationic terthiophene **5.3** in the presence of 0 – 0.65 mM fish sperm DNA in 25 mM MOPS, 50 mM NaCl and 1 mM EDTA, pH 7.0, at 25 °C. Absorbances at wavelengths 336 nm (▲), 380 nm (●) and 397 nm (■) are plotted against DNA concentration and the solid lines represent a global fit to a multiple independent sites model.

8.2 Isothermal titration calorimetry

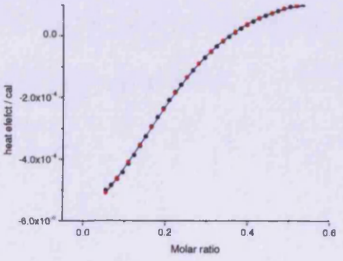

Figure A63 Titration of 19.8 mM solution of **5.3** into 5.0 mM solution of FS DNA. Fits to one binding site model with ligand self aggregation included: *n*-merisation model (blue fit), Kegeles' model (red-fit)

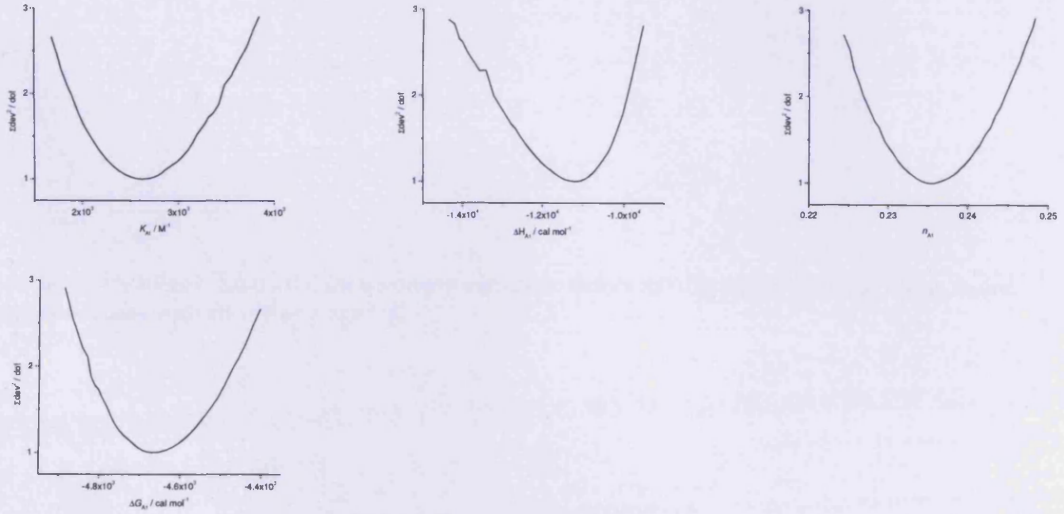

Figure A64 Normalised $\Sigma dev^2/dof$ for binding parameters. Errors are calculated from the fitting to one binding site model and n-merisation model.

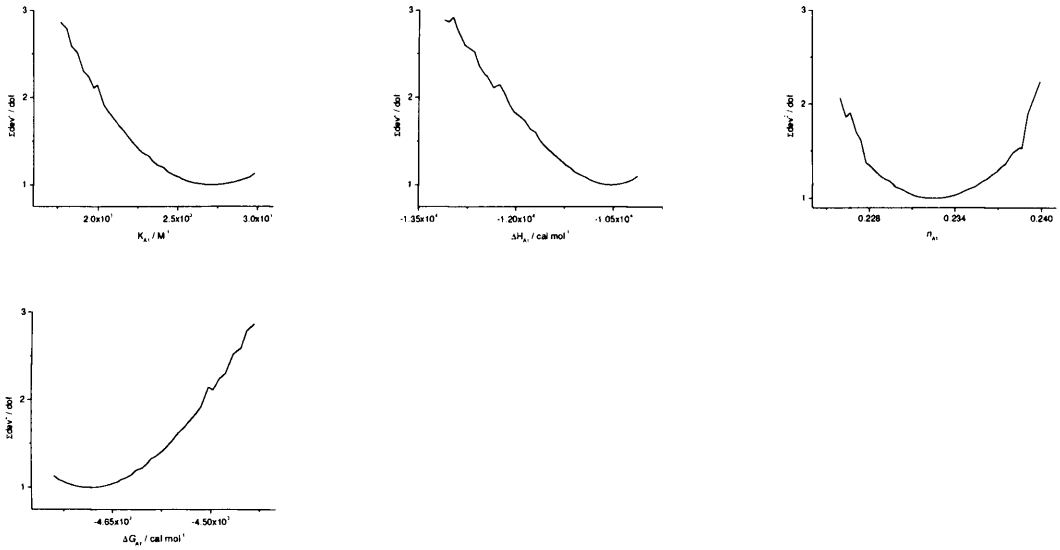

Figure A65 Normalised $\Sigma dev^2/dof$ for binding parameters. Errors are calculated from the fitting to one binding site model and n-merisation' model.

A9 Cationic furan derivative 5.6 binding to DNA

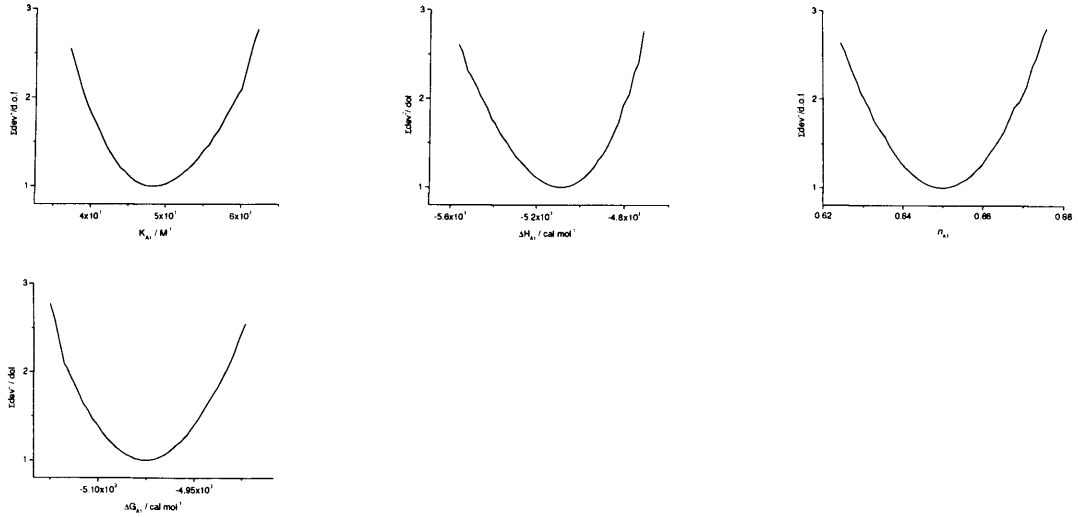

Figure A66 Normalised $\Sigma dev^2/dof$ for binding parameters. Errors are calculated from the fitting to one binding site model without self aggregation

A9 Dicationic terthiophene binding to DNA

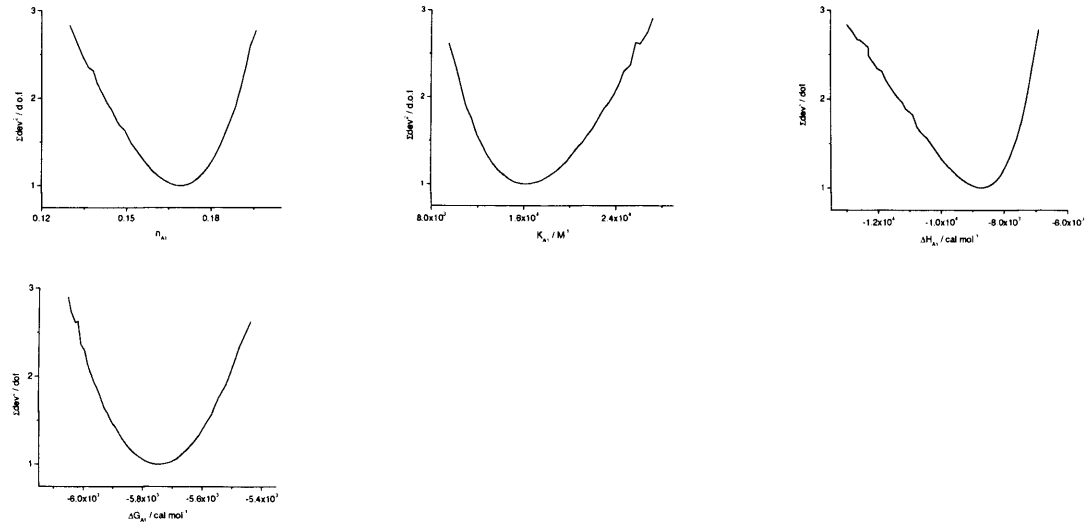

Figure A67 Normalised $\Sigma dev^2/dof$ for binding parameters. Errors are calculated from the fitting to one binding site model without self aggregation